Development, characterization, and application of novel *in vitro* human eccrine sweat gland models for studying new mechanisms to regulate sweating

Inaugural dissertation

for the attainment of the title of doctor
in the Faculty of Mathematics and Natural Sciences
at the Heinrich Heine University Düsseldorf

presented by

Jessica Welzel
from Melle

Düsseldorf, May 2021

externally conducted at Henkel AG & Co. KGaA, Düsseldorf
under the supervision of Prof. Dr. Dr. h. c. Holger Stark
from the Institute of Pharmaceutical and Medicinal Chemistry
at the Heinrich Heine University Düsseldorf

Published by permission of the
Faculty of Mathematics and Natural Sciences at
Heinrich Heine University Düsseldorf

Supervisor: Prof. Dr. Dr. h. c. Holger Stark
Co-Supervisor: Prof. Dr. Wilhelm Stahl

Date of the oral examination: 25.08.2021

Abstract

Thermoregulation of the human body mainly relies on sweating. Thereby, aqueous sweat fluid secreted by eccrine sweat glands onto the skin surface evaporates and cools the skin. Although this is a natural, highly efficient process providing humans with an evolutionary advantage, appearance of wet patches on clothes is mostly undesired today. Especially in case of sweat-related disorders such as hyperhidrosis, where excessive sweating occurs, this poses a high burden for the individual. Underlying dysregulation of sweating is, up to now, only partly understood and just few alleviating agents are available. For some of them the mechanism of action is well investigated, whereas the one of the most common antiperspirant ingredient, aluminum chlorohydrate (ACH), is still only partly disclosed. It is assumed to encompass physical blockage of the eccrine sweat gland.

To intensify the knowledge of the sweating mechanism on a cellular level and to elucidate possible physiological effects of ACH, a cell-based *in vitro* test procedure was developed. As sweating is mainly a process of ion fluxes between eccrine sweat gland cells, gland lumen, and surrounding tissue, herein established methodical test system relies on monitoring of intracellular changes of calcium, potassium, sodium, and chloride ions using cultured primary human eccrine sweat gland cells. Employing this novel procedure ACH was demonstrated to also evoke physiological reactions in human eccrine sweat gland cells. Strikingly, a distinct class of substances, Cl^--containing ammonium solutions, elicited the same characteristic ion changes as ACH. With further testing, polyols were identified as another class of substances dysregulating the ion equilibrium *in vitro*. For both substance classes the antiperspirant effect was verified in humans. Strengthening herein developed reliable *in vitro* test system, even proposals for underlying cellular mode of action of these agents are possible. This highlights the capabilities of these methods and contributes significantly to understanding sweating on a cellular basis.

Adding to the latter aspect, an organotypic three-dimensional model of the human eccrine sweat gland was developed in this work to facilitate detailed scrutiny of cell-cell-interactions between the cell types of secretory coil and reabsorbing duct. In a further step, those cells were successfully integrated into newly designed *in vitro* dermal equivalents comparable to the natural environment in human skin. Both these *in vitro* models emphasized cellular interdependency of coil and duct cells in developing certain proteins and revealed some alterations in protein expression of cultured cells compared to native eccrine sweat gland cells.

Those deviances were also apparent in herein generated eccrine sweat gland duct cell line. After transduction with simian virus 40 large T antigen-containing lentiviral vector and overcoming of a short proliferation crisis, transduced eccrine duct cells exhibited an extended lifespan with stable growth suggesting their immortalized state. As duct cells represent the primary target of topically applied products and, so far, no immortalized duct cell line is available for research, this newly generated and described transduced duct cell line represents an important tool for standardization of cellular material in future *in vitro* sweat gland research. It should facilitate more detailed elucidation of physiological sweating processes and pose a defined source of cellular material for generation of organotypic sweat gland models.

Results of this PhD thesis add significantly to understanding the mechanism of sweating including required cellular interactions. With the help of newly generated eccrine sweat gland duct cell line standardization of these *in vitro* approaches is feasibly in future, which allows for further detailed investigation of perspiration and cellular interdependency with relevance for treating dermal disorders.

Zusammenfassung

Die menschliche Körpertemperatur wird überwiegend durch Schwitzen reguliert. Durch Sezernierung des wässrigen Schweißes aus ekkrinen Schweißdrüsen auf die Hautoberfläche und der dortigen Evaporation wird die Kühlung der Haut erreicht. Obwohl dieser natürliche, hoch effiziente, physiologische Prozess den Menschen in der Evolution einen wichtigen Vorteil liefert, ist die Entstehung von Schweißflecken auf der Kleidung in der heutigen Gesellschaft verpönt. Vor allem für Menschen, die unter Hyperhidrose, also überproportional starkem Schwitzen, leiden, stellt dies eine große Belastung dar. Die zugrunde liegende Dysregulierung des Schwitzmechanismus ist bis heute nicht vollständig aufgeklärt und nur wenige lindernde Wirkstoffe finden Anwendung. Während der Wirkmechanismus einiger Stoffe detailliert beschrieben ist, bleibt die genaue Wirkweise des meistgenutzten Inhaltsstoffs aus Antitranspirantien, das Aluminiumchlorohydrat (ACH), unklar. Wissenschaftlich anerkannt ist der physische Verschluss des Schweißdrüsen-ausführungsgangs durch einen gelartigen aluminiumhaltigen Pfropfen.

Um das Verständnis des Schwitzmechanismus zu vertiefen und mögliche physiologische Effekte des ACH zu untersuchen, wurde in dieser Arbeit ein zellbasiertes in-vitro-Testsystem entwickelt. Da Schwitzen in erster Linie durch Ionenströme zwischen Schweißdrüsenzellen, dem Drüsenlumen und dem umgebenden Gewebe beschrieben werden kann, basiert der hier entwickelte methodische Testansatz auf der Messung von intrazellulären Veränderungen der Ionen Kalzium, Kalium, Natrium und Chlorid in kultivierten, primären, Zellen der ekkrinen Schweißdrüse. Mit Hilfe dieses Verfahrens konnte eindeutig eine charakteristische, physiologische Wirkung des ACH in Schweißdrüsenzellen dargestellt werden. Erstaunlicherweise zeigten sich im Zuge der Wirkstoffsuche identische Modifikationen der Ionenlevel auch durch die Applikation von bestimmten, Chlorid haltigen Ammoniumlösungen. In weiteren Untersuchungen konnte überraschenderweise auch für Polyole eine Dysregulierung des Ionengleichgewichts in Zellen beobachtet werden. Beide Substanzklassen zeigten in anschließenden humanen Studien deutliche schweiß-reduzierende Wirkungen. Besonders erwähnenswert ist die Möglichkeit auf Grundlage der hier erhaltenen in-vitro-Ergebnisse, eine erste fundierte Hypothese über den zellulären Wirkmechanismus der Substanzen ableiten zu können. Dies hebt die umfassenden Fähigkeiten dieses Testsystems hervor und trägt maßgeblich zum Verständnis des Schwitzmechanismus auf zellulärer Ebene bei.

Im Hinblick auf zelluläre Aspekte wurde in dieser Arbeit ebenfalls ein organotypisches, dreidimensionales Modell der humanen ekkrinen Schweißdrüse konstruiert. Mit dessen Hilfe konnten detaillierte Untersuchungen zu Interaktionen zwischen den Zelltypen des sekretorischen Coils und des resorbierenden Duktes der ekkrinen Schweißdrüse unternommen werden. In einer weiteren Entwicklung wurden diese unterschiedlichen Zelltypen erfolgreich in ein speziell für diesen Zweck konzipiertes dermales Hautmodell integriert, welches die natürliche Situation in der menschlichen Haut nachempfindet. Unter Verwendung beider in-vitro-Modelle konnte die zelluläre Wechselbeziehung zwischen Coil- und Duktzellen unter anderem im Hinblick auf die Ausprägung von speziellen Proteinen näher untersucht werden. Gleichzeitigen kristallisierten sich Differenzen in der Protein-

expression zwischen kultivierten Schweißdrüsenzellen und solchen in der Haut heraus, die vor allem die Duktzellen umfasste.
Ähnliche Beobachtungen wurden auch während Charakterisierung der in dieser Arbeit erstellten ekkrinen Duktzelllinie offenbar. Dafür wurden kultivierte, primäre Duktzellen mit einem das Simianvirus 40 large T Antigen-enthaltenden, lentiviralen Vektor transfiziert und kultiviert. Nach dem Überwinden einer kurzen Proliferationskrise zeigten die genetisch veränderten Zellen ein stabiles Wachstum und werden somit als immortalisiert eingestuft. Solch eine immortalisierte Duktzelllinie ist bislang für wissenschaftliche Untersuchungen nicht verfügbar, wobei jedoch Duktzellen als primäres Ziel von topisch applizierten Produkten angesehen werden können. Somit stellt die hier beschriebene immortalisierte ekkrine Schweißdrüsen-Duktzelllinie ein standardisiertes Zellmaterial für zukünftige in-vitro-Untersuchungen zur ausführlichen Erforschung des Schwitzmechanismus dar. Außerdem ermöglicht diese Zelllinie eine definierte Quelle für die Erstellung weiterer organotypischer Schweißdrüsenmodelle.

In dieser Dissertation wurde erstmalig ein zellbasiertes in-vitro-Testsystem beschrieben, dessen Eignung für die Untersuchung des Schwitzmechanismus auf zellulärer Ebene sowie die Identifizierung von alternativen Antitranspirant-Wirkstoffen gezeigt werden konnte. Erstaunlicherweise lässt sich unter Verwendung dieses mehrstufigen Prozesses auch eine fundierte Hypothese über den zellulären Wirkmechanismus der Substanzen erstellen. Zusammen mit den hier entwickelten in-vitro-Modellen der humanen ekkrinen Schweißdrüse trägt dies maßgeblich zum Verständnis des Schwitzprozesses und der zellulären Interaktion bei. Des Weiteren ermöglicht die in dieser Arbeit generierte immortalisierten Duktzelllinie eine Standardisierung der in-vitro-Bedingungen, was wiederum eine detailliertere Beschreibung des Schwitzens inklusive der zellulären Wechselwirkungen erleichtert. Auch im medizinischen Kontext erscheint der Einsatz der hier entwickelten Methoden sinnvoll, um schweißdrüsenassoziierte Erkrankungen zu erforschen.

TABLE OF CONTENTS

I. Abbreviations

$[Ca^{2+}]_i$	intracellular calcium concentration
$[Cl^-]_i$	intracellular chloride concentration
$[K^+]_i$	intracellular potassium concentration
$[Na^+]_i$	intracellular sodium concentration
°C	degree Celsius
µg	microgram
µl	microliter
µm	micrometer
1,2-PD	1,2-propanediol
1,3-PD	1,3-propanediol
2D	two dimensional (referring to a monolayer culture of sweat gland cells in contrast to the organotypic 3D sweat gland model)
3D	three-dimensional (referring to the spheroidal organotypic sweat gland model)
ACH	aluminum chlorohydrate
AM	acetoxy methyl ester
ANO1/ TMEM16A	Anoctamin 1 (Ca^{2+}-dependent Cl^- channel)
ANOVA	analysis of variance
AP	antiperspirant(s)
AQP5	aquaporin 5
AS	active substance
AUC	area under the curve
BfR	German Federal Institute of Risk Assessment (Bundesministerium für Risikobewertungen)
BMP	bone morphogenetic protein
CA II	carbonic anhydrase II
cAMP	cyclic adenosine monophosphate
cDNA	complementary desoxyribonucleic acid
CEACAM5	carcinoembryonic antigen-related cell adhesion molecule 5
CFTR	cystic fibrosis transmembrane conductance regulator (cAMP-dependent Cl^- channel)
CK	cytokeratin
Cl^-	chloride ion
CMV	cytomegalovirus
co-culture	eccrine sweat gland cell culture derived from isolated whole glands and consisting of predominantly coil cells with few duct cells in between
COL1	Collagen type I
COL3	Collagen type II
DAG	diacylglycerol
DAPI	4′,6-diamidino-2-phenylindole
DG	diglycerol
DMEM	Dulbecco’s Modified Eagle Medium
DMP-HCl	Dimethyl piperazine solution with hydrochloric acid
DMSO	dimethyl sulfoxide
DNA	deoxyribonucleic acid
DPG	dipropylene glycol, isomeric mixture

e.g.	for example
EDA	ectodysplasin
EGF	epidermal growth factor
ENaC	epithelial sodium channel
ER	endoplasmic reticulum
Fox	forkhead-box
GCDFP-15	gross cystic disease fluid protein 15
GFP	green fluorescent protein
GPCR	G protein-coupled receptor
h	hour
HCl	hydrochloric acid
HE	hematoxylin and eosin
HEPES	N-(2-Hydroxyethyl)piperazine-N′-(2-ethanesulfonic acid)
HIV	human immunodeficiency virus
hTERT	human telomerase reverse transcriptase
$InsP_3$ R	inositol triphosphate receptor
IP_3	inositol triphosphate
log $P_{O/W}$	*n*-octanol-water partition coefficient
LTR	long terminal repeats
M_3	muscarinic acetylcholine receptor subtype 3
mg	milligram
min	minute
miRNA	micro ribonucleic acid
ml	milliliter
mRNA	messenger ribonucleic acid
MTS	[3-(4,5-dimethylthiazol-2-yl)-5-(3-carboxymethoxyphenyl)-2-(4-sulfophenyl)-2H-tetrazolium, inner salt
Na^+	sodium ion
NaOH	sodium hydroxide solution
NGS	normal goat serum
NHE 1	Na+/H+ exchanger 1
NKCC1	Na^+-K^+-Cl^- cotransporter 1
nl	nanoliter
OD	optical density
ORAI1	calcium release-activated calcium channel protein 1
PEI-HCl	polyethylene imine solution with hydrochloric acid
PG	polyglycerol
PIP_2	phosphatidylinositol 4,5-bisphosphate
PKA	protein kinase A
PLC	phospholipase C
PPD	polypropanediol
PVA	polyvinyl amine
PVAm-HCl	Polyvinyl amine solution with hydrochloric acid
qRT-PCR	quantitative real-time polymerase chain reaction
RFU	relative fluorescence units
RNA	ribonucleic acid
rpm	revolutions per minute
RT	room temperature

SCCS	Scientific Committee on Consumer Safety
sec	second
SGDC-SV40T	eccrine sweat gland duct cells transduced with simian vacuolating virus 40 large T antigen
SGDC-1D10	immortalized eccrine sweat gland duct cell line derived from clone 1D10
Shh	sonic hedgehoc
SPQ	6-methoxy-N-(3-sulfopropyl)quinolium, inner salt
STIM1	stromal interaction molecule 1
SV40T	simian vacuolating virus 40 large T antigen
TPSA	topological polar surface area
TQ	TelQuel, as it is
Wnt	wingless-type integration site family

1 Introduction

Living beings have developed a multitude of mechanism during evolution to adapt to all kinds of extreme environmental conditions. Many of them are faced with the lethal risk of hyperthermia due to external heat exposure (e.g., solar energy) and endogenous metabolic heat production. For dissipating surplus endogenous heat mammals have developed several mechanisms with a small percentage of them relying on sweating for that purpose (Best and Kamilar 2018). Among them are humans, horses, and some primates. Thermoregulation via sweating allows humans to survive in a hot environment or under heat stress, e.g., due to physical exertion. This physiological cooling process occurs naturally via evaporative heat dissipation from the skin surface. As aqueous sweat is secreted by sweat glands residing in the skin, integrity and correct functioning of skin and sweat glands are crucial components in physiological thermoregulation and survival (Wilke et al. 2007; Shibasaki and Crandall 2010; Bovell 2015).

A high density of sweat glands is present in the axilla, palms, and soles. As a result, strong sweating with release of high amounts of aqueous fluid occurs in these areas which is often regarded as socially distressing (Cheshire and Fealey 2008; Lu and Fuchs 2014). Cosmetic antiperspirants (AP) seek to reduce perspiration and have satisfactorily achieved so in using aluminum chlorohydrate (ACH) - the most often employed active AP substance since its patenting in the 1940s (Untied 2004; Mandriota 2017; Montenier 1941). However, it has become a topic of public concern as ACH is under discussion to contribute to the development of diseases such as Alzheimer's and breast cancer (Fischer 2014; Hohmann-Jeddi 2014; Kalogria et al. 2014; Mandriota 2017). Although convincing scientific proof is still missing and some controversial results have been published (Rodrigues-Peres et al. 2013; Mandriota et al. 2016; Linhart et al. 2017), concern remains in the public opinion. Thus, finding a suitable and safe alternative to ACH with comparable AP efficacy is of particular interest not only for the cosmetic industry but also to medically treat excessive sweating.

A deep understanding of the complex physiological mechanism of sweating on a cellular basis is necessary to find such an alternative. In this regard especially ionic fluxes as the major components of the sweat secretion process are of relevance. An *in vitro* model of the human sweat gland provides the indispensable research tool for investigating these cellular events for cosmetic, pharmaceutical, and toxicological applications and improvements. Besides, such a cell-based research model constitutes an essential basis to develop an effective *in vitro* screening procedure enabling the targeted search of alternative AP actives. Concomitantly, a more detailed characterization of discovered sweat-reducing agents would be feasible using such a sophisticated eccrine sweat gland model. Even more, with the availability of a defined and characterized cell line further variations in these investigations could be reduced adding even more standardization to the screening process.

1.1 Human skin and skin appendages

The skin constitutes the largest organ of the human body with an average surface area of about 2 m² (Wilke et al. 2007; Slominski et al. 2013; Lai-Cheong and McGrath 2017). Its most important functions of protecting the health of the whole human body and of maintaining the

body homeostasis are achieved by efficient local and systemic regulatory mechanisms. Among them are immune defense properties to fight against infectious agents and to communicate with the systemic immune system (Slominski et al. 2012; Slominski et al. 2015; Prescott et al. 2017). Together with its highly sophisticated structure this builds an epidermal barrier to protect the body against harmful environmental influences such as UV and thermal radiation as well as mechanical, chemical and biological disturbances (Slominski and Wortsman 2000; Menon 2002). Furthermore, skin is involved in sensory functions through integrated cutaneous nerve fibers and participates in electrolyte regulation, insulation, and production of various chemical factors like cytokines, hormones, and neurotransmitters. Social communication is transmitted by visible pigmentation of the skin and manifestation of adnexal organs (Slominski et al. 2012; Slominski et al. 2015). Among the latter are hair follicles and thereto associated sebaceous and apocrine sweat glands as well as nails. Eccrine sweat glands constitute the main adnexal structure for thermal regulation, emphasizing the skin as the primary organ for body temperature regulation. Cooling of the body is achieved by means of vasodilation with increased blood flow as well as sweat secretion and heat dissipation (Lee et al. 2006; Bovell 2015). A complex interplay of thermal and mechanosensory receptors is necessary for perceiving the skin's level of humidity which greatly contributes to retaining the body's thermal balance (Filingeri et al. 2014; Filingeri and Havenith 2015).
Structurally, human skin is composed of three distinct compartments: the epidermis, the dermis and the subcutis (**Fig 1.1**) (Slominski et al. 2013; Abd et al. 2016; Lai-Cheong and McGrath 2017).

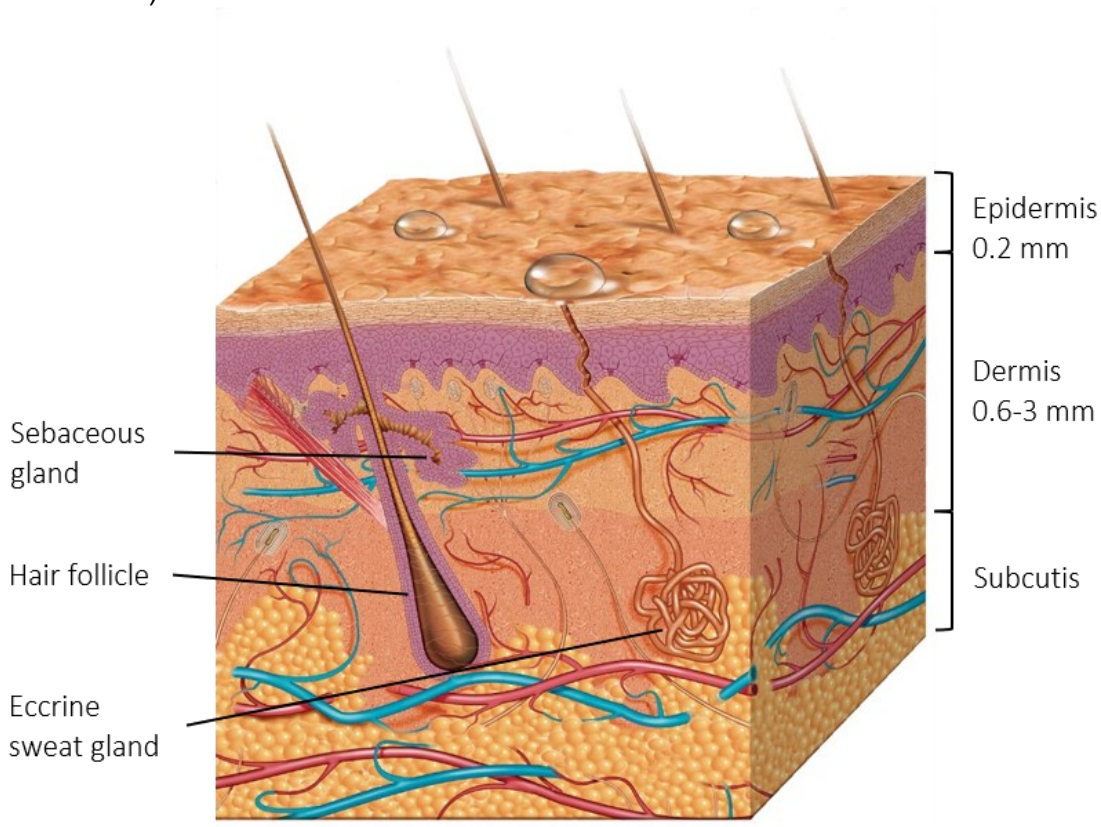

Fig 1.1: Structure of the human skin with skin appendages.
Human skin is subdivided into three main layers of upper epidermis, interjacent dermis and lower subcutis. Embedded in the skin and mainly located in the dermis are skin appendages such as sweat glands, hair follicles, sebaceous glands, and nails (not depicted).

The stratified epidermis constitutes the outermost avascular layer which is predominantly composed of keratinocytes (about 95 %) (Slominski and Wortsman 2000; Menon 2002; Lai-Cheong and McGrath 2013). It can be further subdivided into four different layers: the stratum corneum as the uppermost coat, the stratum granulosum, the stratum spinosum and the stratum basale as the deep border to the dermis (Urmacher 1990; Menon 2002). Cuboidal keratinocytes regenerate via mitosis in this inner basal layer and differentiate on their way through the other epidermal layers towards the surface, thereby losing their nuclei and organelles. During this transition they flatten and terminally differentiate to corneocytes (Bouwstra and Honeywell-Nguyen 2002; Lee et al. 2006; Brodell and Rosenthal 2008; Chamcheu et al. 2011). Surrounded by the cornified envelop, which consist of hydrophobic extracellular matrix proteins, embedded corneocytes comprise the stratum corneum as the main epidermal barrier. Skin is subject to a continuous renewal process which takes about 40 days from replication of the cells in the stratum basale to shedding off of the cornified layer at the surface. The latter step is described as desquamation (Lee et al. 2006; Chamcheu et al. 2011; Lai-Cheong and McGrath 2013). Apart from keratinocytes, melanocytes can be found in the stratum basale which synthesize the UV protective pigment melanin (Slominski et al. 2013). The stratum spinosum is interspersed with Langerhans and Merkel cells contributing to immune defense as dendritic cells or conveying mechanosensory information, respectively (Brodell and Rosenthal 2008; Seneschal et al. 2012; Nakatani et al. 2015).

Connected to the epidermis via the basement membrane zone is the vascular dermis, a connective tissue composed of extracellular matrix elements and cellular components. Mesenchymal derived fibroblasts are the dominant type of cells in this cutaneous layer. They secrete extracellular matrix proteins such as collagens, elastic fibers, glycoproteins, and adhesive molecules thereby providing the basis for elasticity, integrity, and strength of the skin and contributing to wound repair. Apart from fibroblasts, the dermis contains cells of the immune system like mast cells, lymphocytes, dendritic cells and histocytes (Menon 2002; Kim et al. 2007; Lai-Cheong and McGrath 2013; Slominski et al. 2013). Two plexuses of blood vessels (deep and superficial), lymphatic channels, sensory nerves and nerve receptors reside in this skin layer which are major contributors to immune and sensory functions. Cutaneous appendages located in the dermis are of epidermal origin and include sebaceous glands, sweat glands of the eccrine and apocrine type, hair follicles and nails (Slominski et al. 2012; Slominski et al. 2013; Slominski et al. 2015; Abd et al. 2016; Lai-Cheong and McGrath 2017).

The deepest skin layer, the subcutis, is composed of lipocytes - fat lobules separated by fibrous septae - and constitutes the subcutaneous fat tissue of the skin. About 50 to 80% of the body fat is situated within this adipose tissue. Consequently, this innermost skin layer plays a role in insulation and energy storage and has endocrine functions such as production of hormones, too. Due to presence of blood vessels this layer also serve to nourish the upper skin layers of dermis and epidermis (Slominski et al. 2012; Abd et al. 2016; Lai-Cheong and McGrath 2017).

1.2 Human sweat glands

In human skin, sweat glands constitute the adnexa responsible for sweat secretion and body odor formation (Sato et al. 1989a; Saga 2001). Two distinct types of human sweat glands are distinguished, apocrine and eccrine ones, which were first distinguished and described by Schiefferdecker in 1922. Highly discussed is the existence of a third type of sweat gland present in the axilla, the apoeccrine gland. It is supposed to combine morphological features of eccrine and apocrine glands and was first described by Sato et al. in 1987 (Sato and Sato 1987b; Wilke et al. 2007; Bovell et al. 2011). In any case, apocrine and eccrine sweat glands are clearly discriminable based on their secretory functionality, morphological structure, localization and distribution as described in the following chapters (Sato et al. 1989a; Saga 2001; Lu and Fuchs 2014).

1.2.1 Apocrine sweat glands

Apocrine sweat glands represent remnants of odorous glands and, thus, they primarily contribute to body odor formation but not significantly to thermoregulation (Saga 2001; Saga 2002; Best et al. 2019). Attributed to their osmic nature they secrete precursors of odoriferous substances as well as hormone-like compounds possibly acting in pheromonal communication (Savic et al. 2001; Hu et al. 2018). The secretory portion of these large glands resides in the subcutis of hairy skin as their short, thick duct ends in the upper follicle shaft of hair (epitrichial). According to this epitrichial classification their distribution in skin is restricted to hairy areas mainly the axilla and the pubic region, but they are also found in other body parts such as the eyelids and the auditory canal of the ears (Bunting et al. 1948; Sato et al. 1989a; Saga 2001; Wilke et al. 2007; Farkaš 2015). Structurally, the secretory coil of apocrine glands is composed of columnar secretory cells surrounded by myoepithelial cells. These secretory cells possess a high number of luminally located microvilli and of mitochondria in the cytoplasm. Its apocrine secretion is characterized by pinching off and liberation of cellular components into the wide gland lumen. Due to the release of intracellular content the secreted fluid is milky, viscous and rich in proteins (Sato et al. 1989a; Saga 2001; Saga 2002; Farkaš 2015). Sweaty malodor is thereby produced by bacterial conversion of secreted substances on the skin surface (Natsch 2015).

Concerning their development, apocrine sweat glands evolve during embryogenesis in connection with the hair follicle but only become active during puberty and accompanying hormonal changes (Saga 2002; Lu and Fuchs 2014). From then on, they discharge sweat in an intermitted fashion triggered by emotional stimulation which expresses itself in release of adrenergic neurotransmitters such as adrenaline and noradrenalin (Sato et al. 1989a; Wilke et al. 2007).

In other mammals, apocrine sweat glands represent the majority of glands, whereas in mice apocrine sweat glands are completely absent. Unique evolutional changes in humans gave them a survival advantage by transition to predominant eccrine sweating and, thus, effective thermoregulation (Lu and Fuchs 2014). Due to this, apocrine glands are described in this work to complete the picture, but the following parts focus on eccrine sweat glands only.

1.2.2 Eccrine sweat glands

1.2.2.1 Structure and function of human eccrine sweat glands

Apart from apocrine glands, the second type of sweat glands, the smaller eccrine ones, reside in the dermis of hairy and non-hairy skin and end up directly on the skin surface (atrichial). About 1.6 to 4 million of them are distributed almost over the entire human body with the highest density of up to 600-700 /cm² on the palms of the hands and soles of the feet and about 100 /cm² in the axilla and facial skin (Bunting et al. 1948; Sato 1977b; Sato et al. 1989a; Wilke et al. 2007). These highly specialized eccrine glands are unique for humans and ensure sufficient thermoregulation of body temperature even under significant heat stress (Zancanaro et al. 1999). Liberation of the content from small vesicles (exocytosis) originating from the Golgi apparatus or the endoplasmic reticulum defines eccrine/merocrine secretion of aqueous fluid (Bunting et al. 1948; Wilke et al. 2007; Bovell et al. 2011; Lu and Fuchs 2014). Other mammals like rats, mice, and dogs also possess eccrine sweat glands but only in the palmar-plantar region and their eccrine sweat glands are less effective regarding thermoregulation. In those animals sweat glands in paws and feet rather contribute to increase friction and grip. In horses, thermoregulation is predominantly achieved by apocrine sweat glands which are found on their whole body surface in a number comparable to human eccrine sweat glands (Montgomery et al. 1984; Lu and Fuchs 2014; Cui and Schlessinger 2015; Best and Kamilar 2018). Also neural control of sweating differs among mammals: While human eccrine sweating is prevailingly triggered by acetylcholine horses mainly sweat in response to β-adrenergic agonists (Ko et al. 1996).

Structurally, eccrine glands are composed of different compartments which all are built up of epithelial cells. Within the gland structure those cells possess a distinct polarity expressed as an apical/luminal and basolateral side which enables the directed transport of salts and water across the cells (Saint-Criq and Gray 2017). Seen as a whole, the eccrine sweat gland represents an unbranched, single tubule with a length of 3 to 8 mm which can be separated into three main parts (Morphology and structure of the human eccrine sweat gland.**Fig 1.2a**): the irregularly coiled fluid secreting portion located in the deep dermis (coil); the mainly salt reabsorbing duct which connects to the coil (duct); and the surface-opening acrosyringium traversing the epidermis (Bunting et al. 1948; Holyoke and Lobitz 1952; Hibbs 1958; Wilke et al. 2007; Lei et al. 2013; Cui and Schlessinger 2015). Eccrine sweat glands were regarded as separate skin appendages until a recent study described the coils of those glands to be closely associated with the hair follicle and the sebaceous gland in the upper subcutis forming one morphological entity (Poblet et al. 2018).

The self-entangled, deepest part of the tubule, the coil, has an inner luminal diameter of 5 to 40 µm whereas the overall diameter of the gland reaches up to 700 µm at the skin surface (Sonner et al. 2015; Kurata et al. 2017). The coil is composed of two different cell types, so called clear and dark cells - a designation ascribed to the absence or presence of basophilic granules within the cells, respectively (Montagna et al. 1953; Kurata et al. 2017). The larger flask-shaped clear cells show a basal location within the coil and less contact to the lumen while the dark cells are mainly located close to the lumen and reach the basal lamina only via small processes (**Fig 1.2b**) (Zancanaro et al. 1999; Bovell et al. 2011). Especially between the cells of the basal layer several intercellular canaliculi can be found which increase the luminal

surface (Hibbs 1958; Bovell 2015), while tight junctions and desmosomes connect adjacent cells (Wilke et al. 2007).

Regarding their function, clear cells contain several relevant membrane proteins such as ion channels and transporters to facilitate secretion of the isosmotic, sodium chloride rich, primary sweat (for a detailed description of the secretion mechanism see 1.2.2.4). Its production and release into the lumen is the main role of the secretory coil (Bovell et al. 2011; Bovell 2015). Dark cells, however, are postulated to take part in intercellular transport and secretion of macromolecules such as glycoproteins into the sweat (Lu and Fuchs 2014; Sonner et al. 2015). Solely the coiled tubule of the gland is surrounded by a discontinuous layer of longitudinally arranged spindle-shaped myoepithelial cells. In accordance with expressing the alpha isoform of smooth muscle actin (α-SMA) they give structural support, facilitate contraction of the coil and, thus, aide in sweat expulsion (Bunting et al. 1948; Sato 1977a; Montgomery et al. 1984; Kurata et al. 2017).

Attached to the coil, the reabsorbing duct as the upper part of the gland is divided into a lower coiled portion and a straight tubule which ascends to the epidermis (Hibbs 1958). The hollow 10 to 20 µm wide lumen of the duct is encircled by two layers of cuboidal epithelial cells of the same kind, a basal and a luminal layer (**Fig 1.2c**). Those epithelial duct cells are connected by desmosomes and gap junctions (Bovell 2015). In contrast to the coil, no basal lamina is present, but the luminal parts of the cells form a cuticular-like structure of varying width with protruding microvilli which borders the lumen (Bunting et al. 1948; Holyoke and Lobitz 1952; Montagna et al. 1953; Sato and Sato 1983; Cui and Schlessinger 2015; Sonner et al. 2015). In the duct lumen, ions are reabsorbed from the isotonic primary sweat to prevent massive ion loss (Quinton 2007; Saint-Criq and Gray 2017). The hypotonic sweat fluid is released onto the skin surface through the dilated and cornified lumen of the acrosyringium (Wilke et al. 2007; Lu and Fuchs 2014).

The total sweat volume secreted per gland is associated with the age of the individual and reaches the maximum amount of sweat release during puberty (Murota et al. 2015; Best et al. 2019). Its decrease over lifetime is attributed to declining thermal sensitivity and atrophy of sweat glands (Kenney and Fowler 1988; Natsume et al. 1992; Smith et al. 2013). Already in the 80s, Sato and Sato postulated a proportional correlation between size of the eccrine sweat gland and sweat rate per gland, respectively per length of the coil (Sato and Sato 1983). Assumed sex-related variations in sweating could be ascribed to morphological differences according to a recent study (Notley et al. 2017). Apart from these interindividual variations further intraindividual and regional variabilities exist (Baker 2017).

Vital for its correct functioning blood vessels, which are convoluted with the whole gland, provide nutrient supply and aid in sweat reabsorption while nerve fibers, located close to and around the secretory coil, transmit sympathetic innervation (Kurata et al. 2017).

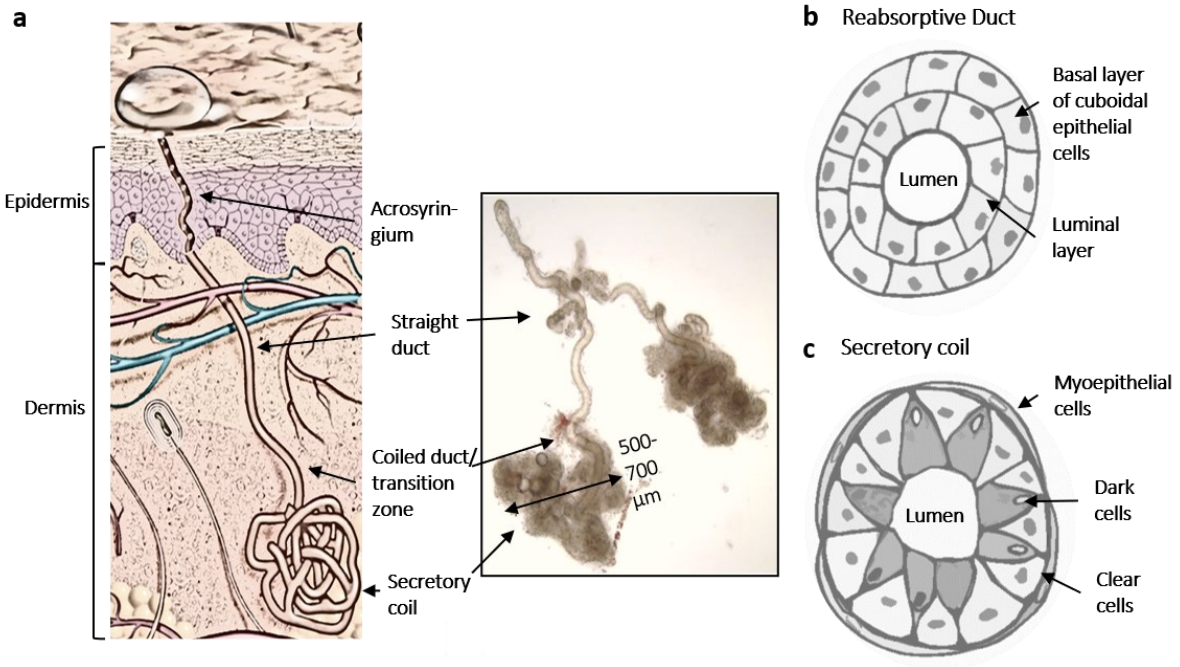

Fig 1.2: Morphology and structure of the human eccrine sweat gland.
The human eccrine sweat gland resides in the dermis and opens onto the skin surface. It is composed of a secretory coil, a transition zone separating coil and duct, a straight duct which ascends to the epidermis and an intraepidermal acrosyringium (**a**). The framed section depicts isolated native eccrine sweat glands. Note the visible transition zone separating the darker coil and the nearly transparent duct. Clear cells and dark cells constitute the secretory coil of the eccrine sweat gland around the gland lumen (**b**). A discontinuous layer of myoepithelial cells surrounds this tubule. The straight and coiled duct is made up of cuboidal epithelial cells arranged in two layers around the gland lumen (**c**).

Apart from its main function of thermoregulation, eccrine sweat glands contribute to wound repair and skin homeostasis by harboring nestin-positive stem cells. Especially myoepithelial cells and epithelial cells of the gland duct possess a multipotent potential and contribute to the regeneration of injured glands and the epidermis as they are mitotically active. Those cells are even capable to rebuild a functional stratified epidermis (Biedermann et al. 2010; Petschnik et al. 2010; Lu et al. 2012; Lei et al. 2013; Nagel et al. 2013; Gao et al. 2014; Liao et al. 2019). Eccrine sweat glands also play a role in innate immune defense of the skin by production of antimicrobial peptides such as dermcidin, cathelicidins and β-defensins (Schittek et al. 2001; Murakami et al. 2002; Rieg et al. 2004; Schittek 2012). These exocrine glands also secrete moisturizing factors including various amino acids, lactate and urea acting as humectants and contributing to skin homeostasis (Cui and Schlessinger 2015; Baker 2019).

1.2.2.2 Ontogenesis of eccrine sweat glands

Already in the 1960s embryonic development of human eccrine sweat glands was scrutinized in more detail. Thereby, onset of formation in skin of palms and soles as early as in gestational week 12 was reported. It starts as small invaginations from the germinal layer, the *stratum germinativum*. During the following weeks, the early ectodermal buds grow deeper into the dermis forming the duct which later begins to coil. The gland lumen emerges from united intracytoplasmic cavities across several inner cells in a process of pinching-off and resolution (Hashimoto et al. 1965; Cui et al. 2014).

Eccrine sweat gland morphogenesis is comparable to the development of other skin appendages and is closely linked to the emergence of hair follicles (Lu et al. 2016). Intense signaling between ectoderm and mesenchyme characterizes sweat gland ontogenesis which is initiated by Wnt/β-catenin (wingless-type integration site family) signaling. At different developmental stages further downstream signaling cascades including EDA (ectodysplasin), Shh (sonic hedgehog), BMP (bone morphogenic protein) and Fox (forkhead-box) family transcription factors are involved (Cui and Schlessinger 2006; Cui et al. 2014; Lu and Fuchs 2014). Wnt triggers an EDA cascade responsible for the formation process of the duct (Cui et al. 2009; Cui et al. 2014). Being dependent on EDA, other signaling molecules like Shh and, further downstream, Fox family transcription factors mainly influence development of the eccrine sweat gland coil (Kunisada et al. 2009; Cui and Schlessinger 2015). Apart from those genes, micro ribonucleic acids (miRNA) were identified to be involved in early stages of sweat gland ontogenesis (Cui et al. 2017).
Corresponding with the structural formation of the gland, cytokeratin (CK) marker expression changes. All cells of the eccrine sweat gland derive from multipotent CK14-positive progenitors (Lu et al. 2012). Quickly after evolvement of the first duct structure, differentiation specific markers CK1 and CK10 are detectable in luminal duct cells as found in the mature gland. Comparably, distal parts of the gland attain distinct CK markers of the mature coil as soon as coiling begins; those are CK8, CK18 and CK7 which are especially expressed in the inner, luminal coil cells. Later during ontogenesis basal cells of the coiled portion differentiate into myoepithelial cells indicated by the specific markers CK5, CK14, CK17 and α-SMA (Moll and Moll 1992; Lu and Fuchs 2014).
Despite these reports and progressive uncovering of signaling cascades and their interplay during ontogenesis, *de novo* generation of sweat glands for, e.g., transplantation purposes after severe skin burning still remains a challenge (Lu and Fuchs 2014; Lu et al. 2016). Especially because eccrine sweat gland are structurally completely formed before birth, at around the eight gestational month, and already resemble adult glands with no further ones being built postnatal (Li et al. 2009; Gao et al. 2014; Cui and Schlessinger 2015; Ma et al. 2018). Although structurally mature at birth there is a transition of the neuronal innervation phenotype from noradrenergic to cholinergic during the early postnatal phase. This in turn evokes adaptions within the gland for proper sweat production (Habecker et al. 1996; Cui and Schlessinger 2015; Best et al. 2019). Later on, during infancy, initially inactive eccrine sweat glands become active with the extent seeming to dependent on the thermal environment; in hot climates, the active-to-inactive ratio is significantly higher (Murota et al. 2015; Best et al. 2019).

1.2.2.3 Innervation and neural control of human eccrine sweat glands

Sweat secretion of human eccrine sweat glands is controlled by the central as well as the autonomic nervous system (Hu et al. 2017). There are three distinct types of sweating postulated: *Gustatory sweating* is triggered by hot and spicy food and leads to sweat output especially in the facial area (Sato et al. 1989b). *Emotional sweating*, in contrast, mainly occurs on the palms and soles (Wilke et al. 2007; Cui and Schlessinger 2015) and is supposed to be centered in the limbic system of the brain. Catecholamines such as noradrenalin are tightly

linked to emotional sweating via action on α_1- and β-adrenoceptors and thereby triggered increase of intracellular cyclic adenosine monophosphate (cAMP). *Thermal sweating* is the third and most important type of perspiration. It is regulated by the thermoregulatory center in the pre-optic anterior hypothalamus in which thermoreceptors assess the body core temperature. Peripheral thermoreceptors, e.g., in the skin, also affect thermal sweating by sending afferent impulses to the hypothalamus and thalamus. Apart from that, temperature-independent influencing factors exist such as the hydration status, the electrolyte concentration and exertion (Sato et al. 1989a; Low 2004; Shibasaki and Crandall 2010; Hu et al. 2018). Thermal sweating is predominantly driven by the internal body core temperature and to a lesser extent by the mean skin temperature (Ogawa and Sugenoya 1993; Wilke et al. 2007). In general, it is triggered if the body's temperature deviates from the internal set point temperature which is postulated to be located in the posterior hypothalamus. From the brain, efferent signals travel via the spinal cord and pre- and postganglionic sympathetic neurons to eccrine sweat glands (Low 2004; Shibasaki and Crandall 2010; Hu et al. 2017). Non-myelinated class C postganglionic fibers, which are mainly of the cholinergic type, encompass especially myoepithelial cells around the secretory coil of the gland. Thermal sweating is therefore predominantly regulated by the cholinergic neurotransmitter acetylcholine. It exerts its effect through muscarinic acetylcholine receptors of the M_3 type located with a high density in the basolateral membrane of coil parts (Kurata et al. 2017; Baker 2017; Hu et al. 2017). Apart from cholinergic stimulation eccrine sweat glands also possess adrenergic innervation although the sweating response triggered by catecholamine amounts to only about 10% of cholinergic perspiration (Sato 1973; Sato and Sato 1981). Further neuromodulators regulating sweating to a slight extent have been identified, among them calcitonin gene-related peptide, nitric oxide, vasoactive intestinal peptide and galanin (Bovell et al. 2013; Baker 2017). All these sweating regulators predominantly influence secretory coil cells as innervation of gland ducts is sparse. This suggests reabsorption taking place in the duct to be mainly determined by sweat rate rather than neural control (Ouyang et al. 2018).

1.2.2.4 Physiological mechanism of sweat secretion

Thermal sweating is predominantly cholinergic triggered. Thereby, the neurotransmitter acetylcholine acts on the muscarinic acetylcholine receptor subtype 3 (M_3) which subsequently triggers release of Ca^{2+} as the intracellular second messenger (Prompt and Quinton 1978; Cui and Schlessinger 2015; Hu et al. 2017). Generally, five distinct subtypes of muscarinic receptors are distinguished (M_1 to M_5) which are expressed in the central and peripheral nervous system. All of them are transmembrane G protein-coupled receptors (GPCR) and activated non-selectively by acetylcholine (Conn et al. 2009; Dencker et al. 2012). However, they vary in their sequence of amino acids at certain locations and, in consequence, in their coupled G protein: M_2 and M_4 transduce their signaling via G_i proteins, while M_1, M_3 and M_5 function via proteins of the G_q-type. The M_3 receptor is expressed in the brain, smooth muscle and glandular tissues such as the intestine and pancreas (Langmead et al. 2008; Nathanson 2008). Further, this receptor subtype is found in secretory and myoepithelial cells of the eccrine sweat gland (Cui and Schlessinger 2015).

Upon binding of acetylcholine and activation of the M_3 receptor, the G_q protein is released into the cytosol and a distinct intracellular signaling cascade is elicited (**Fig 1.3**). G_q protein activates phospholipase C (PLC) in secretory cells which converts phosphatidylinositol 4,5-bisphosphate (PIP_2) into diacylglycerol (DAG) and inositol 1,4,5-triphosphate (IP_3). The latter binds to the IP_3 receptor subtype 2 ($InsP_3R_2$) at the membrane of the endoplasmic reticulum triggering the release of Ca^{2+} from internal stores into the cytosol (Sato et al. 1989a; Cui and Schlessinger 2015; Bovell 2015). Additionally, the intracellular Ca^{2+} concentration ($[Ca^{2+}]_i$) is increased due to influx of Ca^{2+} from the interstitium through calcium release-activated calcium channel protein 1 (ORAI1). ORAI1 channels are opened upon binding of stromal interaction molecule 1 (STIM1) which is activated when Ca^{2+} stores in the ER are depleted. This influx leads to a sustained high level of $[Ca^{2+}]_i$ essential for sweat production (Concepcion et al. 2016).

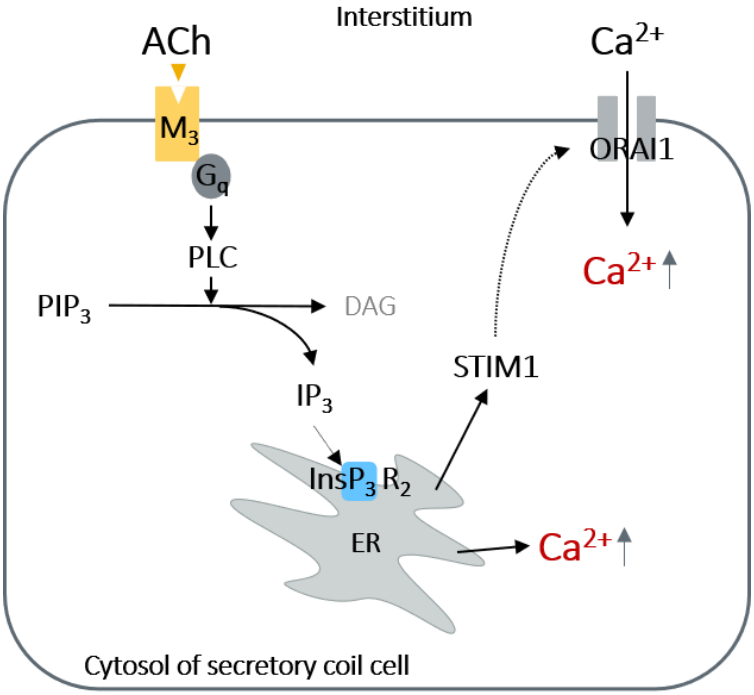

Fig 1.3:Signaling pathway upon cholinergic stimulation in secretory coil cells.
Binding of acetylcholine (ACh) to the muscarinic acetylcholine receptor subtype 3 (M_3) triggers an intracellular signaling cascade via activation of the G_q protein. This encompasses activation of phospholipase C (PLC), resulting production of inositol triphosphate (IP_3), and finally leads to release of Ca^{2+} from intracellular stores in the endoplasmic reticulum (ER) and influx of Ca^{2+} through ORAI1 channels from the extracellular space. Intracellular Ca^{2+} as the second messenger increases and is the basis for further signaling and sweat production. PIP_2: phosphatidylinositol 4,5-bisphosphate; DAG: diacylglycerol; $InsP_3R_2$: inositol triphosphate receptor subtype 2; STIM1: stromal interaction molecule 1; ORAI1: calcium release-activated calcium channel protein 1.

Apart from acetylcholine, sweating is also elicited via adrenergic stimulation mediated by β-adrenoceptors, though to a lesser extent. This kind of perspiration is associated with a stress response and is therefore sometimes referred to as stress-induced sweating. Generally, β-adrenoceptors also belong to the class of GPCR but release their coupled G_s protein upon binding of catecholamines such as adrenaline and noradrenaline (**Fig 1.4**). Liberated G_s protein activates membrane bound adenylate cyclase (AC) to convert ATP into cAMP as the

second messenger (Lefkimmiatis and Zaccolo 2014; Bovell 2015; Hu et al. 2018). Either directly or via cAMP-activated protein kinase A (PKA) phosphorylation, this second messenger is able to modulate $InsP_3R_2$ and associated Ca^{2+} release. This constitutes an important cross-talk mechanism linking cAMP production to Ca^{2+}-activated sweat release (Wojcikiewicz and Luo 1998; Vervloessem et al. 2015).

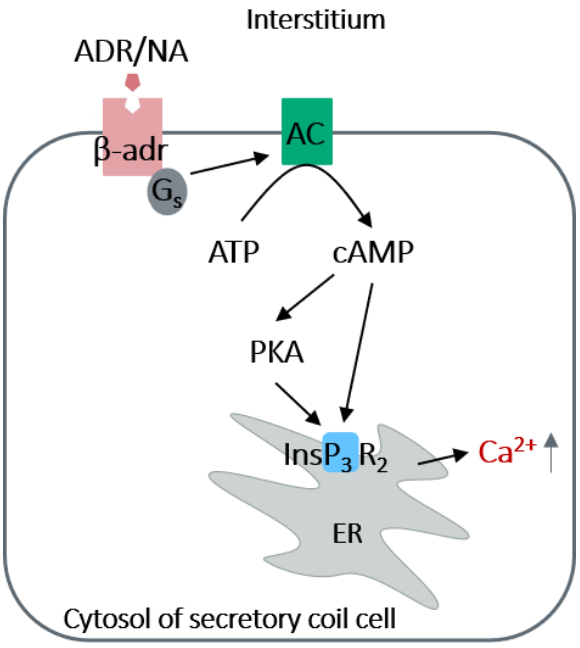

Fig 1.4: Signaling pathway upon adrenergic stimulation in secretory coil cells.
Binding of catecholamines such as adrenaline (ADR) or noradrenalin (NA) to β-adrenoceptors (β-adr) releases receptor-coupled G_s protein which activates adenylate cyclase (AC). The latter produces cyclic adenosine monophosphate (cAMP) from adenosine triphosphate (ATP). Via cAMP-transmitted activation of protein kinase A (PKA) and its phosphorylating activity or in a direct manner cAMP modulates inositol triphosphate receptor subtype 2 ($InsP_3R_2$). Thereby, cAMP signaling pathway is linked to and influences intracellular Ca^{2+} release. ER: endoplasmic reticulum.

Intracellular Ca^{2+} serves as a second messenger and activates further ion channels as postulated in the Na^+-K^+-Cl^- cotransport model (**Fig 1.5a**). According to this model, increase in $[Ca^{2+}]_i$ leads to higher opening probability of basolateral und luminal K^+- and luminal Cl^- channels in secretory coil cells. As a result, efflux of K^+ into the extracellular space and of Cl^- into the sweat gland lumen occurs (Sato et al. 1989a; Cui and Schlessinger 2015; Murota et al. 2015). While involved K^+ channels are not yet fully elucidated, Anoctamin (ANO1 or TMEM16A) is the relevant Ca^{2+} activated Cl^- channel located in luminal membranes of the coil facilitating Cl^- outflow (Ertongur-Fauth et al. 2014; Bovell 2015). Another cAMP activated Cl^- channel, cystic fibrosis transmembrane conductance regulator (CFTR), has been shown to exist in luminal membranes of clear cells and, thus, might contribute to luminal Cl^- secretion (Sato and Sato 2000; Quinton 2007; Saint-Criq and Gray 2017). In some tissues, however, CFTR has been reported to be at least partially activated also by Ca^{2+} (Billet and Hanrahan 2013).
Efflux and thus decrease in intracellular K^+ and Cl^- produces a chemical gradient which stimulates basolateral Na^+-K^+-Cl^- cotransporter 1 (NKCC1) to carry Na^+, K^+ and two Cl^- into

coil cells. Subsequently, increasing $[Na^+]_i$ promotes basolateral Na^+/K^+-ATPase which pumps three Na^+ out of the cell in exchange for two K^+ (Quinton and Tormey 1976; Takemura et al. 1991). Resulting intracellular negative charge propels further luminal efflux of Cl^- into the gland lumen and raises a chemical gradient attracting Na^+ via paracellular movement through intercellular gap junctions into the gland lumen (Sato et al. 1989a; Bovell 2015). Salt ions secreted into the coil lumen cause passive osmotic flow of water through luminally located aquaporin 5 (AQP5) water channels. Hence, produced primary sweat is isotonic to plasma with a physiological pH of 7.4 (Song et al. 2002; Granger et al. 2003) and ion concentrations of about 135-145 mM of Na^+, 95-110 mM of Cl^- and 4-5 mM of K^+ (Baker 2017).

Participation of dark cells in sweat secretion has yet to be fully elucidated, but contribution of Best2, a protein exclusively expressed in dark cells, as a Cl^- and/or HCO_3^- channel has been presumed (Cui and Schlessinger 2015). However, cell shrinkage after muscarinic stimulation was only observed in clear, but not in dark cells (Takemura et al. 1991).

In contrast to highly ion permeable secretory coils, eccrine sweat gland ducts are relatively impermeable (Quinton 1981). Thus, reabsorption of primarily NaCl from primary isotonic sweat into duct cells occurs through various ion channels and results in production of hypotonic sweat (**Fig 1.5b**). Na^+/K^+-ATPase, expressed in basolateral membranes of both duct cell layers, is the driving force for ion movements across epithelia duct cells. As in the coil, this ion channel conveys three Na^+ out of while two K^+ enter the cell. In the following, K^+ exits duct cells through basolateral K^+ channels. Due to the concentration gradient created by the Na^+/K^+-ATPase, Na^+ is passively reabsorbed from the primary sweat through luminally located epithelial sodium channel (ENaC) into duct cells (Bovell 2015; Murota et al. 2015). Apart from ENaC, CFTR is the major Cl^- channel present in luminal membranes and, at a lower density, is also found in basolateral membranes of ducts. It reabsorbs Cl^- from primary sweat into duct cells driven by the electrochemical gradient created by Na^+ fluxes. Reddy and Quinton demonstrated activity of ENaC to be functionally coupled to Cl^- conducting activity and transport direction of CFTR (Reddy et al. 1999; Reddy and Quinton 2003; Quinton 2007). CFTR is constitutive active since it is phosphorylated by cAMP-dependent PKA (Reddy and Quinton 2009). Finally, hypotonic sweat (with regard to Na^+ and Cl^-) is generated by this complex mechanism of ion movements and fluxes and is released onto the skin surface (Murota et al. 2015; Bovell 2015).

Up to now, single ion movements have been investigated in several studies (Reddy et al. 1999; Reddy and Quinton 1987; Reddy and Quinton 2003; Ohtsuyama et al. 1994; Sato and Sato 1988), but their complex interplay as a whole was rarely in the center of attention so far (Sato and Sato 1990; Takemura et al. 1991).

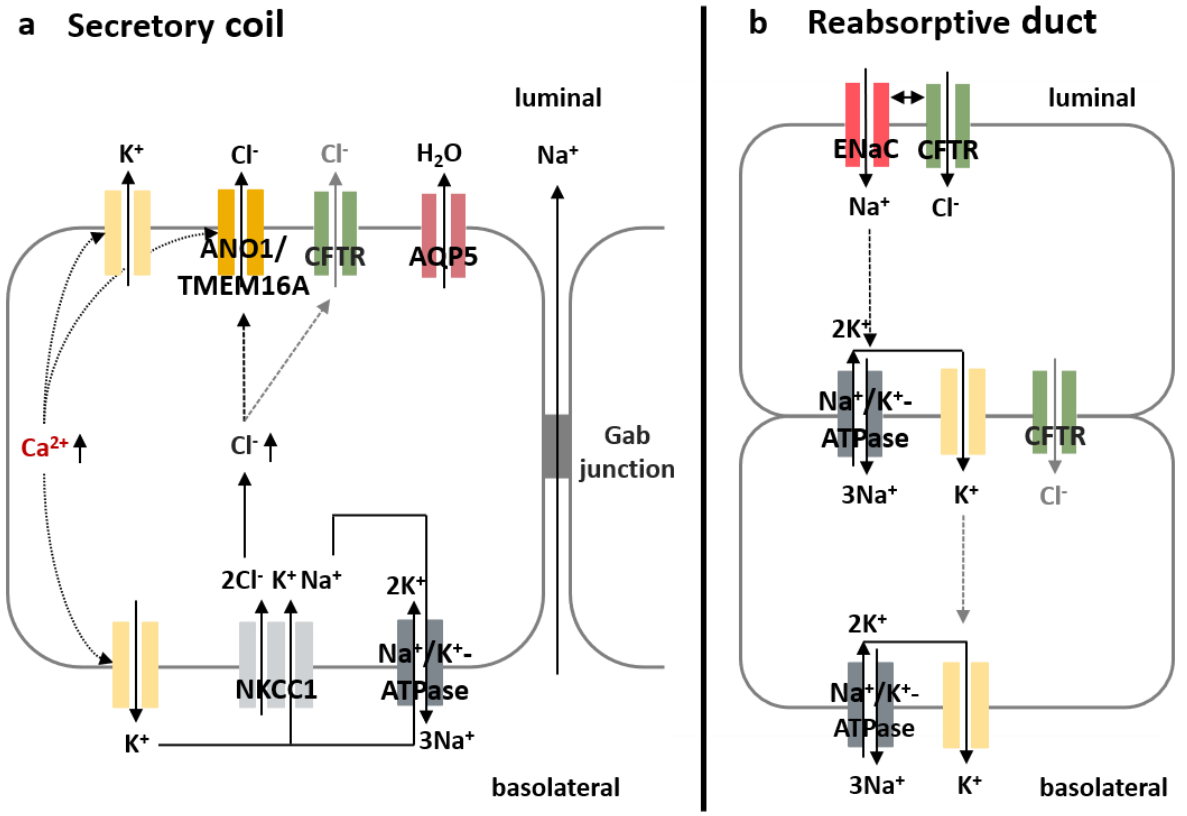

Fig 1.5: Ion transport processes during sweat secretion.
Production of primary sweat in coil cells is described by the Na^+-K^+-Cl^- cotransport model (**a**). Activated by Ca^{2+}, K^+ and Cl^- efflux (through anoctamin 1 (ANO1)) creates a chemical gradient which triggers Na^+-K^+-Cl^- cotransporter 1 (NKCC1) to transport one Na^+ and K^+ and two Cl^- in an electroneutral fashion into the cell. Increasing intracellular Na^+ stimulates Na^+/K^+-ATPase to transport Na^+ out of and K^+ into the cell. Increasing intracellular Cl^-, in contrast, causes a negative intracellular potential which constitutes the driving force for luminal Cl^- secretion. This in turn causes paracellular attraction of Na^+ into the lumen while water follows osmotically facilitated by aquaporin 5 channels (AQP5) to produce the primary isotonic sweat. Reabsorption of NaCl in the duct is dominated by activity of Na^+/K^+-ATPase (**b**). Created intracellular Na^+ deficiency is counteracted by passive entering of sweat Na^+ through luminal epithelial sodium channels (ENaC). Simultaneously, luminal Cl^- crosses the cell membrane through cystic fibrosis transmembrane conductance regulator (CFTR) Cl^- channels. K^+ brought into cells in exchange for Na^+ exists through basolateral K^+ channels.

pH of final sweat strongly depends on sweat rate and ranges between 5 at low sweat rates and up to 8 at high rates. This variable pH is attributed to presence of Na^+/H^+ exchanger 1 (NHE1) in duct cells with its effectiveness of transport being dependent on the luminal concentration of Na^+ and Cl^- and, thus, coupled to sweat rate (Herrmann and Mandol 1955; Granger et al. 2003). Further, also NKCC1 was discovered to be weakly expressed in eccrine ducts (Nejsum et al. 2002; Cui and Schlessinger 2015).

Apart from mentioned ions, secreted sweat contains further components such as lactate, glucose and ammonia related to gland metabolism; hydrogen carbonate for pH regulation; urea and amino acids contributing to skin moisturization; and other proteins among them previously mentioned antimicrobial peptides (Sato et al. 1989a; Baker 2019).

1.2.2.5 Interference of physiological sweating

Under physiological conditions ion concentrations in primary and final sweat are well-balanced within defined ranges. Interestingly, although primary sweat is isotonic and its composition unaffected by sweating rate, ion concentrations of final sweat as secreted onto the skin surface are affected by released sweat amount: With increasing rates of secretion absorptive processes in the duct become saturated and NaCl content in final sweat increases (Quinton 2007; Sonner et al. 2015). Several non-thermal modulators have been identified to interfere with sweating and sweat rate. During exercise, muscle metaboreflex and activation of muscle mechanoreceptors affect sweat output. Similarly, hypohydration due to profuse sweating and hyperosmolar blood conditions reduce the sweat rate drastically. However, baroreceptors seemingly exert no effect on secreted sweat amount (Shibasaki and Crandall 2010).
Apart from these physiological perturbations pharmacologically acting agents are known to influence the sweat process at different stages and to act on different key regulatory proteins of sweating. Commonly applied, iontophoresis with cholinergic agonists like acetylcholine, pilocarpine, methacholine and carbachol induces spontaneous perspiration *in vivo* (Simmers et al. 2018). Consequently, the competitive muscarinic receptor antagonist atropine abolishes sweat production (Sato 1973; Quinton 1981). Similarly acting and a common measure to treat excessive sweating is local injection of the anticholinergic agent botulinum toxin. It functions by blocking acetylcholine release from sympathetic nerve terminals (Semkova et al. 2015). Sweating is also inhibited by administration of ouabain, an inhibitor of Na^+/K^+-ATPase, which emphasizes the vital role of this ion transporter in sweat generation (Sato 1973; Quinton 1981). Loop diuretics such as bumetanide and furosemide, which block NKCC1, exert the same inhibitory effect on perspiration. Prohibition of K^+ channel activity by Ba^{2+} also completely abolishes sweat secretion. Only a slight and partial reduction of sweating is achieved with amiloride which inhibits ENaC and with 4,4'-diisothiocyanostilbene-2,2'-disulphonic acid (DIDS) blocking the Cl^--HCO_3 exchanger (Sato and Sato 1987a; Cui and Schlessinger 2015). However, administration of amiloride fully suppresses Na^+ reabsorption in eccrine gland ducts (Quinton 1981). Several other drugs are known to either lower or increase sweating, inducing hypo- or hyperhidrosis, respectively. Among them are drug classes like antidepressants, antiepileptics, opioids, and antipsychotics (Cheshire and Fealey 2008). A completely different mode of action is postulated for the common AP agent ACH though its exact effect remains unknown. It is supposed to act topically within ducts of the eccrine sweat gland via formation of a physical plug of precipitated aluminum hydrogel (McWilliams et al. 1987; Mandriota 2017). Overall, these different modes of action emphasize relevance of unperturbed ion movements for physiological sweating and suggest ionic dysregulation as cause for sweating disorders. Although single ion fluxes haven been studied in detail in eccrine sweat glands and isolated cells for identifying effects of above-mentioned inhibition of ion transporters (Sato 1973; Quinton 1981), comprehensive investigation of several ion movements and their interaction after substance application was scarcely realized (Saga and Sato 1989; Takemura et al. 1991).

1.2.2.6 Disorders associated with eccrine sweat glands

Being a vital physiological mechanism disorders of sweating significantly affect life and well-being of individuals. Commonly known diseases relate to produced volume of sweat: Hyperhidrosis is characterized by secretion of unnaturally high amounts of sweat without morphologic alterations of eccrine sweat glands. It is seen as a consequence of dysfunctions in the nervous or endocrine system, systemic illnesses such as diabetes and congestive heart failure or cutaneous diseases (Sato et al. 1989b; Schlereth et al. 2009; Bovell 2015). Hypohidrosis, characterized by a reduced sweat volume, or anhidrosis, absence of sweating, are attributed to different conditions including failure of autonomic responses, diabetes, impaired or damaged sweat glands after skin lesions or mutated ORAI1 and STIM1 yielding lower levels of $[Ca^{2+}]_i$ (Sato et al. 1989b; Low 2004; Bovell 2015; Concepcion et al. 2016). Mutations in the gene coding for EDA1 manifest in defective development of eccrine sweat glands and are the cause for hypohidrotic ectodermal dysplasia (Reyes-Reali et al. 2018). Generally, impact of hypohidrosis is more severe compared to hyperhidrosis as it can lead to hyperthermia or even heat exhaustion, heat stroke and finally death (Cheshire and Fealey 2008; Hu et al. 2017).

Independent of the secretion rate sweat contains 3-5 time more NaCl in case of cystic fibrosis, a condition in which function of CFTR is impaired. Due to abundant occurrence of this Cl^- channel many tissues and organs are affected by this disease, but diagnosis is commonly attained by determination of extremely salty sweat. As a result of significantly reduced Cl^- reabsorption in ducts, concomitantly, Na^+ uptake from primary sweat is also downscaled (Sato and Sato 1984; Lee et al. 1986; Reddy et al. 1999; Quinton 2007). However, expression and function of Na^+ channel ENaC is not affected in case of cystic fibrosis (Brown et al. 2011).

Miliaria is restricted to eccrine sweat glands and displays itself in obstruction of gland ducts by an augmented sweat volume, keratinized plugs or solidified bacterial remnants. Symptoms include formation of small, localized vesicles on the skin surface due to retention of sweat in the upper skin layer (Shelley et al. 1948; Lu and Fuchs 2014).

Malignant tumors originating from eccrine sweat glands are rare appearances with less than 0.01% of skin carcinomas and mostly occur in elderly patients. They display a high degree of morphologic variation with inconsistent designation. Besides, eccrine carcinomas exhibit a high probability of local recurrence and metastasis (Rütten 2002; Sidiropoulos et al. 2011; Lu and Fuchs 2014).

1.2.2.7 Marker of eccrine sweat glands

As previously mentioned, different compartments of eccrine sweat glands are characterized by expression of distinct proteins. Based on these markers, identification of sweat glands within the skin additional to distinguishing of apocrine and eccrine glands is feasible. Even more, various sweat gland cell types, their location within glands, and their embryonic developmental stages can be differentiated (Lei et al. 2013; Cao et al. 2019). The latter is predominated by succession of skin structure-determining CK (Li et al. 2009). Additionally, markers proved useful in delineating sweat glands from other adnexal organs such as hair follicles and sebaceous glands. As early as in the 1980s the glycoprotein carcinoembryonic antigen (CEA) was discovered as an exclusive sweat gland marker (Cotton 1986). Other

proteins with this exclusive feature include CK7, glycoprotein epithelial membrane antigen (EMA), and membrane-bound ion transporters such as Na^+/K^+-ATPase and NKCC1 (Cao et al. 2019). Both types of sweat glands are distinguishable by CK77, a marker exclusively expressed in eccrine glands. Being an integral part of this work, structural differentiation of eccrine sweat gland coil and duct compartments is also feasible with the help of CK: Typically, epithelial duct cells are characterized by CK1, 5 and 10, whereas secretory cells express CK8 and 15 (Lei et al. 2013; Gao et al. 2014; Xie et al. 2016). Apart from CK, other functional and structural proteins have been discovered to discern reabsorbing duct, secretory coil and surrounding myoepithelial cells (**Tab 1.1**). Due to its secretory function, AQP5 water channel is exclusively expressed in coil cells (Song et al. 2002; Inoue et al. 2013). Among others, the same holds true for cell surface antigens CD44 and CD34 as well as S100 protein (Wang et al. 1992; Lei et al. 2013). In contrast, solely eccrine duct cells express stage-specific embryonic antigen-4 (SSEA-4) suitable for distinction of eccrine from apocrine ducts (Borowczyk-Michalowska et al. 2017). On the cellular level, clear and dark cells of secretory coils are also distinguishable by specific proteins: calcitonin gene-related peptide (CGRP) and gross cystic disease fluid protein 15 (GCDFP15) are found in dark cells while substance P, carbonic anhydrase II (CAII), vacuolar proton pump (V-ATPase) and CK31 label clear ones. Surrounding the coil, myoepithelial cells are marked by presence of α-SMA, nitric oxide synthase type I (NOS-I) and choline-acetyltransferase (ChAT) (Zancanaro et al. 1999; Bovell et al. 2011; Ma et al. 2018; Du et al. 2020).

Tab 1.1: Differentiation markers of eccrine sweat gland compartments and cells.
Different compartments and cell types of the eccrine sweat gland are characterized by distinct expression of certain marker proteins. This helps to identify the various cell types and structures in histological skin sections and cell cultures. CK – cytokeratin, SSEA-4 – stage-specific embryonic antigen-4, AQP5 – aquaporin 5, CD – cluster of differentiation, CAII – carbonic anhydrase II, V-ATPase – vacuolar proton pump, CGRP – calcitonin gene-related peptide, GCDFP15 - gross cystic disease fluid protein 15, α-SMA – alpha isoform of smooth muscle actin, NOS-I – nitric oxide synthase type I, ChAT – choline-acetyltransferase.

Location	Marker
Reabsorbing duct	CK1, CK5, CK10, SSEA-4
Secretory coil	CK8, CK15, AQP5, CD44, CD34, S100
Clear cell	Substance P, CAII, V-ATPase, CK31
Dark cell	CGRP, GCDFP15
Myoepithelial cells	α-SMA, NOS-I, ChAT

1.3 *In vitro* 2D and 3D cell culture models

Research on sweat and sweating started with identification of its causes and composition using animal models and human volunteers. Later, skin biopsies and micro-dissecting techniques to isolate single glands allowed for structural characterization of human sweat glands in and outside the dermal environment. For detailed investigations on functional properties of different cellular comparts, monolayer (2D) cells were explanted from isolated human gland substructures, which quickly replaced animal studies (Bovell 2018). However, primary 2D cell cultures stretch to their limits regarding maintenance of physiological features

and longevity. While the latter is coped with by developing immortalized cell lines, functional deficiencies including altered protein expression patterns are partly overcome by three-dimensional (3D) tissue culture models (Lee and Dessi 1989; Santos et al. 2012; Bovell 2018). Using this sophisticated culturing technique, cellular microenvironments are closer to native situations with intensified cell-cell-contact and improved cellular interaction (Santos et al. 2012). Consequently, development of 3D tissue models for biomedical research has increased in recent years. Different techniques are employed which can be categorized into scaffold-free and matrix-assisted culturing methods with the latter relying on e.g. hydrogel and Matrigel (Lin et al. 2008; Dutta and Dutta 2009). Generation of multicellular spheroids in hanging-drop or low attachment plates is based on self-assembling properties of suspension cells (Lin et al. 2008). These methods refrain from using an extra scaffold comprised of extracellular matrix components and are thus called scaffold-free techniques. Such models are easily prepared and consequently represent attractive organotypic tissue models for biological research and development, drug screening and toxicological assessments (Dutta and Dutta 2009; Klaka et al. 2017). Sophisticated *in vitro* 3D tissue models may even open the chance to be used instead of animal testing in some areas such as toxicity testing (Kunz-Schughart et al. 2004; Dutta and Dutta 2009). Highly important, degree of cell viability and detoxification capacities increases with establishment of a differentiated cellular orientation within the organoids (Lin et al. 2008).

In contrast, scaffold-assisted culturing commonly relies on different natural or synthetic hydrogels, or Matrigel, a solubilized basement membrane originating from a mouse chondrosarcoma rich in laminin, collagen type IV, perlecan, nidogen, various proteases, growth factors and other proteins (Kleinman and Martin 2005; Dutta and Dutta 2009). Thereby, Matrigel simulates the extracellular matrix (ECM) of native tissue to a certain degree (Santos et al. 2012). Cells cultured in this environment exhibit a pronounced differentiation pattern regarding morphology as well as gene expression indicating a biological activity of this scaffold material. Furthermore, 3D interaction of cells within Matrigel is enhanced evident by formation of cellular substructures comparable to the ones in the native tissue, e.g. luminal-like structures which are otherwise difficult to obtain (Kleinman and Martin 2005).

Employing this technique, a research group around Haihong Li generated an *in vitro* 3D human eccrine sweat gland model with distinctly differentiated cells and a certain structural organization. It resembles the native gland in that sphere-like and duct-like structures developed which even exhibited a small central lumen (Li et al. 2013). When freshly prepared Matrigel-cell mixtures were subcutaneously implanted into nude mice and cultured for some weeks, isolated constructs showed a distinct apical-basal cellular orientation evident by expression of certain eccrine sweat gland markers such as structural proteins, ion channels and CEA. Even more, observed cell polarization was highly similar to native gland structure indicating interaction with other reconstituted glands and the extracellular matrix (Li et al. 2015; Li et al. 2016b). By analysis of cell-type specific proteins not only coil-like and duct-like compartments could be discerned but also clear and dark cells within coil-like structures (Li et al. 2017a; Li et al. 2017b). Concerning time course of cell differentiation during development, analysis of those isolated 3D reconstituted eccrine sweat glands revealed a distinct succession of protein expression including keratins, α-SMA, CA II, S100 proteins and GCDFP-15, comparable to ontogenesis of native eccrine sweat glands (Li et al. 2016a; Zhang et al.

2018b). Besides, proliferation capacity of especially coil cells was demonstrated to diminish rapidly after implantation corresponding with increasing cell differentiation status (Li et al. 2017c). Demonstration of presence of FOXA1, Na^+-K^+-ATPase and NKCC1, vital contributors of sweating *in vivo*, as well as innervation with adrenergic and cholinergic fibers and nutrient supply by blood vessels suggested implanted 3D reconstitutes to possess a secretory function which was subsequently determined using magnetic resonance imaging (Li et al. 2018a; Zhang et al. 2018a; Li et al. 2018b).

Another working group used a similar approach of Matrigel-assisted 3D eccrine sweat gland reconstitutes to cultivate sweat gland cells. They reported good proliferation of cells within organoids while simultaneously enriching stem cells. Besides, these 3D constructs were successfully integrated into wounded skin with the ability to regenerate skin and assisting in wound healing (Diao et al. 2019).

A scaffold-free organotypic 3D model of the human eccrine sweat gland was established and characterized at the beginning of this project. It relies on the HD technique where cells out of a single cell suspension self-aggregate to form a spheroid in the tip of a medium droplet. Like Matrigel-assisted 3D reconstituted glands, a cellular orientation was determined within this construct based on protein expression and localization. Furthermore, ion transporters essential for sweat secretion such as AQP5, ANO1 and NKCC1 were abundantly present. All this demonstrates superiority of this simply generated model over conventional 2D cell cultures. Even more, this polarization of cells developed without assistance of an extracellular matrix component and transplantation into mice. Therefore, this HD-based 3D model is easier to prepare and, due to omitting transplantation steps, suitable for screening in cosmetics where tests involving animals are prohibited. Physiological functionality of this HD model was demonstrated by its reaction upon cholinergic and purinergic stimulation characterized by increase in the second messenger Ca^{2+}. On the downside, adequate cell viability within spheroids was restricted to less than seven days limiting research application of these models to a quite narrow time window (Klaka and Giesen 2015; Klaka et al. 2017).

1.4 Cell lines

Generation of above-described *in vitro* 3D models of eccrine sweat glands is based on employing isolated primary human cells. Unfortunately, like other primary cell types, also primary eccrine sweat gland cells go into senescence after only few rounds of passaging. Thus, the number of cells originating from the same donor is limited introducing the unwanted factor of interindividual variability into comparative studies for detailed, in depth understanding of molecular and physiological processes. Besides, primary cells differentiate during culture resulting in culture heterogeneity as another variability factor. To add, availability of skin biopsy tissue is sparse and isolation procedures are time-consuming. To circumvent these limitations and standardize the experimental conditions as far as possible, immortal cell lines of one defined cell type or those with extended lifespan constitute superior research tools for long-term and comparative investigations (Buchanan et al. 1990; Bovell 2018). Given this background, also an eccrine sweat gland cell line would be desirable for exploring the

sweating mechanism in more detail, discovering alternative AP actives, and generating standardized *in vitro* models for studying cell-cell-interactions.

Generally, development of cell lines and especially of immortalized ones is an ongoing research topic for already several decades. To achieve immortalization, one way is to overrule cell cycle checkpoints. This can be achieved by different means including mutations in the controllers of this pathway or modifications in expression of oncogenes and oncoproteins which regulate cell cycle checkpoints. Further, elongation of telomers via induction of telomerase might lead to immortalization by stabilizing chromosomes beyond the normal stage. However, infinite cell growth does not come cheap and is often associated with various drawbacks such as phenotypic changes, induction of tumorigenesis, and cellular crisis characterized by a high degree of apoptotic cells. Nonetheless, a lot of research takes recourse on immortalized cell lines to explore biological mechanisms and traits of different cell types and tissues (Maqsood et al. 2013). Therefore, an eccrine sweat gland cell line would be of great help to standardize conditions with respect to cellular material in sweating-related studies.

1.4.1 Lentiviral transduction

Generation of immortal cell lines requires changes in the cell's genome to overcome cell death which is normally induced by endogenous regulatory mechanisms like senescence and apoptosis. Those intentional, targeted genetic alterations are often implemented with the help of viral vector-assisted gene transfer. Thereby, lentiviral vectors provide a well-established, effective vehicle for target gene delivery into cells for immortalization. Belonging to the group of retroviral vectors, lentiviral vectors are originally derived from human immunodeficiency virus (HIV). Owing to their big advantage of being able to transduce nondividing cells lentiviral vectors are ideal gene delivery systems. Furthermore, they provide stable integration of the transgene into the target genome ensuring long-term expression, large cloning capacity, and omittance of undesired viral gene transfer into cells. However, due to their origin from the human pathogenic HIV, safety is a major concern when working with lentiviral vectors (Zufferey et al. 1998; Dull et al. 1998). To increase biosafety the complex genome of the virus was altered and packed into different plasmids to prevent formation of replication-competent viruses (Iwakuma et al. 1999). In the latest state-of-the-art third generation of lentiviral vectors several modifications of viral RNA were performed and only those genes vital for viral replication, integration and packaging were retained. Basically, only three of nine protein-coding genes of the original HIV, being *gag, pol,* and *rev*, were preserved (Zufferey et al. 1998). Removal of *tat* from the viral vector by substituting the U3 region of the 5' long terminal repeats (LTR) with a chimeric cytomegalovirus (CMV) promotor drastically reduced the possibility of recombination of a wild-type virus and, thus, increased the safety without compromising mRNA expression (Iwakuma et al. 1999; Lee and Cobrinik 2020). Besides, deletion of some base pairs in the 3' LTR not only minimized the risk of activation of cellular oncogenes but also lead to generation of self-inactivating vectors due to deletion of the enhancer and promotor function (Zufferey et al. 1998). To further reduce the possibility of viral recombination and production of replication competent viruses respective genes were split into different plasmids resulting in a recombinant lentiviral vector system composed of a

transgene vector, a packaging vector, and an envelope plasmid (Iwakuma et al. 1999). While the envelope plasmid includes a surface glycoprotein to enable transmembrane entry into target cells, the packaging plasmid encodes *gag, pol,* and *rev* for efficient entry and integration of the viral genome (Zufferey et al. 1998; Dull et al. 1998). Most importantly, the transfer plasmid encodes the desired transgene of interest together with the improved, self-inactivating 5' and 3' LTR regions to facilitate viral RNA transcription (Lee and Cobrinik 2020).
Life cycle of unaltered lentivirus starts with binding of the virus to the cell surface through surface glycoprotein encoded by the respective envelope gene. This triggers cellular entry via endocytosis of the cell membrane and release of the virus core into the target cell. In the target cell's cytoplasm reverse transcription of viral RNA is initiated and resulting complementary desoxyribonucleic acid (cDNA) is actively transported into the host cell's nucleus where the so-called provirus integrates into chromosomes. There, full-length transcription of the provirus occurs facilitated by the host cell's RNA polymerase II and associated transcription factors. All components of the proviral genome are transcribed and transported into the cytoplasm where they are subject to translation. Encoded structural elements wrap the full-length viral genome into viral buds close to the cell membrane and enable the release of newly infectious viruses (Dufait et al. 2012).
Due to splitting of named different genes into several plasmids, lentivirus-like particles are generated which can integrate into the target cell's chromosomes. In the following, those transgenes are transcribed and translated, but fail to generate new infectious viruses (Dufait et al. 2012).

1.4.2 Cell immortalization with SV40 large T antigen

In the course of ongoing proliferation primary cells enter a state of replicative senescence characterized by growth arrest and often accompanied by changes in gene expression and activation (Hayflick and Moorhead 1961). Overcoming of this proliferation stop can be achieved by compromising pathways of genetically steered cell cycle checkpoints, which may result in generation of an immortal cell line (Maqsood et al. 2013). Additionally, ongoing shortening of chromosome's telomeric ends needs to be dealt with. While in primary cells age-related alterations of genes directly lead to cell's growth arrest, telomer shortening destabilizes chromosomes which in turn activates DNA damage responses thereby evoking cell cycle arrest and senescence. In both cases, cell cycle regulation and telomer shortening, integration of certain genetic alterations via viral gene transfer represents a key component to circumvent programmed cell death. Targeting telomer shortening, this might be overcome by activation of human telomerase reverse transcriptase (hTERT) as the main regulator protein of telomerase (Kim et al. 2001; Smith et al. 2016; Shin et al. 2018). Alternatively, viral transduction of cells with certain target genes and thereby evoked genetic transformation can induce immortalization which constitutes nowadays most frequently applied technique as described above (Kirchhoff et al. 2004). However, the probability of successful immortalization increases when overexpression of hTERT is combined with viral oncogene expression; the latter interfering with cell cycle checkpoint pathways (Shin et al. 2018). One of the most widely used viruses to convert an array of cell types is simian vacuolating virus 40 (SV40) (Tegtmeyer 1975; Anderson and Martin 1976; Lee and Dessi 1989; Kohli and Jorgensen 1999; Kim et al.

2001; Kirchhoff et al. 2004; Shin et al. 2018), a polyomavirus originating from the Rhesus macaque as the host. Core protein encoded in the circular, double-stranded DNA of SV40 is the large tumor antigen (SV40T), which is essential for induction and maintenance of transformation, and thus, immortalization. Most vital for vast application of SV40T is its easy propagation in cell cultures. Steps of viral infection encompass penetration of the virion through the cell membrane, translocation into the nucleus where the viral chromatin is liberated and activation of cellular transcription resulting in expression of SV40T. Viral DNA is integrated randomly into the host cell's nuclear DNA. However, only when gene sequence of viral promoter and SV40T remain unaltered during integration daughter cells are able to maintain expressing SV40T and, thus, become immortal (Sáenz-Robles et al. 2001; Pipas 2009).

Functionally, SV40T undertakes many vital aspects of infection and transformation. First, it is the key protein binding to viral origin of replication and simultaneously attracts all relevant cellular components to induce viral DNA replication. Secondly, SV40T causes cellular transformation by affecting endogenous proteins of cell cycle regulation. It interacts with two major tumor suppressors, p53 and members of the retinoblastoma (Rb) family, with both complex formations being essential for cell transformation and immortalization. Binding of the carboxy-terminal half to p53 inhibits expression of p53-dependent genes omitting their growth-suppressing action. Likewise, interaction with proteins of the Rb family through the conserved LXCXE motif of SV40T blocks further downstream growth-arresting processes, especially liberation of Rb-dependent E2F. The latter inhibition results in initiation of gene expression and drives the cell into the cell cycle. As a third structural domain, amino-terminal J domain of SV40T is responsible for recruiting hsc70 chaperone which mediates ATP hydrolysis. Thereby liberated energy is required for separating Rb family proteins from their target (Sáenz-Robles et al. 2001; Pipas 2009).

Studies report these interactions of SV40T to be essential but not sufficient for cell transformation and further targets of SV40T haven been found. However, their exact contribution and importance for cell transformation and immortalization still needs to be elucidated (Sáenz-Robles et al. 2001; Pipas 2009).

1.4.3 Eccrine sweat gland cell lines

In the past, generation of more than one eccrine sweat gland cell line by viral transformation with SV40T has been reported. The first eccrine sweat gland cell line, called NCL-SG3, was established by Lee and Dessi in 1989. Being the only eccrine cell line used for extensive research in the further course, it has been well characterized. Although initially cellular origin was unknown functional and morphologic traits strongly suggest NCL-SG3 to stem from secretory coil cells (Bovell et al. 2008). This is corroborated by its missing response towards amiloride application as thereby targeted sodium channel is known to be present in duct cells. Despite successful creation of an immortal eccrine sweat gland cell line, it still shows some limitations, especially regarding functional behavior. Unfortunately, cholinergic activation of ion transport processes was lost upon transformation to immortalized cells, which under physiological conditions represents the major regulatory pathway of thermal sweating *in vivo*. However, NCL-SG3 exhibit ion transport capacity upon treatment with lysyl-bradykinin and

isoproterenol implying functioning β-adrenergic stimulation (Lee and Dessi 1989). Cellular reaction upon activation of PAR2 receptor by agonists and demonstration of its mRNA indicated presence and function of this receptor in NCL-SG3 (Bovell et al. 2008). Further characterization revealed expression of functioning Ca^{2+}-activated chloride channel TMEM16A (ANO1) and therewith associated Ca^{2+}-activated chloride transport (Ring et al. 1995; Servetnyk and Roomans 2007; Ertongur-Fauth et al. 2014). In contrast, presence of cAMP dependent CFTR could not be confirmed which coincides well with the cell's origin from secretory coils. Nonetheless, treatment of these cells with cAMP triggered Cl^- and K^+ currents suggesting the involvement of other Cl^- channels (Mörk et al. 1996; Servetnyk and Roomans 2007).

In the later course, another secretory coil cell line, EC23, was created at the Queen Marry University of London, and some immortal clones were isolated and characterized. This cell line as well as derived clones were demonstrated to express most important markers of eccrine secretory coil cells. Besides, EC23 and to a lesser extent its clones could be stimulated by both, adrenergic agonist isoproterenol and cholinergic agonist carbachol. Comparing those reactions with the ones of NCL-SG3, EC23 cells exhibited a stronger reaction leading to the conclusion of the EC23 cell line to be better suited for research on sweat secretion processes (Robles-Munoz 2014).

Apart from those cell lines, also generation of reabsorbing duct cell lines is reported in literature. Buchanan et al. (1990) created several cell lines with extended lifespan from sweat gland coil and duct tissue of patients with and without cystic fibrosis. However, only one of those cell lines originating from secretory coil cells exhibited no phenotypic alterations and senescent features and was therefore termed immortal (Buchanan et al. 1990). Later on, a SV40T-transduced eccrine sweat gland duct cell line was described which retained fundamental duct characteristics including cAMP-steered Cl^- conductance and amiloride-sensitive Na^+ absorption (Bell and Quinton 1995). However, no further studies with this duct cell line were reported. Thus, up to now a scientifically available duct cell line for in depth research of sweat reabsorption processes is lacking.

1.5 Antiperspirants and deodorants

Sweat secretion is a natural physiological phenomenon important for thermoregulation of the human body and is conducive to reinforcing the skin barrier (Bovell 2015). However, due to high density of apocrine and eccrine sweat glands in the semi occlusive area of the axilla formation of unpleasant wet stains and malodor is especially noticeably in this body region (Natsch 2015; Wilke et al. 2007). Therefore, cosmetic products to reduce underarm perspiration and odor formation are widely and daily used. Different product types are available including sticks, aerosols, sprays or roll-ons (Laden 1999). In general, deodorants and AP have to be distinguished (Rosenthal and Burchum 2017): Active ingredients in deodorants inhibit bacterial conversion of mainly apocrine secreted precursor of malodorous volatile substances (fatty acids and amines) and, thus, prevent formation of body malodor (Natsch 2015). Apart from antimicrobial agents diminishing cutaneous microorganism deodorants contain various fragrances and perfumes to mask remaining and emerging

unpleasant smell (Zirwas and Moennich 2008). Beyond that, AP combine functions of deodorants with additional reduction of watery sweat output from eccrine sweat glands. Mainly used active ingredients to achieve sweat reduction are metallic salts and especially aluminum salts such as ACH, which is already known since the early 1900s with the first patent claiming its astringent properties being filed in 1941 (Moore 1935; Montenier 1941; Toedt et al. 2005). Recently published, simulating *in vitro* studies examined details of AP mechanism of action of ACH. They support commonly accepted blockage of eccrine gland ducts by formation of gelatinous hydrogel plugs and thereby reduced cutaneous liberation of watery sweat. More elaborate, initial aggregation of those plugs is triggered by reaction of aluminum polycations with basic proteins present in sweat. With more proteins adhering to initially formed gelatinous membrane, the plug growths until covering the whole diameter of the orifice (Bretagne et al. 2017; Chen et al. 2016). As a consequence of this neutralization reaction a substantial amount of hydrochloric acid (HCl) is formed which is responsible for occurrence of skin irritations (Swaile et al. 2012). Despite this well accepted mode of action, some research postulates aluminum salts to also exert cellular effects in deeper compartments of eccrine sweat glands. This suggests another and/or additional AP action of these actives apart from plug formation (Papa and Kligman 1967; Scholes et al. 1978; McWilliams et al. 1987).

In recent years a discussion about possible negative health impacts of these aluminum salts has started (Untied 2004). Triggered by so far scientifically unconfirmed public concern and coinciding with intensified awareness for natural and clean beauty, more and more consumers seek for natural aluminum-free formulations without any compromise on efficacy. Especially in Germany there is a high demand for ACH alternatives due to still lingering, disproportionate public doubts about the safety of aluminum salts (Guinaugh 2020; Osserman 2020). Altogether, this poses a consumer and market requirement still needing fulfillment which was the main reason for starting herein described research on eccrine sweating and development of a standardized screening system to identify alternative sweat-reducing agents.

1.6 Toxicological aspects of antiperspirants

In line with public concerns about their health, cosmetic formulations need to be safe for daily application. Routine use of various cosmetic products on different parts of the body has become habitual to improve wellbeing and personal feeling of hygiene. Safety assurance of these consumer goods is therefore indispensable to protect the health of the applicant. Ideally, easy to perform *in vitro* methods with fast receipt of results should be available not only to screen for new actives, but also to pose the potential for simultaneous assessment of the ingredients' toxicological safety (Eisenbrand et al. 2002).

Legally, all cosmetic products, which are intendent to be placed on the market, need to be safe according to the Cosmetics Regulation 2009/1223/EC. This directive also prohibits use of animal testing to assess the risk of ingredients and formulations since march 2013 (European Parliament and Council 2009). Apart from this European legislation the Scientific Committee on Consumer Safety (SCCS) constitutes another important institution providing opinions and statements on the safety risk of consumer goods and gives advice on the safety evaluation process (SCCS 2016).

As mentioned above, use of aluminum in consumer goods as received public attention due to possible negative health effects linking aluminum, among other things, to initiation of Alzheimer's and breast cancer (Untied 2004; Mandriota et al. 2016; Mandriota 2017). Regarding these public health concerns of aluminum in cosmetic products the SCCS as well as the local German Federal Institute for Risk Assessment (BfR) currently released opinions concerning safety of aluminum-containing formulations. In their statement the local BfR suggested a reduced or at least careful usage of aluminum-containing AP especially on pre-damaged skin as is the case after shaving. However, the German institution does not dissuade from application of AP as they judge aluminum uptake from cosmetics as low compared to relatively high aluminum intake from food sources (Bundesinstitut für Risikobewertung 2019a, 2019b). Based on more recent available data, SCCS reassessed the toxicological risk of AP and finally stated concentrations of up to 10.6% of aluminum in AP as safe. Most important for their conclusion, a recent study reports more than 95% of topically applied aluminum to remain on external body parts resulting in a dermal bioavailability of only 0.00052%. Taking these values into account additional, systemically available aluminum attributable to dermal exposure is considered negligible compared to other routes of exposure such as oral intake via food consumption (Scientific Committee on Consumer Safety 2019).
Altogether, need for aluminum replacements in AP is mitigated by these official statements. However, consumers are alert and in view of currently growing consciousness towards clean beauty, sustainability, and natural ingredients an alternative AP combining these demands will probably prove popular and find market acceptance (Guinaugh 2020; Jindal 2020).

1.7 Aim of the study

Aim of this study was to get detailed scientific knowledge of sweating on a molecular level which should aid in identifying aluminum-free alternatives as AP actives. To achieve this, several aspects were investigated: First, a reliable eccrine sweat gland cell-based *in vitro* test system should be established. Therewith, the physiological mechanism of sweating should be further elucidated while simultaneously facilitating the discovery of sweat-reducing substances including indications for their cellular mode of action. Cellular monitoring of ion fluxes seems a suitable approach to achieve these aims as sweating is mainly a process of water and ion transport. In the following, validity of this *in vitro* procedure should be confirmed with the help of well-established, standardized *in vivo* sweat reduction studies with human volunteers.
Furthermore, available 3D *in vitro* model of the human eccrine sweat gland should be further optimized. It is desired to elaborate in more detail the cell-cell interactions between eccrine sweat gland coil and duct cells and to scrutinize their coordination regarding orientation and protein expression. Additionally, interdependency of eccrine sweat gland cell constructs with surrounding skin cells should be evaluated as a crucial step for development of an organotypic *in vitro* model comprising reconstructed sweat glands in artificial skin.
To standardize sweat gland-associated research and avoid interindividual variations in the future, an immortalized eccrine sweat gland duct cell line should be created and its characteristics elucidated. A duct cell line is of especial interest as, so far, only cell lines derived from the secretory coil compartment have been widely employed. However, with dermal application of cosmetic products penetration of active ingredients into the deeper secretory parts of the eccrine sweat gland are not expected, rendering duct cells the primary target for interaction with topically applied agents.

2 Material and Methods

2.1 Materials

2.1.1 Chemicals and reagents

Description	Article no.	Supplier
Antibody Diluent	S3022	Dako
Carbachol chloride	C4382	Sigma
CellTiter 96® Aqueous One Solution Cell Proliferation Assay (containing [3-(4,5-dimethylthiazol-2-yl)-5-(3-carboxymethoxyphenyl)-2-(4-sulfophenyl)-2H-tetrazolium, inner salt (MTS))	G3581	Promega
Collagen type I, high concentrated, rat tail	354249	Corning
Cytoseal™ XYL	8312-4	Thermo
dNTP Mix	U1511	Promega
Dulbecco's Modified Eagle Medium (DMEM) + GlutaMAX™ with phenol red	31966021	Gibco
Dulbecco's Modified Eagle Medium (DMEM), no phenol red	31053044	Gibco
Dulbecco's phosphate buffered saline (DPBS), 1x, no Ca and Mg	BE17-512F	Lonza
Fetal Bovine Serum	10270106	Gibco
FetalClone II Serum	SH30066.03	HyClone
Hematoxylin 7211	7211	Thermo
M-MLV RT 5x Buffer	M531A	Promega
M-MLV RT RNase (H-), Point Mutant	M3688	Promega
Normal goat serum (10%)	501972	Life
Phosphate buffered saline (PBS) buffer, 10x solution	70011044	Gibco
Polybrene	TR-1003-G	Merck
Proteinase K	19131	Qiagen
Puromycin dihydrochloride solution	ant-pr-1	InvivoGen
Random Primers	C1181	Promega
Recombinant RNasin®, RNase Inhibitor	N2515	Promega
RNase-Free DNase Set	79254	Qiagen
Tissue Freezing Medium	14020108926	LeicaB
TrypLE™ Express + Phenol Red	12605-010	Gibco
William's Medium E (1x) + GlutaMAX™	32551-020	Gibco

Further reagents were acquired from standard chemical suppliers like Merck or Thermo Fisher Scientific. Detailed information about mentioned suppliers are listed in the supplementary (IV.1.4).

2.1.2 Disposables

Description	Article no.	Supplier
96-well QPCR Plates, non-skirted	401333	Agilent
Biopsy cassettes and capsules		Leica
Bottle top filter, sterile, 0.45 µm CA, different sizes		Corning
Cell culture flasks, dishes, and plates		Corning
Centrifuge tubes, sterile, 15 ml and 50 ml		Corning
Cryogenic vials, CryoTube™ Vials, 1.8 ml	V7634	Nunc
GravityPLUS™ Hanging Drop System, 96 well	ISP-06-010	InSphero
Microscope slides 76 x 26 x 1 mm, frosted	1000200	Marien
Multiple well plate, 96-well, clear flat bottom, black	3340	Corning
Multiple well plate, 96-well, clear flat bottom, clear	3596	Corning
Optical strip caps for QPCR plates	401425	Agilent
Pipette tips, epT.I.P.S.® Reloads, various sizes		Eppend
Safe-lock test tubes, different sizes		Eppend
Serological glass pipettes, Stripette®, different sizes		Corning

2.1.3 Kits

Description	Article no.	Supplier
Brilliant® II SYBR® Green QPCR Master Mix	600828	Agilent
Elecsys® HIV Duo, HIV-1 p24 antigen kit		Roche
RNeasy Micro Kit	74004	Qiagen
RNeasy Mini Kit	74104	Qiagen

2.1.4 Technical devices

Description	Supplier
1-channel pipettes, electrical and manual various sizes	Eppend/Sator
8-channel pipettes, electrical and manual, various sizes	Eppend/Sator
Automated unheated slide stainer, Gemini AS	Thermo
Cryostat SM 1900	Leica
Centrifuges	Heraeus
Centrifuge Labofuge™ 400	
Benchtop centrifuge, 4-15C	
Incubator, CB 220	Binder
Microscope	Olympus
Inverse microscope CKX41 (ocular magnification 10x)	
Fluorescence microscope BX51 (ocular magnification 10x)	
Stereo microscope SZX7 (ocular magnification 10x)	
Microscope digital cameras DP71 and XC10, magnification 0.5x	Olympus
Multimode microplate reader Tecan Spark®	Tecan
Nanodrop ND-1000 Spectrophotometer	PEQLAB
Nitrogen tank Locator 4 Plus	Thermo

pH meter CG840	Schott
PTJ-200, Peltier Thermal Cycler	Bio-Rad
Sterile laminar flow hood/Clean bench, HERAsafe™	Thermo
Stratagene Mx3000P qPCR System	Agilent

2.1.5 Software and Programs

CellSense Dimension	Olympus
Fiji/ImageJ 1.52i	NIH
Microsoft Office 365	Microsoft
GraphPad Prism version 9.0 for Windows	GraphPad
SparkControl™ Software	Tecan
Marvin JS	ChemAxon
MxPro qPCR Software version 4.10	Agilent

2.1.6 Solutions and buffers

If not mentioned differently, chemicals and reagent were of high purity grade and acquired from Merck.

3,3',5-triiodo-L-thyronine solution (0.2 mM)
6.8 mg of 3,3',5-triiodo-L-thyronine sodium salt were dissolved in 0.75 ml of 0.02 M NaOH solution. 0.75 ml of this solution were carefully dropped into 49.25 ml of aqua dest. and filtered through a sterile filter.

Adenine solution (2.43 g/ml)
240 mg of adenine were dissolved in 12 ml of 0.5 M HCl, filled up to 100 ml with aqua dest. and filtered through a sterile filter. Aliquots of 5 ml were stored at -20°C.

Cholera toxin solution (0.1 µM)
0.5 mg of cholera toxin from *Vibrio cholerae* were dissolved in 0.59 ml of aqua dest. 0.5 ml of this solution were added to 99.5 ml of DMEM with phenol red containing 10% FetalClone II (HyClone) and filtered through a sterile filter.

Citrate buffer pH 6.0
4.5 ml of 0.1 M watery citric acid stock solution were added to 20.5 ml of 0.1 M watery sodium citrate stock solution. Stored at 2-8°C.

Epidermal growth factor (EGF) solution (10 µg/ml)
0.5 mg of EGF from murine submaxillary gland were dissolved in 50 ml of DMEM GlutaMAX™ containing 10% FetalClone II und sterile conditions.

HEPES buffer
0.3485 g of potassium sulphate (Roth) (2 mM), 0.2465 g of magnesium sulphate heptahydrate (1 mM) (both from Roth), 7.597 g of sodium chloride (130 mM), 0.9008 g of D-(+)-glucose (5 mM), 2.383 g of N-(2-Hydroxyethyl)piperazine-N′-(2-ethanesulfonic acid) (HEPES) (10 mM) and 0.1009 g of calcium carbonate (1 mM) were dissolved in aqua dest., filled up to 1 L with aqua dest., adjusted to pH 7.4 with 2 M NaOH, and filtered through a sterile filter. Stored at 2-8°C.

Hydrocortisone solution (200 µg/ml)
25 mg of hydrocortisone were dissolved in 5 ml of ethanol. 4 ml of this solution were added to 96 ml of DMEM with phenol red and filtered through a sterile filter.

Insulin solution (40 UI/ml resp. 28 UI/mg))
14.28 mg of insulin were dissolved in 10 ml of aqua dest. and sterile filtered. Aliquots of 1.5 ml were stored at -20°C.

L-ascorbic acid 2-phosphate solution (100 mM)
5 g of L-ascorbic acid 2-phosphate sesquimagnesium salt hydrate were dissolved in 195 ml of DMEM with phenol red and filtered through a sterile filter. Aliquots of 5 ml were stored at -20°C.

Penicillin G solution (50.000 UI/ml)
Dependent on the concentration of the batch a stock of 50000 U/ml was prepared by dissolving penicillin G sodium salt in aqua dest. and filtered through a sterile filter. Aliquots of 1 ml were stored at -20°C.

Supplement mixture
50 ml of 3,3',5-triiodo-L-thyronine solution, 50 ml of cholera toxin solution, 50 ml of EGF solution and 100 ml of hydrocortisone solution were mixed under sterile conditions. Aliquots of 2.5 ml were stored at -20°C.

2.1.7 Cell culture media and dishes

If not indicated differently, chemicals and reagent were acquired from Merck. Final concentrations of each ingredient are stated in brackets behind the respective chemical. Preparation of all cell culture media and dishes was conducted under sterile conditions.

Collagen I-coated cell culture flasks and well plates (5 µg/cm²)
Cell culture flasks and well plates were filled with 1x DPBS so that the bottom was covered. Rat tail Collagen type I was added to a final concentration of 5 µg/cm². Stored at 4°C.

Dye-loading solution
38 µL of 330 mM probenecid stock solution in DMSO were added to 10 ml of phenol red-free DMEM (1.25 mM) and either 4 µM Fluo-4, 2 µM Sodium Green tetraacetate or 5 µM PBFI with 0.05% Pluronic F-125 were added. Freshly prepared before use.

Fibroblast medium (FB medium)
500 ml of DMEM GlutaMAX™, 50 ml of Fetal Bovine Serum (10%), 1 ml of penicillin G solution (100 UI/ml) and 0.25 ml of gentamicin solution (ready to use in 200 mM) (25 µg/ml) were mixed. Stored at 2-8°C.

Isolation medium (0.5% (w/v) collagenase V, 0.25 mg/ml thermolysin)
1% (w/v) collagenase type V stock solution and 0.5 mg/ml thermolysin stock solution were mixed 1:1. Freshly prepared before use.

MTS-solution (1:6)
Aqueous One Solution Reagent and DMEM without phenol red were mixed 1:6. Freshly prepared before use.

Sweat gland cell culture medium
275 ml of DMEM GlutaMAX™, 150 ml of Ham/F-12 (HyClone), 50 ml of FetalClone II (10%), 10 ml of L-glutamine (4 mM), 5 ml of adenine solution (2.43 µg/ml), 1.5 ml of insulin solution (0.12 UI/ml), 5 ml of L-ascorbic acid 2-phosphate solution (1 mM), 1 ml of penicillin G solution (100 UI/ml), 0.25 ml of gentamicin solution (ready to use in 200 mM) (25 µg/ml) and 2.5 ml of supplement mixture (10 ng/ml EGF, 0.4 µg/ml hydrocortisone, 0.1 nM cholera toxin, 2 nM 3,3',5-triiodo-L-thyronine) were mixed. Stored at 2-8°C.

Sweat gland cell culture selection medium
Sweat gland cell culture medium was supplemented with 1.0 µg/ml puromycin dihydrochloride. Stored at 2-8°C.

2.1.8 Primer

Primers were manufactured at Sigma-Aldrich as customarily designed with the stated sense (s) and anti-sense (as) strands. Ready designed primers of ANO1, CFTR, SCNN1A and GAPDH were acquired from Qiagen; therefore, only the primer name and the catalog number are known.

Gene symbol	Gene name	Gene sequence (5'-3')
ANO1	Anoctamine-1	Hs_ANO1_1_SG (QT00076013)
AQP5	Aquaporin 5	s: CCACCTTGTCGGAATCTACTT as: CTGAACCGATTCATGACCAC
CEACAM5	carcinoembryonic antigen related cell adhesion molecule 5	s: TCATCCTGAATGTCCTCTATG as: GTGATGTTGGAGATAAAGAGC
CFTR	Cystic fibrosis transmembrane conductance regulator	Hs_CFTR_1_SG (QT00070007)
CHRM3	Muscarinic acetylcholine receptor subtype 3	s: ACAATAAGGTTTTGGGTC as: AACCAATACAATGTGTCCAG
COL1A1	Collagen type I alpha 1	Hs00164004_m1

COL3A1	Collagen type III alpha 1 chain	Hs00943809_m1
GAPDH (SYBR Green)	Glyceraldehyde-3-phosphate dehydrogenase	Hs_GAPDH_1_SG (QT00079247)
GAPDH (TaqMan)	Glyceraldehyde-3-phosphate dehydrogenase	Hs02786624_g1
NKCC1	Sodium-potassium-chloride cotransporter 1	s: AGGATGGCAAGACTGCAACT as: CGTGCAACTGGGAGACTCAT
SCNN1A	Sodium channel epithelial subunit 1	Hs_SCNN1A_1_SG (QT00022883)

2.1.9 Antibodies

2.1.9.1 Primary antibodies

Antibody	**Dilution**	**Host (Clonality)**	**Article no.**	**Producer**
Alpha smooth muscle actin (α-SMA)	1:200	Mouse (monoclonal)	M0851	Dako
Anoctamin-1 (ANO1)	1:300	mouse (monoclonal)	ab190721	Abcam
Aquaporin 5 (AQP5)	1:1000	Rabbit (polyclonal)	ab92320	Abcam
Carcinoembryonic antigen-related cell adhesion molecule 5 (CEACAM5) (CD66e)	1:250	Rabbit (polyclonal)	ab15987	Abcam
CD276 (B7 homolog 3 protein)	1:4000	Rabbit (monoclonal)	ab219648	Abcam
CD44 (Hyaluronic acid receptor)	1:200	Mouse (monoclonal)	ab6124	Abcam
CD9 (Tetraspanin-29)	1:50	Mouse (monoclonal)	ab2215	Abcam
Collagen type I (COL1)	1:1000	Mouse (monoclonal)	C2456	Sigma
Collagen type III (COL3)	1:200	Rabbit (polyclonal)	ab7778	Abcam
Cystic fibrosis transmembrane conductance regulator (CFTR)	1:100	Mouse (monoclonal)	ab2784	Abcam
Cytokeratin 15 (CK15)	1:150	Mouse (monoclonal)	CBL272	Milli
Dermcidin	1:100	Rabbit (polyclonal)	ab175519	Abcam

Muscarinic acetylcholine receptor 3 (CHRM3)	1:100	Rabbit (polyclonal)	ab60981	Abcam
Na-K-2Cl-Cotransporter (NKCC1)	1:200	Rabbit (polyclonal)	ab59791	Abcam
SCNN1A, Epithelial sodium channel (ENaC), subunit 1 alpha	1:500	Rabbit (polyclonal)	HPA012743	Sigma
Stage-specific embryonic antigen 4 (SSEA-4)	1:300	Mouse (monoclonal)	41-4000	Thermo

2.1.9.2 Secondary antibodies

Antibody	**Dilution**	**Host (Clonality)**	**Article no.**	**Producer**
Anti-Mouse IgG, Alexa Fluor 488 (FITC)	1:200	Goat (polyclonal)	A11017	Invitrogen
Anti-Rabbit IgG, Alexa Fluor 568 (TRITC)	1:200	Goat (polyclonal)	A11011	Invitrogen
2-(4-Amidinophenyl)-6-indolecarbamidine dihydrochloride (DAPI)	1:1000		D9542	Sigma

2.1.10 Fluorescence dyes

Fluo-4, AM-ester, Ca2+ indicator

Molecular formula:	C51H50F2N2O23
Molecular weight:	1096.95 g/mol
Fluorescence:	Ex/Em: 494/506 nm
Supplier:	Thermo
Article number:	F14217
Batch number:	1739650

PBFI, AM-ester, K+ indicator

Molecular formula:	C58H62N2O24
Molecular weight:	1171.00 g/mol
Fluorescence:	Ex/Em: 340/500 nm
Supplier:	Abcam
Article number:	ab142804
Batch number:	GR243631-3

Sodium Green tetraacetate, Na+ indicator

Molecular formula:	C76H64Cl4N4O23
Molecular weight:	1543.17 g/mol
Fluorescence:	Ex/Em: 507/532 nm
Supplier:	Thermo
Article number:	S6901
Batch number:	1754485

6-methoxy-N-(3-sulfopropyl)quinolium, inner salt (SPQ), Cl^- indicator

Molecular formula:	$C_{13}H_{15}NO_4S$
Molecular weight:	281.33 g/mol
Fluorescence:	Ex/Em: 344/443 nm
Supplier:	Thermo
Article number:	M440
Batch number:	2088709

2.1.11 Test substances

For testing of Cl^--containing substances (amines and ACH), stock solutions in distilled water were prepared and adjusted to pH 3.5 with hydrochloric acid (HCl). Those stock solutions were then diluted in DMEM to attain final treatment concentrations.
Besides, listed here and further used throughout this thesis are chemical lead substances of tested cosmetic raw materials which may also contain other impurities. Therefore, trade names of applied substances are also stated for reference.

1,2-Propanediol (1,2-PD)
Molecular formula: $C_3H_8O_2$
Molecular weight: 76.09 g/mol
Supplier: various

1,3-Propanediol (1,3-PD)
Molecular formula: $C_3H_8O_2$
Molecular weight: 76.09 g/mol
Supplier: Dupont

1,4-Dimethylpiperazine (DMP)
Molecular formula: $C_6H_{14}N_2$
Molecular weight: 114.19 g/mol
Supplier: Huntsman
Tradename: Jeffcat DMP

3,3'-Oxydipropanol (PPD-2) [1]
Molecular formula: $C_6H_{14}O_3$
Molecular weight: 134.17 g/mol
Supplier: WeylChem
Trade name: Sensatis H134

3,3'-[Oxybis(1,3-propanediyloxy)]bis(1-propanol) (PPD-4) [1]
Molecular formula: $C_{12}H_{26}O_5$
Molecular weight: 250.33 g/mol
Supplier: WeylChem
Trade name: Sensatis H250

Aluminum chlorohydrate (ACH)
Molecular formula: $Al_nCl_{(3n-m)}(OH)_m$
Molecular weight: not applicable, mixture
Supplier: Elementis

Diglycerol (DG)
Molecular formula: $C_6H_{14}O_5$
Molecular weight: 182.65 g/mol
Supplier: Solvay

Dipropylene glycol, isomeric mixture (DPG)
Molecular formula: $C_6H_{15}ClN_2O_2$
Molecular weight: 134.17 g/mol
Supplier: BASF

Glycerol
Molecular formula: $C_3H_8O_3$
Molecular weight: 92.09 g/mol
Supplier: AppliChem
Product number: A2926

Polyvinyl amine (PVAm, Copolymer of vinyl formamide and vinyl amine)
Molecular formula: $(C_6OH_{12}N_2)_n$
Molecular weight: <10000 g/mol (average)
Supplier: BASF
Trade name: Lupamin 1595

Polyethyleneimine, branched (PEI)
Molecular formula: $(C_2H_5N_1)_n$
Molecular weight: 1300 g/mol
Supplier: BASF
Trade name: Lupasol® G20 water free

Polyglycerol-4 (PG-4) [2]
Molecular formula: $C_{12}H_{26}O_9$
Molecular weight: 314.35 g/mol
Supplier: Inovyn

Polyglycerol-6 (PG-6) [2]

Molecular formula:	$C_{18}H_{38}O_{13}$
Molecular weight:	462.5 g/mol
Supplier:	Lonza
Trade name:	Natrulon® H-6

Polyglycerol-10 (PG-10) [2]

Molecular formula:	$C_{30}H_{62}O_{21}$
Molecular weight:	758.8 g/mol
Supplier:	Lonza
Trade name:	Natrulon® H-10

[1] Solution of polyether polyols having an average molecular weight equivalent to that of PPD-2 and PPD-4, respectively.
[2] Aqueous solutions of polyglycerols having an average molecular weight equivalent to that of PG-4, PG-6, and PG-10, respectively.

2.1.12 Lentiviral vectors

GFP Control Lentivirus, pLenti-GFP

Reporter gene (GFP) containing lentiviral vector

Overexpressed gene:	Green fluorescent protein (GFP)
Viral Titer:	at least $1 \cdot 10^6$ IU/ml
Vector map:	pLenti-GFP
Selection gene marker:	Kanamycin, Neomycin
Supplier:	Applied Biological Materials Inc. (abm)
Category number:	ABM-LV006
Lot number:	0196845135013

Lenti-SV40T (Puro) Lentivirus, High Titer

High Titer Lentivirus expressing SV40 large T antigen (vector map displayed in Supplemental **Fig 6.1**)

Overexpressed gene:	Simian vacuolating virus 40 large T antigen (SV40T)
Viral Titer:	at least $1 \cdot 10^9$ IU/ml
Vector map:	pLenti-SV40-T (Puro)
Selection gene marker:	Puromycin
Supplier:	Applied Biological Materials Inc. (abm)
Category number:	ABM-LV613
Lot number:	0072845128006

2.2 Methods

2.2.1 Cell culture

2.2.1.1 Isolation of primary eccrine sweat gland cells from facial skin biopsies

Human facial skin biopsies were obtained from cosmetic surgeries conducted by plastic surgeons and were in compliance with the German “Gesetz über die Spende, Entnahme und Übertragung von Organen und Geweben” (§8 ff.) (Bundesministerium der Justiz und für Verbraucherschutz sowie Bundesamt für Justiz 9/4/2007), omitting prior authorization by an ethics committee (Klaka et al. 2017). Experiments were performed in accordance with the World Medical Association’s Declaration of Helsinki (World Medical Association 1964). Human facial skin biopsies were obtained with prior written informed consent from healthy adult volunteers. Data were analyzed anonymously with knowledge of only the region of sampling, the sex, and the age of the patient.

Eccrine sweat glands isolated from facial human skin are suited for investigations on elucidating the sweating process as eccrine glands contained in the axilla are morphologically and functionally the same as in the face. Merely density of sweat glands might be slightly higher in the axilla (Wilke et al. 2007). Facial skin biopsies, mostly from the forehead, having an average density of 130-170 eccrine sweat glands/cm² were cut into pieces of about 1cm² with a scalpel. To liberate eccrine sweat glands from surrounding cutaneous connective tissue, enzymatic digestion with 0.5% (w/v) collagenase type V and 0.25 mg/ml thermolysin was conducted by completely immersing the skin pieces in a 50 ml falcon tube. Incubation lasted for 3 hours (h) at 37°C with 95% humidity and 5% CO_2 as the optimal time for isolating a maximal number of intact sweat glands. After thoroughly shaking, the enzymatic reaction was stopped by adding at least twice the amount of DMEM. Centrifugation at 1200 revolutions per minute (rpm) for 5 minutes (min) enabled removal of fat as supernatant. With the help of a stereo microscope, intact human eccrine sweat glands were isolated from the remaining fluid by suctioning into a 20 µl glass capillary connected to a pipette. In case of cultivation of single gland compartments (coil or duct), those parts were carefully separated at the transition zone (Fig 1.1) with a canula under the microscope prior to extraction from the medium. Mixed cell cultures of the entire gland (both compartments) are from hereon called co-cultures to distinguish it from separate coil and duct cell cultures (short coil or duct, respectively). Whole isolated sweat glands or respective compartments were transferred into sterile cell culture flasks pre-treated with collagen type I and supplemented with sweat gland cell culture medium and 10 µM of acetylcholine. Collagen I is the most abundant collagen in the human body and is be found especially in the dermis and connective tissue (Lai-Cheong and McGrath 2017). Thus, collagen-coating in combination with nutrient-rich culture medium ensured optimal environmental conditions for the growth of isolated sweat gland cells. Acetylcholine was added for improved expression of sweat-relevant proteins (Klaka et al. 2017).

Henceforth, culturing was conducted under sterile conditions with incubation at 37°C, 95% humidity and 5% CO_2. Medium was renewed every 2-3 days only after adherence of the isolated primary tissue (*in situ* tissue) to the culture dishes to prevent vacuuming off the isolated glands. Within a few days newly formed cells migrated from the *in situ* tissue forming a two-dimensional (2D) monolayer culture. About 28 days (d) after isolation, primary cells reached a confluency of about 80-90%.

2.2.1.2 Culturing of primary eccrine sweat gland cells

When covering about 80-90% of the culture flask primary eccrine sweat gland cells were subcultured. For that, the old culture medium was aspired, and cells were washed with DPBS once to remove remaining medium, serum and dead cells. Afterwards, as much of 0.05% of trypsin-EDTA with phenol red was added to completely cover the cells. Incubation at 37°C for about 10 min detached the cells from the culture dish while easy shaking eased off stronger adhesive cells. Addition of at least twice the amount of serum-containing medium terminated the enzymatic activity of trypsin and, thus, prevented degradation of the cells.
In case of first sub-culturing of outgrown cells from the *in situ* tissue, strongly adhering cells were mechanically detached with a cell scraper. The cell suspension was passed through a cell strainer with a pore size of 100 µm to retain *in situ* eccrine sweat glands as their cellular cohesion was too intense to separate them. After centrifugation (5 min at 1200 rpm) of the cell suspension in a falcon the supernatant was aspired, and the cell pellet resuspended in 1or 2 ml of the culture medium depending on the size of the pellet. Before counting with a hemocytometer, 50 µl of the cell suspension were mixed with 50 µl of trypan blue. Trypan blue stains the cytoplasm of dead cells as their cell membrane is impaired. In contrast, viable cells maintain a clear cytoplasm enabling their distinction and the exclusive counting of living cells (Strober 2015). Considering the mean number of cells from four quadrants, the intrinsic chamber factor, and the respective dilution the number of cells per ml and the total number of cells in the suspension were determined. An appropriate quantity was seeded into collagen I-coated culture dishes, supplemented with a certain volume of medium, gently shaken to mix the cells with the medium after seeding, and incubated (37°C, 95% humidity, 5% CO2). Every 2-3 days the medium was renewed.
For generation of 3D eccrine sweat gland models (refer to 2.2.1.4) and eccrine sweat gland matrix models (refer to 2.2.2) detached 2D primary and immortalized eccrine sweat gland cells were utilized and integrated to form the new 3D models. In case of substance testing including cytotoxicity measurements (refer to 2.2.6.1) and determination of intracellular ion levels (refer chapter 2.2.6.2 and 2.2.6.3) detached 2D cells were seeded into 96-well plates 2-3 d prior to conduction of the experiments. Seeding occurred with an initial density of 20,000 or 30,000 cells/well in a volume of 100 µl 2 or 3 d in advance, respectively.

2.2.1.3 Cryopreservation and thawing of primary eccrine sweat gland cells

For preservation of intact primary eccrine sweat gland cells and immortalized duct cells, they were stored in liquid nitrogen for up to several years in aliquots of 1 ml containing 1 to $3*10^6$ cells. For that, freshly prepared cell suspension was diluted with cell culture medium, and dimethyl sulfoxide (DMSO) was added to a final concentration of 10% preventing the cells from bursting due to freezing. 1 ml of the suspension was transferred into each cryogenic vial and slowly cooled down to -80°C in a freezer. After some days of storage, the vials were transferred into a nitrogen tank. In case of utilization, deeply frozen eccrine sweat gland cells were taken out of the nitrogen tank and quickly thawed by suspending in 10 ml of pre-warmed cell culture medium. After centrifugation (5 min, 1200 rpm) to separate the cells from DMSO-containing medium, cells were resuspended in cell culture medium and seeded into collagen I-coated cell culture flasks for cultivation as described in chapter 2.2.1.2.

2.2.1.4 Generation of spheroidal sweat gland models

Contrasting to conventional 2D cell cultures, the spheroidal three-dimensional (3D) sweat gland cell model exhibits characteristics closer resembling the physiological conditions in the native gland *in vivo* (Klaka et al. 2017). These *in vitro* 3D sweat gland models were produced using the hanging drop (HD) culturing method utilizing the scaffold-free 96-well GravityPLUS™ Hanging Drop System (**Fig 2.1**). This highly sophisticated system enables the stable and reproducible cultivation of 3D cell models which can be directly harvested into 96-well plates as kinds of *in vitro* sweat glands and further employed in flowing analyses.

Fig 2.1: GravitiyPLUS™ Hanging Drop System.
Depicted are several hanging drops (HD) as they are arranged in this culture system. 50 µl of a cell suspension were added into each slot to obtain a stable HD with sufficient nutrient supply for the cells to aggregate at the tip of the droplet. Picture was taken from below where under normal culture conditions a bottom plate is tightly combined with the HD bearing upper plate. Everything is covered by a lid to assure sterile conditions.

During preparation, the rim of the microtiter plate was filled with about 2 ml of sterile aqua dest. to minimize evaporation of the medium. Additionally, a provided sterile filter paper was soaked with about 15 ml of sterile 1x DPBS and placed below the seeding cavities on the bottom of the plate for the same purpose. After detachment, counting and appropriate dilution of cells with sweat gland culture medium (for detailed description refer to chapter Culturing of primary eccrine sweat gland cells2.2.1.2), 50 µl of the cell suspension containing 25,000 cells were carefully transferred into each cavity with a manual multichannel pipette as depicted in **Fig 2.2a** and **b**. Cell-loaded plates were carefully placed into the incubator (37°C, 95% humidity, 5% CO_2) to prevent the HD from falling off. Within three days of incubation, the primary eccrine sweat gland cells aggregated to stable mature spheroids (Fig 2.2c) ready for harvesting and experimental measurements.
For harvesting the 3D eccrine sweat gland models were initially collected into the bottom plate. For that, the filter paper was removed from the bottom while about 20 ml of sterile DMEM without phenol red were added. Next, 70 µl of the same medium were added into each cavity with a multichannel pipette resulting in an increased drop size and its plunging (Fig 2.2d and e). The swimming spheroids were then carefully transferred into a 5 ml tube with a pipette, ready for further application.

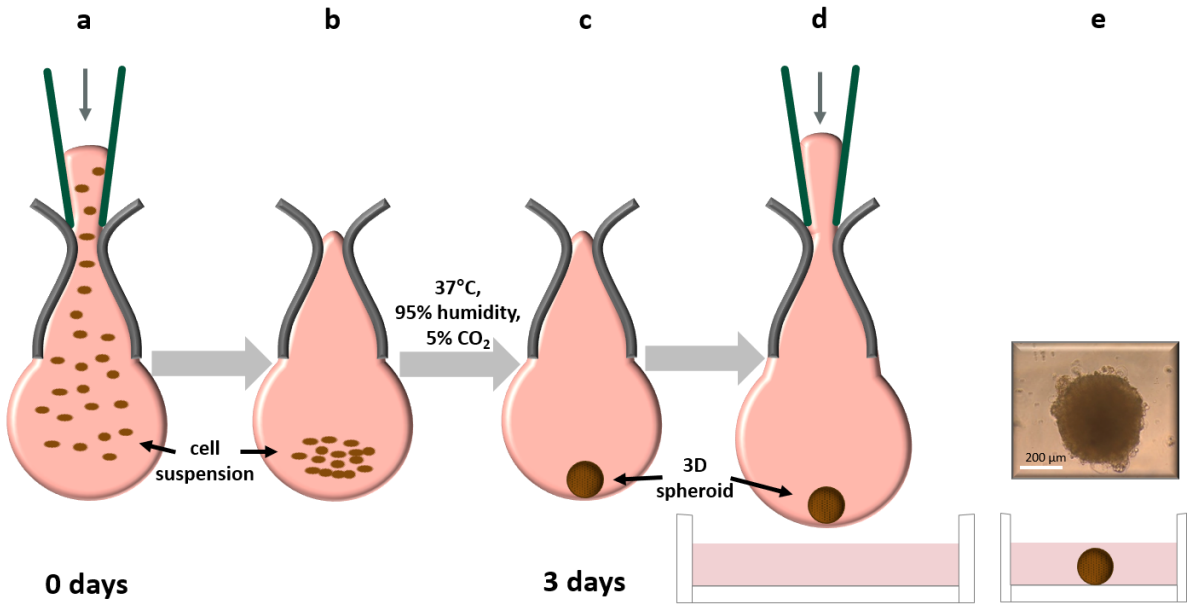

Fig 2.2: Scheme for the generation of the 3D eccrine sweat gland model.
Using a multichannel pipette, 50 µl of the suspension medium (containing 25,000 primary eccrine sweat gland cells) were seeded into each cavity of the GravityPLUS™ Plate (**a**) and sweat gland cells started to aggregate at the lower end of the medium droplet (**b**). After three days of incubation at 37°C, 95% humidity and 5% CO_2 the eccrine sweat gland cells formed a stable spheroidal 3D model of the eccrine sweat gland (**c**). By adding 70 µl of DMEM the HD fell off into the bottom plate provided with DMEM to soften the impact of the spheroid (**d**). Afterwards, 3D sweat gland models swimming in medium could be collected with pipettes and used for further experiments (**e**). The framed insert is a microscopic image of a harvested 3D eccrine sweat gland model after 3 days of incubation.

Conventionally, *in vitro* 3D models of the human eccrine sweat gland were prepared from primary cells of the entire gland (co-culture). Herein established improved *in vitro* 3D HD models of the eccrine sweat gland were generated by consecutive seeding of duct and coil cells. For that, about 12,000 duct cells were plated into HD 24 h prior to adding coil cells. Before coil cell supplementation, 20 µl of the culture medium were aspirated using a multichannel pipette and 20 µl of fresh culture medium containing 12,000 coil cells added. As with the other 3D models, they aggregated within three days prior to harvesting and experimental use.
To examine characteristics of in this study generated SV40T-immortalized eccrine sweat gland duct cells, they were incorporated into 3D models instead of primary duct cells.

2.2.2 Generation of eccrine sweat gland matrix models

In native skin eccrine sweat glands are integrated into the dermis, traverse the epidermis and open onto the skin surface. One focus of this study is to examine the interdependency of eccrine sweat gland cells with the surrounding skin. To simulate intense cell-cell-contact between eccrine sweat gland cells and fibroblasts in the dermis an advanced skin model was designed in this work where eccrine sweat gland cells were integrated into a dermal matrix.
The artificial dermis consisted of a cross-linked collagen I mixture (1 M NaOH, 10x PBS, Collagen I in a ratio of 1:8,75:42,5). With the help of a 3D-printed mold (**Fig 2.3**), made of

durable resin and kindly provided by Henkel Adhesive Technologies, 16 defined slots (0.5 mm in diameter, 4 mm in length; 1 mm apart) were built into the scaffold. 750 µl of the collagen I mixture supplemented with 100,000 primary human skin fibroblasts was poured around the mold into a 12-well insert featuring a polyethylene membrane. Addition of fibroblasts ensured emergence of proper conditions in the dermal matrix equivalent including the deposition of extracellular matrix components produced by the fibroblasts. After solidification for 1.5 h at 37°C the mold was removed with remaining slots being hollow imprints of eccrine sweat glands in the skin regarding shape and size. To rebuild the native situation, cultured eccrine sweat glands cells were then seeded into these slots. With focus on achieving a situation as close as possible to the native one in the human skin (coil deep down in the skin and duct connecting to the surface), sweat gland coil cells were added 24 h prior to the duct cells into these slots. For that, 50 µl of a coil cell suspension in sweat gland culture medium containing between $2 \cdot 10^6$ cells was prepared and thereof 2.5 µl were added directly into each microwell (50,000 coil cells/slot) with a fine pipette. Concomitantly, 1.5 ml of culture medium was added to the well and 30 min later 200 µl of culture medium were pipetted on top. Matrix models were incubated at 37°C with 95% humidity and 5% CO_2 to allow for deposition of the coil cells into the slots. On the next day, 50 µl of a duct cell suspension in culture medium comprising $8.75 \cdot 10^6$ cells was prepared and again 2.5 µl of the suspension (220,000 duct cells/slot) was added per microwell. As before, duct cells were allowed to sink into the slots while incubating for 2 h. Finally, 0.5 ml of culture medium was provided per insert and the eccrine sweat gland models were incubated for another one two four weeks with culture medium which was replaced every 2-3 days.

Culturing of eccrine sweat gland matrix models was terminated after one, two, three, and four weeks and the models prepared for histological investigations as paraffin or frozen sections (refer to 2.2.5) to determine the integration, marker expression and differentiation status of the sweat gland cells in the dermal matrix equivalent.

Culturing of eccrine sweat gland matrix models was terminated after one, two, three, and four weeks and the models prepared for histological investigations as frozen sections (refer to 2.2.5) to determine the integration, marker expression and differentiation status of the sweat gland cells in the dermal matrix equivalent and to compare it with the *in vivo* situation.

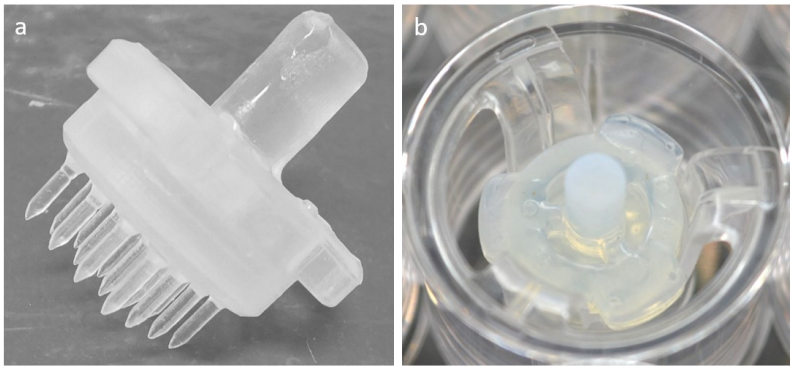

Fig 2.3: 3D-printed mold for preparation of slot-bearing dermal matrix models.
The mold is made of durable resin and was fabricated using a 3D printer (**a**). Its diameter of 12 mm is adapted to fit the size of a 12-well insert (**b**). The tube-like shape and size of each pin imitates the tubular structure of eccrine sweat glands in the skin regarding length (4 mm) and diameter (0.5 mm). Distance between single pins equals 1 mm.

2.2.3 Eccrine sweat gland duct cell line

To conduct experiments under standardized conditions it is desirable to always work with the same cellular material preventing measurement uncertainties due to interindividual variations (Buchanan et al. 1990). Given this background, one objective of this study was the generation of a cell line derived from human eccrine sweat gland duct cells. Those could then be used in substance screenings in search of alternative AP actives as well as in generation of sophisticated *in vitro* 3D models of the human eccrine sweat gland.
Initially required primary human eccrine sweat gland duct cells were isolated from a facial skin biopsy (denoted 19-01) (refer to 2.2.1.1) and expanded (refer to 2.2.1.2). Cryopreserved aliquots of primary, parental cells were ship to the external institute trenzyme GmbH, Konstanz, for conduction of the transduction procedure as this step required special laboratory safety measures not established at Henkel. The aim was to immortalize eccrine sweat gland duct cells by transduction with a SV40T-containing lentiviral vector.

2.2.3.1 Transduction with a lentiviral GFP control virus

After shipping and a first quality control at the external institute, primary eccrine sweat gland duct cells 19-01 were transduced with a lentiviral green fluorescent protein (GFP) control vector to assess the MOI (multiplicity of infection) for later successful transduction with the SV40T-containing lentiviral vector. The MOI expresses the average number of viral particles applied per infection cell and is calculated according to formula (1):

$$(1) \qquad MOI = \frac{\text{Product Titer} \cdot \text{Infection Sample Volume}}{\text{Final Volume}} \cdot \frac{1}{\text{Total Cell Number}}$$

At trenzyme, the optimal MOI for these cells was determined. For that, primary duct cells were seeded with about 30% confluency into collagen I-coated 12-well plates and five hours later infected with different MOIs of the GFP control vector. For infection, transduction medium, supplemented with 8 µg/ml of polybrene to enhance transduction efficiency, replaced the culture medium. Medium containing viral particles was removed 16 h after transduction and exchanged for fresh culture medium. Three days post-transduction duct cells were dissociated from the plate, fixated with formaldehyde, and analyzed in a flow cytometer for GFP expression. Three best suiting MOIs displaying a high amount of green fluorescence were chosen for transduction of the duct cells with the SV40T-containing lentiviral vector.

2.2.3.2 Transduction of primary human eccrine sweat gland duct cells with a SV40T-containing lentiviral vector

Stable integration and expression of the SV40T is a pre-requisite for immortalization of primary cells. To obtain a stably immortalized duct cell line, primary eccrine sweat gland duct cells 19-01 were transduced with a third generation SV40T-containing lentiviral vector where the respective gene is regulated by a cytomegalovirus (CMV) promotor (**Fig 2.4**). Besides, the vector contained a puromycin resistance gene for selection of successfully SV40T-transduced cells.

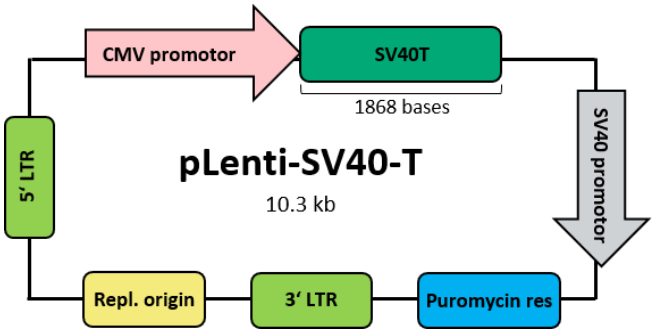

Fig 2.4: Vector map of the used transfer lentiviral vector containing the SV40T transgene. The HIV-1 derived lentiviral vector containing simian vacuolating virus 40 large T antigen (SV40T) as a transgene has a total length of 10.3 kilobases (kb). The length of the 1868 bases long SV40T-transgene is under control of a cytomegalovirus (CMV) promotor. Additional to the origin of replication (Repl. origin) the single stranded RNA also encompasses a puromycin resistance gene (Puromycin res) to select successfully transduced cells. 5' LTR – 5' long terminal repeat, 3' LTR – 3' long terminal repeat.

For transduction performed at the external partner trenzyme, primary duct cells were seeded into collagen I-coated 6-well plates five hours prior to infection with a density of $1 \cdot 10^4$ cells/cm², corresponding to about 30% confluency and a total of $9.6 \cdot 10^4$ cells/well. Afterwards, the culture medium was replaced by 3 ml of virus-containing medium with three different MOIs (MOI of 10, 25 and 50) and supplemented with 8 µg/ml of polybrene. As with the GFP control vector, medium containing viral particles was replaced by fresh culture medium after 16 h. Passage number was set to 0 on the day of transduction and the transduced cell pool termed SGDC-SV40T (sweat gland duct cell-SV40T).

After three days cells were passaged for the first time by diluting 1:1.5 and re-seeding into 6-well plates. To select for duct cells stably transfected with the SV40T, cell culture selection medium with three different concentrations of puromycin (0.5, 0.75 and 1.0 µg/ml) was added after cells had attached to the culture dish.

Parental primary duct cells were cultivated in parallel with and without the selection marker puromycin to compare the growth behavior of parental and transduced duct cells and to control the selection pressure. Basically, the same culture procedure was used as described in 2.2.1.2.

Additionally, cell culture supernatants of the transduced cells in passage one and five were collected and tested for the presence of viral particles using Roche HIV Ag p24 kit (Centre hospitalier universitaire Vaudois). After assuring of viral clearance transduced cells were classified as BSL 1. The pool of SV40T-transduced duct cells was cryopreserved and ship back to Henkel AG & Co. KGaA.

2.2.3.3 Determination of growth behavior of SGDC-SV40T

Upon arrival at Henkel, SGDC-SV40T were seeded in collagen I-coated culture flask and analyzed regarding their morphology and growth behavior in several rounds of passaging. SGDC-SV40T were cultured in selection medium containing 1 µg/ml puromycin, but otherwise handled as the primary eccrine sweat gland cells (refer to 2.2.1.2 and 2.2.1.3). Morphological characteristics were observed under an inverse microscope and pictures were taken with a microscope mounted digital camera.

Growth rate and population doubling time (PDT) are two common measures to characterize growth behavior of cells. While the growth rate provides information about proliferation pace and, thus, physiological fitness of cells, PDT quantifies the time needed for a population to double its number of cells (Hashimoto et al. 2016).
Growth behavior of SGDC-SV40T was monitored by cell counting during passaging (refer to 2.2.1.2) and reseeding of $0.5 \cdot 10^6$ cells in T75 flasks. Out of the determined number of cells growth rate λ and population doubling time (PDT) t_d were calculated using the following formulas (2) and (3):

(2) Growth rate: $$\lambda = \frac{\ln\left(\frac{N(t)}{N_0}\right)}{t}$$

(3) PDT: $$t_d = \frac{\ln(2)}{\lambda}$$

with: λ – growth rate; N_0 – number of seeded cells at time 0; N(t) – number of cells at time t; t – time in h between seeding and harvesting; t_d – population doubling time in h

2.2.3.4 Single cell cloning using SGDC-SV40T

A cell line is defined as a rather homogenous population of cells with certain functional and phenotypic traits. Cloning of single cells increases the genetic uniformity within the cell line (Sato et al. 2016).
To obtain a defined immortalized eccrine sweat gland duct cell line with distinct characteristics out of the pool of SGDC-SV40T single cells were isolated and used as the origin for colony forming. To achieve this, an aliquot of a SGDC-SV40T suspension was adjusted with selection medium to contain on average one cell per 96-well cavity (10 cells/ml) and seeded into three 96-well plates. After 24 h wells were inspected and those containing one cell were noted. From then on, wells were regularly checked (every 2-3 d) for formation of colonies. Occasionally, images were taken in bright field mode using the microscope CKX41 with the mounted digital camera XC10. Selection medium was renewed every 2 to 7 d by preconditioned selection medium in wells of single cell cloning plates. This preconditioned selection medium was composed of selection medium carefully removed from cultures of SGDC-SV40T (stored at 4°C until used) mixed with fresh selection medium in a ratio of 1:1 prior to application to single cell cloning plates. When reaching 80-90% confluency colonies were expanded by transferring into collagen I-coated 24-well, then 12-well and 6-well plates followed by 60 mm and 100 mm Petri dishes. At this stage, medium was renewed every 2 to 3 d with fresh selection medium. The first 15 clones reaching this stage were then subject to more extensive molecular analyses (refer to 2.2.4), were examined regarding their functional properties in the substance screening procedure (refer to 2.2.6) and generated 3D models comprising these transduced duct cells were histologically scrutinized (refer to 2.2.1.4 and 2.2.5). For every characteristic, cell clones were compared to primary cells and, when applicable, to native eccrine sweat glands.

2.2.4 Molecular biological analyses

2.2.4.1 Isolation of RNA and determination of the concentration

Studying molecular biological characteristics of cells gives deeper insight into vital cellular functions and mechanism as well as thereof changes caused by altered environmental conditions. Special focus is thereby often set on scrutinizing the cell's nucleic acid content as the first indicator for modified cellular reactions and its adaptation.
Ribonucleic acid (RNA) from native human tissue, 2D eccrine sweat gland cells, transduced duct cells, and their clones was extracted using the RNeasy Mini Kit or for *in vitro* 3D models using the RNeasy Micro Kit. In case of 2D cells, one aliquot comprised 400,000 cells whereas for extraction from 3D models 16-20 models were pooled.
Prior to RNA extraction tissue and cells were lysed in 150 µl RLT buffer, thoroughly vortexed for cell disruption and additionally shaken for 30 to 40 min on a lab shaker. Lysed samples were either stored at -20°C until further processed or directly set for protein degradation, especially RNases, in 20 mg/ml Proteinase K in RNA-free water at 55°C for 1 h. Addition of 500 µl of 99% ethanol precipitated the RNA by mixing through pipetting. Following the sample transfer onto RNeasy Mini Spin Columns (2D cells and native tissue) or RNeasy MinElute® Spin Columns (3D models) the columns were centrifuged at 13,000 rpm and 4°C for 1 min and the filtrate was discarded while RNA and DNA were retained on the column. Washing of the column was performed with 500 µl of RW1 buffer and another centrifugation step where, again, the filtrate was discarded. Next, the DNA was digested in a 1:8 mixture of the supplied DNase1 reagent in RDD buffer (341 Kunitz units/ml) for 15 min at RT. Again, washing was conducted by addition of 500 µl of RW1 buffer, centrifuging and discarding of the filtrate. For preparing of the sample elution, the columns were washed twice with 500 µl of RPE buffer, followed by centrifugation and discarding of the filtrate. To get rid of remaining liquid in the columns they were again centrifuged at 13,000 rpm for 5 min. Finally, the columns were transferred onto collection tubes and 25 ml of RNase-free water was supplied directly into the membrane of the column. After a short incubation time of a few minutes elution of the RNA was achieved by centrifugation. This time the filtrate contained the RNA which was photometrically quantified using the Nanodrop device. Thereby, the aromatic rings of the nucleic acids (RNA and DNA) absorb light in the UV-range with an absorption maximum at 260 nm. The optical density (OD) at this wavelength was used for calculation of the RNA concentration. Simultaneously, the OD at 280 nm was also measured as an indicator of the purity of the sample as proteins exhibit an absorption maximum at 280 nm. By calculating the quotient OD_{260}/OD_{280} the degree of impurities, such as proteins, phenolic compounds etc., could be determined. A quotient value between 1.8 and 2.0 indicates a sample free of contaminants. Quantified RNA samples were stored at -20°C.

2.2.4.2 Synthesis of complementary DNA

For determination of relative gene expression (ref. 2.2.4.3) isolated RNA (ref. 2.2.4.1) needs to be transcribed into complementary DNA (cDNA). This is achieved with the help of the reverse transcriptase which is produced in *E. coli* from the retrovirus *Moloney murine leukemia virus* (MMLV) (Gerard et al. 1997). This specific enzyme processes the synthesis of cDNA from single-stranded RNA (e.g., mRNA) or DNA templates in presence of primers.

Herein, 500 ng of RNA were dissolved in a total amount of 10 µl of RNase-free water to which 1 µl of random primer was added, centrifuged at 1,000 rpm for 1 min and set for primer annealing at 65°C for 10 min. After addition of 4 µl of 5x Reaction buffer, 1 µl of dNTP mixture (containing dATP, dGTP, dCTP and dTTP), 0.5 µl of RNasin, 2.5 µl of RNase-free water and 1 µl of the MMLV enzyme, samples were again centrifuged for mixing and primer extension toke place at 42°C for 1 h. Finally, the MML enzyme was heat inactivated at 70°C for 15 min, the samples cooled to 4°C and their concentration adjusted to 5 ng/µl with RNase-free water. Diluted cDNA samples were stored at -20°C.

2.2.4.3 Analysis of gene expression using RT-qPCR

To determine relative gene expression of tissue and cell samples initially their RNA was isolated, quantified and transcribed into cDNA (ref. 2.2.4.1 and 2.2.4.2). In real-time quantitative polymerase chain reactions (RT-qPCR) those cDNA strands were amplified and simultaneously, in real-time, their amount determined using the intercalating fluorescence dye *SYBR Green Brilliant II*. Thereby, the measured fluorescence intensity is directly proportional to the amount of generated cDNA copies.
RT-qPCR was conducted in 96-well plates with an initial amount of 25 ng of cDNA of the respective sample. 4.7 µl of RNase-free water, 12.5 ml of *SYBR Green Brilliant II*, 0.3 µl of ROX reference dye and 2.5 µl of the primer of the gene of interest were added and the samples centrifuged at 6,000 rpm for 1 min. The reference dye ROX enables normalizing of the fluorescence and determining its threshold. Glyceraldehyde 3-phosphate dehydrogenase (GAPDH) served as the housekeeping gene which is constitutively expressed in all cells and is mostly unsusceptible to gene regulation. RNase-free water instead of cDNA was used as the negative control to detect unspecific primer bindings and, thus, contaminations. As a positive control a cDNA sample containing a mixture of several isolated native human eccrine sweat glands from different donors was adduced. The thermal profile in the Stratagene Mx3000p cycler composed 1 cycle of 10 min at 95°C for heat activation of the hot start polymerase and 40 cycles of DNA amplification. Amplification cycles were subdivided into DNA denaturation at 95°C for 30 sec, primer annealing at 55°C for 1 min and primer elongation at 72°C for 1 min. Each cycle is terminated by recording of a melting curve with successively increase temperature up to 95°C informing about the specificity of the PCR reaction.
Quantitative analysis of the sample was conducted using the MxPro software and was based on the delta-delta-cycle threshold-method (ΔΔCt). As a first step, Ct value of the target gene, signifying the start of the exponential growth phase, is related to the Ct value of the housekeeping gene GAPDH according to the following formula (4):

$$\Delta Ct = Ct\,(\text{gene of interest}) - Ct\,(\text{housekeeping gene}) \quad (4)$$

Relative gene expression levels of the gene of interest were calculated as $2^{-\Delta Ct}$.
To compare relative gene expressions of different samples ΔΔCt values were calculated according to formula (5) from which relative gene expression levels of, e.g., cell line and native gland could be compared by taking the value of $2^{-\Delta\Delta Ct}$:

$$\Delta\Delta Ct = \Delta Ct\,(\text{sample 1}) - \Delta Ct\,(\text{sample 2}) \quad (5)$$

2.2.5 Histological examinations

From a molecular analytical perspective, quantity of mRNA constitutes no direct indicator for abundance of protein expression due to intermediate regulatory mechanism affecting mRNA translation into protein (Liu et al. 2016b). Therefore, paraffin and frozen sections of native human facial skin specimen, spheroidal 3D sweat gland models, and sweat gland matrix models were prepared and specifically stained with antibodies of sweat gland-associated proteins to examine their structure and the localization and distribution of distinct proteins.

2.2.5.1 Preparation of frozen sections

Tissue specimen and 3D models were placed into cryomolds, slightly frozen using a cryostat and fixated by imbedding in Tissue Freezing Medium. Frozen blocks were kept at -80°C for long-term storage and frozen sections were prepared using the Cryostat SM 1900 when needed. For that, deeply frozen blocks were equilibrated to -30°C, removed from the cryomold and mounted onto specimen stages with Tissue Freezing Medium. Sections of 5-8 µm thickness were prepared, mounted onto Super Frost Plus microscope slides and shortly dried at RT. Slides were then stored at -20°C until used for histological staining.

2.2.5.2 Hematoxylin and eosin staining

Hematoxylin and eosin staining (HE staining) is one of the most common routine methods for staining of histological sections. All staining techniques enable the distinction of various morphological structures within a tissue sample based on their differential reaction with cellular substructures. Hematoxylin and eosin, the two dyestuffs of this technique, also exhibit specific chemical reactions: The naturally occurring hematoxylin colors acidic and basophile structures such as nucleic acids in the nucleus and ribosomes with a deep blue to purple hue. In contrast, synthetically produced eosin stains basic and acidophile structures including proteins and collagen fibers slightly red to pink. So, in a common tissue sample, the cell's nucleus appears deep blue while the cytoplasm and extracellular matrix are displayed with differing hues of red to pink (Fischer et al. 2008; Titford 2009).

Prepared frozen sections were automatically stained using the HistoTek Slide Stainer. Procedure consisted of the following incubation steps: xylol (2 min), pure ethanol (20 sec), 50% ethanol (20 sec), hematoxylin (3.5 min), 70% ethanol (20 sec), ammonium hydroxide ethanol (1.5% / 80%) (20 sec), 95% ethanol (20 sec), eosin (20 sec), 2x pure ethanol (20 sec), xylol (20 sec). All ethanol solutions were prepared in distilled water. Afterwards, stained slides were coated with Cytoseal mounting medium to prevent fading of the color and covered with a cover glass. Morphological features of the samples were inspected using an inverse microscope in bright field mode (BX51) at different magnifications and pictures were taken with a microscope-mounted digital camera (DP71).

2.2.5.3 Immunofluorescence staining

Frozen sections of native human facial skin specimens, *in vitro* 3D, and sweat gland matrix models served to examine the expression and localization of specific proteins therein.
Indirect immunofluorescence (IF) staining is a two-step-process based on the binding of a primary antibody to the target protein as the epitope and specific recognition including binding of this primary antibody by a fluorophore-conjugated secondary antibody. Each secondary antibody is thereby tagged with an individual fluorophore which is stimulated by a distinct wavelength to emit a fluorescence signal. This enables the simultaneous detection of more than one specific protein in one sample (Im et al. 2019).
As a fixation step, prepared frozen sections were incubated in ice-cold acetone for 10 min prior to staining. Slides were air dried and subsequently unspecific binding sites were blocked off by incubation with 10% normal goat serum (NGS) for 1 h at RT to reduce background staining. Incubation with the primary antibody occurred overnight at 4°C in Dako Antibody Diluent in dilutions of the respective antibodies as stated in chapter 2.1.9.1. Negative controls only received Dako Antibody Diluent omitting any primary antibody. Subsequently, sections were washed three times with 1x PBS to remove remaining primary antibody and incubated with the secondary antibody for 45 min at RT. Secondary antibodies were also diluted in Dako Antibody Diluent in the concentrations stated in chapter 2.1.9.2 with 0.1% of 4′,6-diamidino-2-phenylindole (DAPI) added for staining of the cell nuclei. After washing three times in 1x PBS, specimens were coated with Dako Fluorescence Mounting Medium to prevent fading of the fluorescence and mounted with a cover glass.
The presence and location of stained proteins was evaluated using a fluorescence microscope (BX51) at different magnifications with a microscope-mounted digital camera (DP71) after the mounting medium had dried.
Sections of all specimens exclusively incubated with a secondary antibody served as negative controls to establish unspecific background staining of the secondary antibody and for determination of the fluorescence exposure time. Stainings of native facial skin sections were carried along as positive controls.

2.2.6 Experimental procedures for substance screening

Major driver for this project was the development of a cell-based *in vitro* screening approach for identification of alternative AP actives. Core of this procedure was establishment of methods to determine intracellular ion levels as indicators for *in vitro* sweat simulation. As a prerequisite, however, sufficient viability of eccrine sweat gland cells under substance treatment was ascertained.
For all *in vitro* experiments conducted within this work and involving new actives primary eccrine sweat gland cells from one donor (15-24) were used. This prohibited the occurrence of interindividual variations throughout the measurements. More stringent, primary cells in passage five or six were applied in these assays to further minimize possible age-related variations. To assess the functional, physiological behavior of generated immortalized duct cells, they were also employed in these *in vitro* tests together with their parental cells (19-01) as a reference.

2.2.6.1 Cell viability assay

To ensure the reliability of data in measurements of ion fluxes, cell viability had to be sufficiently high to prevent unspecific cell reactions. In the current project, a cell viability of 80% was set as the minimum prerequisite when studying the physiological influence of a substance treatment.

Conventional cytotoxicity assays are based on measurement of exclusion of vital dyes, of intracellular protein release or metabolic activities of the cells. The latter principle includes the often used colorimetric MTS(T) assay with the employment of tetrazolium salts (Méry et al. 2017). Relying on the enzymatic activity of mitochondria, the NADPH-dependent dehydrogenase in living cells converts the tetrazolium salt (e.g. MTS) into a water-soluble formazan dye (Barltrop et al. 1991) which is easily detectable due to its specific absorbance at 490 nm. Thus, the level of produced formazan is directly proportional to the number of viable cells (Capasso et al. 2003).

In this work, test substances were analyzed *in vitro* regarding their cytotoxic effects on primary human eccrine sweat gland cells as well as on immortalized duct cell clones. For that, cells were seeded into transparent, flat bottom 96-well plates 2-3 days prior to assay performance (refer to chapter 2.2.1.2). Blanks remained without cells. At the day of the experiment, the culture medium was replaced by test substance containing DMEM without phenol red (further denoted only as DMEM) as phenol red would interfere in the subsequent photometric measurement. The untreated control received plain DMEM. Additionally, the pH of each test solution and DMEM were determined with a calibrated electrical pH meter. After 1 h of incubation with different concentrations of the test substance at 37°C, cells were washed once with DMEM to remove remaining substance. Afterwards, cells were again incubated for 1 h at 37°C with 100 µl of MTS-solution followed by quantitative photometric measurement of the produced formazan at 490 nm using the microplate reader Tecan Spark® with the SparkControl software. Treatments were determined in sextuplet. For quantification purposes, measured individual optical densities (OD) were corrected by the mean of the respective blanks. Blank-corrected mean intensities were then related to the mean intensity of untreated cells according to formula (6). Untreated was set to represent 100% viability.

$$(6) \qquad V(\text{substance})\ [\%] = \frac{(\overline{x}_{\text{substance}})}{(\overline{x}_{\text{untreated}})} \cdot 100\%$$

V(substance) – cell viability in % after incubation with the test substance
$\overline{x}_{\text{substance1}}$ – blank-corrected mean absorbance intensity of cells incubated with the substance
$\overline{x}_{\text{untreated}}$ - blank-corrected mean absorbance intensity of untreated control cells

2.2.6.2 Determination of intracellular Ca^{2+}-, Na^{+}- and K^{+}-ions

During sweating various ion channels, transporters and receptors are activated within the cells to produce the primary isotonic sweat in the coil and to reabsorb ions from the sweat while passing the duct, resulting in a hypotonic sweat output (Wilke et al. 2007). Apart from the anion chloride (Cl^{-}), especially calcium (Ca^{2+}), sodium (Na^{+}) and potassium (K^{+}) cations contribute to the ion conductivity within cells and across cell membranes (Sonner et al. 2015). While Ca^{2+} release from intracellular stores is the main electrophysiological regulator in secretory glands

(Bovell 2015), Na^+ and K^+ are the major cations found in the primary sweat (Sato et al. 1989a) (for detailed mechanistic explanations refer to 1.2.2.4). Therefore, the relative intracellular concentrations of these three cations (further designated $[Ca^{2+}]_i$, $[Na^+]_i$ and $[K^+]_i$) and their specific change upon treatment with different substances were considered suitable indicators for *in vitro* sweat simulation and, thus, were taken as the core of herein established *in vitro* AP screening procedure. Development of such a sufficiently robust and reliable *in vitro* test system provided an ideal basis for gaining a better mechanistical understanding of sweating and identifying new actives as alternative AP (Welzel et al. 2021).

Fluorometric determination of the relative intracellular ion levels was achieved by loading the sweat gland cells with cation-sensitive fluorescence dyes - each one specific for one cation of interest. As a Ca^{2+} indicator Fluo-4 was chosen, while Sodium Green tetraacetate detected Na^+ and PBFI is sensitive for K^+. These fluorescence indicators were brought into cells in their ion-insensitive from in which acetoxy methyl ester (AM) groups obscure present charges. The uncharged forms are membrane-permeable and get into the cytoplasm where ubiquitous esterases liberate the respective ion-sensitive, charged indicator by cleaving off the AM groups (de-esterification) as soon as getting in contact with the dyes. As charged molecules cross the membrane less readily they accumulate inside the cells (Bird et al. 2008). Supplementation of the dye-loading solution with the surfactant Pluronic F-125 dissolved in DMSO enhances loading efficiency even further (Hamad et al. 2015). As a measuring principle, the respective indicator reversibly forms a fluorescent complex with its specific cation (Meuwis et al. 1995) whereby the fluorescence intensity increases with increasing concentration of the respective ion (Despa et al. 2000).
To implement the AP test procedure, standard assay protocols for measurement of these cations were available but had to be adopted for the applicability in eccrine sweat gland cells. For experiments with monolayer cultures, primary and immortalized eccrine sweat gland cells were seeded into black 96-well plates with flat, clear bottoms (refer to 2.2.1.2). Assays were performed in indicator-free DMEM. On the day of experiment, nearly confluent cells were washed twice with DMEM to remove remaining serum as this might inhibit loading of the dyes. Cells were then incubated for 4 h at RT in the dark with the dye-loading solution containing probenecid, Pluronic F-125 and one of the fluorescence indicators (**Fig 2.5a**). Probenecid was added to prohibited leakage of the dye by blocking organic anion transporters (Steinberg et al. 1987; Malgaroli et al. 1987). After loading of the dye, cells were washed three times with DMEM to remove extracellularly remaining indictor. De-esterification of the AM esters occurred during 1.5 h of incubation in probenecid supplemented DMEM at RT in the dark and resulted in intracellular release of cation-sensitive indicators. Fluorescence measurements were performed with the Spark multiplate reader and the SparkControl software. Prior to treatment with different test substances the baseline fluorescence intensity (F_0) was recorded as the mean of four cycles of 1 min each (**Fig 2.5b**). Determination of F_0 ensured adjusting for cell confluency and loading efficacy of the cells. Intensities of Fluo-4 and Sodium Green were measured with an excitation wavelength of 485 nm and an emission wavelength of 535 nm, while PBFI intensity was determined with excitation at 360 nm and emission of 505 nm. For substance testing, equal volumes of test substances diluted in DMEM were applied and after a 4 min incubation (4 cycles) 10 µM of the stimulant carbachol (in DMEM) was added.

Untreated controls received DMEM to compensate for volumetric changes: Resulting fluorescence intensities (F) were determined in 20 cycles of 1 min keeping the same instrument parameters as for F_0. Using kinetic measurements fluorescence values over a longer time span were recorded. This was especially important as the time of onset of action of the test substances was unknown.

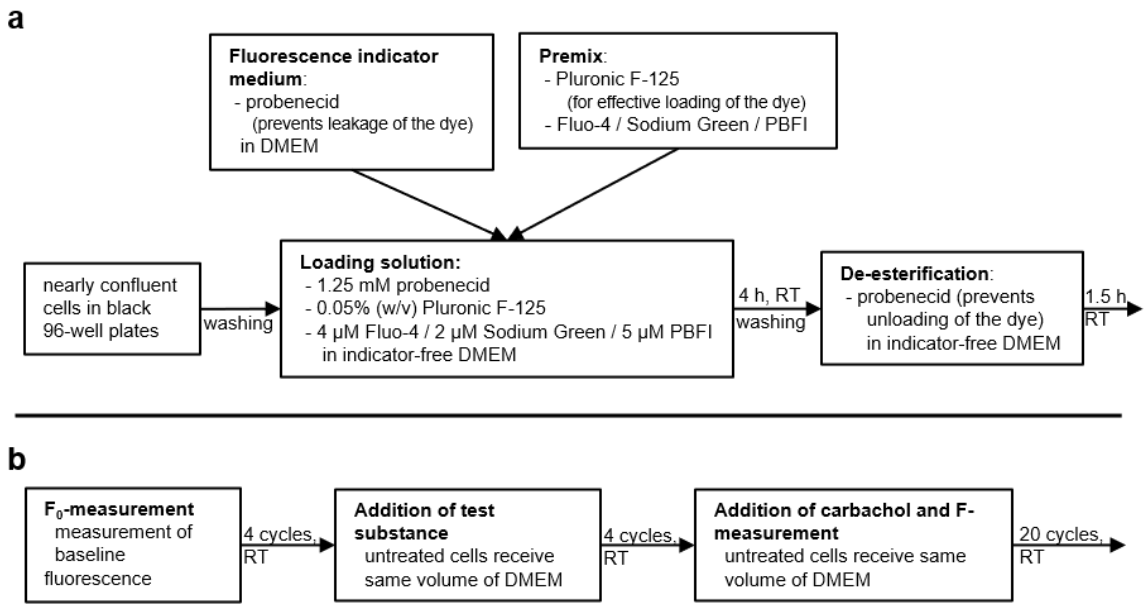

Fig 2.5: Experimental workflow for determination of changes of intracellular cations.
Effective loading of cells with the respective fluorescence indicator was achieved by supplementation of indicator-free DMEM with probenecid and Pluronic F-125 and occurred at room temperature (RT) (**a**). De-esterification liberated the ion-sensitive, fluorescent dye. Following fluorescence measurement was standardized but excitation and emission wavelength were specific for each indicator (**b**). Test substances were diluted in indicator-free DMEM. One measurement cycle had a time frame of 1 min.

Relative changes in the fluorescence intensities upon treatment with the test substance were calculated relative to F_0 as means of sextuple replicates according to formula (7):

$$(7) \qquad F_{rel} = \frac{(F_x - blank_{Fx})}{(F_0 - blank_{F0})}$$

F_{rel} – relative change in fluorescence intensity; F_x – fluorescence intensity at timepoint x after addition of stimulant; $blank_{Fx}$ – fluorescence intensity of substance-treated cell-blank; F_0 – baseline fluorescence intensity determined as mean of four measurements; $blank_{F0}$ – fluorescence intensity of blanks in the F_0-measurement

Calculated values were given as a function of time and the ion changing potential of a substance was summed up as the area under the curve (AUC) according to formula (8).

$$(8) \qquad AUC = \sum_{i=1}^{n} [y_i \cdot (x_i - x_{i-1})] - [(y_i - y_{i-1}) \cdot (x_i - x_{i-1})]$$

AUC – area under the curve; timepoint x_i, y_i – relative fluorescence intensity at timepoint x_i

Treatments were determined in sextuple replicates with two cell-blanks and are stated as relative intracellular ion levels with the AUC of untreated control set to 100%.

2.2.6.3 Determination of intracellular Cl^--ions

Apart from the mentioned cations Cl^- is the most important anion in the sweat process, both, in the secretory portion and the reabsorption in the gland duct (refer to 1.2.2.4). Measuring its intracellular concentration ($[Cl^-]_i$) and its changes upon treatment therefore complemented the *in vitro* screening procedure for alternative AP.

Contrary to the measurement principle of cations, the fluorescence intensity of the halide indicator SPQ decreases with an increasing concentration of Cl^-. Upon reversible binding of a Cl^- ion the excited fluorescence molecule returns to its non-fluorescent ground state. This process is called dynamic quenching (Arosio and Ratto 2014). Due to its hydrophilicity SPQ poorly permeates the cell membrane and, thus, different loading techniques, solutions, and times have been proposed. Successful and effective dye-loading was achieved by transient permeabilization of the cell membrane when cells were exposed to a hypotonic solution. As this procedure left membrane integrity and transepithelial characteristics of the cells unaffected, this approach was applied in this work (Ram and Kirk 1989; Chao et al. 1989; Chao et al. 1990).

Seeding and treatment with test substances including blanks was the same as described for the cation measurement (refer to 2.2.6.2). Loading of the dye, however, was different in that cells were washed with HEPES buffer and incubated for 30 min at 37°C with 5 mM of SPQ in a hypotonic solution - a 1:1 mixture of aqua dest.: HEPES buffer (**Fig 2.6a**). The dye-loading solution was replaced by HEPES buffer and cells reconstituted from the hypotonic shock for 15 min at 37°C. Prior to measurement of F_0 cells were extensively washed with HEPES buffer to remove extracellularly remaining dye. Following substance application and fluorescence measurements in the microplate reader were conducted as for the cations, except for adjusted wavelengths for excitation of 360 nm and emission at 465 nm (**Fig 2.6b**).

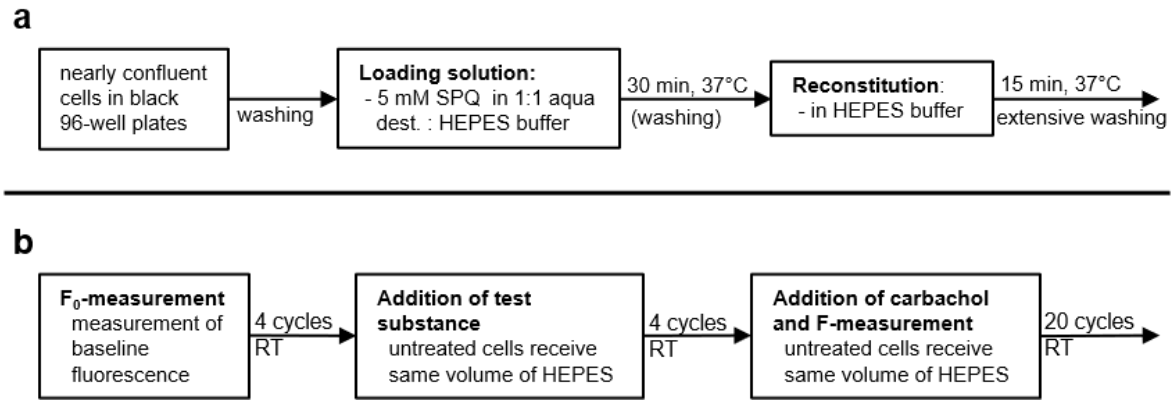

Fig 2.6: Experimental workflow for determination of intracellular chloride.
Effective loading of cells with the fluorescence indicator SPQ was achieved by hypotonic shock rendering the cell membrane transiently permeable (**a**). Following fluorescence measurement was also standardized but excitation occurred at 360 nm and emission was recorded at 465 nm (**b**). Test substances were diluted in HEPES buffer. One measurement cycle had a time frame of 1 min.

Due to quenching of the fluorescence with increasing $[Cl^-]_i$, relative changes in the intensities were calculated with an adapted formula (7) in which numerator and denominator were interchanged. See formula (9):

$$(9) \qquad F_{rel} = \frac{(F_0 - blank_{F0})}{(F_x - blank_{Fx})}$$

Calculation of AUC and evaluations were performed according to formula (8) (refer to 2.2.6.2).

2.2.7 *In vivo* sweat reduction studies

Substances identified as potential sweating inhibitors in *in vitro* screenings were further characterized in *in vivo* sweat reduction studies on the back of volunteers. These studies were performed in collaboration with the contracted research institute proDERM in Hamburg, Germany, and gathered data were placed at the disposal for comparison with generated and herein presented *in vitro* screening results.

In general, procedure of *in vivo* studies was based on a published protocol (Brandt et al. 2008). Prior to begin of the *in vivo* study, test samples were assessed for their safety and approved for application under defined test conditions by internal toxicologists to ensure safety of human study participants. The recommendations of the current World Medical Association's Declaration of Helsinki (World Medical Association 1964) and the ICH Good Clinical and Research practices (GCP) (World Health Organization 2005) were observed as applicable to a non-drug study. All volunteers were informed about the objective and possible risks of the study and gave their informed written consent prior to initiation of the study.

For each study, a panel of 18 to 20 female volunteers aging between 18 and 70 years was selected. Three days prior to the first substance application and during the whole study participants were advised to refrain from applying neither leave-on cosmetic products nor detergents on the test area on the back. 16 measurement spots (size 4 cm x 5 cm) were defined on the back and arranged as 8 rows of two contralateral columns. Contralateral positioning of treated and respective untreated control area ensured the best comparability and reduced variations as the secreted amount of sweat is depended on the horizontal position on the back. At each test site 35 or 75 µl of the test substance were applied by a technician and allowed to dry for 5 min. Control spots remained untreated. Test areas were covered with an occlusive, non-absorbing plastic foil attached with Fixomull® for 2 h simulating the humid situation in the human axillae. This procedure was repeated on four consecutive days. 2, 6 or 24 h after the last treatment, gravimetrical determination of the sweat amount took place. For that, pre-weight cotton pads were placed onto the treated areas after careful cleaning of the back with water. Study participants were stimulated to sweat in a sauna at 80°C for 10-15 min while in a prone position until visible sweat drops appeared. The locally produced sweat was absorbed, the pads collected with a tweezer when the volunteers left the sauna, and the amount of secreted sweat immediately determined gravimetrically. Comparison of the treated with the respective untreated control site allowed for quantification of sweat-reducing efficiency of the respective test substance.

In all *in vivo* studies, an aqueous solution of the well-known AP ingredient ACH served as a reference eliciting a quite constant sweat reduction across all studies.

2.2.8 Statistical analysis

2.2.8.1 *In vitro* experiments

Data represent mean values ± SD. Graphical representation of the results was achieved with GraphPad Prism version 6.0. Single datapoints were considered outliers when lying outside the range of mean ± 4 times the standard deviation of all relevant datapoints. Statistical analysis was performed with XRealStat Excel Plug-In and consisted of determination of normal distribution of the results and thereon based significance calculation. Data with normal distribution were analyzed by One-way analysis of variance (ANOVA) with Bonferroni correction followed by Tukey's multiple comparisons test ($\alpha = 0.05$). Non-normal distributed data were tested for significance using Kruskal-Wallis test followed by Dunn's multiple comparison test ($\alpha = 0.05$). In both cases, differences were considered statistically significant with $p<0.05$ (*), $p<0.001$ (**) and $p<0.0001$ (***).

2.2.8.2 *In vivo* studies

The relative sweat reduction of the test substance was calculated as the percentage quotient of the gravimetrical difference between the treated and the respective untreated control spot. For every test substance the mean relative sweat reduction was stated as percentage of the untreated control. Study participants showing a sweat reduction of less than 0% at the sites treated with the benchmark ACH were considered non-responders and their results were completely excluded from the study evaluation. Additionally, outlier values were defined as values outside mean ± 2.5 times the standard deviation of all responders. These single values were also excluded from data analysis. Stated data represent mean sweat reduction values ± 95% confidence intervals. Sweat-reducing effect was termed effective and significant if the lower 95% confidence interval excluded zero.

3 Results

3.1 Screening for antiperspirant actives

Between the 1960s and today barely any solid knowledge was added to identifying the actual mechanism of action of aluminum-based AP actives. Early on, there was a discussion between physical blockage of sweat ducts resulting in obstruction of sweat output versus physiological effects on sweat glands cells triggering altered sweat secretion or reabsorption (Papa and Kligman 1967; Gordon and Maibach 1968; Quatrale et al. 1981; McWilliams et al. 1987). Today, the first theory of plug formation is well scrutinized and widely approved (Swaile et al. 2012; Bretagne et al. 2017; Scientific Committee on Consumer Safety 2019), while the latter is only scarcely mentioned in literature (Scholes et al. 1978). Up to now, research on possible cell-based, physiological effects of ACH has not been focused and remains to be proven.
Taking this idea further, a new *in vitro* testing strategy was developed here focusing on physiological, cellular changes induced by substance application to investigate the sweating mechanism in more detail and to search for alternative AP actives. Employing this approach two distinct classes of substances were identified showing a distinct pattern of *in vitro* physiologic reactions. Subsequently, their sweat-reducing potential was verified *in vivo*.

Prior to *in vitro* testing of physiological effects of the substances, their non-cytotoxic concentration was determined by application on isolated, cultured eccrine sweat gland monolayer cells (2D) and measurement of their cell viability. Proper AP testing strategy then consisted of treating 2D eccrine sweat gland co-culture cells (mixture of predominantly coil with duct cells) with suitable substance concentrations and determination of evoked relative changes in intracellular ion concentrations of Ca^{2+}, K^+, Na^+ and Cl^- by using ion-specific fluorescence dyes. Taking all ion measurements together, obtained ion profiles were substance-specific and revealed important information about their mechanism of action, including the one of ACH.

3.1.1 Chloride-containing substances

3.1.1.1 Impact of concentration on *in vitro* ion profile

ACH represents the aluminum salt predominantly found in cosmetic AP products today (Bundesinstitut für Risikobewertung 2019b, 2019a; Scientific Committee on Consumer Safety 2019). To address possible physiological effects of ACH on eccrine sweat gland cells, its impact on intracellular ion levels was extensively scrutinized in this work. In the following, ACH was used as the benchmark in *in vivo* sweat reduction studies due to its well-known sweat reducing properties.
When applying a 1% active substance (AS) (w/w) aqueous solution of ACH (prepared from a 10% AS (w/w) stock solution by dilution in DMEM) to 2D eccrine sweat gland co-culture cells, a distinct ion pattern was elicited characterized by markedly reduced $[K^+]_i$ and $[Na^+]_i$ whereas $[Cl^-]_i$ was slightly elevated (Fig 3.1). No changes were observed for the second messenger $[Ca^{2+}]_i$. In accordance with well-established plug forming properties in the native eccrine gland, application of ACH solutions to 2D co-culture cells also left a thin gelatinous layer on the cells.

In contrast, application of the muscarinic agonist carbachol at a concentration of 10 µM exerted no significant changes of mentioned ions (see Supplemental **Fig 6.2**) as was already described for this *in vitro* test system before (Welzel 2017).
However, results of affected intracellular ion equilibria after treatment with ACH are first indications for this substance to possess an additional physiological effect on the cellular level apart from plug formation and physical blockage of the gland.

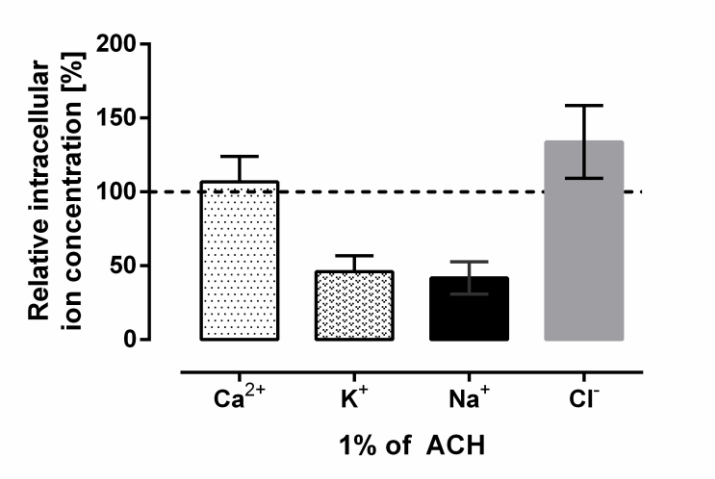

Fig 3.1: *In vitro* ion profile of a 1% solution of ACH.
Depicted are relative intracellular ion concentrations of cations calcium $[Ca^{2+}]_i$, potassium $[K^+]_i$, and sodium $[Na^+]_i$ as well as of the anion chloride $[Cl^-]_i$ evoked by a DMEM-based, aqueous solution with 1% AS (w/w) of aluminum chlorohydrate (ACH). Nearly confluent 2D eccrine sweat gland co-culture cells were treated and resulting changes of fluorescence intensities measured with a microplate reader reflecting fluctuation of intracellular ion levels relative to an untreated control which was set as 100%. Data represent mean ± SD of one (Ca^{2+} and K^+) or three (Na^+ and Cl^-) experiments. Modified from Welzel et al. 2021.

Uncovering this effect, different concentrations of ACH and other Cl^--containing substances were tested for their impact on intracellular ion equilibria in eccrine sweat gland coil and duct co-cultures (**Fig 3.2**). Of note, the following investigations with Cl^--containing substances focused on the measurement of intracellular changes of Na^+ and Cl^- as those ions were revealed to be most important for determination of effects and their magnitude. Respective measured values are summarized in **Tab 3.1** at the end of chapter 3.1.1.3 on page 62.
With increasing concentrations of ACH, $[Na^+]_i$ decreased gradually down to a level of 42% (Fig 3.2a). There was a significant impact measurable down to a concentration of 0.125% (w/w) of ACH resulting in a relative Na^+ level of 69%, while next lower concentration of 0.0625% exerted no changes in neither $[Na^+]_i$ nor $[Cl^-]_i$. Generally, alterations in $[Cl^-]_i$ were not as continuous as those of $[Na^+]_i$. Therefore, significant elevations of $[Cl^-]_i$ with values higher than 140% were detected for concentrations starting from 0.25% upwards, without a clear concentration-dependence as seen for $[Na^+]_i$. As ACH creates an acidic pH in aqueous solutions, this acidity and its chloride content were considered essential for triggered effects.
Based on these observations, various other chemical compounds from different substance classes were screened. Inspired by published results stating flocculating amine-bearing aqueous polymer solutions as effective sweat-reducing agents (Lemoine and Beau 2005b, 2005a), a specific group of substances amines, or more precisely here ammonium chlorides,

were further investigated. This group consisted of commercially available raw material solutions containing either polyethylene imine (PEI), or polyvinyl amine (PVAm), or dimethyl piperazine (DMP) as the chemical lead substance. Aqueous stock solutions of these raw materials were adjusted to an acidic pH value of 3.5 with hydrochloric acid (HCl) (stock concentrations: PEI-HCl 5% (AS) (w/w), PVAm-HCl 10% TelQuel (TQ) (w/w) (roughly 3% AS), DMP-HCl 3% TQ (w/w)), which transformed aminic lead substances into ammonium chlorides and, thus, introduced a certain amount of Cl^-. Those ammonium chloride solutions were then comparable to ACH solutions in that all of them provided a certain amount of Cl^-. *In vitro* testing of DMEM-based dilutions of these stock solutions revealed concentration-dependent decreases of $[Na^+]_i$ accompanied by elevations of $[Cl^-]_i$ (Fig 3.2b-d) - similar to what was observed for ACH. However, no precipitation or flocculation of these ammonium chloride solutions was detected.

For the highest concentration of 0.5% AS (w/w) of PEI-HCl, significantly reduced $[Na^+]_i$ down to a level of 23% and increased $[Cl^-]_i$ up to over 200% were detected (Fig 3.2b). Overall, recorded changes in intracellular ion levels were significant down to a concentration of 0.1% AS (w/w).

Similarly, treatment with PVAm-HCl resulted in significantly diminished $[Na^+]_i$ down to a concentration of 0.0625% TQ (w/w), whereas significantly elevated $[Cl^-]_i$ was observed down to 0.125% TQ (w/w) (Fig 3.2c). The highest concentration tested (0.5% TQ (w/w)) exerted a minimum $[Na^+]_i$ value of 50% while concurrently increasing $[Cl^-]_i$ to a level of 116%.

The third tested substance, DMP-HCl, reduced $[Na^+]_i$ significantly down to a concentration of 0.25% TQ (w/w), while its increasing effect on $[Cl^-]_i$ was significant down to a substance concentration of 0.125% TQ (w/w) (Fig 3.2d). Here again, the highest concentration applied (0.5% TQ (w/w)) yielded diminished $[Na^+]_i$ of 45% and concomitantly increasing $[Cl^-]_i$ up to 135%.

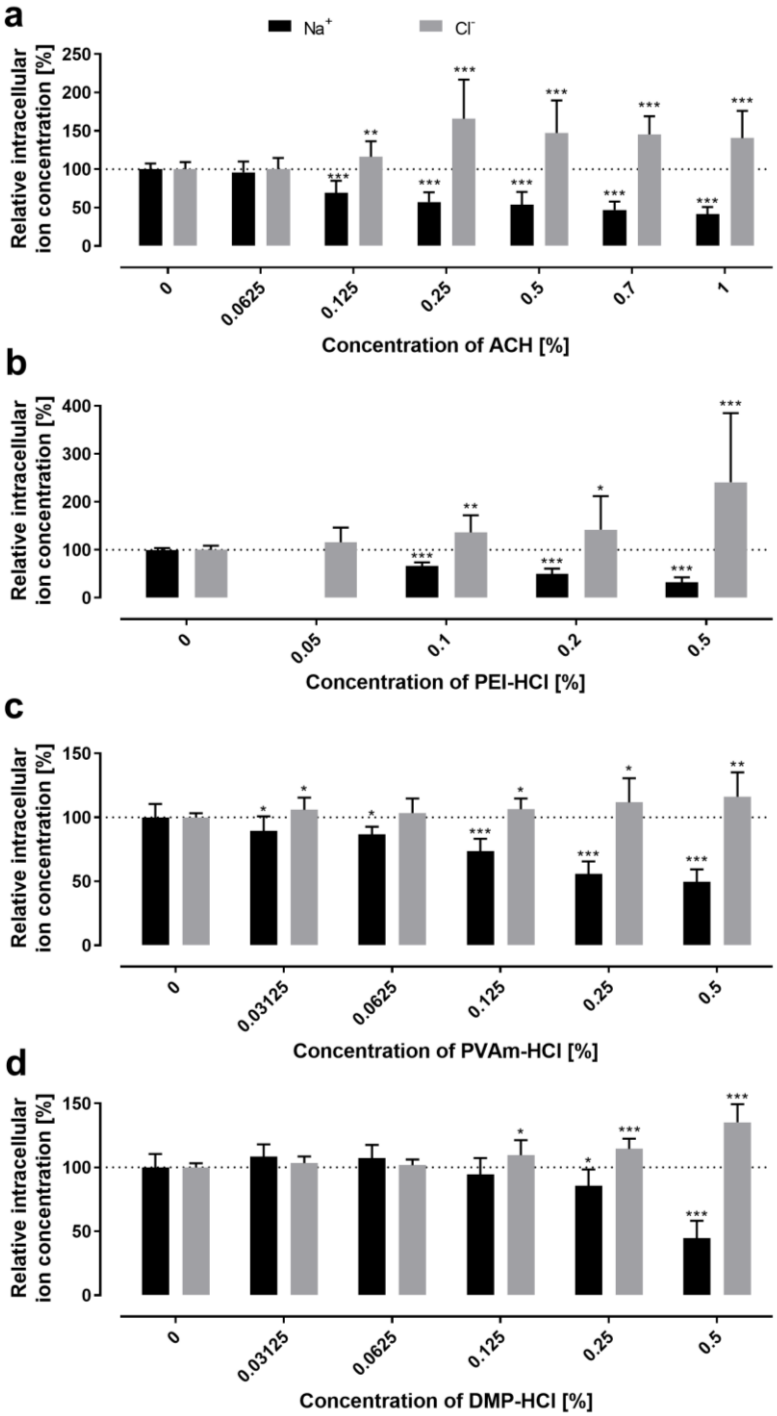

Fig 3.2: Concentration-dependent effect of chloride-containing substance on relative intracellular sodium and chloride concentrations.
Depicted are relative intracellular concentrations of sodium $[Na^+]_i$ and chloride $[Cl^-]_i$ ions in monolayer eccrine sweat gland co-culture cells after treatment with different concentrations of Cl^--containing substances. DMEM-based, aqueous solutions of (**a**) aluminum chlorohydrate (ACH), (**b**) polyethylene imine adjusted to pH 3.5 with hydrochloric acid (PEI-HCl), (**c**) PVAm adjusted to pH 3.5 with hydrochloric acid (PVAm-HCl), (**d**) dimethyl piperazine adjusted to pH 3.5 with hydrochloric acid (DMP-HCl) were diluted to stated concentrations with DMEM. Nearly confluent cells were treated and resulting changes of fluorescence intensities measured with a microplate reader reflecting fluctuation of intracellular ion levels relative to an untreated control (0%) which was set as 100%. Data represent mean ± SD of three experiments performed in sextuple replicates (Kruskal-Wallis test with Dunn's multiple comparison test (Cl^- values of ACH, PEI-HCl, and PVAm-HCl) or one-way ANOVA with Tukey's multiple comparison test (all Na^+ values and Cl^- value of DMP-HCl); */**/*** statistically significant difference to untreated with $p<0.05/0.001/0.0001$). Data are summarized in Tab 3.1 on page 62. Part a and b taken and modified from Welzel et al. 2021.

Above stated results outline the potency of ammonium chloride solutions to alter the *in vitro* ion profile in cultured eccrine sweat gland cells in a concentration dependent manner. To elaborate this effect and the mechanism behind in more detail, additional experiments were performed with PEI-HCl. Therefore, 5% AS (w/w) stock solutions were adjusted to pH 3.5, 4.5, 5.5, and 7.5 with HCl, respectively, with each solution requiring addition of a distinct amount of HCl. Afterwards, each of the four separate stock solution was diluted with DMEM to contain a final concentration of PEI-HCl of 0.2% AS (w/w). These dilutions were then tested for their effect on intracellular ion levels revealing similar impacts with only slight differences in magnitude (**Fig 3.3**). Especially for $[Na^+]_i$ proportional pH-dependency was observed with lower initial pH values evoking stronger reduction of $[Na^+]_i$ and effects ranging between 49% and 58% for pH 3.5 and 7.5, respectively. However, only differences in $[Na^+]_i$ of pH 3.5, pH 4.5, and pH 5.5, respectively towards pH 7.5 were significant. In contrast, $[Cl^-]_i$ was elevated in all treatments reaching values of 132% to 162% with a tendency of higher $[Cl^-]_i$ with lower pH values of stock solutions. However, the impact on $[Cl^-]_i$ was not coherent with adjusted pH of the stock solution. Data are also summarized in Tab 3.1 on page 62.

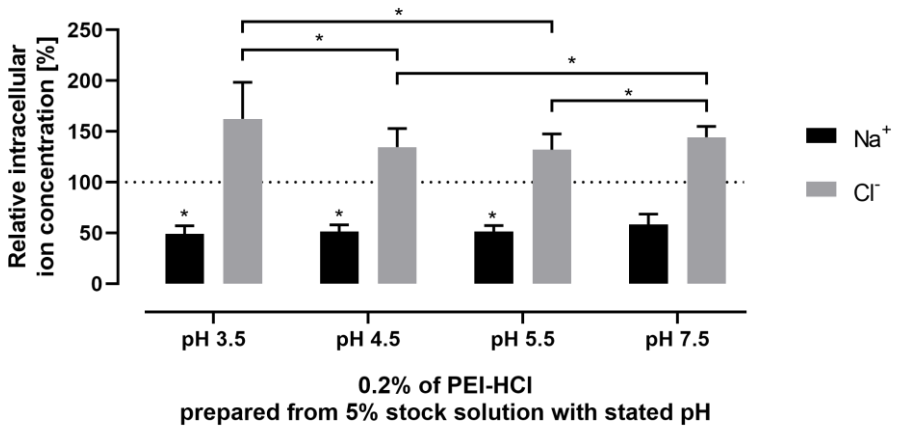

Fig 3.3: Influence of pH of the stock solution on relative intracellular sodium concentrations. Depicted are relative intracellular concentrations of sodium $[Na^+]_i$ and chloride ions $[Cl^-]_i$ determined in monolayer eccrine sweat gland co-culture cells after treatment with 0.2% AS (w/w) dilutions prepared from 5% AS (w/w) stock solutions with different, stated pH values. pH of stocks was adjusted with HCl to 3.5, 4.5, 5.5, and 7.5 respectively, and those solutions were diluted to stated concentrations with DMEM. Nearly confluent 2D eccrine sweat gland co-culture cells were treated and resulting changes of fluorescence intensities were measured with a microplate reader reflecting fluctuation of intracellular ion levels relative to an untreated control which was set as 100%. Data represent mean ± SD of three experiments performed in sextuple replicates (Kruskal-Wallis test with Dunn's multiple comparison test (Cl^- values) or one-way ANOVA with Tukey's multiple comparison test (Na^+ values); * statistically significant difference with $p<0.05$). Data are summarized in Tab 3.1 on page 62. Taken and modified from Welzel et al. 2021.

Of note, all examined Cl^--containing substances were shown to reduce $[Na^+]_i$ while simultaneously increasing $[Cl^-]_i$ in monolayers of eccrine sweat gland co-culture cells in a concentration-dependent manner. However, due to different concentrations of the stock solutions (also being AS and TQ) and the requirement of distinct amounts of HCl to adjust their pH, a direct comparison of efficacy between the different substances was not feasible. Especially fitting of ACH was challenging as no HCl was added to it. Therefore, a common basis needed to be established for inter-substance comparison of effects.

3.1.1.2 Effect of the amount of chloride

For initial tests, all stock solutions of the amines were adjusted to pH 3.5 with HCl for which each solution required a specific amount of HCl. Likewise, stock solutions of PEI adjusted to different pH values consumed a specific amount of HCl to reach stated pH values. ACH, in contrast, naturally contains a certain amount of Cl^- due to its chemical composition. Therefore, the parameter of chloride equivalent was established, denoting the amount of Cl^- added by the substances to prepared dilutions. It served as the basis for comparison of the different substances and equals the amount of extra Cl^- added to monolayer eccrine sweat gland co-culture cells per treatment. Thereby, the amount of Cl^- in a 50% AS (w/w) ACH solution is specified by the supplier to lie between 7.9 and 8.4% (w/w) and therefore, mean value of 8.15% (w/w) was used for calculation of the chloride equivalent of ACH. For the other Cl^--containing substances the amount of HCl added to stock solutions to reach a pH of 3.5 was taken as the basis for computation of this parameter.
For correlation with chloride equivalents $[Na^+]_i$ was selected since effects on this intracellular feature could be measured more precisely and showed a stronger concentration-dependency. Strikingly, plotting those recorded $[Na^+]_i$ versus calculated chloride equivalents revealed decreasing Na^+ levels with increasing amounts of Cl^- for all tested substances (**Fig 3.4** and Tab 3.1 on page 62).
Having a closer look on the exact position of the data in the diagram two data sets were identified: On the one hand, datapoints of ACH (circles), PEI-HCl (triangles), and PVAm-HCl (squares) lay close together while, on the other hand, those of DMP-HCl (diamonds) ranged above. Thus, dilutions of DMP-HCl showed higher $[Na^+]_i$ for similar chloride equivalents. Data obtained with different PEI-HCl stock solutions were pooled with those of different PEI-HCl concentrations and are all depicted as triangular symbols.

Taken together, introduction of the parameter of chloride equivalent facilitated comparison of effects of the different substances and revealed two data clusters: datapoints of DMP-HCl ranged above those of ACH, PEI-HCl, and PVAm-HCl. Based on these observations, chloride equivalent of the applied dilution has a marked influence on evoked $[Na^+]_i$. Yet, this comparison excludes from consideration slight differences in pH of tested dilutions which requires for a more detailed assessment.

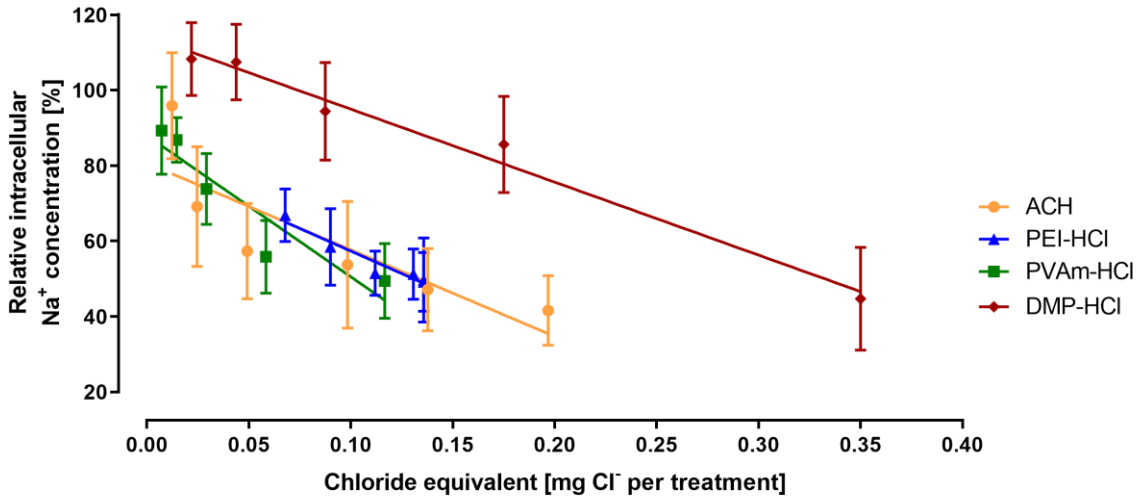

Fig 3.4: Effect of the chloride equivalent on relative intracellular sodium concentrations.
Relative intracellular sodium concentrations $[Na^+]_i$ were determined in nearly confluent monolayer eccrine sweat gland co-culture cells treated with different substances and concentrations thereof. Application of DMEM-based substance solutions resulted in changes of fluorescence intensities which were measured with a microplate reader reflecting fluctuation of intracellular Na^+ levels relative to an untreated control which was set as 100%. The chloride equivalent, denoting the amount of chloride contained in each treatment solution, was calculated, and is plotted on the abscissa instead of applied substance concentrations. Note the clustering of datapoints obtained with Aluminum chlorohydrate (ACH, circles), polyethylene imine hydrochloride solution (PEI-HCl, triangles), and polyvinyl amin hydrochloride solutions (PVAm-HCl, squares) below those of dimethyl piperazine hydrochloride solutions (DMP-HCl, diamonds). Data represent mean ± SD of three experiments performed in sextuple replicates. Data are summarized in Tab 3.1 on page 62.

3.1.1.3 Influence of pH

Several studies investigated the influence of extracellular changes of pH on its intracellular regulation and the mechanisms involved in different cell types (Bischof et al. 1996; Yatani et al. 1984). Due to these known influence of external pH on cellular ions, especially Na^+, effect of the acidity of tested dilutions was further examined.

Although stock solutions were diluted in bicarbonate buffered DMEM addition of the substances altered the physiological pH of the medium towards slightly more acidic values due to presence of HCl. To investigate the impact of pH on herein focused ion levels, obtained $[Na^+]_i$ were plotted against respective pH values of prepared dilutions (**Fig 3.5** and Tab 3.1 on page 62). Again, changes in $[Na^+]_i$ were taken into account as above stated results indicate $[Na^+]_i$ to yield more reliable results.

Generally, $[Na^+]_i$ decreased with lower pH values. Comparable to the diagram of $[Na^+]_i$ versus chloride equivalent distinct positioning of datapoints was discernible where those of ACH, PEI-HCl, and PVAm-HCl lay close together while datapoints of DMP-HCl ranged above.

As all those test solutions contained a certain amount of Cl^-, DMEM was adjusted to different pH values with glycolic acid to investigate the effect of pure pH changes without contribution of additional Cl^-. Remarkably, datapoints of glycolic acid dilutions ranged close to those of DMP-HCl. Furthermore, effect of plain DMEM with a physiological pH of 7.4 served as the untreated control having a set $[Na^+]_i$ of 100% (cross). Like glycolic acid, this datapoint coincided with those of DMP-HCl.

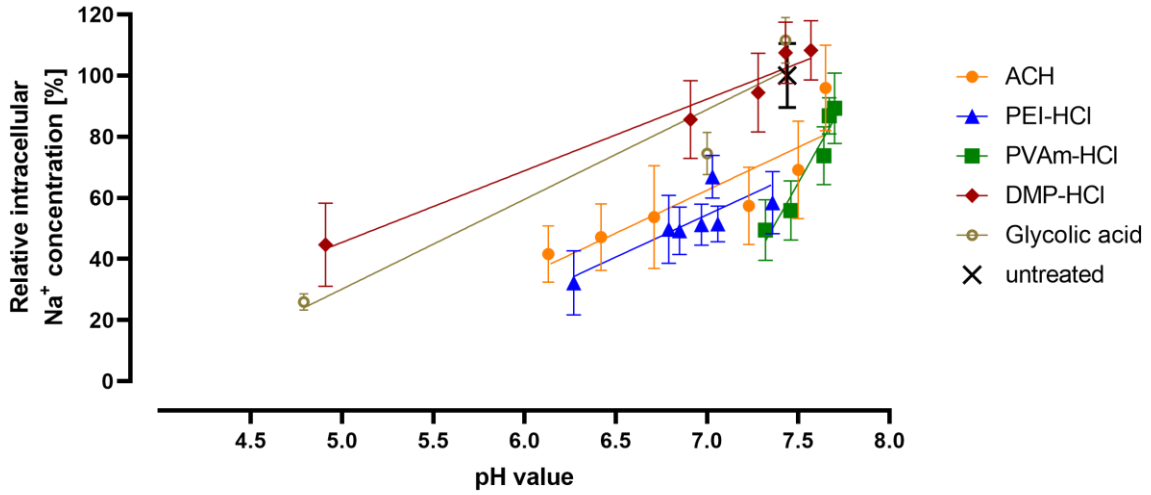

Fig 3.5: Influence of pH on intracellular sodium concentrations.
Depicted are pH values of substance dilutions prepared in bicarbonate buffered DMEM and resulting relative intracellular sodium concentrations measured as changes of fluorescence intensities in eccrine sweat gland monolayer co-culture cells as obtained with a microplate reader. pH values were measured once with an electrical pH meter. Untreated control received plain DMEM with a physiological pH of 7.4 and its fluorescence signal was set as 100% (cross). Filled circles represent datapoints of various dilutions of Aluminum chlorohydrate (ACH) while triangles reflect those of polyethylene imine (PEI-HCl), polyvinyl amine dilutions (PVAm-HCl) are depicted as squares, and dimethyl piperazine values (DMP-HCl) are shown as diamonds. Data are mean ± SD of three independent experiments performed in sextuple replicates. Dilutions of glycolic acid represent pH controls without addition of chloride ions (hollow circles) and data reflecting mean ± SD of one representative experiment performed in sextuple replicates. Data are summarized in Tab 3.1 on page 62.

Given the demonstrated linkage between pH and measured $[Na^+]_i$, the question remains whether and in how far the chloride equivalent impacts the pH of the dilution. To scrutinize this aspect, pH value of each tested dilution was plotted against the respective chloride equivalent (**Fig 3.6** and Tab 3.1 on page 62).
Overall, pH slightly decreased with increasing chloride equivalent for investigated Cl^--containing substances. However, in this diagram distinguishing or separation of data points of the different test substances based on these parameters was not feasible. Nonetheless, the datapoint of the untreated control (cross) seemed to range below those of the test substances.

Taken together, $[Na^+]_i$ decreased slightly with decreasing pH of applied DMEM-based dilutions. Highly important though, the overall effect was not uniform across all tested substances. Rather, application of DMP-HCl resulted in higher $[Na^+]_i$ compared to treatment with ACH, PEI-HCl, and PVAm-HCl at similar pH. Even more, those datapoints of DMP-HCl could be grouped with those of chloride-free glycolic acid dilutions.
Such a distinct substance-dependent effect of chloride equivalent on pH was not apparent, but instead dependence of pH on chloride equivalent was coherent for all tested Cl^--containing substances.

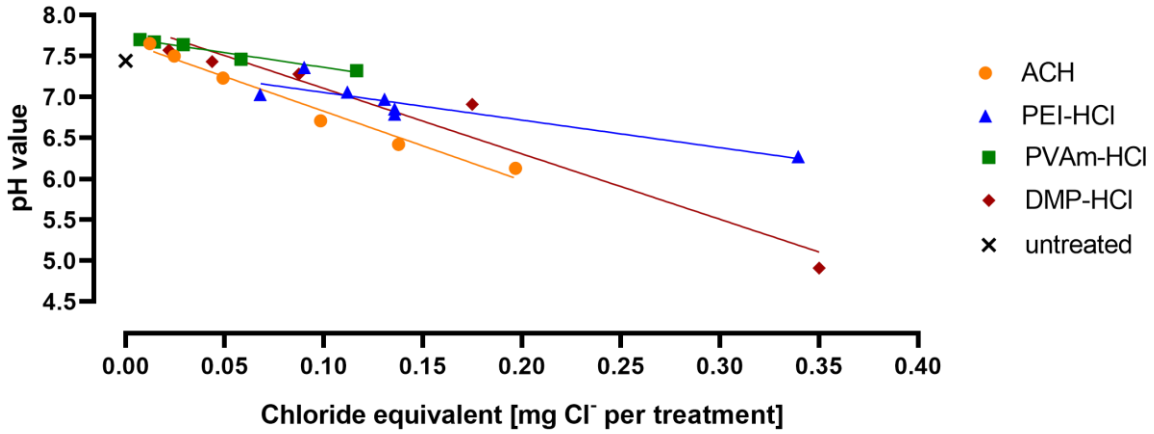

Fig 3.6: Influence of the chloride equivalent on pH of the test solution.
Plotted are pH values of substance dilutions prepared in bicarbonate buffered DMEM versus the chloride equivalent calculated from added amount of hydrochloric acid (HCl). Plain DMEM without any substance was set as the reference with a Cl^- equivalent of 0.0 and a physiological pH of 7.4 (cross). Filled circles represent datapoints of various dilutions of Aluminum chlorohydrate (ACH) while triangles reflect those of polyethylene imine (PEI-HCl), polyvinyl amine dilutions (PVAm-HCl) are depicted as squares and dimethyl piperazine ones (DMP-HCl) as diamonds. Data represent one measurement performed with an electrical pH meter and are summarized in Tab 3.1 on page 62.

Tab 3.1: Summary of *in vitro* characteristics of chloride-containing substances.
Substance concentrations reflect conditions surrounding treated eccrine sweat gland co-culture cells and are stated as % (w/w). Substance dilutions for treatment were prepared from pH-adjusted stocks by dilution in bicarbonate buffered DMEM. Chloride equivalents in mg chloride (Cl^-) per treatment were calculated from amount of hydrochloric acid (HCl) added to substance stock solutions to adjust the pH to 3.5 or – if differing – to stated pH values. Listed chloride equivalents reflect the amount of Cl^- contained in the substance dilution due to addition of HCl. Specified pH values reflect cell surrounding conditions and were measured with an electrical pH meter. After substance treatment relative changes in the intracellular sodium (Na^+) and chloride (Cl^-) concentration of monolayer eccrine sweat gland co-culture cells were recorded and are listed in percent [%] of untreated. Untreated control (0%) received plain DMEM, and its intracellular ion levels were set as 100%. Data represent mean ± SD of three independent experiments performed in sextuple replicates. Dilutions of glycolic acid represent pH controls without addition of chloride ions with data reflecting mean ± SD of one representative experiment performed in sextuple replicates. Table represents a summary of all data of Fig. 3.2 to Fig 3.6. n.d. - not determined.

Treatment concentration (w/w)	Chloride equivalent [mg Cl^- per treatment]	pH value	Relative intracellular ion concentration [%]	
			Na^+	Cl^-
ACH				
0.0%	0.0000	7.44	100.00 ± 7.63	100.00 ± 9.28
0.0625%	0.0123	7.65	95.93 ± 14.06	100.36 ± 14.24
0.125%	0.0246	7.50	69.14 ± 15.90	116.25 ± 20.28
0.25%	0.0492	7.23	57.37 ± 16.81	165.87 ± 50.90
0.5%	0.0984	6.71	53.74 ± 16.81	147.36 ± 42.41
0.7%	0.1378	6.42	47.15 ± 10.89	145.56 ± 23.51
1%	0.1968	6.13	41.60 ± 9.22	140.71 ± 35.42
PEI-HCl				
0.0%	0.0000	7.44	100.00 ± 4.39	100.00 ± 8.56
0.05%	0.0340	n.d.	n.d.	115.60 ± 30.82
0.1%	0.0679	7.03	66.89 ± 7.01	136.51 ± 35.35
0.2%	0.1358	6.79	49.69 ± 11.16	142.06 ± 69.84
0.5%	0.3396	6.27	32.22 ± 10.52	240.88 ± 144.06
0.2%, pH 3.5	0.1358	6.85	49.22 ± 7.81	162.30 ± 36.21
0.2%, pH 4.5	0.1307	6.97	51.22 ± 6.71	134.56 ± 18.38
0.2% pH 5.5	0.1120	7.06	51.51 ± 5.87	131.98 ± 15.48
0.2%, pH 7.5	0.0901	7.36	58.46 ± 10.16	144.31 ± 10.75
PVAm-HCl				
0.0%	0.0000	7.44	100.00 ± 10.48	100.00 ± 3.24
0.03125%	0.0073	7.70	89.33 ± 11.56	105.90 ± 9.54
0.0625%	0.0146	7.67	86.81 ± 5.91	103.47 ± 11.30
0.125%	0.0292	7.64	73.81 ± 9.43	106.43 ± 8.42
0.25%	0.0584	7.46	55.88 ± 9.68	111.71 ± 18.98
0.5%	0.1167	7.32	49.47 ± 9.90	116.21 ± 19.03
DMP-HCl				
0.0%	0.0000	7.44	100.00 ± 10.48	100.00 ± 3.24
0.03125%	0.0219	7.57	108.28 ± 9.66	103.37 ± 5.16
0.0625%	0.0438	7.43	107.49 ± 10.05	101.70 ± 4.45
0.125%	0.0875	7.28	94.41 ± 12.94	109.54 ± 11.73
0.25%	0.1751	6.91	85.62 ± 12.77	114.49 ± 7.99
0.5%	0.3501	4.91	44.71 ± 13.61	135.14 ± 14.23
Glycolic acid				
0.083%	0.0000	7.43	111.54 ± 7.46	n.d.
0.167%	0.0000	7.00	74.51 ± 6.89	n.d.
0.33%	0.0000	4.79	25.96 ± 2.65	n.d.

3.1.1.4 Effect on *in vivo* sweat reduction

ACH constitutes the most common AP ingredient from the large class of aluminum-based substances. In general, this group is characterized by their unique feature of water solubility at low pH ranges and gel-forming quality when reaching more neutral pH values. Due to this plug forming properties, they represent effective means to attenuate human perspiration by physically blocking sweat secretion. Additionally, biochemical interaction of these substances with sweat gland cells is discussed as another or supplementary mechanism in reducing sweating (Papa and Kligman 1967; McWilliams et al. 1987; Exley 2004; Scientific Committee on Consumer Safety 2019). Efficacy of AP substances is verified by in vivo studies which are either performed in the axillae or on the back of human volunteers. Simultaneous testing of up to eight substances provides a huge advantage of back studies compared to those performed in the axillae where only one agent can be applied (Blackwenn et al. 2018). Therefore, *in vivo* studies on the back were used to generate data provided for in this work assessing AP characteristics of aqueous solutions of Cl^--containing substances PEI-HCl, PVAm-HCl, and DMP-HCl. Due to its well-known AP effect and its reproducible results yielding relative sweat reduction values around 50%, ACH was carried along in each *in vivo* study as the reference for comparison and as a benchmark. For cross-study comparison of all Cl^--containing substances, obtained relative sweat reduction values were normed to the effect of a 10% AS (w/w) aqueous solution of ACH which was set to 50% relative sweat reduction when measured 24 h after the last substance application. Of note, while 37 µl of ACH were applied per treatment, ammonium chloride solutions were tested with an amount of 75 µl. Sweat-reducing effects were termed significant if the 95% confidence interval excluded zero.

Results demonstrate increasing concentrations of PEI-HCl (triangles) adjusted to pH 3.5 to evoke higher relative sweat reduction values (**Fig 3.7a** and **Tab 3.2**). Strikingly, the highest tested concentration of 3% AS (w/w) reached an AP efficacy of over 60% which was in the range of sweat reduction induced by the benchmark ACH, but already a 2% AS (w/w) solution of PEI-HCl evoked a significant AP effect. Interestingly, with decreasing HCl-adjusted pH but constant PEI concentration of 3% AS (w/w) the sweat-reducing effect of the solutions gradually decreased. Most astonishingly, a 3% AS (w/w) aqueous solution of PEI adjusted to pH 3.5 with citric acid instead of HCl (PEI-Citrate, hollow triangle) evoked no considerable sweat reduction. This indicates the chloride content to contribute substantially to observed AP effect.

In comparison, a 5% TQ (w/w) aqueous solution of PVAm-HCl (squares) and 2.5% TQ (w/w) aqueous solution of DMP-HCl (diamonds), both adjusted to pH 3.5 with HCl, yielded drastically reduced sweat reduction effects with only the one of PVAm-HCl being just significant (**Fig 3.7b** and Tab 3.2).

Furthermore, for neither of the tested ammonium chloride solutions *in vivo* plug forming characteristics were observed. Solely ACH showed its well-known hydrogel plug precipitation.

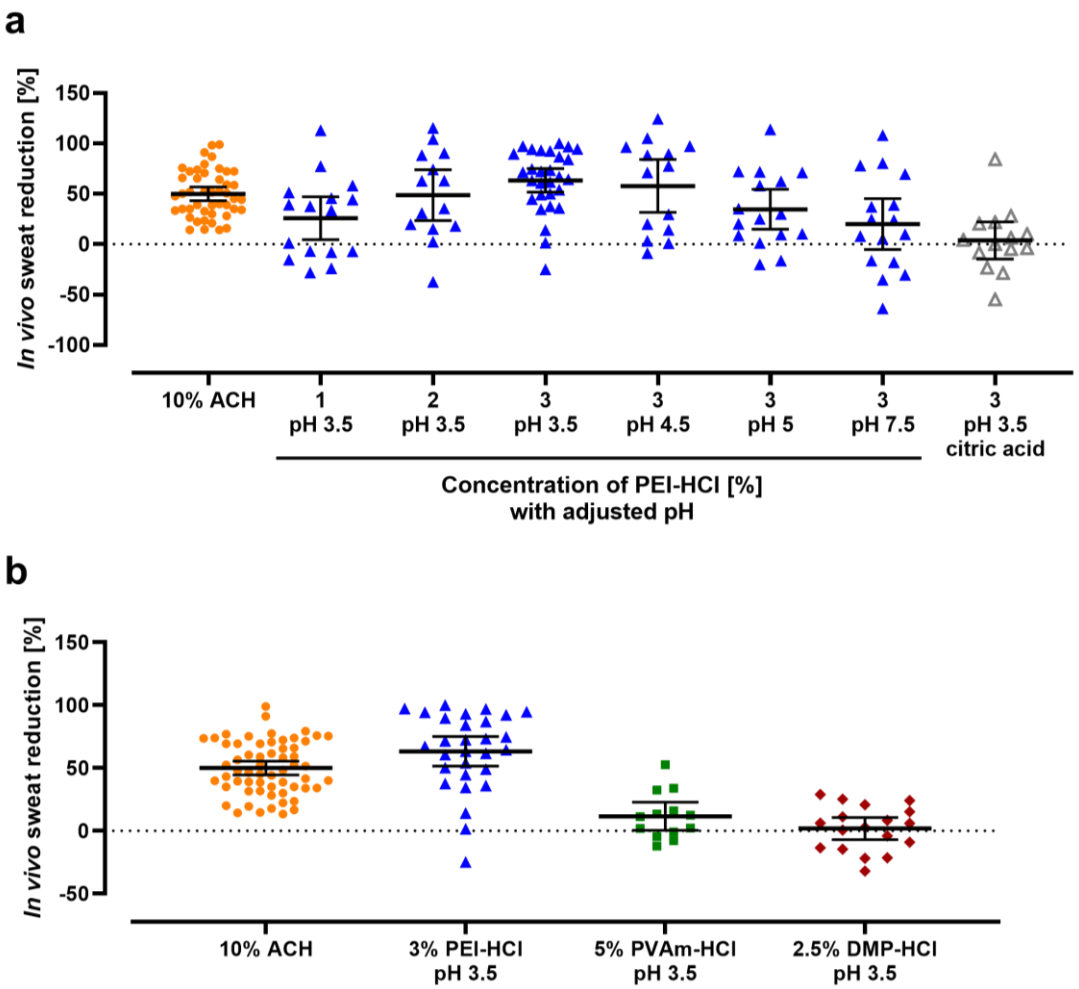

Fig 3.7: *In vivo* sweat-reducing effect of chloride-containing substances and the benchmark aluminum chlorohydrate.
In vivo relative sweat reduction in percent (%) of untreated control area was measured 24 h after the last substance application. Increasing concentrations of a polyethyleneimine solution adjusted to pH 3.5 with hydrochloric acid (PEI-HCl, triangles) evoked progressive sweat-reducing effects on the back of volunteers. Efficiency of 75 µl of a 3% AS (w/w) solution ranged among sweat reduction values produced by 37 µl of a 10% AS (w/w) solution of aluminum chlorohydrate (ACH, circles). With increasing pH of the prepared PEI-HCl solution relative sweat reduction decreased (**a**). In comparison, 75 µl of 5 and 2.5% TQ (w/w) aqueous solutions of PVAm and DMP, respectively, adjusted to pH 3.5 with HCl (PVAm-HCl, squares, and DMP-HCl, diamonds) achieved markedly lower sweat reduction values (**b**). As data were taken from different *in vivo* studies, values are normed to ACH evoking a relative sweat reduction of 50% in each study (mean ± 95% confidence interval; data from n=1-3 independent studies with each 13-18 volunteers). Numerical data are listed in Tab 3.2.

Tab 3.2: Summary of *in vivo* sweat reduction efficacies achieved with chloride-containing test substances.
Aqueous solutions of test substances with indicated concentrations in % (w/w) were adjusted to stated pH with hydrochloric acid (HCl) or citric acid (Citrate). 75 µl thereof, resp. 37 µl for ACH, were applied to the back of 13-20 volunteers per study (n) on four consecutive days. Resulting sweat reduction was determined 24 h after the last application relative to an untreated control spot on the contralateral side. To allow cross-study comparison, relative sweat reduction values were normed to ACH set to a sweat reduction of 50% in each study. Listed are the mean ± 95% confidence interval (CI) of n=1-3 independent studies with each 13-18 volunteers, as well as the resulting upper and lower 95% CI. Sweat reduction efficacy of tested solution was termed significant (#) if the lower 95% CI was higher than zero. Chloride equivalents of the solutions were calculated from added amount of HCl to achieve stated pH values.

Treatment characteristics	Chloride equivalent [mg Cl^- per treatment]	Mean *in vivo* sweat reduction [%]	Upper 95% CI	Lower 95% CI	n
10% ACH	0.6068	50.00 ± 6.87#	56.87	43.13	3
1% PEI-HCl, pH 3.5	0.4376	25.78 ± 21.35#	47.13	4.43	1
2% PEI-HCl, pH 3.5	0.8751	48.78 ± 25.25#	74.03	23.54	1
3% PEI-HCl, pH 3.5	1.3419	63.33 ± 11.69#	75.02	51.64	2
3% PEI-HCl, pH 4.5	0.9481	57.82 ± 26.32#	84.14	31.50	1
3% PEI-HCl, pH 5	0.6564	34.63 ± 19.78#	54.40	14.85	1
3% PEI-HCl, pH 7.5	0.6126	20.06 ± 25.30	45.35	-5.24	1
3% PEI-Citrate, pH 3.5	0.0001	3.74 ± 18.41	22.15	-14.67	1
5% PVAm-HCl, pH 3.5	0.7351	11.66 ± 11.28#	22.93	0.38	1
2.5% DMP-HCl, pH 3.5	1.1377	9.68 ± 10.19	19.87	-0.51	1

Already *in vitro* experiments the considerable influence of the amount of Cl^- present in the solutions on relative $[Na^+]_i$ was demonstrated (refer Fig 3.4). In analogy to that, influence of the chloride equivalent on *in vivo* sweat reduction was also graphically correlated showing an increase in *in vivo* AP efficacy with increasing amount of Cl^- (**Fig 3.8**). This linear relation was especially strong for PEI-HCl samples (triangles) with different concentrations and varying adjusted pH values. For PEI-Citrate (hollow triangle) a chloride equivalent of 0.0 was allocated and nearly no AP effect was measured. However, this data point fitted well with linear regression line of PEI-HCl data points suggesting the chloride content to have substantial influence on AP effect. In contrast, data point of ACH (circle) ranged above those of PEI-HCl, while the one of PVAm-HCl (square) lay slightly and the one of DMP-HCl (diamond) substantially below PEI-HCl data.

Overall, *in vitro* tested ammonium chloride solutions PEI-HCl and PVAm-HCl also evoked substantial sweat-reducing effects *in vivo* with the intensity depending on the chloride equivalent of the applied solution. DMP-HCl, in contrast, was not able to elicit considerable AP effects *in vivo*. Besides, neither of the tested solutions showed any signs of flocculation or sweat gland pore obstruction as is the case for the well-known AP agent ACH.

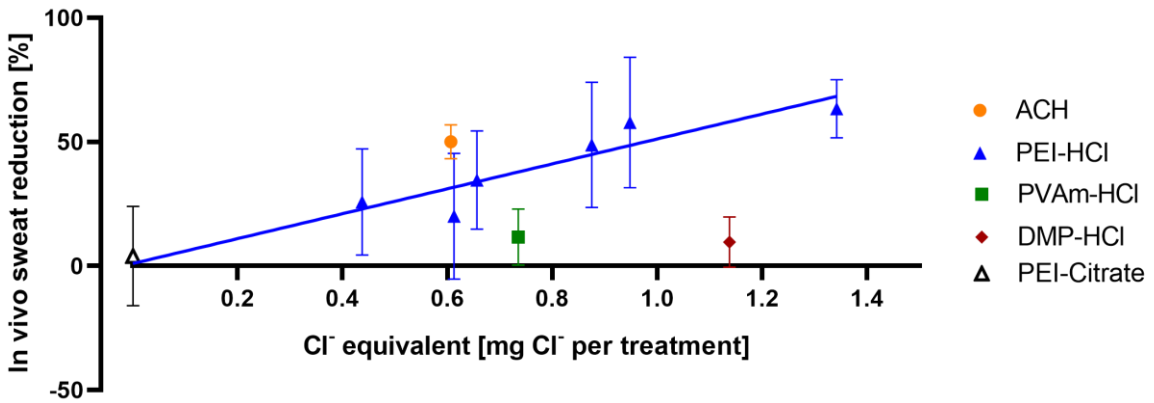

Fig 3.8: Influence of chloride equivalent of chloride-containing substance solutions on *in vivo* sweat reduction.
In vivo sweat reduction in percent (%) of control area was measured 24 h after the last substance application and correlated with calculated chloride equivalents of applied amounts of the solutions. Chloride equivalents are based on the amount of hydrochloric acid (HCl) added to the samples to adjust their pH and reflect the milligram amount of chloride present in each sample applied in the back of volunteers. Samples of PEI-HCl (triangles) exhibited a good linear correlation with coefficient of correlation R^2 = 0.8255. Data point of PEI-Citrate (hollow triangle) fits well with this linear regression line. ACH (circle) ranges above this line while PVAm-HCl (squares) and DMP-HCl (diamonds) lie below. As data were taken from different *in vivo* studies, values are normed to ACH evoking a relative sweat reduction of 50% in each study (mean ± 95% confidence interval; n=1-3 independent studies with each 13-18 volunteers). Numerical data are listed in Tab 3.2. Taken and modified from Welzel et al. 2021.

3.1.2 Polyols such as diols

3.1.2.1 Impact of different diols on *in vitro* ion profile

Apart from Cl^--containing substances, further chemical substance from other substance classes were tested in parallel. Strikingly, a 4% AS (w/w) aqueous solution of 1,2-propanediol (1,2-PD) evoked a different ion print when applied on 2D eccrine sweat gland co-culture cells. It is characterized by elevated $[Na^+]_i$ while $[Cl^-]_i$ was concomitantly reduced (**Fig 3.9**Fig 3.10), which is the exact opposite of the ionic changes induced by Cl^--containing substances. In contrast, $[Ca^{2+}]_i$ and $[K^+]_i$ remained constant after application of 1,2-PD and, thus, further detailed investigations with similar substances were again focused on changes in $[Na^+]_i$ and $[Cl^-]_i$.
Noteworthy, a quite high concentration of 1,2-PD was applied to yield cellular effects with intensities comparable to those of Cl^--containing substances (refer to 3.1.1.1).

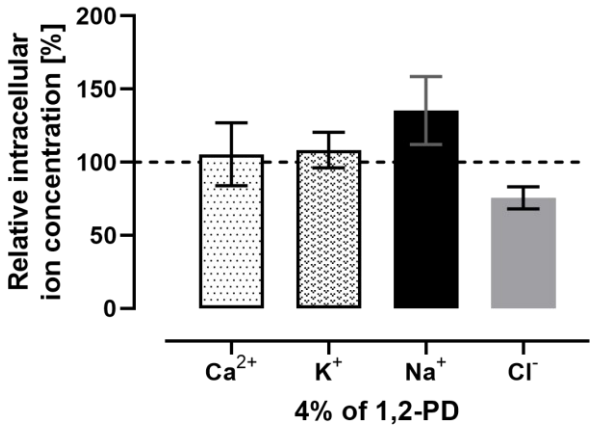

Fig 3.9: *In vitro* ion profile of a 4% (w/w) solution of 1,2-PD.
Relative intracellular ion concentrations of cations calcium $[Ca^{2+}]_i$, potassium $[K^+]_i$, and sodium $[Na^+]_i$ as well as of the anion chloride $[Cl^-]_i$ evoked by an DMEM-based solution with 4% (w/w) of 1,2-propanediol (1,2-PD) are depicted. Nearly confluent 2D eccrine sweat gland co-culture cells were treated and resulting changes of fluorescence intensities measured with a microplate reader reflecting fluctuation of intracellular ion levels relative to an untreated control which was set as 100%. Data represent mean ± SD of two (Ca^{2+} and K^+) or three (Na^+ and Cl^-) experiments.

Additional experiments revealed these changes in intracellular ion levels to be concentration dependent: Down to a concentration of 2% AS (w/w) of 1,2-PD measured reduction of $[Cl^-]_i$ was significant, whereas the impact on $[Na^+]_i$ was significant only at 4% AS (w/w) (**Fig 3.10a**). Based on these results further representatives of this substance class of polyols were selected and their impact on intracellular ion levels established: 1,3-propylene glycol (1,3-PD) as an isomer of 1,2-PD (Fig 3.10b), an isomeric mixture of dipropylene glycol (DPG) as dimers of 1,2-PD (Fig 3.10c), and diglycerol (DG) as a polyol closely related to DPG regarding molecular weight (Fig 3.10d). Consistent across all tested substances $[Na^+]_i$ increased whereas $[Cl^-]_i$ diminished with higher applied concentrations. Numerical data of all substances are summarized in **Tab 3.3** on page 70.
Comparable to 1,2-PD, its isomeric form 1,3-PD yielded a significant elevation of $[Na^+]_i$ only at the highest tested concentration of 4% AS (w/w). $[Cl^-]_i$ was significantly reduced at 2 and 4% AS (w/w). DPG, in contrast, evoked significant changes in $[Na^+]_i$ and $[Cl^-]_i$ down to a concentration of 1% AS (w/w). Effects produced by the polyol DG were significant only at 8% AS (w/w) in case of diminished $[Cl^-]_i$ or 4 and 8% AS (w/w) regarding elevation of $[Na^+]_i$.
Again, attention is put on the high concentrations of the polyols needed to elicit an intracellular response as compared to effective concentrations of Cl^--containing substances (refer to 3.1.1.1).

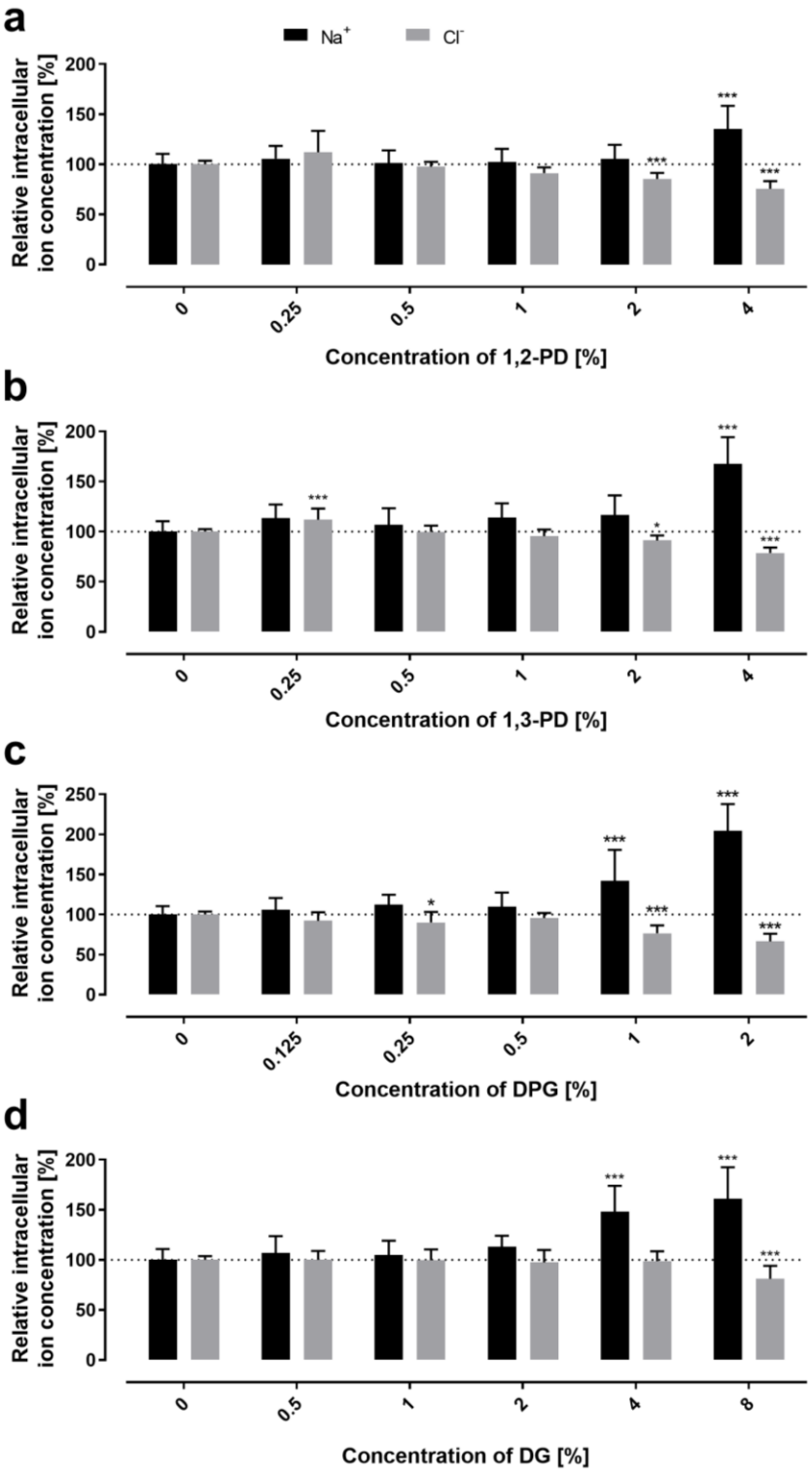

Fig 3.10: Concentration-dependent effect of polyols on relative intracellular sodium and chloride concentrations.

Depicted are relative intracellular concentrations of sodium $[Na^+]_i$ and chloride $[Cl^-]_i$ ions in monolayer eccrine sweat gland co-culture cells after treatment with different concentrations of polyols. DMEM-based solutions of (**a**) 1,2-propanediol (1,2-PD), (**b**) 1,3-propanediol (1,3-PD), (**c**) dipropylene glycol (DPG), and (**d**) diglycerol (DG) with different concentrations were applied to nearly confluent cells. Resulting changes of fluorescence intensities were measured with a microplate reader reflecting fluctuation of intracellular ion levels relative to an untreated control (0%) which was set as 100%. Data represent mean ± SD of three independent experiments performed in sextuple replicates (Kruskal-Wallis test with Dunn's multiple comparison test (DPG) or one-way ANOVA with Tukey's multiple comparison test (1,2-PD, 1,3-PD, and DG); */**/*** statistically significant difference to untreated (0%) with $p<0.05/0.001/0.0001$). Data are summarized in Tab 3.3 on page 70.

In analogy to Cl^--containing substances and to be able to compare effects of tested polyols, elicited changes in $[Na^+]_i$ were plotted against the respective substance concentration (**Fig 3.11**). This overview revealed DPG to exert by far the strongest intracellular effect of all polyols with values of $[Na^+]_i$ amounted to over 200% for 2% AS (w/w) of DPG. In contrast, the other tested polyols - 1,2-PD, 1,3-PD, and DG – elicited values not exceeding 150% though applied at the same concentration. Among those other three, 1,3-PD exhibited slightly higher $[Na^+]_i$ compared to 1,2-PD and DG.

Condensed, *in vitro* testing of polyols in monolayers of eccrine sweat gland co-culture cells revealed applied polyol substances to evoke consistent and concentration-dependent changes of intracellular Na^+ and Cl^- levels. Thereby, DPG outranked all other so far examined polyols regarding the impact on elevation of $[Na^+]_i$.

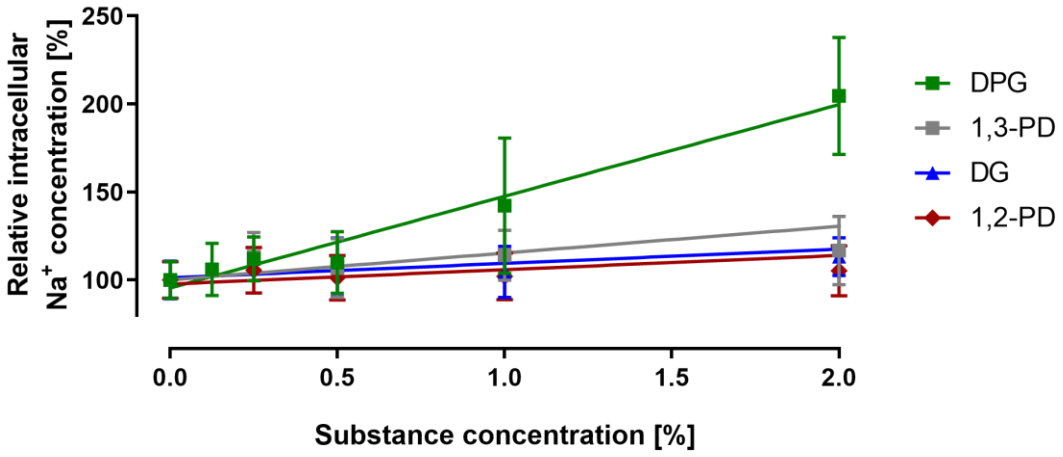

Fig 3.11: Concentration-dependent comparison of polyols regarding their effect on relative intracellular sodium concentrations.
Depicted are relative intracellular sodium concentrations $[Na^+]_i$ of monolayer eccrine sweat gland co-culture cells after treatment with different concentrations of polyols. DMEM-based solutions of 1,2-propanediol (1,2-PD, circles), 1,3-propanediol (1,3-PD, squares), dipropylene glycol (DPG, triangles), and diglycerol (DG, diamonds) with different concentrations were applied to nearly confluent cells. Resulting changes of fluorescence intensities were measured with a microplate reader reflecting fluctuation of intracellular ion levels relative to an untreated control (0%) which was set as 100%. Data represent mean ± SD of three independent experiments performed in sextuple replicates. Data are summarized in Tab 3.3 on page 70.

Tab 3.3: Summary of *in vitro* characteristics of polyols.
Substance concentrations reflect conditions surrounding treated monolayer eccrine sweat gland co-culture cells and are stated as % AS (w/w). Substance dilutions of 1,2- and 1,3-propanediol (1,2-PD and 1,3-PD, respectively), dipropylene glycol (DPG) and diglycerol (DG) were prepared in bicarbonate buffered DMEM. Stated pH values reflect cell surrounding conditions and were measured with an electrical pH meter. After substance treatment relative changes in the intracellular sodium (Na^+) and chloride (Cl^-) concentrations of monolayer eccrine sweat gland co-culture cells were recorded with a multiplate reader and are listed in percent [%] of untreated. Untreated control (0%) received plain DMEM, and its intracellular ion levels were set as 100%. Data represent mean ± SD of three independent experiments performed in sextuple replicates. Table is a summary of data displayed in Fig 3.10 and Fig. 3.11.

Treatment concentration (w/w)	pH value	Relative intracellular ion concentration [%]	
		Na^+	Cl^-
1,2-PD			
0.0%	7.44	100.00 ± 10.50	100.00 ± 3.36
0.25%	7.80	105.57 ± 12.84	112.17 ± 21.32
0.5%	7.80	101.30 ± 12.66	97.65 ± 4.77
1%	7.80	102.18 ± 13.22	91.14 ± 5.78
2%	7.80	105.22 ± 14.23	85.38 ± 6.08
4%	7.80	135.31 ± 23.20	75.63 ± 7.58
1,3-PD			
0.0%	7.44	100.00 ± 10.50	100.00 ± 2.41
0.25%	7.80	113.34 ± 13.81	111.94 ± 11.18
0.5%	7.80	106.82 ± 16.69	99.95 ± 6.07
1.0%	7.80	114.05 ± 14.26	95.42 ± 6.68
2.0%	7.80	116.82 ± 19.47	91.29 ± 4.92
4.0%	7.80	167.78 ± 26.59	78.78 ± 5.35
DPG			
0.0%	7.44	100.00 ± 10.50	100.00 ± 3.80
0.125%	7.80	106.06 ± 14.76	92.30 ± 10.50
0.25%	7.80	112.07 ± 12.48	90.15 ± 13.22
0.5%	7.80	110.00 ± 17.53	95.62 ± 6.34
1.0%	7.80	142.26 ± 38.35	76.64 ± 9.85
2.0%	7.80	204.56 ± 33.20	66.65 ± 9.37
DG			
0.0%	7.44	100.00 ± 10.78	100.00 ± 3.80
0.5%	7.81	107.08 ± 16.77	100.17 ± 8.78
1.0%	7.81	104.68 ± 14.52	99.74 ± 10.69
2.0%	7.81	113.37 ± 10.84	97.59 ± 12.35
4.0%	7.81	148.17 ± 25.85	98.85 ± 9.68
8.0%	7.77	161.01 ± 31.46	81.22 ± 13.02

3.1.2.2 Influence of molecular size

Following up on initial *in vitro* observations, the spectrum of examined polyols was extended. Based on stated results showing DPG, the reaction product of two molecules of 1,2-PD, to exert strong effects on $[Na^+]_i$, polymerized derivatives of 1,2-PD, 1,3-PD, and glycerol with varying molecular sizes were tested with monomeric entities being linked via ester group formation. For comparison, all substances were applied at an equimolar concentration of 84 mM (maximum tolerable concentration as determined by cell viability assay) (**Fig 3.12** and **Tab 3.4**). Tested family of 1,2-PG derivatives consisted only of this substance and an isomeric mixture of DPG. In contrast, family of 1,3-PD derivatives was augmented by 3,3'-oxydipropanol (polypropanediol-2, PPD-2) and 3,3'-[oxybis(1,3-propanediyloxy)]bis(1-propanol) (polypropandiol-4, PPD-4) being reaction products of, on average, two or four molecules of 1,3-PD, respectively. Similarly, family of glycerol as the monomer included previously tested DG and was extended by solutions of polymerized derivatives with on average four, six or ten glycerol molecules. They were named polyglycerol-4 (PG-4), PG-6 and PG-10, respectively.

For all investigated families $[Na^+]_i$ rose with increasing molecular size. However, differences were revealed regarding the magnitude of effects. While 1,2-PD and DPG evoked small elevations, 1,3-PD and its derivatives showed significant and marked augmentation of $[Na^+]_i$. Especially PPD-4 reached values of over 250%. Polymerized glycerol derivatives showed a gradual increase of $[Na^+]_i$ which was significant starting from PG-4 onwards and reaching maximal levels of 150% for PG-10.

Concerning $[Cl^-]_i$, there was a clear trend observed only for glycerol and its derivatives with values ascending with greater molecular size. In case of 1,3-PD, PPD-2 evoked a slight though significant elevation in $[Cl^-]_i$ whereas PPD-4 reduced this level. Similarly, $[Cl^-]_i$ decreased by DPG treatment compared to 1,2-PD application.

Regarding pH, irrespective of the type of polyol and its concentration pH value of each solution was always constant at 7.8, which is close to the pH value of pure DMEM (pH 7.4). Therefore, polyols exerted no considerable change of pH of the extracellular medium implying this not to have any relevance for their mode of action.

Taken together, investigation of further, long-chained polyols clearly demonstrated intensity of evoked cellular effects to depend on molecular size of tested substance. Thereby, magnitude of elicited ionic changes unambiguously increased with chain-length.

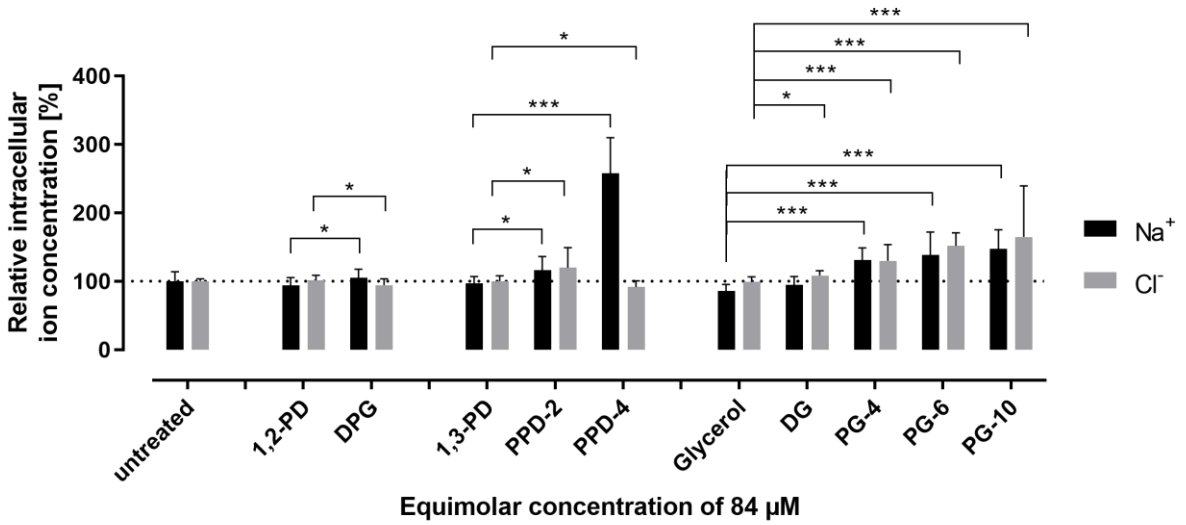

Fig 3.12: Effect of equimolar concentrations of different polyols with varying chain length. Relative intracellular concentrations of sodium $[Na^+]_i$ and chloride $[Cl^-]_i$ ions were determined in nearly confluent monolayer eccrine sweat gland co-culture cells after treatment with different polyols but with the same concentration of 84 µM. DMEM-based solutions of 1,2-propanediol (1,2-PD), dipropylene glycol (DPG), 1,3-propanediol (1,3-PD), 3,3'-oxydipropanol (PPD-2), 3,3'-[oxybis(1,3-propanediyloxy)]bis(1-propanol) (PPD-4), glycerol, diglycerol (DG), and polyglycerol (PG)-4, PG-6 and PG-10 were applied. Resulting changes of fluorescence intensities were measured with a microplate reader reflecting fluctuation of intracellular ion levels relative to an untreated control which was set as 100%. Data represent mean ± SD of three independent experiments performed in sextuple replicates (Kruskal-Wallis test with Dunn's multiple comparison test; */**/*** statistically significant difference to family-specific basic molecule with $p<0.05/0.001/0.0001$). Data are summarized in Tab 3.4.

Tab 3.4: Summary of *in vitro* characteristics of different polyol families.
Nearly confluent eccrine sweat gland co-culture cells were treated with a final concentration of 84 µM of each of the listed polyols. Substance dilutions were prepared in bicarbonate buffered DMEM and pH was always constant at 7.8 close to the one of plain DMEM. After substance treatment relative changes in the intracellular sodium (Na^+) and chloride (Cl^-) concentrations in monolayer eccrine sweat gland co-culture cells were recorded with a multiplate reader and are listed in percent [%] of untreated. Data represent mean ± SD of three independent experiments performed in sextuple replicates. Stated number of hydroxyl groups reflects the average amount present per molecule. 1,2-/1,3-PD: 1,2-/1,3-propanediol, DPG: dipropylene glycol, PPD-2/-4: polypranediol-2/-4, DG: diglycerol, PG-4/-6/-10: polyglycerol-4/-6/-10.

Test substance	Number of hydroxyl groups	Relative intracellular ion concentration [%]	
		Na^+	Cl^-
untreated	0	100.00 ± 13.89	100.00 ± 3.43
1,2-PD family			
1,2-PD	2	93.75 ± 11.51	101.15 ± 7.66
DPG	2	104.87 ± 12.64	94.38 ± 9.24
1,3-PD family			
1,3-PD	2	96.85 ± 10.16	100.17 ± 7.85
PPD-2	2	116.15 ± 19.84	119.85 ± 29.30
PPD-4	2	257.94 ± 51.86	91.83 ± 8.65
Glycerol family			
Glycerol	3	85.94 ± 9.48	99.04 ± 7.41
DG	4	95.17 ± 11.55	108.39 ± 6.89
PG-4	6	130.87 ± 17.77	129.99 ± 23.71
PG-6	8	138.23 ± 33.69	151.75 ± 19.20
PG-10	12	147.57 ± 27.77	164.60 ± 74.82

3.1.2.3 Effect of polyols on *in vivo* sweat reduction

Equal to the procedure pursued with Cl^--containing substances, *in vitro* results gathered with polyols require *in vivo* verification to allocate obtained ion profiles to sweat-reducing potential. In case of these polyols *in vivo* studies were particularly interesting as their characteristic ion profile was completely opposing the one of Cl^--containing substances including the well-known AP active ACH: While polyols increased $[Na^+]_i$ Cl^--containing substances decreased it. Therefore, examination of sweat-reducing characteristics of polyols served not only the purpose of establishing their AP potential, but should also add conclusive insight to the mechanism of sweating. As mentioned above, ACH was carried along in each *in vivo* study as the benchmark and for comparison of efficacies. Similar to *in vitro* experiments also *in vivo* high concentrations of the polyols were applied on the back of volunteers. Otherwise, those studies were performed identical to the ones stated above, meaning 75 µl of polyol solutions but 37 µl of 10% AS (w/w) aqueous solution of ACH was applied on the back on four consecutive days.

Determination of sweat reduction 24 h after the last application revealed 40% AS (w/w) solutions of 1,2-PD and DPG to exert no significant effect with means between 9-10% (**Fig 3.13a** and **Tab 3.5**). As explained above, average sweat reduction value of the standard 10% AS (w/w) ACH solution was again set as 50% allowing for cross-study comparison of the tested substances.

Inspired by immediate and short-term mode of action of other biologically acting substances such as drugs, the protocol of *in vivo* studies was adapted and sweat-reducing effects on the back of volunteers were determined already 2 h after the last application. Apart from that, study procedure was kept constant. Strikingly, the same 40% AS (w/w) solutions of 1,2-PD and DPG evoked significant AP effects with means of 34% and 39%, respectively (Fig 3.13b). Concerning the benchmark ACH its performance was also slightly improved reaching a mean of 65% sweat reduction.

To obtain information about longevity of effects, the time of measurement after the last application was again changed to 6 h. Further, the potency of DG, an additional polyol already well described above by *in vitro* tests, was also investigated in this *in vivo* study (Fig 3.13c). Sweat-reducing efficiency of all polyols was reduced with 40% AS (w/w) solutions of 1,2-PD and DG evoking nonsignificant mean sweat reductions of 13% and 10%, respectively. However, the same concentration of DPG diminished sweating significantly by 23%. Interestingly, effect of the benchmark ACH was markedly increased reaching an average sweat reduction efficiency of 81%.

Due to time constraints and the efforts required for those *in vivo* studies, unfortunately, no more candidates from the class of polyols were examined for their sweat-reducing potential.

In short, investigation of *in vivo* sweat-reducing impact of several polyols at multiple time points unequivocally demonstrated those substances to possess AP properties. Strikingly, a prominent dependency of observed intensity of sweat reduction on the time passed between last application and sweat induction was revealed with polyols eliciting a strong short-term effect.

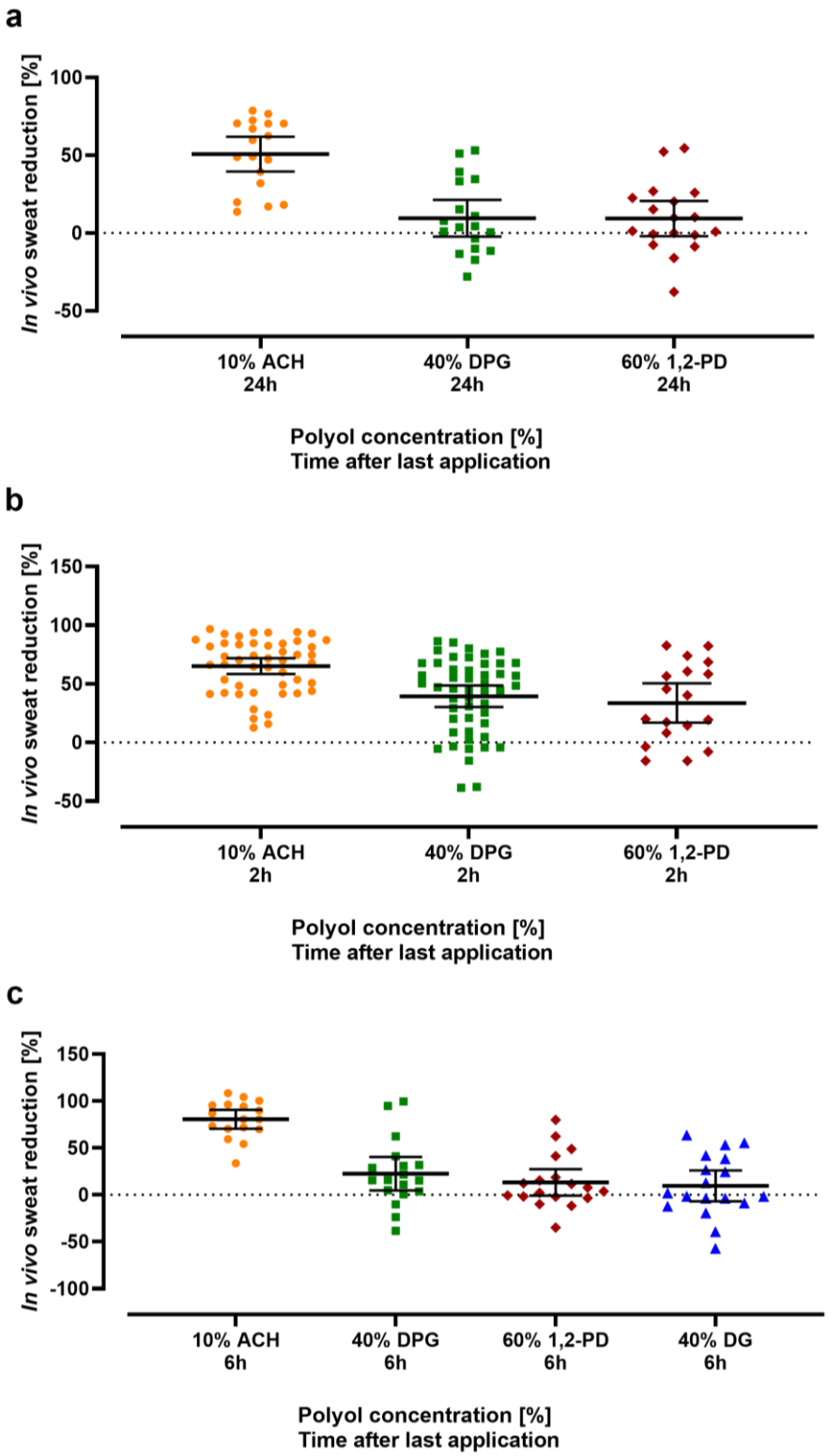

Fig 3.13: *In vivo* sweat-reducing effects of polyols and the benchmark aluminum chlorohydrate. Relative *in vivo* sweat reduction in percent (%) of control area was measured 24 h (**a**), 2 h (**b**), or 6 h (**c**) after the last of four substance applications performed on consecutive days. After 24 h benchmark solution of 10% AS (w/w) aluminum chlorohydrate (ACH) achieved about 50% sweat reduction while 40% AS (w/w) solutions of 1,2-propanediol and diglycerol (DG) exerted no significant antiperspirant effect (**a**). Measurement 2 h after the last application resulted in drastically higher and significant sweat-reducing behavior. Response of the standard ACH solution was also slightly elevated (**b**). Intermediate sampling after 6 h yielded the highest sweat-reducing effect of ACH. For the polyols, only a 40% (w/w) solution of DPG exerted a significant sweat reduction while those of the same concentration of 1,2-PD and diglycerol (DG) were marginal (**c**). Data represent mean ± 95% confidence interval of n=1-3 independent studies with each 13-18 volunteers. Numerical data are listed in Tab 3.5.

Tab 3.5: Summary of *in vivo* sweat reduction efficacies achieved with test substances from the class of polyols.
Aqueous solutions of tested substances with indicated concentrations in % AS (w/w) were applied to the back of 13-20 volunteers per study (n) on four consecutive days. While for aluminum chlorohydrate (ACH) 37 µl were put on per application polyols were tested with an amount of 75 µl per application. Resulting sweat reduction was determined 2 h, 6 h or 24 h after the last application relative to an untreated control spot on the contralateral side. To allow cross-study comparison, relative sweat reduction values of 24 h studies were normed to ACH achieving a sweat reduction of 50% in each study. Listed are the mean ± 95% confidence interval (CI) of n=1-3 independent studies with each 13-18 volunteers, as well as the resulting upper and lower 95% CI. Sweat reduction efficacy of tested solution was termed significant (#) if the lower 95% CI was higher than zero. 1,2-PD: 1,2-propanediol, DPG: dipropylene glycol, DG: diglycerol

Treatment characteristics	Mean *in vivo* sweat reduction [%]	Upper 95% CI	Lower 95% CI	n
10% ACH, 2 h	65.16 ± 6.71#	71.87	58.45	3
10% ACH, 6 h	80.63 ± 10.11#	90.74	70.52	1
10% ACH, 24 h	50.74 ± 11.17#	61.91	39.56	1
40% 1,2-PD, 2 h	33.67 ± 16.67#	50.43	16.90	1
40% 1,2-PD, 6 h	13.36 ± 14.06	27.42	-0.70	1
40% 1,2-PD, 24 h	9.31 ± 11.26	20.57	-1.95	1
40% DPG, 2 h	39.40 ± 9.13#	48.53	30.27	3
40% DPG, 6 h	22.58 ± 17.74#	40.32	4.83	1
40% DPG, 24 h	9.49 ± 11.83	21.32	-2.33	1
40% DG, 6 h	9.58 ± 16.39	25.97	-6.81	1

3.2 Eccrine sweat gland cell models

3.2.1 Optimization of the 3D hanging drop model

Widely used since several decades, monolayer cell cultures represent a convenient research tool to find aswers to a variety of scientific questions. However, isolated 2D cultured cells are prone to losing functional properties such as expression of certain proteins compared to their native state. Many of those deficiencies can be overcome by employing three-dimensional (3D) tissue culture methods (Lee and Dessi 1989; Santos et al. 2012; Bovell 2018). Therefore, a standardized and well characterized 3D model of the human eccrine sweat gland might improve above-described AP testing strategy and add further insight to the underlying mechanism of action of examined substances.

Generally, native eccrine sweat glands encompass two distinct compartments: the secretory coil and the reabsorbing duct, which consist of different cell types termed coil and duct cells (Bovell 2015). As monolayer cultures, these two cell types are easily told apart by their distinct cell shape: While coil cells feature a cuboidal cobblestone morphology, duct cells are longer and spindle-shaped (**Fig 3.14a-c**). Besides, coil cells grew in dense colonies whereas duct cells were distributed over the culture plate as individual cells.

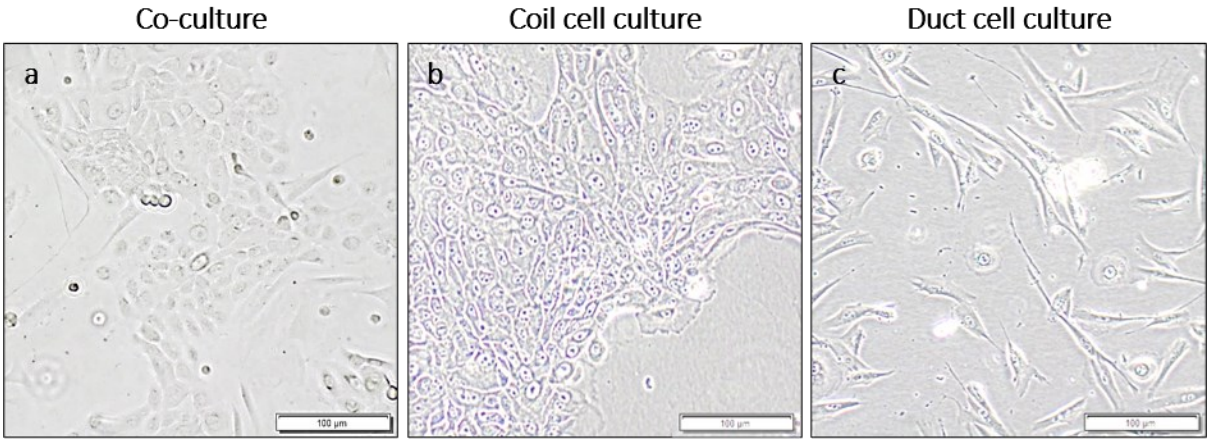

Fig 3.14: Morphological characteristics of eccrine sweat gland co-cultures, coil cell and duct cell cultures.
Morphological traits of co-cultured cells originating from whole gland explants and containing coil and duct cells (**a**) were compared with features of isolated coil cell (**b**) and duct cell cultures (**c**), respectively. While cuboidal coil cells and spindle-shaped duct cells were visible in co-cultures, solely cobblestone-like coil cells or longish duct cells made up their respective monoculture. Images were taken in in bright field mode at 10x object magnification using CKX14 microscope with the digital camera XC10. Bar represents 100 µm.

Initially developed and characterized *in vitro* 3D HD models were generated using either whole gland, coil or duct cell cultures, respectively (Klaka et al. 2017; Klaka 2017). However, due to dominating growth behavior of coil cells over duct cells, whole gland cell cultures (co-cultures) mainly consisted of coil cells. Thus, with the novel approach of defined combination of coil and duct cells cellular composition of spheroidal 3D HD models should mimic a more physiological environment compared to previously generated ones using co-culture cells. In any case, both strategies are certainly more advanced than conventional monolayer cell cultures and should trigger protein expressions in 3D models which resembles the native situation more closely.

For generation of all below described HD models primary cells derived from the same donor (denoted 15-24) were used. To compare structural characteristics of those 3D HD models with native glands, frozen human skin sections as well as sections of different kinds of generated *in vitro* spheroids were stained with HE (**Fig 3.15a-d**). In sections of native skin, coil and duct compartments were distinguishable since duct parts (*du*) are characterized by a more intense, darker hue compared to coil parts (*sc*) (Fig 3.15a). Initially developed eccrine sweat gland models comprising co-culture sweat gland cells showed little characteristics of duct cells and exposed a loose cellular architecture in the center of the spheroid (Fig 3.15b and Klaka et al. 2017). To optimize this 3D model further, novel approaches were tested in this thesis. By combining initially separately cultured coil and duct cells into one *in vitro* 3D HD model, ideally, a layered structure was obtained which bears higher resemblance to the tubular form of native glands. Besides, defined presence and cell-cell interaction of both cell types was achieved. In the first preparation strategy equal numbers of both cell types were mixed and 25,000 blended cells added per HD (termed coil with duct). Alternatively, in the second variation, 12,500 duct cells were pre-seeded and after 24 h of cultivation the same number of coil cells was added (termed coil on duct). With these approaches the effect of defined seeding and possible interaction of the cell types should be addressed.

After 3 d of cultivation as HD, eccrine sweat gland models were harvested, frozen sections cut, and HE stains prepared to compare their structural characteristics. Attributed to characteristics of used dyes, cell nuclei were stained blue while the cell cytoplasm was colored in different hues of red to pink. Strikingly, distinct regions were discernible in both novel 3D models since cells of the same kind closely self-aggregated (Fig 3.15c and d). Thereby, duct cell regions were in the core of the HD and were characterized by more densely packed nuclei. Coil cells surrounded those duct cell areas and featured cells with larger nuclei and more cytoplasm. Thus, regions of duct cells appeared rather purple while coil cell parts showed a high amount of reddish-pink coloration. Noticeably, regions of duct cells in models prepared by simultaneous addition of both cell types formed smaller demarcated zones lying close together. In contrast, pre-seeding of duct cells resulted in formation of one, relatively round, compact duct cell core with a definite border towards surrounding coil cells. In both models, though, duct cells were always bordered by coil cells.

Unfortunately, a tubular stratified structure where coil and duct cells form separate compartments could not be realized with herein employed 3D culturing technique, which reveals its limitation and difference to native eccrine glands. Yet, generated eccrine sweat gland HD models feature a double-layered appearance with still clearly distinguishable areas formed by the different cell types.

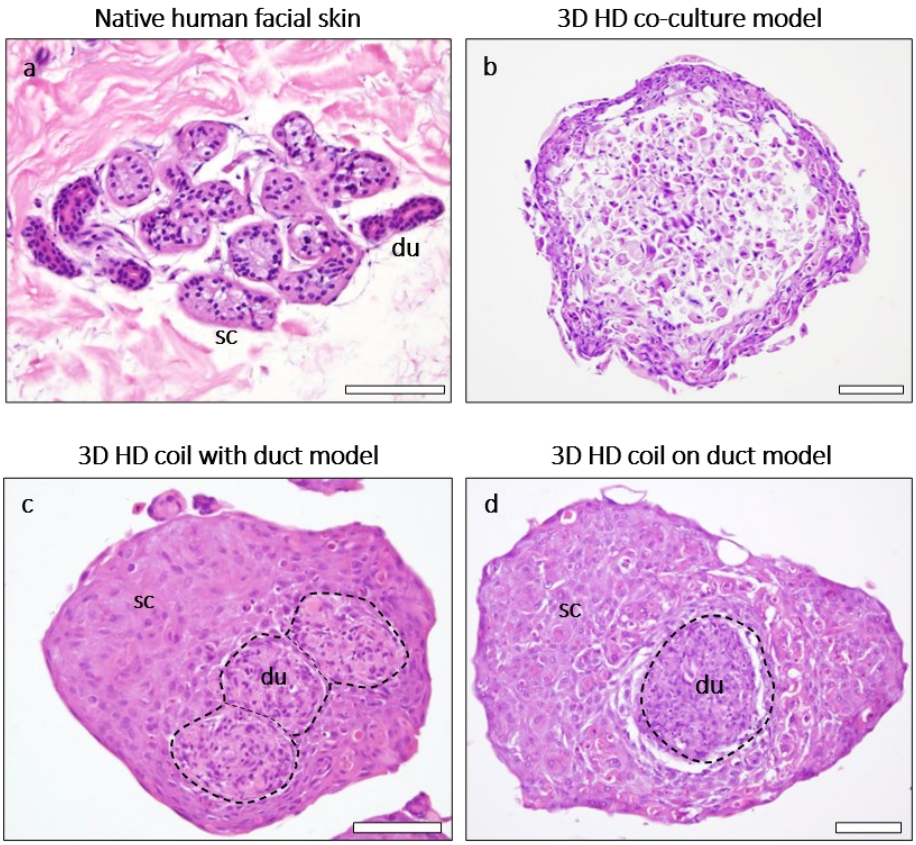

Fig 3.15: Histological hematoxylin and eosin staining of native human skin and 3D Hanging Drop models comprising co-culture or coil and duct cells.
Morphological and structural characteristics of native human skin and *in vitro* 3D human eccrine sweat gland models were compared by hematoxylin and eosin staining. Therefore, frozen sections of human facial skin biopsies (**a**) and 3D hanging drop (HD) models were prepared. Three distinct types of *in vitro* spheroids were generated: One containing eccrine sweat gland co-culture cells (**b**) and novel models prepared by either simultaneous seeding of equal numbers of coil and duct cells (coil with duct, **c**) or pre-seeding of duct cells and addition of the same number of coil cells 24 hours later (coil on duct, d). In all cases, 3D hanging drop models were harvested after 3 days of cultivation. Note the loose cell orientation in the center of the 3D HD co-culture model. Regions of duct cells are marked with *du* and secretory coil cells are denoted with *sc*. Bar represents 100 µm.

Using immunofluorescence staining of selected sweat-relevant proteins reflected by the muscarinic receptor M3, ion channels such as ENaC and specific cell markers like AQP5, dermcidin, CD44, and CEACAM5 the identity of the cell types and their differentiation status was further elucidated in frozen sections of the novel *in vitro* 3D HD models of the eccrine sweat gland (**Fig 3.16** middle and right column). To depict natural protein localization and cell type specificity in the native human eccrine sweat gland, frozen sections of human facial skin served as controls and references (Fig 3.16 left column). Distinction of coil and duct cell areas within the 3D models was based on HE staining as well as visible differences in nuclei density. Respective regions are marked in each image and denoted with *du* for duct cells and *sc* for secretory coil cells. Negative controls of each specimen treated solely with secondary antibodies showed no staining.
Both HD models - prepared by coil with duct and coil on duct cell seeding - showed the same marker expression with only slight alterations in intensity (Fig 3.16 central and right column). In detail, coil cell specific glycoprotein CD44 was identified exclusively in coil compartments

of the native gland but was absent from duct structures (Fig 3.16a). In contrast, this protein was expressed in both, coil and duct cell areas, in the 3D models (Fig 3.16b and c).
Staining for the muscarinic acetylcholine receptor M3, responsible for triggering sweating, and for the antimicrobial peptide dermcidin was detected in coil and duct structures of the native gland but was solely present in coil cell areas of both 3D models (Fig 3.16a-f). Similarly, eccrine sweat gland specific protein CEACAM5 and sodium ion channel ENaC were strongly expressed in both, coil and duct cell compartments, in facial skin sections (Fig 3.16g and j). In *in vitro* 3D models, however, those two proteins showed marked staining in areas of coil cells but were weakly present only in duct cell regions of models with combined coil and duct cell seeding (Fig 3.16h, i, k, and l).
The duct cell specific cell surface antigen SSEA-4 exclusively stained the native duct parts and was weakly identified in duct cell regions of both 3D models (Fig 3.16m-o). Interestingly, SSEA-4 expression was strongest in those parts of duct cells closest to surrounding coil cells. Further, water channel AQP5, which is specific for coil compartments in the native gland, was identified in exactly these coil structures in facial skin sections. Likewise, AQP5 was expressed in coil cell areas of *in vitro* HD models but was absent from duct cell parts (Fig 3.16m-o).
Tab 3.6 summarizes and graduates observed staining intensities as depicted in Fig 3.16.

In summary, herein newly generated improved *in vitro* 3D HD models of the human eccrine sweat gland containing defined numbers of both cell types revealed new insights into cellular interactions and defined marker expression. Interestingly, independent growing behavior of monolayer cultures of coil and duct cells was reflected in 3D HD models when combined: HE stainings revealed that although both cell types were mixed, surprisingly duct cells self-aggregated to form demarcated zones inside the core of the HD surrounded by coil cells. These striking findings were corroborated by immunofluorescence staining with cell type specific markers such as M3, AQP5 and SSEA-4. Similarly, a second approach using pre-seeding of duct cells yielded nearly the same HD structure featuring one solid duct cell core in the center with surrounding coil cells. However, generation of tubular like structures resembling the native eccrine gland could not be realized. Altogether, these novel results indicate a self-sorting and -aggregation behavior of isolated eccrine sweat gland cells in *in vitro* 3D HD models.

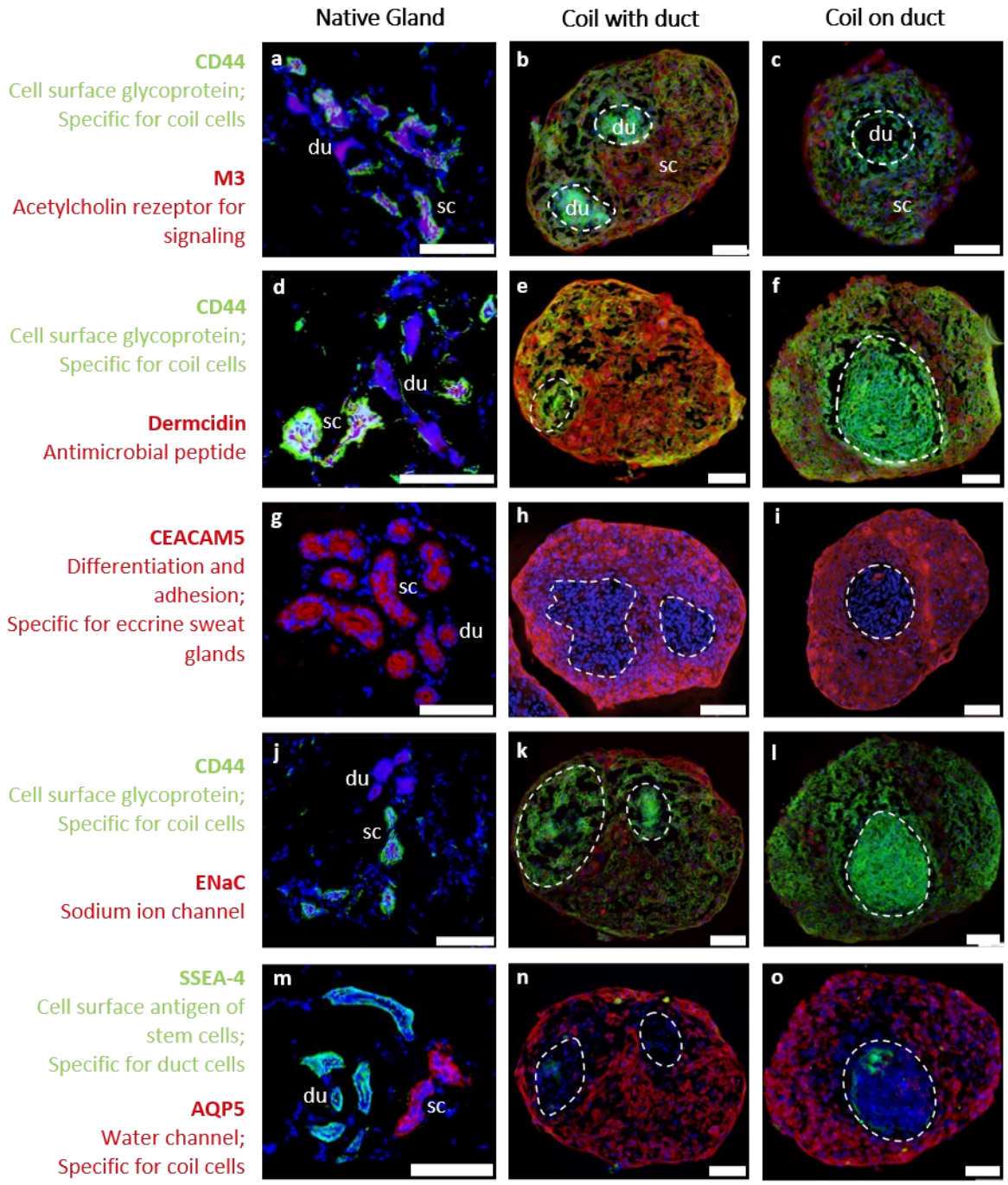

Fig 3.16: Protein expression in native eccrine sweat glands and 3D Hanging Drop models with coil and duct cells.
Localization and distribution of characteristic proteins were compared by immunofluorescence staining in frozen sections of native skin and 3D Hanging Drop (HD) models prepared by either simultaneous seeding of equal numbers of coil and duct cells (coil with duct, middle column) or pre-seeding of duct cells and addition of the same number of coil cells 24 hours later (coil on duct, left column). Again, 3D HD models were harvested after 3 days of cultivation. Regions of duct cells are denoted by *du* and surrounding secretory coil cells are marked with *sc*. Frozen sections of native skin with eccrine sweat glands served as controls for localization of the target proteins (right column). Target proteins are depicted in red (TRITC) and green (FITC) while nuclei are stained in blue (DAPI). Bar represents 100 µm.

Tab 3.6: Comparison of protein expression in coil and duct cells of native glands and novel 3D HD models of the human eccrine sweat gland.
Protein expression of listed sweat gland-associated markers was determined using specific immunofluorescence staining in frozen sections of human facial skin (native gland), of 3D hanging drop (HD) models with joint seeding of eccrine sweat gland coil and duct cells (coil with duct), and of 3D HD models with pre-seeding of duct cells (coil on duct). Staining intensities for the respective proteins were assessed and graduated: +/++/+++ light/middle/high expression intensity; - not detected.

	Native gland		Coil with duct		Coil on duct	
	coil	**duct**	**coil**	**duct**	**coil**	**duct**
CD44	+++	-	+	+++	+	+++
M3	++	++	+++	-	+++	-
Dermcidin	+++	+	+++	-	+++	-
SSEA-4	-	+++	-	+	-	+
AQP5	+++	-	+++	-	+++	-
ENaC	+	+	++	+	+	-
CEACAM5	+++	+++	+++	+	+++	-

3.2.2 Eccrine sweat gland cells in a dermal matrix model

In human skin, secretory coil compartments of eccrine sweat glands reside in the deeper dermis while ducts traverse the dermal layers and the epidermis to open up onto the skin surface (Bovell et al. 2011). To create a structurally more physiological environment isolated and cultivated eccrine sweat gland coil and duct cells were inserted into hollow slots in a fibroblast-supplemented collagen I matrix. While collagen I is one of the predominant collagens in the native dermal compartment fibroblasts represent the major cell type of this skin layer (Lai-Cheong and McGrath 2013).
Identical to above mentioned 3D HD models, all dermal matrix models were prepared using isolated primary eccrine sweat gland cells from donor 15-24. In this approach, coil cells were seeded into slots 24 h prior to addition of duct cells to foster the natural distribution of these two eccrine cell types where coil cells form the lower part of the tubule and duct cells the superficial one. HE staining of such a model after 7 d of cultivation revealed the successful structural integration of eccrine sweat gland cells as well as the loose structure of the dermal equivalent (**Fig 3.17a**). As explained above, cell nuclei were stained blue while cell cytoplasm and collagen scaffold were colored in different shades of red to pink. After only 7 d of cultivation eccrine sweat gland cells already filled the slots in the loose collagen I-fibroblast matrix and were interwoven with the collagen framework along the side walls (**Fig 3.17b**). Besides, in each cavity two different kinds of cell types were distinguishable by means of different color shades. At the bottom and in the middle of each slot reddish-pink colored cells were visible, whereas rather purple appearing cells aligned along the rims of the cavities. Similarly, in HE stains of native human facial skin the coil and duct compartments were distinguishable by their different color intensities in that duct parts featured a darker pinkish hue than coil structures (**Fig 3.17c**).

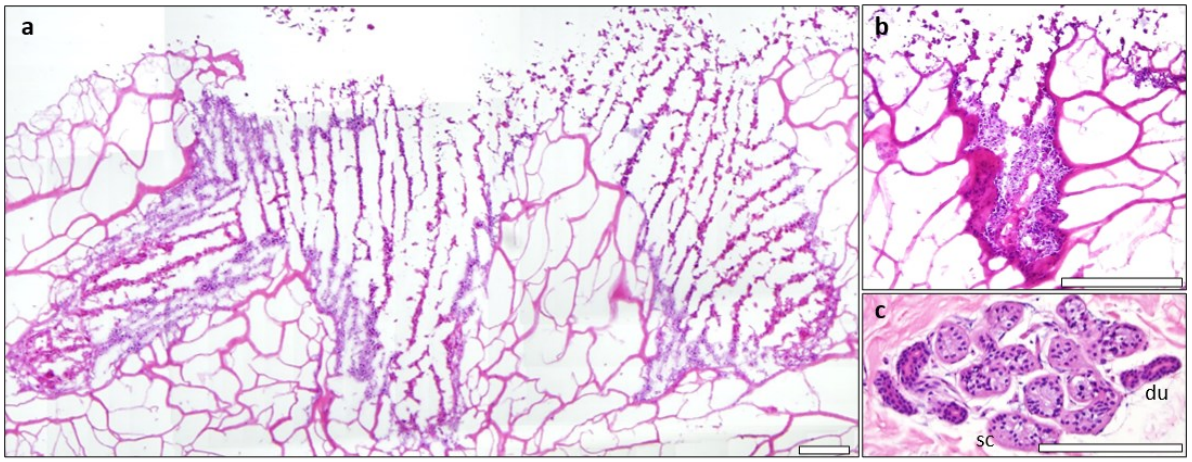

Fig 3.17: Histologic hematoxylin and eosin staining of dermal matrix models with eccrine sweat gland equivalents and native human facial skin.
Frozen sections of prepared dermal matrix models with incorporated eccrine sweat gland coil and duct cells (**a** and **b**) and of native human facial skin (**c**) were stained with hematoxylin and eosin. Morphological structure of the whole model was evaluated regarding integration of the sweat gland cells after cultivation for 7 days (a). Image b depicts another example of this sweat gland matrix model at day 7. In both cases, the top of the picture shows the upper side of the matrix model. In native human facial skin, the two sweat gland compartments of coil (*sc*) and duct (*du*) are discernible by their different color intensities as duct parts exhibit darker staining. Images were taken in brightfield mode at 10x magnification. Bar represents 200 µm.

Models with sweat gland cells integrated into the collagen I matrix were cultured for up to four weeks. After each week of culture one model was terminated, frozen sections were prepared and HE stainings were produced to elucidate structural changes as well as possible differentiation of the cells. Along the time course of four weeks no striking differences regarding degree of integration and cell differentiation were observed (**Fig 3.18**). Structural disparities between timepoints occurred due natural variations of each distinct model. For example, taking the matrix model terminated on d14 a large part of the sweat gland cells aggregated on top of the model (Fig 3.18b). Furthermore, with models of d21 and d28 cell bearing cavities were only partially cut (Fig 3.18c and d). Apart from that, eccrine sweat gland cells were successfully integrated into the loose collagen scaffold at every time point. Also, the above mentioned two distinct cell types were discernible by their individual color shade in every section revealing the presence of both, coil and duct cells, in each model.
Of note, in matrix model of d28 a small layer of keratinized cells was found to cover the surface.

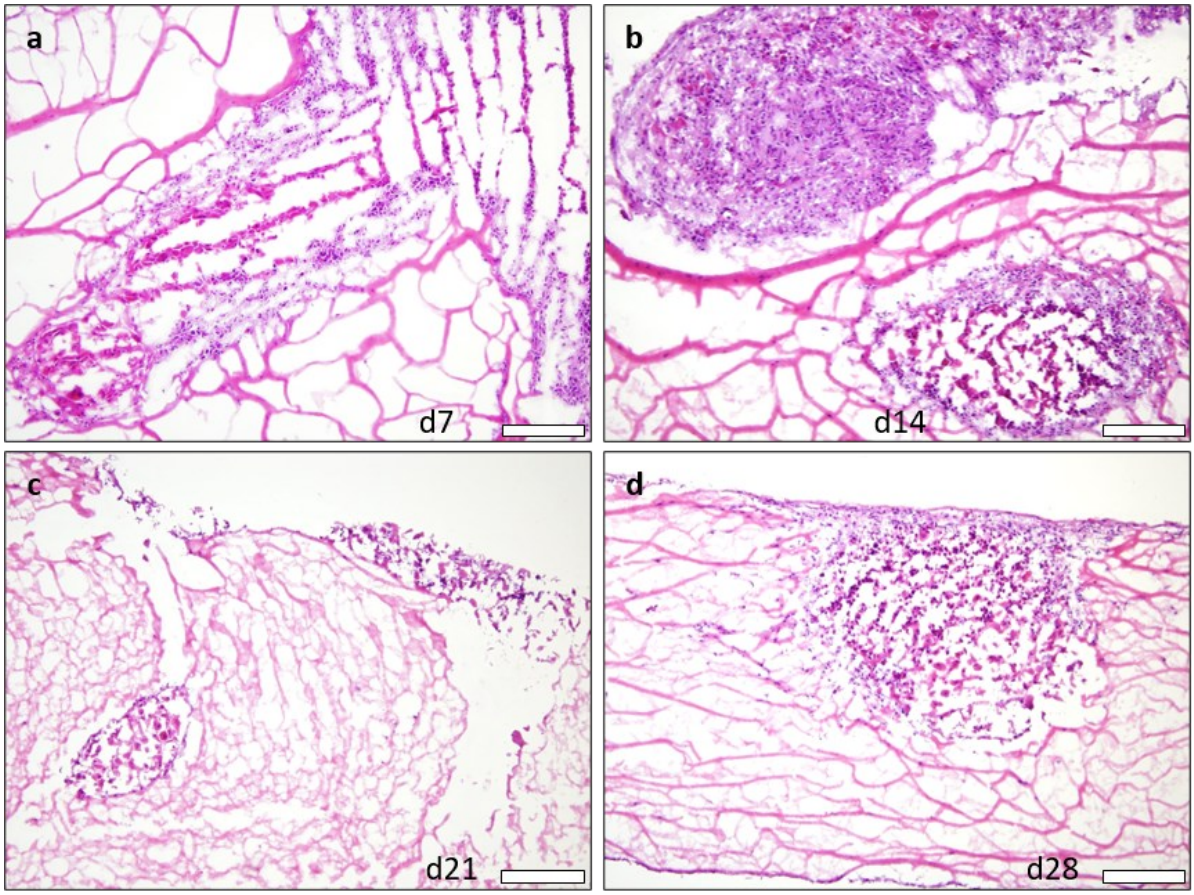

Fig 3.18: Temporal comparison of histologic hematoxylin and eosin staining of dermal matrix models with eccrine sweat gland cells.
Hematoxylin and eosin stainings of frozen sections of dermal matrix models with incorporated eccrine sweat gland coil and duct cells were prepared after 7 (d7 in a), 14 (d14 in b), 21 (d21 in c) and 28 days (d28 in d) of cultivation. Structural changes and degree of cell differentiation were compared over time. Here again, the top of the picture shows the upper side of the matrix model. Images were taken in brightfield mode at 10x magnification. Bar represents 200 µm.

To clarify origin of different cell coloration observed in HE stainings and to gather more detailed information about cell-cell interactions, frozen sections of eccrine sweat gland matrix models of d7 and d28 were investigated for their protein expression pattern using immunofluorescence staining. Description and comparison of the first and the last time point is considered sufficient as occurring differences in protein expression were gradual (see Supplemental **Fig 6.3**). Again, frozen sections of human facial skin sections served as controls and references reflecting protein distribution and cell type specificity in *in vivo* native glands. Besides, negative controls of each specimen were carried along and showed only staining for DAPI.
Concerning distribution of the cell types, coil and duct cell parts were distinguished with the help of prior HE stainings of the models and the different densities of the nuclei. Therewith, regions of coil cells were identified in the lower and central area of the cavities while duct cells lined the sides of the cavities (refer to Fig 3.18).
Miscellaneous markers known to be expressed in the eccrine sweat gland and associated cells were selected revealing the degree of analogy between these sweat gland matrix models and the native eccrine gland (**Fig 3.19**). Among them, α-SMA, a protein characteristic for

myoepithelial cells, was exclusively detected in cells surrounding the native coil compartment but was absent in sections of the matrix models (Fig 3.19a-c).
Staining for the muscarinic acetylcholine receptor M3, antimicrobial peptide dermcidin, and eccrine gland specific marker CEACAM5 was visible in coil and duct compartments of the native gland though expression was weaker in the duct (Fig 3.19a, d, and g). However, in both matrix models, of d7 and d28, these three proteins were only detected in parts of the integrated coil cells but were absent in duct cell parts. Interestingly, the staining was considerably more intense and widespread in the younger model of d7 and only scattered in the older one (Fig 3.19b, c, e, f, h, and i).
Coil cell specific glycoprotein CD44 selectively stained coil cells in the native gland (Fig 3.19d). In the sweat gland matrix model of d7 staining for this marker was weak though detectable in all eccrine sweat gland cells (Fig 3.19e). In the longer cultivated model of d28, in contrast, CD44 was stronger expressed, especially in the upper cell layers of duct cells (Fig 3.19f).
Chloride channel CFTR is another marker vital for sweat secretion in eccrine glands (Reddy and Quinton 1994). Its expression was identified in native eccrine ducts with higher intensity than in coil compartments (Fig 3.19g). Eccrine sweat gland cells in the model of d7 lacked this marker but a slight and scattered staining for CFTR was visible especially in the lower coil cell part of the older model (Fig 3.19h and i).
Exclusively identified in duct cell parts of native glands, the duct specific cell surface marker SSEA-4 was scarcely present in any matrix model (Fig 3.19j-l).
On the contrary, the water channel AQP5, a crucial protein for sweat generation in the secretory coil (Nejsum et al. 2002), stained solely the coil compartment in facial skin sections (Fig 3.19j). However, sweat gland matrix models AQP5 was only detected in the lower tip of the cell-filled cavity on d7 and in a small layer on the bottom as well as the top of the model of d28 (Fig 3.19k and l).
Tab 3.7 summarizes and graduates the staining patterns observed in this Fig 3.19.

Taken together, HE stainings of prepared matrix models with inserted eccrine sweat gland cells demonstrated successful integration of coil and duct cells into the fibroblast-supplemented collagen I matrix. Areas of coil and duct cells were discernible by their distinct hue and more densely located nuclei of duct cells. Additional immunofluorescence staining of sweat gland specific proteins α-SMA, M3, CD44, dermcidin, CEACAM5, CFTR, SSEA-4, and APQ5, corroborated zonal, cell type-related localization of coil and duct cells from HE stainings on a protein level and revealed some differences between native and cultured eccrine sweat gland cells. Thereby, cultured duct cells exhibited the most prominent changes evidenced by loss of expression of SSEA-4 and CEACAM5 and gained expression of CD44. Regarding the culture time only few differences were identified such as more intense detection of CD44 and diminished expression of M3 and dermcidin in the longer cultivated model.

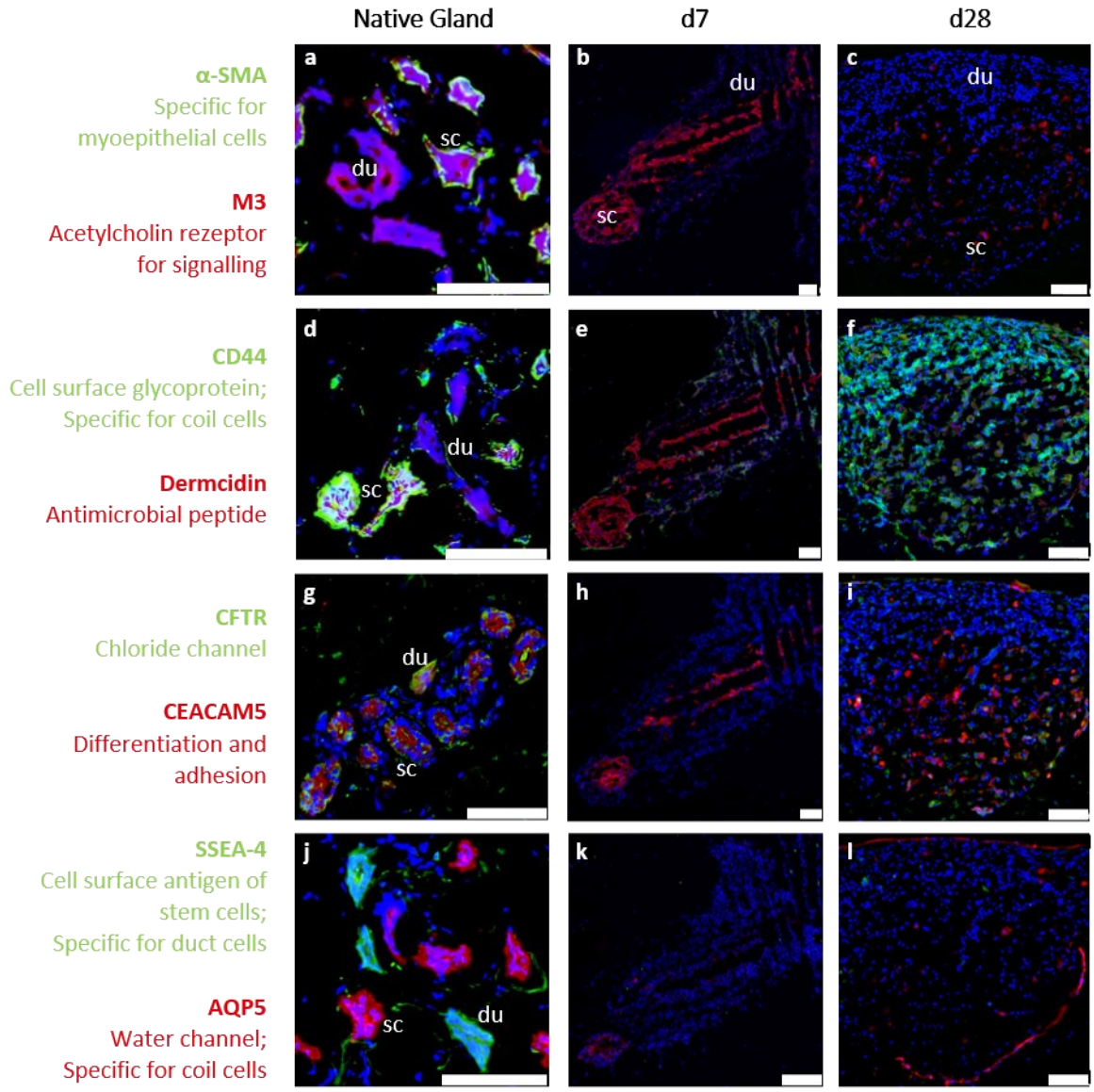

Fig 3.19: Protein expression of sweat gland-related markers in native facial skin and sweat gland matrix models.
Localization and distribution of sweat gland-associated proteins was analyzed in frozen sections of native human facial skin (left column) and in sections of sweat gland matrix models cultivated for 7 days (d7, middle column) and 28 days (d28, right column), respectively. Models were built by pre-seeding of coil cells directly into slots in the fibroblast-supplemented collagen I matrix and addition of duct cells 24 h later. The top of these pictures is the direction of the upper surface of the matrix models. Frozen sections of native skin with eccrine sweat glands served as controls for localization of the target proteins. Parts of coil cells are denoted with *sc*, while *du* signifies duct cells regions as exemplary presented in image a-c. Target proteins are depicted in red (TRITC) and green (FITC) while nuclei are stained in blue (DAPI). Bar represents 200 µm.

Tab 3.7: Comparison of protein expression in coil and duct cells of native eccrine sweat glands and sweat gland matrix models of d7 and d28.
Protein expression of the listed sweat gland-associated markers was determined using specific immunofluorescence staining in frozen sections of human facial skin (native gland) and sweat gland matrix models cultured until day 7 (d7) and day 28 (d28), respectively. Staining intensities for the respective proteins were assessed and graduated: +/++/+++ light/middle/high expression intensity; - not detected; +/- barely detectable.

	Native gland		**sweat gland matrix model d7**		**sweat gland matrix model d28**	
	coil	**duct**	**coil**	**duct**	**coil**	**duct**
α-SMA	++	-	-	-	-	-
M3	++	++	+++	-	+	-
CD44	+++	-	+	+++	++	+++
Dermcidin	+++	+	+++	-	+	-
CFTR	+	+	-	-	+	-
CEACAM5	++	++	+++	-	+++	-
SSEA-4	-	+++	-	-	-	+/-
AQP5	+++	-	+	-	++	-

3.3 Development of an immortalized duct cell line

3.3.1 Transfection and generation of a transduced duct cell pool

Like other primary cell types, also primary eccrine sweat gland cells reach a senescent stage after only few rounds of passaging. This limits the number of cells originating from the same donor. For large comparative studies such as above-described substance testing and investigation of cellular interactions, it is desirable to have recourse to well characterized and standardized cellular material. This eliminates the unwanted factor of interindividual variability from ongoing research and makes comparison between individual experiments far easier. To achieves this cellular standardization for herein described *in vitro* methods, an immortalized eccrine sweat gland duct cell line should be generated as duct cells represent the primary target of topically applied substances and products.

Therefore, primary eccrine sweat gland duct cells were derived from native eccrine sweat glands isolated from a facial skin biopsy (denoted 19-01), propagated in culture until passage 2 (P2) and sent to the external cooperation partner trenzyme GmbH for transfection with simian vacuolating virus 40 large T antigen (SV40T) (vector map of the viral gene is stated in Supplemental Fig 6.1).

After further propagation, feasibility of transduction of specifically these eccrine duct cells was assessed as well as suitable transduction conditions established. For that, part of the primary duct cells was transfected with a GFP-containing lentiviral control vector with and without addition of polybrene and at different MOI.

Independent of virus load, cells grew confluent in all attempts. **Tab 3.8** summarizes flow cytometric determination of percentage of GFP-positive cells and its mean fluorescence intensities reflecting transduction efficiency. Polybrene was added as a transduction enhancer but did not alter neither the number of GFP-positive cells nor their mean fluorescence on its own. With increasing amount of virus both, percentage of GFP-positive cells as well as its mean fluorescence, gradually increased reaching a maximum at a MOI of 10 with 60.7% of GFP-positive cells and an average fluorescence of 725.

Tab 3.8: Flow cytometric analysis of cellular fluorescence for lentiviral transduction efficacy. Primary eccrine sweat gland duct cells were transduced with different amounts of green fluorescent protein (GFP)-containing lentiviral particles per cell (MOI: multiplicity of infection) and without any viral particles as a control. To all but one approach polybrene was added to enhance the transduction efficiency. After fixation with formaldehyde, percentage of GFP-positive cells and their mean fluorescence was measured using a flow cytometer. This served as an indication for transduction efficiency. Data were provided by trenzyme GmbH, Konstanz and represent one experiment.

sample	MOI	% GFP positive	Mean fluorescence
without virus without polybrene	-	0.5	8.8
without virus with polybrene	-	0.3	15.8
transduction 1	1	7.9	487.9
transduction 2	2	12.2	483.8
transduction 3	3	14.5	530.8
transduction 4	4	19.6	489.1
transduction 5	5	24.5	512.1
transduction 6	6	32.4	570.9
transduction 7	7	36.6	582.3
transduction 8	8	40.4	605.0
transduction 9	9	49.5	656.6
transduction 10	10	60.7	752.0

As both indicators for transduction efficiency, percentage of GPF-positive cells and their mean fluorescence, were further increasing at a MOI of 10, primary eccrine sweat gland duct cells in P7 were transduced with a SV40T-containing lentiviral vector with MOIs of 10, 25 and 50 to obtain a transduced duct cell pool with the desired stable and high expression of SV40T.
Irrespective of the virus load all transduced cells grew confluent within three days after transduction. Therefore, further analyses were performed with cells transduced with a MOI of 50. Those cells were further cultivated under selection pressure by adding 1.0 µg/ml of puromycin to the cultivation medium to select cells which had stably integrated the viral RNA including SV40T and a puromycin resistance marker. As a comparison, non-transduced primary duct cells were also cultivated in medium with and without puromycin. While all parental cells under selection pressure died within six days, the transduced cell pool (termed SGDC-SV40T from here on) kept proliferating (**Fig 3.20**). Primary cells cultured in normal medium remained proliferative at first but reached a senescent stage accompanied by higher PDT. Finally, parental cells stopped proliferating beyond P20 and exhibited an altered cell morphology with a broader and less defined cell shape compared to young proliferative duct cells (**Fig 3.21a-c**).
To control if shipping conditions would affect cellular vitality, an aliquot of SGDC-SV40T were cryopreserved in P14 and thawed again for further culturing. Thawed SGDC-SV40T exhibited the characteristic more longitudinal morphology (Fig 3.21c), but their proliferation was slowed with PDT of 40 to 80 h compared to transduced cells prior to freezing which had PDT of 30 to 60 h. Of note, non-cryopreserved SGDC-SV40T also showed increasing PDT in the last rounds of passaging (P18 onwards).

Condensed, successful transduction of primary eccrine sweat gland duct cells with an SV40T-containing lentiviral vector at a MOI of 50 and including a puromycin resistance gene was evidenced by steady proliferation under selection pressure. Transduced cells remained proliferative beyond the normal stage when parental cells became senescent indicating at least a prolonged life span of these cells. Effective immortalization of these cells, however, required further testing. Therefore, transduced duct cells were cryopreserved in P14 and shipped back from trenzyme GmbH for detailed characterization.

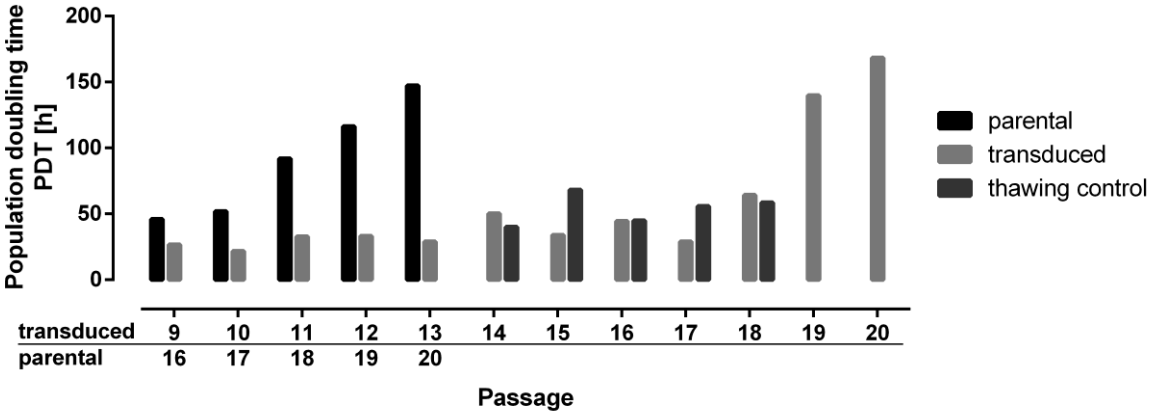

Fig 3.20: Population doubling times of primary and transduced eccrine sweat gland duct cells. Primary eccrine sweat gland duct cells were transduced with a lentiviral vector at a MOI of 50 containing SV40 large T antigen (SGDC-SV40T) and a puromycin resistance gene. They were cultured under selection pressure of 1 µg/ml of puromycin. Depicted is their growth behavior (light grey) in comparison to the one of the primary, parental duct cells (black) and a thawing control of transduced cells (dark grey). Population doubling times (PDT) in hours (h) are stated for each round of passage. Primary cells became senescent throughout passaging, but also the PDT of SGDC-SV40T increased at higher passages. Thawing control showed slightly higher PDT compared to respective passages of SGDC-SV40T without freezing stress.

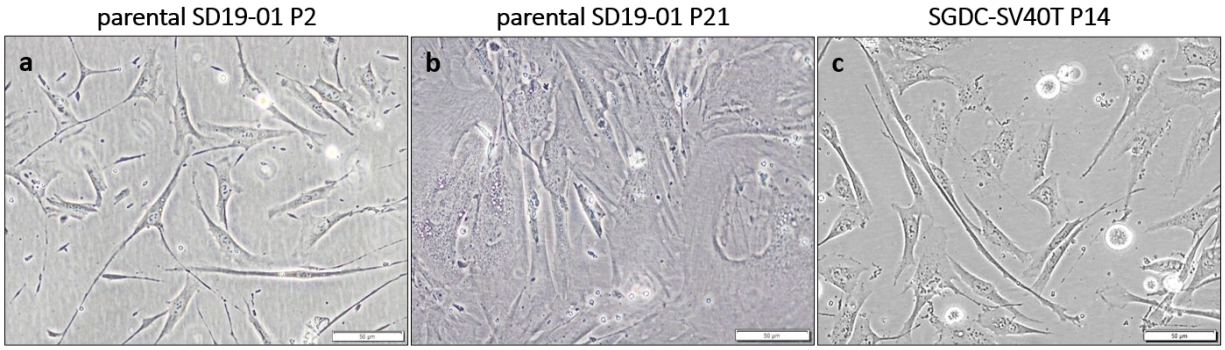

Fig 3.21: Cell morphology of parental and transduced eccrine sweat gland duct cells. Parental and SV40 large T antigen-transduced eccrine sweat gland duct cells (SGDC-SV40T) were cultured until parental cells became senescent while SGDC-SV40T kept proliferating as a proof for successful transduction and increased life span. Proliferative, young parental duct cells in passage 2 (P2) showed the characteristic more longitudinal cell morphology (**a**) while senescent parental cells in P21 exhibited an altered, broader, and less defined cell shape (**b**). SV40T-transduced cells retained their longitudinal cell morphology (**c**). Bar represents 50 µm.

3.3.2 Growth behavior of the transduced duct cell pool

After shipping, SGDC-SV40T were taken into culture in selection medium containing 1 µg/ml of puromycin and their growth behavior was monitored to evaluate their increased life span and possible immortalization (**Fig 3.22**). While initially high PDT in P15 was attributed to thawing of the cells, SGDC-SV40T exhibited gradually slowed growth in the following passages with a maximal PDT of 136 h in P19. Interestingly, starting from P21/22 transduced cells proliferated faster again and finally reached stable PDT of 30 to 40 h from P23 onwards comparable to initial PDT before the "crisis". This indicates mere transduction of primary eccrine sweat gland duct cells with SV40T to be insufficient to achieve immortalization. Contemporaneously with resuming decreased PDT beyond P20, morphology of the SGDC-SV40T slightly changed and initially longitudinal cells in P14 exhibited a slightly rounder shape (**Fig 3.23a** and **b**), suggesting further underlying cellular processes to have occured.

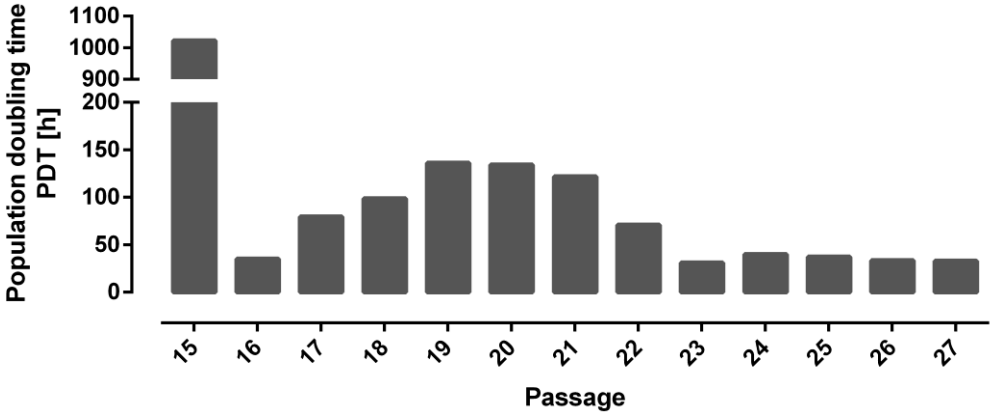

Fig 3.22: Population doubling times of transduced eccrine sweat gland duct cell pool.
Depicted are population doubling times (PDT) in hours (h) of several passages of the eccrine sweat gland duct cell pool transduced with SV40 large T antigen-containing lentiviral vector. After initial slowed growth, cells overcame a small crisis in passage 20 (P20) and gradually resumed to PDT in the range of those prior to the crisis (P16). Afterwards, cells exhibited stable growth and PDT (P23 to P27).

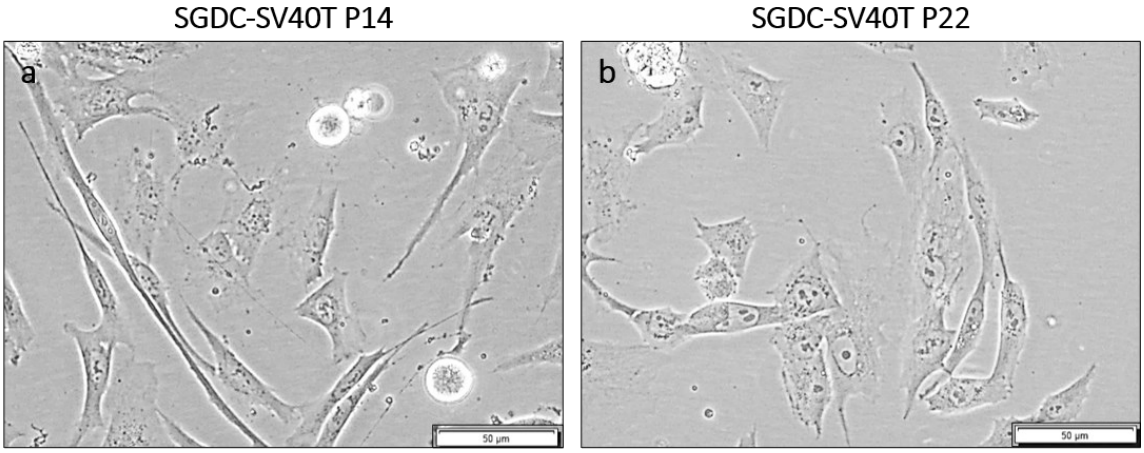

Fig 3.23: Morphological transition of SV40T-transduced eccrine sweat gland duct cells.
Cell morphology of the SV40T-transduced eccrine sweat gland duct cell pool (SGDC-SV40T) in passage 14 (P14) (**a**) and P22 (**b**) are compared. After overcoming the growth crisis in P20 cells were characterized by a slightly rounder shape compared to their rather longitudinal form in P14. Images were taken at 10x objective magnification in bright field mode using CKX14 microscope with the digital camera XC10. Bar represents 50 µm.

3.3.3 Single cell cloning

To obtain a defined eccrine sweat gland cell line with distinct characteristics, single cell cloning was performed with SGDC-SV40T by seeding of one cell per cavity in 96-well plates. In several of these wells colony forming originated from one cell when cultured in preconditioned selection medium but failed to emerge when cloning was performed in fresh selection medium. In the latter case, single cells exhibited slowed proliferation and became senescent before reaching a substantial number. With preconditioned selection medium, which contained metabolic byproducts of therein previously cultured transduced duct cells, single cell cloning was successful and the first 15 clones reaching confluency in 100 mm Petri dishes were further characterized. On average, the PDT of those clones was similar, ranging between 34.4 and 37.2 h (**Fig 3.24**). Also morphologically, those isolated clones exhibited the same appearance of a rather roundish shape comparable to post-crisis SGDC-SV40T. For simplification, clones are designated according to the plate and well they originate from.

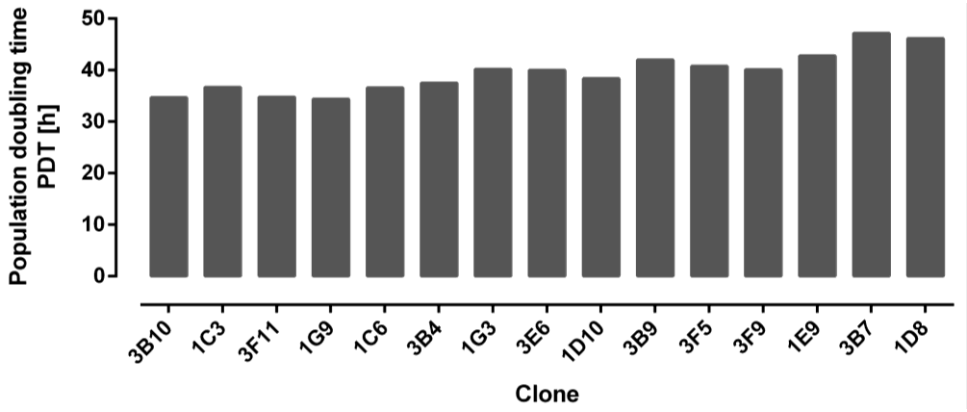

Fig 3.24: Population doubling times of isolated transduced duct cell clones.
Shown are average population doubling times (PDT) in hours (h) of 15 isolated SV40T-transduced duct cell clones which formed colonies in preconditioned selection medium and were further propagated in selection medium until reaching confluency in 100 mm Petri dishes. Single cell cloning was performed with SV40T-transduced duct cell pool by seeding on average one cell per cavity of a 96-well plate.

3.3.3.1 Molecular biological characterization of isolated duct cell clones

As basis of the immortalized duct cell line the duct cell clone with traits closest to the native tissue should be identified. To select this ideal clone aliquots of all isolated SV40T-transduced eccrine sweat gland duct cell clones were analyzed in P21 and compared regarding their gene expression levels using RT-qPCR (**Fig 3.25**). Most important for the salt absorbing function of duct cells are sodium and chloride ion channels represented by ENaC and CFTR. CEACAM5 was chosen as a marker characterizing eccrine sweat gland cells.
Relative gene expression levels arbitrary related to clone 1B10 were determined reaching values between 0.2 and 1.0 as well as 0.5 and 3.0, for ENaC and CFTR, respectively. In case of CEACAM5, clonal variations were pore pronounced: While this marker was undetectable in clones 3F11, 3B4, and 1E9, clones 3B10, 1G9, 3E6, and 3F9 showed low, and clones 1C3, 1C6, 3F5 and 3B9 high relative expression levels of over 50. Based on these data 8 clones (3B10, 1C3, 1C6, 1D10, 3F5, 3B9, 3B7, and 1D9) with overall highest expression levels were chosen for further analyses as they were assumed to exhibit traits closest to the native duct.

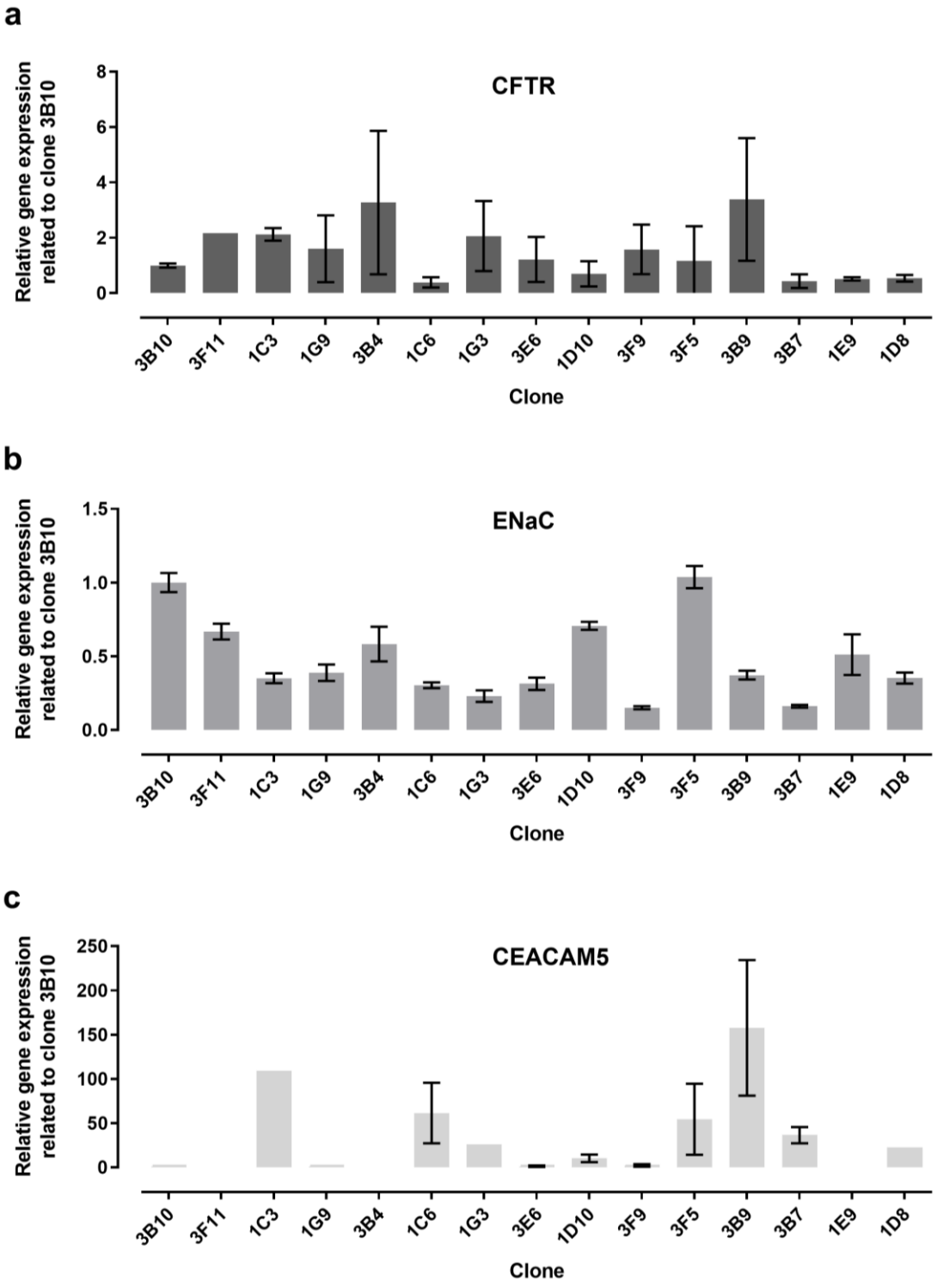

Fig 3.25: Relative gene expression levels of isolated SV40T-transduced duct cell clones.
Depicted are relative gene expression levels for cystic fibrosis transmembrane conductance regulator (CFTR) (**a**), epithelial sodium channel (ENaC) (**b**), and carcinoembryonic antigen-related cell adhesion molecule 5 (CEACAM5) (**c**) quantified by RT-qPCR from 15 isolated SV40T-transduced eccrine sweat gland duct cell clones. Clones were propagated until passage 21 and aliquots sampled for mRNA analysis. Randomly chosen, gene expression value of clone 3B10 was set to 1.0. GAPDH served as the housekeeping gene. Data are mean ± SD of one experiment performed in triplicate replicate. Relative gene expression values related to the ones of the native gland are shown in Supplemental Fig 6.4.

A more extensive gene expression analysis including sweating-related genes ANO1, CFTR, ENaC, NKCC1, M3, and AQP5 and structural genes collagen type I (COL1) and type 3 (COL3) was conducted. For that, primary parental duct cells and selected transduced clones were incorporated into *in vitro* 3D HD eccrine sweat gland models. An advantage of those 3D models is the union of coil and duct cells in one spheroid and, thus, the close cellular interaction of both cell types as delineated in chapter 3.2.1. Furthermore, cellular orientation reflects a more physiological environment compared to conventional monolayer cell cultures. Both factors trigger a protein expression in 3D models which resembles the native situation more closely. To prepare those spheroids the above-described approach of pre-seeding of 12,500 duct cells - primary ones or transduced clones - with following addition of the same number of primary coil cells (from the same donor) was chosen (refer to chapter 3.2.1). After 3 d 3D models were harvested for mRNA extraction. Unfortunately, selected duct cell clones 3B7 and 3B9 experienced drastically slowed growth with the number of cells being insufficient for preparation of 3D models. Thus, they were omitted in following investigations.
As controls, 3D models composed of primary coil and duct cells from standard donor 15-24 and primary cells of donor 19-01 were prepared. Of note, primary duct cells of donor 19-01 are parental cells of the SV40T-transduced duct cells and derived clones. Relative gene expression of each sample was calculated with reference to the expression of model 15-24 having a set value of 1 (**Fig 3.26**). In detail, expression of sweating-relevant gene ANO1, ENaC, NKCC1, M3, and AQP5 varied between 3D models containing primary and SV40T-transduced duct cells with values between 0.5 and 2.0 (Fig 3.26a, c, d, e, and f). Overall, gene expression was lower in *in vitro* 3D models with transduced duct cell clones compared to those prepared with primary cells.
Interestingly, gene expression of the duct specific chloride channel CFTR was nearly undetectable in 3D models containing primary and transduced duct cells originating from donor 19-01 compared to 3D models with cells from donor 15-24 (Fig 3.26c).
Additional to those sweat-relevant markers expression of the structural components COL1 and COL3 was analyzed (Fig 3.26g and h). Notably, all 3D models with transduced duct cells exhibited virtually no expression of both, COL1 and COL3. Parental duct cells 19-01, however, showed an increased expression of COL3 compared to the other primary cells 15-24.

Altogether, molecular biological analyses of gene expression patterns of *in vitro* 3D HD models containing isolated SV40T-transduced duct cell clones and comparison with those of primary cells revealed the 3D models with transduced cells to exhibit, on average, lower expression of sweating-related genes. Besides, variations among the transduced duct cells clones and interindividual differences between the two primary cell pools were detected. The latter variation was especially obvious regarding CFTR expression. Drastically reduced expression of COL1 and COL3 in 3D models with transduced duct cell clones was also quite prominent. Apart from that, transduction seemed to have no significant impact on gene expression of sweating-relevant markers.
Among the SV40T-transduced duct cells, 3D models prepared with clones 1D10, 1D8, 3B10, and 1C6 showed highest gene expression and closest resemblance to primary duct cells.

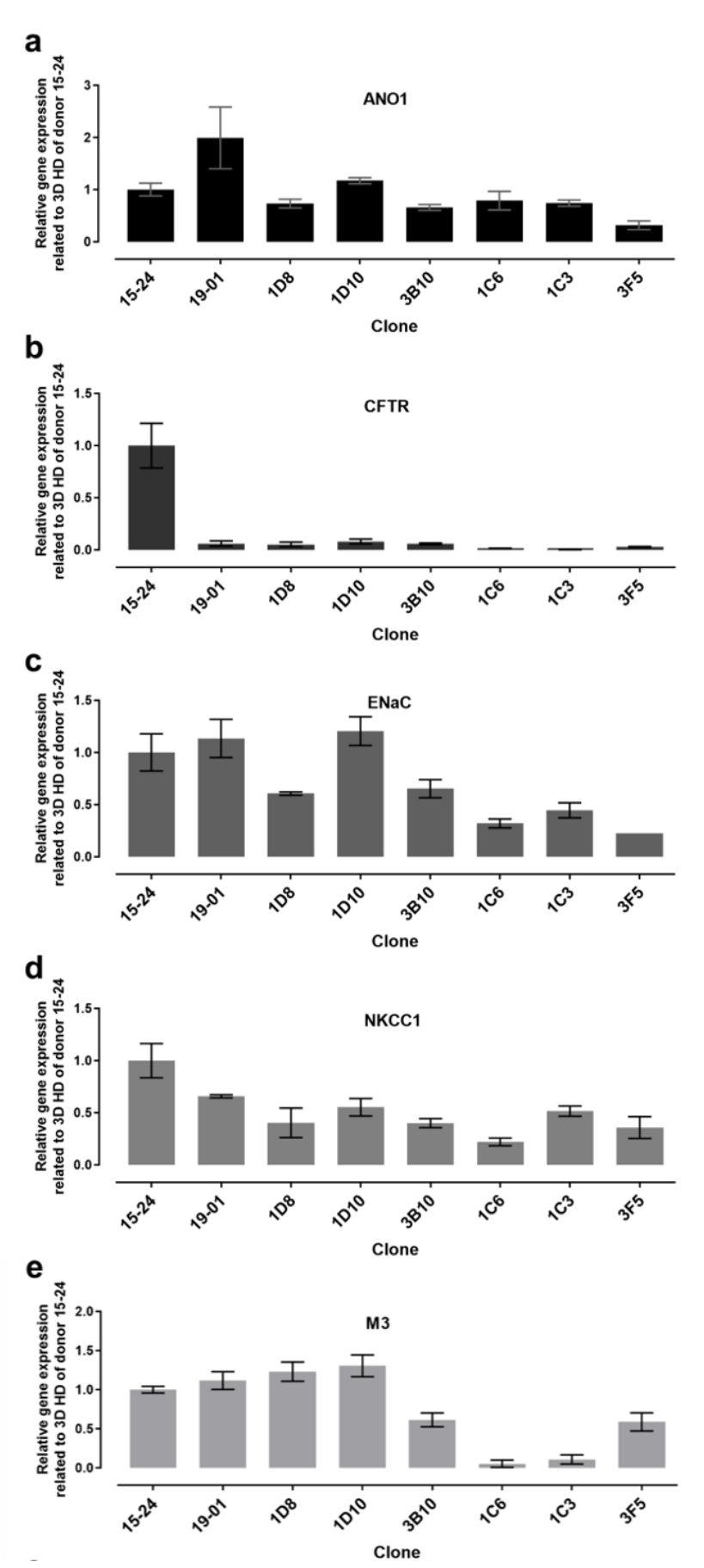
a
ANO1
Relative gene expression related to 3D HD of donor 15-24
3
2
1
0
15-24
19-01
1D8
1D10
3B10
1C6
1C3
3F5
Clone
b
CFTR
Relative gene expression related to 3D HD of donor 15-24
1.5
1.0
0.5
0.0
15-24
19-01
1D8
1D10
3B10
1C6
1C3
3F5
Clone
c
ENaC
Relative gene expression related to 3D HD of donor 15-24
1.5
1.0
0.5
0.0
15-24
19-01
1D8
1D10
3B10
1C6
1C3
3F5
Clone
d
NKCC1
Relative gene expression related to 3D HD of donor 15-24
1.5
1.0
0.5
0.0
15-24
19-01
1D8
1D10
3B10
1C6
1C3
3F5
Clone
e
M3
Relative gene expression related to 3D HD of donor 15-24
2.0
1.5
1.0
0.5
0.0
15-24
19-01
1D8
1D10
3B10
1C6
1C3
3F5
Clone

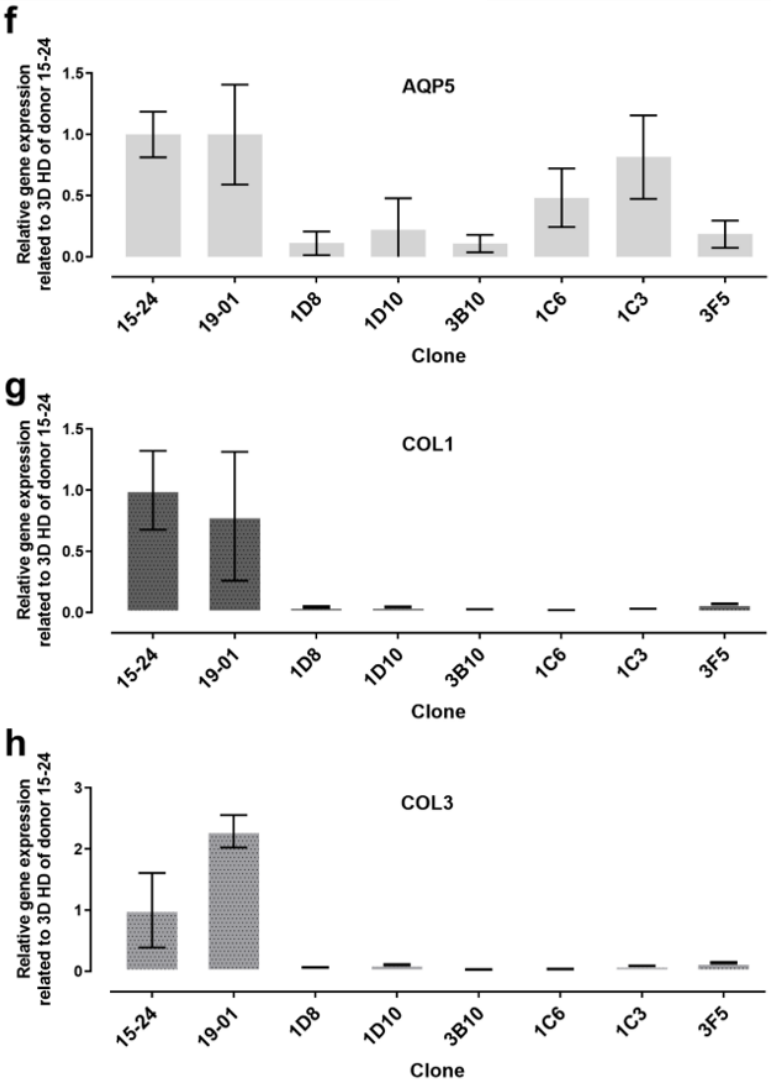

Fig 3.26: Comparison of relative gene expression levels of *in vitro* 3D eccrine sweat gland models with primary duct cells and transduced duct cell clones.
Depicted are relative gene expression levels of anoctamin 1 (ANO1) (**a**), cystic fibrosis transmembrane conductance regulator (CFTR) (**b**), epithelial sodium channel (ENaC) (**c**), sodium-potassium-chloride channel 1 (NKCC1) (**d**), muscarinic acetylcholine receptor 3 (M3) (**e**), aquaporin 5 (AQP5) (**f**), as well as collagen type 1(COL1) (**g**) and type 3 (COL3) (**h**) of *in vitro* 3D models of the human eccrine sweat gland. 3D models are composed of primary coil and duct cells from standard donor 15-24 or donor 19-01, the latter being the origin of the SV40T-transduced duct cell clones. 3D models comprising each one SV40T-transduced duct cell clone together with primary coil cells are abbreviated with the clone name. Gene expression was quantified by RT-qPCR of 3 d old hanging drop cultures each containing 12,500 coil and duct cells. Gene expression of standard donor 15-24 was set to 1.0 and GAPDH served as the housekeeping gene. Data are mean ± SD of one experiment performed in triplicate replicate.

3.3.3.2 Histological characterization of isolated duct cell clones in 3D models

Closely linked to gene expression of transduced duct cells clones is their expression of sweating-associated as well as structural proteins. As a further step in the characterization process, localization and distribution of specific markers was scrutinized by immuno-histological staining of frozen sections of above-described *in vitro* 3D sweat gland models. Examination of duct cells incorporated into those 3D models was chosen over staining of monolayer cells as expression of certain proteins is only observed in more physiological cell

surroundings with intensified cell-cell-contact. Besides, mutual presence of coil and duct cells exhibits higher resemblance to the natural situation in the native gland and might reveal cell contact-related expression patterns.

Prior to localization of selected proteins via specific antibodies the structure of the 3D models was scrutinized using HE staining of frozen sections (**Fig 3.27**). Therein, cell nuclei appeared bluish violet while the cell cytoplasm was colored in shades of purple to pink. All *in vitro* 3D models were characterized by a dense core of duct cells, primary (a and b) or SV40T-transduced (c-h), which was surrounded by varying shapes of coil cells. Thus, these 3D models showed spherical structures identical to the ones described above (refer to 3.2.1).

Regardless of the type of duct cells, their structure was more compact evidenced by close aggregation of nuclei and intense purple staining. In contrast, cell organization of coil cells appeared less dense with larger and loosely situated nuclei and their cytoplasm featured a rather pink staining. Interestingly, coil cells in direct contact with the duct cells formed a denser structure. Further, 3D models with cells from donor 15-24 were more compact compared to those with cells derived from donor 19-01. As an exception, 3D model including clone 3F5 was strikingly compact with a defined outside border (Fig 3.27h).

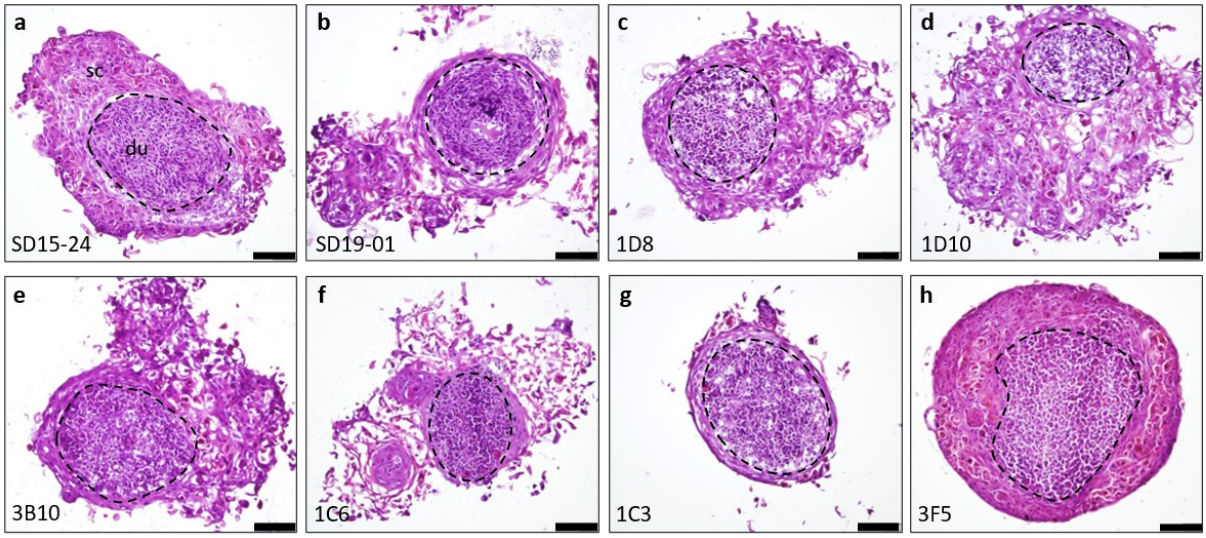

Fig 3.27: Hematoxylin and eosin staining of *in vitro* 3D eccrine sweat gland models with primary duct cells and SV40T-transduced duct cell clones.
Morphological and structural characteristics of *in vitro* 3D eccrine sweat gland models were compared by hematoxylin and eosin staining. Frozen sections of 3D models prepared with primary duct and coil cells from donor 15-24 (**a**) or donor 19-01 (**b**) and frozen sections of 3D models formed by primary coil cells (donor 19-01) with an SV40T-transduced duct cell clone (**c-h**) are compared. 3D models were generated by pre-seeding of 12,500 duct cells 24 h prior to addition of 12,500 coil cells. Exemplary for all, regions of duct cells in the core (denoted by *du*) and surrounding secretory coil cells (denoted with *sc*) are delineated in a. Bar represents 100 µm.

Immunofluorescence-based examination of expression of sweating-relevant proteins was also conducted in *in vitro* 3D models. Like for description of protein distribution in the eccrine sweat gland matrix models, here again frozen sections of human facial skin served as controls and as references revealing cell type specificity and protein distribution in native glands. *In vitro* 3D models generated with primary, parental duct cells (19-01) were also stained to reveal

possible changes in protein expression evoked by the immortalization process. Once again, no staining was observed in negative control sections of neither of facial skin nor 3D models.
As determined by HE staining, duct cells formed the core of 3D models with coil cells surrounding this core. In skin sections, in contrast, sweat gland coils and ducts from separate, consecutive tubular structures. As a limitation of herein employed 3D culturing technique, and as already mentioned before, such a tubule cannot be generated using the HD culture approach. Therefore, transition to a spherical model is required.
Protein expression analyses included sweating-related and structural markers already included in gene expression determination (M3, AQP5, CFTR, CEACAM5, ANO1, NKCC1, COL1, COL3, and ENaC) as well as additional characteristic proteins (α-SMA, CD44, dermcidin, SSEA-4, CD9, CD276, CK15) (**Fig 3.28** and **Fig 3.29**).
In detail, microfilament α-SMA was only located around the native gland coil as it is specifically expressed by myoepithelial cells surrounding the coil (Fig 3.28a), but it was completely absent in both, primary 3D models and those with transduced duct cells (Fig 3.28b and c).
In contrast, muscarinic receptor M3, antimicrobial peptide dermcidin and eccrine gland-characterizing marker CEACAM5 were detected in the native coil as well as in the duct, though weaker (Fig 3.28a, d, and g). Strikingly, in all 3D models these proteins were only expressed in coil cells but neither in primary nor transduced duct cells (Fig 3.28b, c, e, f, h, and i).
Cell surface glycoprotein CD44 was specific for the native coil (Fig 3.28d), but a different expression pattern was observed in 3D models. There, CD44 was exclusively present in duct cells, primary and transduced ones (Fig 3.28e and f).
Localization of the chloride channel CFTR in native glands was, as expected, more intense in the duct portion and scattered in the coil (Fig 3.28g). In contrast, neither 3D model showed any staining for this protein (Fig 3.28h and i).
Recently described as a marker exclusively present in eccrine ducts, localization of the cell surface antigen SSEA-4 was restricted to this compartment, while secretion-related water channel AQP5 was only detected in the native coil (Fig 3.28j). Similar to their *in vivo* distribution, SSEA-4 was solely detected in primary as well as transduced duct cells, while presence of AQP5 was confined to the coil cell area in all *in vitro* 3D models (Fig 3.28k and l).

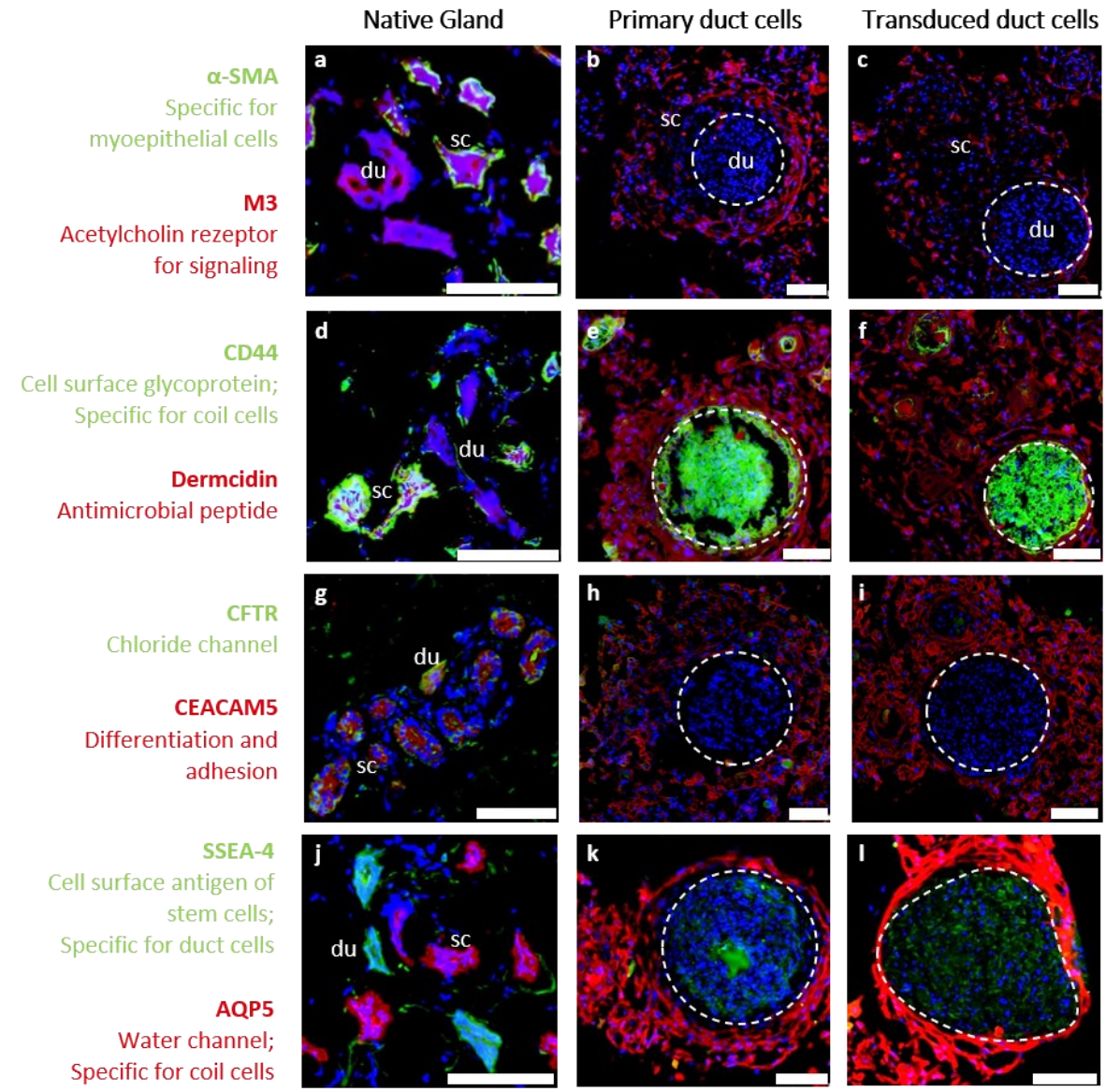

Fig 3.28: Protein expression in native sweat glands and 3D models with primary duct cells or transduced duct cell clones.
Localization and distribution of characteristic proteins were compared by immunofluorescence staining in frozen sections of 3D models prepared with primary duct and coil cells from donor 19-01 (primary cells) and in frozen sections of 3D models formed by primary coil cells (donor 19-01) with an SV40T-transduced duct cell clone. 3D models were built by pre-seeding of 12,500 duct cells 24 h prior to addition of 12,500 coil cells. Frozen sections of native skin with eccrine sweat glands served as controls for localization of the target proteins. Parts of secretory coil cells are denoted with *sc*, while *du* signifies duct cells regions. Target proteins are depicted in red (TRITC) and green (FITC) while nuclei are stained in blue (DAPI). Bar represents 100 µm.

Furthermore, secretion-related chloride channel ANO1 and ion co-transporter NKCC1 were specifically found in the native sweat gland coil with ANO1 confined to the luminal membrane (Fig 3.29a). Strikingly, in both *in vitro* 3D models ANO1 was strongly expressed in those coil cells having direct contact with duct cells, but only scarcely detected in other parts of coil cells region and was completely absent from duct cells (Fig 3.29b and c). Expression of NKCC1, in contrast, was equally intense in both, primary coil and primary duct cells, of *in vitro* 3D models (Fig 3.29b), but its presence was weaker in transduced duct cells (Fig 3.29c).

Cell surface protein CD9 stained coil cells in the native eccrine sweat gland and was also detected around the duct compartment (Fig 3.29d). Similarly, coil cells in the 3D models were positive for CD9, while incorporated duct cells, primary and transduced ones, exhibited only scattered and weak staining (Fig 3.29e and f).
Both structural proteins, COL3 and COL1, surrounded the native gland coil and duct compartments and stained parts of the connective tissue of native dermal skin (Fig 3.29d and g). Surprisingly, primary and transduced duct cells expressed COL3 (Fig 3.29e and f), whereas COL1 was only detected in primary duct cells (Fig 3.29h and i). Coil cells, in contrast, were negative for these structural proteins.
Opposed to this, CD267, the transmembrane protein of prominin-1, was detected in transduced but not in primary duct cells (Fig 3.29h and i). In facial skin sections, small areas with weak staining of CD276 were present in the proximity of eccrine sweat glands (Fig 3.29g). Intermediate filament CK15 was merely weakly detectable in the native coil and absent from the duct compartment, while expression of the sodium channel ENaC was stronger in native ducts compared to coils (Fig 3.29j). In all 3D models, however, coil and duct cells showed in equally intense staining for ENaC with no difference between primary and transduced duct cells (Fig 3.29k and l). Structural protein CK15 was confined to coil cell regions of all 3D models, like the native distribution *in vivo* (Fig 3.29k and l).
Tab 3.9 summarizes and grates protein stainings depicted in Fig 3.28 and Fig 3.29.

In short, with the help of HE staining structural similarity of all 3D models with primary and transduced duct cells was demonstrated. Further, immunofluorescence-based location of sweat gland-associated proteins revealed cell type-specific distribution of certain markers such as APQ5, SSEA-4, ANO1, CK15, and ENaC which were identical to the distribution in the native gland. In contrast, staining for NKCC1, CD44, CEACAM5, M3, COL3, and CD276 uncovered differences between native glands and *in vitro* 3D HD models. Additionally, findings of gene expression analyses were confirmed showing absent expression of CFTR in *in vitro* 3D models and lost expression of COL1 in models with SV40T-transduced duct cells.

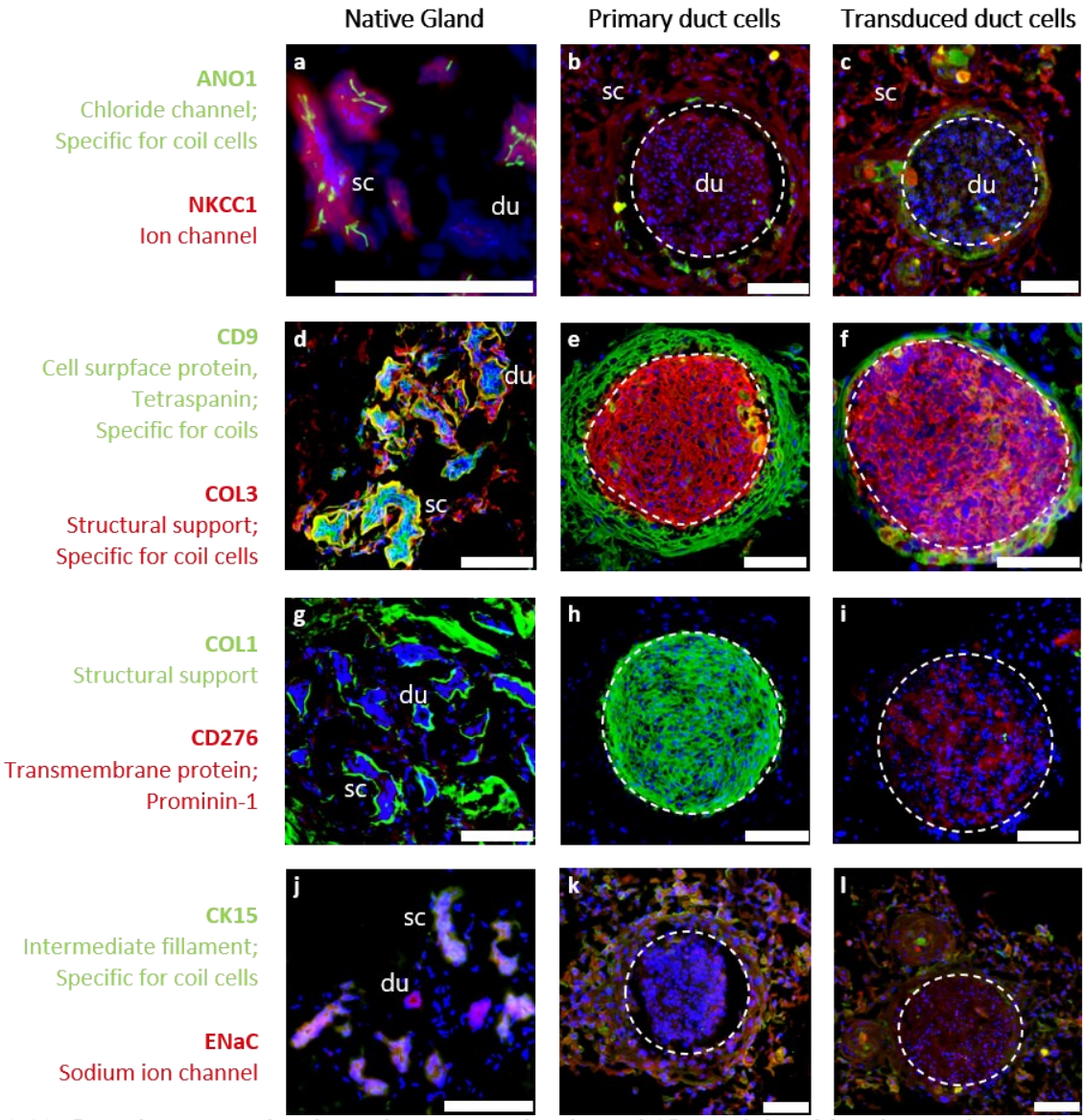

Fig 3.29: Protein expression in native sweat glands and 3D models with primary duct cells or transduced duct cell clones.
Localization and distribution of characteristic proteins were compared by immunofluorescence staining in frozen sections of 3D models prepared with primary duct and coil cells from donor 19-01 (primary cells) and in frozen sections of 3D models formed by primary coil cells (donor 19-01) with an SV40T-transduced duct cell clone. 3D models were built by pre-seeding of 12,500 duct cells 24 h prior to addition of 12,500 coil cells. Frozen sections of native skin with eccrine sweat glands served as controls for localization of the target proteins. Parts of secretory coil cells are denoted with *sc*, while *du* signifies duct cells regions. Target proteins are depicted in red (TRITC) and green (FITC) while nuclei are stained in blue (DAPI). Bar represents 100 µm.

Tab 3.9: Overview of protein expression in coil and duct cells of native eccrine sweat glands and 3D HD models containing primary or SV40T-transduced duct cells.
Protein expression of the listed sweat gland-associated markers was determined using antibody-based immunofluorescence staining in frozen sections of human facial skin (native gland) or 3D HD models prepared by pre-seeding of primary or SV40T-transduced duct cells and addition of primary coil cells. Staining intensities for the respective proteins were graduated: +/++/+++ light/middle/high expression intensity; - not detected; +/- barely detectable.

	Native gland		Primary duct cells		Transduced duct cells	
	coil	duct	coil	duct	coil	duct
α-SMA	++	-	-	-	-	-
M3	++	++	++	-	++	-
CD44	+++	-	-	+++	-	+++
Dermcidin	+++	+	+++	+	+++	+
SSEA-4	-	+++	-	++	-	++
AQP5	+++	-	+++	-	+++	-
CFTR	+	+	+/-	-	+/-	-
CEACAM5	++	++	++	-	++	-
ANO1	++	-	+	+/-	+	+
NKCC1	++	+	++	++	++	+
CD9	++	+	+++	+	+++	+
COL3	+	+	-	+++	-	++
COL1	+	+	-	+++	-	-
CD276	+/-	+/-	-	-	-	++
CK15	++	+	++	+	++	+
ENaC	+	++	++	++	++	++

3.3.3.3 Functional characterization of isolated duct cell clones

Availability of unlimited and standardized cellular material is a big advantage when having an immortalized cell line. Thus, development of an immortalized eccrine sweat gland duct cell line was desired for the research at hand to circumvent donor-dependent variations which is the case when using primary cell material. Ideally, generated cell line should give further insight into the salt-reabsorption mechanism of the duct and should be used for testing of AP actives. Therefore, picked SV40T-transduced duct cell clones were assessed for their reaction upon treatment with above well-described test substances selected from both substance classes: PEI-HCl and DPG (**Fig 3.30**). As controls, primary duct cells from the standard donor 15-24 and primary parental cells of the transduced duct clones (19-01) were carried along.
All, primary duct cells and transduced clones, showed tendentially the same changes of $[Na^+]_i$ and $[Cl^-]_i$ when they were treated with either 0.2% AS (w/w) of PEI-HCl or 2% AS (w/w) of DPG. However, intensities of the changes varied among the different cell cultures.
As described above (refer to 3.1.1.1), application of PEI-HCl also reduced $[Na^+]_i$ to values of 30-60% of the respective untreated control in these experiments but increased $[Cl^-]_i$ up to 234%. Notably, primary duct cells 19-01 exhibited by far the strongest changes in $[Cl^-]_i$ compared to thereof derived clones reaching an intracellular level of over 600%.
In contrast, addition of DPG increased $[Na^+]_i$ yielding relative concentrations of 125-163%, which was comparable to reactions seen before (refer to 3.1.2.1). Simultaneously, $[Cl^-]_i$ was

diminished to values of 70-75%. Solely clone 1C6 reacted with an exceptionally low $[Cl^-]_i$ value of 31%.

In sum, functional analyses of SV40T-transduced duct cell clones confirmed their ability to react towards substance application with changes of intracellular ion levels identical to the ones of standard donor 15-24 and parental cells 19-01. This sensitivity of all isolated clonal cultures towards substance application is supposed to show functionality of biochemical processes. Thus, all of them are suited for utilization in testing procedures. Most qualified, though, seemed clones 1C3, 1D8, 1D10 and 3B10 as they exhibit ion profiles with closest resemblance to primary cells.

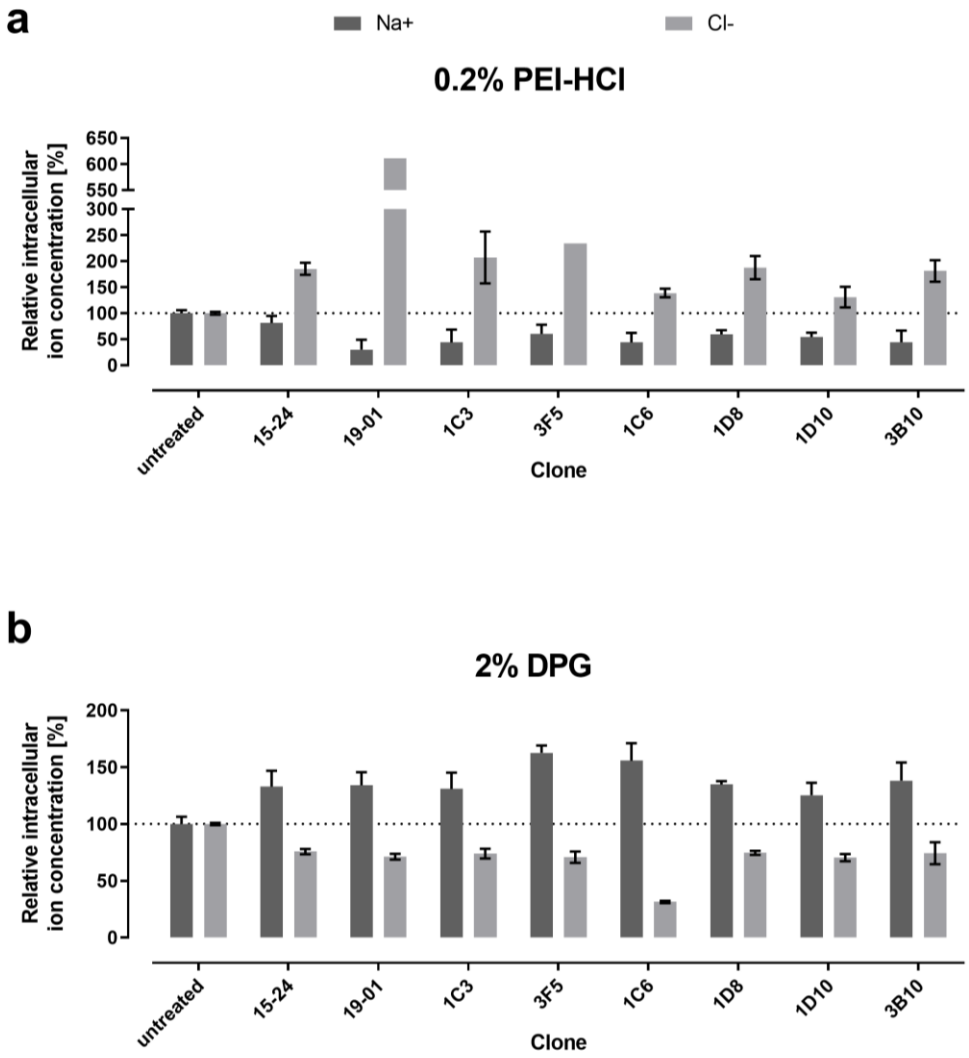

Fig 3.30: Functional characterization of primary duct cells and SV40T-transduced duct cell clones after treatment with PEI-HCl and dipropylene glycol.
Relative intracellular ion concentrations were determined in monolayers of primary eccrine sweat gland duct cells from the standard donor 15-24, of primary duct cells from donor 19-01, and of the selected SV40T-transduced duct cell clones after treatment with 0.2% AS (w/w) of PEI-HCl (**a**) or 2% AS (w/w) of DPG (**b**) in DMEM. Relative intracellular ion concentrations in percent [%] of untreated (100%) were determined from measured fluorescence intensities using a microplate reader. Data are mean ± SD of one representative experiment performed in sextuple replicates.

3.3.3.4 Characterization of duct cell clone 1D10

Ideally, an immortalized cell line stems from one cloned cell to limit initial genetic diversity. Based on above-described molecular, histological, and functional analyses all SV40T-transduced, isolated eccrine sweat gland duct cell clone cultures exhibited comparable characteristics. Out of them, culture of clone 1D10 was chosen as the basis for the immortalized duct cell line as above-delineated analyses showed it to be best qualified and having traits closest to primary cells regarding gene expression, protein structure and functional behavior.

Investigations on morphology and growth behavior of this clonal culture during passaging revealed no abnormalities. After thawing in P22, clonal cells exhibited a slowed propagation with a PDT of nearly 350 h. With progressing culture time PDT gradually decreased until reaching steady PDT of 30-35 h from P26 onwards (**Fig 3.31**). Over the whole timespan morphology of the cells remained constant showing a mixture of longitudinal and cuboidal cell shapes (**Fig 3.32a** and **b**). In comparison, young non-transduced parental cells featured a similar though more longitudinal morphology as described previously (Fig 3.32c).

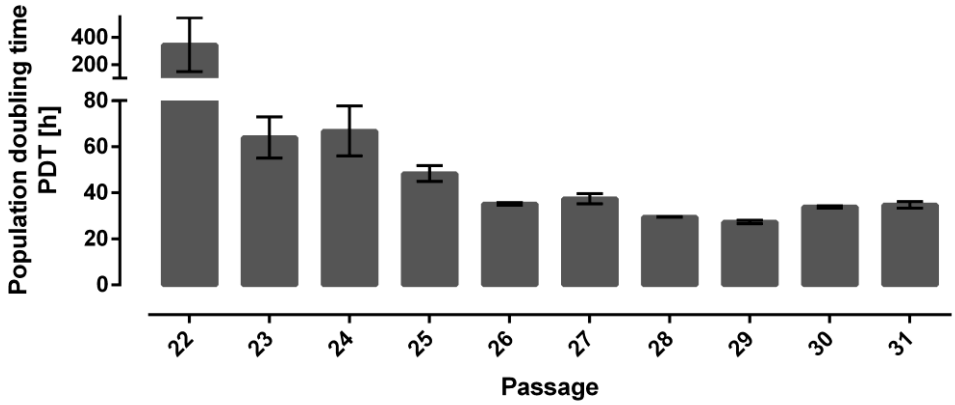

Fig 3.31: Population doubling times of cultures of SV40T-transduced eccrine sweat gland duct cell clone 1D10.
Depicted are population doubling times (PDT) in hours (h) over several passages of the culture of SV40 large T antigen (SV40T)-transduced duct cell clone 1D10. Initial slow growth was observed after thawing in passage 22 (P22). PDT decreased from then on and reached stable values from P26 onwards.

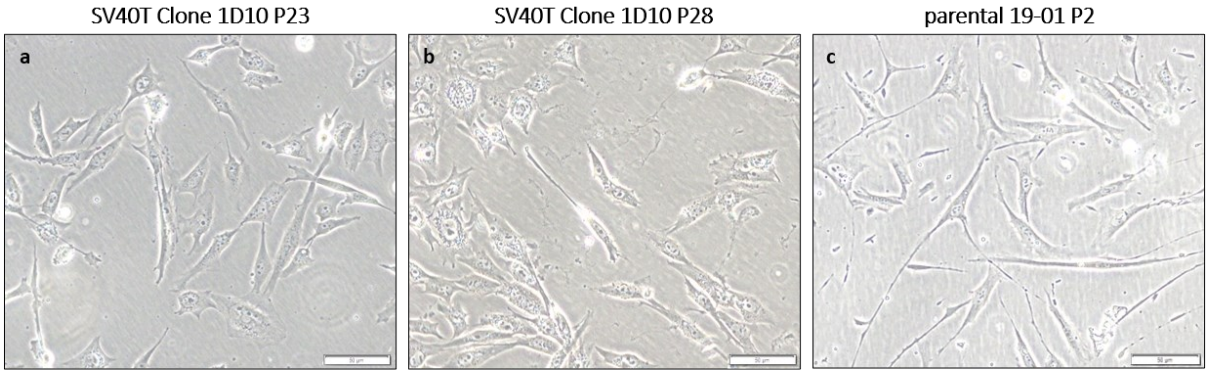

Fig 3.32: Morphological characteristics of cultures of SV40T-transduced eccrine sweat gland duct cell clone 1D10 and primary parental cells.
Cell morphology of the SV40T-transduced eccrine sweat gland duct cell culture from clone 1D10 (SV40T Clone 1D10) in passage 23 (P23) (**a**) and P28 (**b**) are depicted. For comparison, non-transduced parental cells 19-01 exhibited a similar though more longitudinal cell shape (**c**). Throughout cultivation (P22 to P31) those clonal cell cultures retained their characteristic cell shape reflecting a mix of cuboidal and longitudinal features. Images were taken at 10x objective magnification in bright field mode using CKX14 microscope with the digital camera XC10. Bar represents 50 µm.

Additional to these easily detectable though meaningful features, gene expression over several passages was analyzed (**Fig 3.33**). Although there was no clear trend in the expression values, early passages (P21 to P25) showed tendentially slightly higher gene abundance. This was especially observed in case of ANO1 where relative expression values of up to 10 in P24 were recorded. Apart from that, relative expression ranged between 2.0 and 0.5 for all investigated genes. Parental, non-transduced cells 19-01 in P3 exhibited relative gene expression values in range of the ones of SV40T-transduced cells in P21 to P25.

Condensed, characterization of newly generated culture of SV40T-transduced eccrine sweat gland duct cell clone 1D10 exhibited stable and fast proliferation and retained its morphological features during cultivation up to so far examined P31. Regarding gene expression, younger passages showed slightly higher relative values compared to advanced passages above P27.

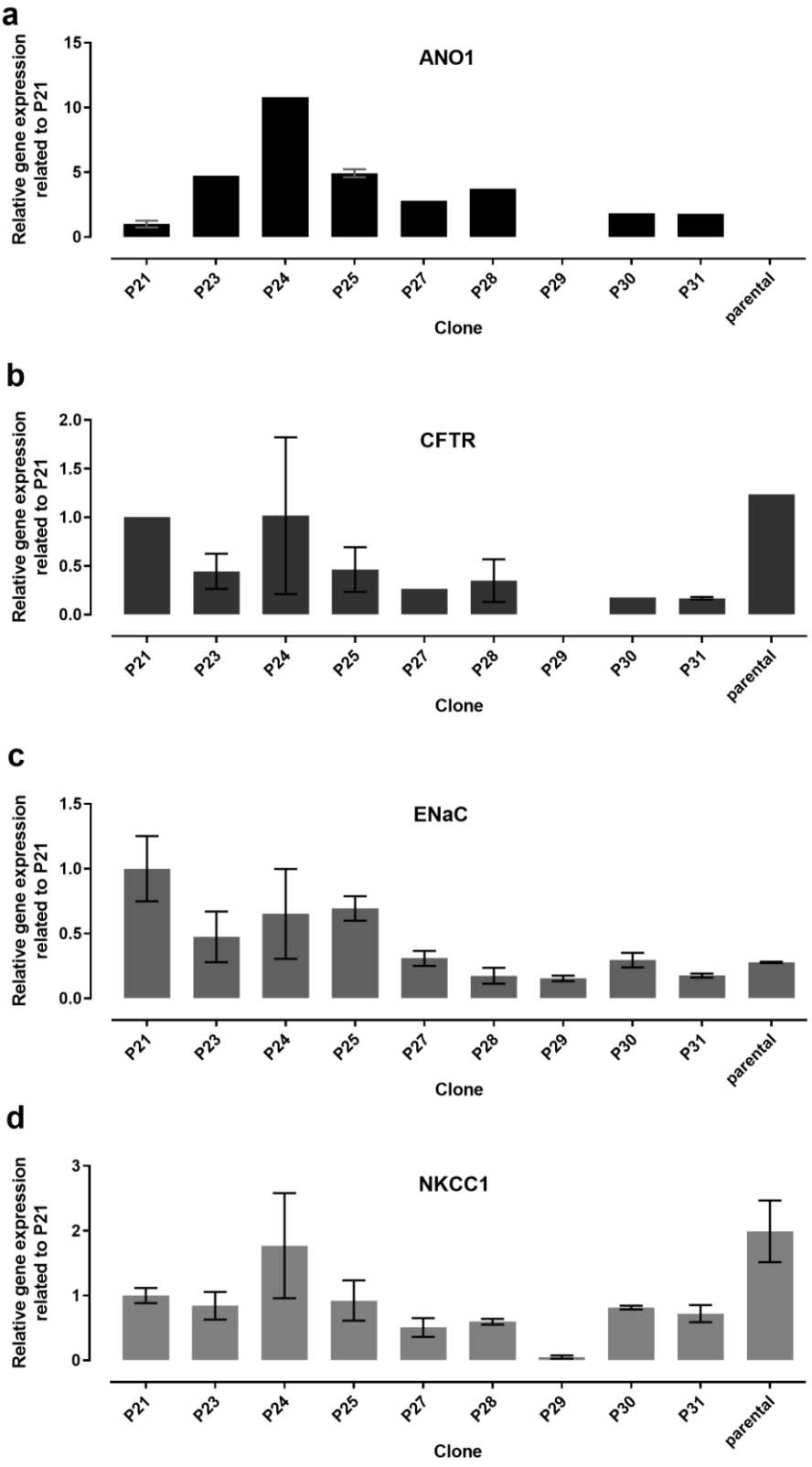

Fig 3.33: Comparison of relative gene expression of several passages of SV40T-transduced duct cell clone 1D10 culture with parental duct cells.
Depicted are relative gene expression levels of anoctamin 1 (ANO1) (**a**), cystic fibrosis transmembrane conductance regulator (CFTR) (**b**), epithelial sodium channel (ENaC) (**c**), and sodium-potassium-chloride channel 1 (NKCC1) (**d**), in several passages (P21 to P31) of SV40T-transduced eccrine sweat gland duct cell clone 1D10 cultures and parental, primary cells 19-01 in P3. Gene expression was quantified by RT-qPCR from monolayer cells. Gene expression value of clonal cell culture at P21 served as the reference and was set to 1.0. GAPDH served as the housekeeping gene. Data are mean ± SD of one experiment performed in triplicate replicate.

4 Discussion

The process of sweating, first regarded as vaporous emission of body substances, is already known since the times of Hippocrates. However, dating back as far as 1833, Purkinjé was the first to describe the general existence of sweat glands in human skin responsible for discharging of those vaporous substances (Kuno 1956). Again it took some time until research on the detailed histological characterization of apocrine and eccrine sweat glands was undertaken (Way and Memmesheimer 1936). From then on, substantial efforts were made to elucidate histologic ultrastructure of eccrine glands (Holyoke and Lobitz 1952; Hibbs 1958; Montagna et al. 1953), their physiological functioning including their cholinergic innervation (Randall 1946; McSwiney 1934) and the chemical composition of secreted sweat (Lobitz and Osterberg 1945; Adolph 1923).
Starting in the 1970s, isolation of single eccrine sweat glands from human skin opened new possibilities for detailed scrutiny of eccrine sweat gland characteristics (Wolfe et al. 1970; Sato 1973; Sato and Dobson 1971) and paved the way for establishment of eccrine sweat gland cell cultures (Lee et al. 1986; Brayden et al. 1988; Pedersen 1989). Despite this extensive research contributing to the current scientific knowledge, there are still some undiscovered aspects, especially regarding the sweating process on a cellular and molecular level. Therefore, establishment of sophisticated *in vitro* models which physiologically mimicking the native human eccrine sweat gland is of scientific interest (Okada et al. 1983).
Tightly linked to the process of sweating is its inhibition. Currently, this is effectively achieved by aluminum salts contained in AP cosmetic products (Untied 2004; Scientific Committee on Consumer Safety 2019). In the last years, however, aluminum was discussed due to its possible negative impacts on human health (Darbre 2001; Mandriota 2017; Ellsworth et al. 2004). Although official statements from the SCCS (2019) and BfR (2019b) classify the use of prevailing concentrations of aluminum salts in cosmetics as safe, there is still a negative connotation lingering in the mind of especially German consumers (Osserman 2020).

Following these scientific and consumer demands, this work combined three research topics: First and foremost, eccrine sweat gland cell-based *in vitro* methods were evaluated to create an innovative test system for intensified understanding of the sweating mechanism. Simultaneously, identification of alternative AP actives as substitutes for ACH was aimed at. Subsequently performed *in vivo* studies involving human volunteers served to establish reliability of the implemented test procedure and to verify *in vitro* derived estimates of substance effects.
As a second aspect, *in vitro* 3D eccrine sweat gland models should be optimized and scientifically described to improve meaningfulness and interpretation of these physiological results. By defined combining of cultured coil and duct cells, this elaborate 3D model enabled more detailed investigation and characterization of eccrine sweat gland cell interactions.
Furthermore, an immortalized eccrine sweat gland duct cell line was to be generated and characterized. With this availability of a standardized, more homogenous cellular material for developed AP testing procedure is accomplished and circumvents interindividual variations in future investigations which poses a problem when primary cells from different donors need to be used.

4.1 Effective antiperspirant actives

The whole mechanism of sweating is complex. It includes and relies on the coherent functioning of numerous receptors, ion channels, and transport proteins. Therefore, scientists are far from understanding its detailed biochemical steps and their interlacing which directly impacts and impedes fast and easy identification of substances to treat sweating-associated diseases such as anhidrosis, hyperhidrosis, and hypohidrosis (Cui and Schlessinger 2015). Public funding supporting dedicated research on this scientific field is sparse due to low economic importance. However, the German Federal Ministry of Education and Research (Bundesinstitut für Bildung und Forschung, BMBF) attended itself to this scientific field by funding sweating-related joint research projects within the frame of NatLifE2020. Part of this thesis contributed to successful outcomes of named BMBF project. Especially the topic of detailed investigation of the sweating process should be addressed within this framework and has high relevance as development of effective AP products with alternative technologies replacing ACH is difficult to realize without the necessary knowledge behind. Up to now, resource-intensive *in vivo* screening studies were the primary method for seeking alternatives to aluminum chlorohydrate (ACH). Availability of qualified and reliable *in vitro* approaches would yield a tremendous reduction of those efforts and, simultaneously, constitute the foundation for cell-based investigations to elucidate the sweating mechanism in more detail.
First actions were taken to fill this void , among others, by Ertongur-Fauth *et al.* who employed the immortalized eccrine sweat gland coil cell line NCL-SG3 to investigate the influence of isoforms of the Cl^- channel ANO1 (TMEM16A) on the sweating process (Lee and Dessi 1989; Ertongur-Fauth et al. 2014; Ertongur-Fauth Torsten et al. 2016). While this approach exclusively revolves around chloride ions and their role in sweating, herein described multilevel *in vitro* screening system encompasses investigation of Ca^{2+}, K^+, Na^+, and Cl^- as the four ions with highest concentrations in sweat (Baker 2019). Based on ion-specific fluorescence probes intracellular variations of these ion concentrations were determined in substance-treated primary eccrine sweat gland co-culture cells and, finally, characteristic ion prints were identified within this work. This novel cell-based approach allows deeper understanding of the sweating mechanism and facilitates cost-effective and rapid substance screening to identify possible replacements for ACH. Ensuing *in vivo* studies on the back of volunteers with selected substance candidates verified their AP potential and helped to correlate *in vitro* determined ion flux processes to *in vivo* sweat-reducing properties (Welzel et al. 2021). Even more, developed systematic screening approach allowed for postulation of the substances' mechanism of action.

4.1.1 Insights from chloride-containing substances

4.1.1.1 Chloride-content and cation structure influence the cellular response

For over 100 years aluminum-based actives have been used in various cosmetic products, mostly in AP where they effectively reduce watery sweat output, for which the first widely marketed formulation was patented in 1941 (Moore 1935; Montenier 1941). However, the exact mechanism of action of these ingredients, including the commonly used and studied ACH, remains elusive. Widely held opinion states physical blockage of the sweat gland duct

by formation of a hydrogel plug and, consequently, inhibition of sweat output (Kennon 1965; Schlereth et al. 2009; Swaile et al. 2012; Lee and Levell 2014; Swary et al. 2015; Bretagne et al. 2017). Some investigations, in contrast, postulate ACH to take effect deeper down in the eccrine sweat gland outreaching mere obstruction of the duct. With sole tape stripping of treated skin areas, and thereby achieved removal of plugs, normal sweating could not be reinstated. This implies an additional cause for the AP effect apart from plug formation (Papa and Kligman 1967; Gordon and Maibach 1968). A study of McWilliams *et al.* found evidence for both hypothesized mechanisms, plug formation and physiological cellular interference. One the one hand, they observed superficial occlusion of the duct by an aluminum-containing plug in treated skin and, on the other hand, recorded unresponsiveness of aluminum-treated eccrine sweat gland coil cells during sweat stimulation (McWilliams et al. 1987).

Although these results represent important indications for a binary mechanism of action of aluminum salts, precise knowledge of underlying physiological processes remains elusive. With the help of described *in vitro* test system closer scrutiny of AP effects on a cellular level is feasible contributing to elaboration of the sweating mechanism (Welzel et al. 2021).

In this thesis, employed *in vitro* test system using primary eccrine sweat gland co-culture cells revealed to be unresponsive for cholinergic stimulation by the agonist carbachol (refer to Fig 6.2). Similarly, lacking reaction upon treatment with carbachol was also reported for the coil cell line NCL-SG3 indicating that such a loss of cholinergic reactivity of cultured eccrine sweat gland cells seems not uncommon (Lee and Dessi 1989).

In any case, *in vitro* testing of ACH revealed this AP active to exert substantial impact on intracellular ion equilibria in primary eccrine sweat gland cells evidenced by a concentration-dependent diminution of $[Na^+]_i$ and simultaneous elevation of $[Cl^-]_i$ (refer to Fig 3.1). Alterations in $[Ca^+]_i$ by ACH treatment were not detected. Based on these findings a physiological mode of action of ACH is proposed which is assumed to complement physical obstruction of sweat glands by hydrogel plugs. These herein described observations of changes in ion equilibria upon substance application correspond with measurements of McWilliams et al. (1987) showing aluminum zirconium tetrachlorohydrate treatment to interfere with normal physiological alterations of intracellular ion levels of especially Na^+ and K^+. Altogether, these results strongly point towards a biochemically steered inhibitory mechanisms of sweating. Based on this assumption the existence of further biologically acting, non-aluminum containing AP actives is presumed and was elaborated in more detail in this thesis.

Chemically seen, ACH is a molecule consisting of aluminum, chloride, and hydroxide which in aqueous solutions dissociated into aluminum hydroxide and chloride ions. Due to its chemical nature a certain amount of Cl^- is attributed to each ACH solution as determined by its chemical formula Al_2OH_5Cl (Nail et al. 1976) (**Fig 4.1a**). Based on this Cl^--containing characteristic of ACH and combined with reports of AP effects of flocculating amine-containing polymer solutions, other substances with similar features were screened in this thesis. They belong to the chemical class of organic amines which, due to their specific chemical structure, offer a great opportunity for easy protonation of their inherent nitrogen atoms in an acidic, HCl-containing solution (Fig 4.1b-d). Simultaneously, present Cl^- serve as counterions. Therewith, a large cationic molecule with a small Cl^- as the counterpart is created which is comparable to the situation of ACH where attached Cl^- outbalance charge differences of large cationic aluminum hydroxide complexes such as $Al_{13}O_4(OH)_{24}(H_2O)_{12}^{7+}$ (Teagarden et al. 1981).

Structural basis of herein screened aminic compound PEI-HCl is polyethyleneimine, a branched polymer formed by several repeating units of the aziridine monomer ethyleneimine with an average molecular weight of 1300 g/mol (BASF - Care Chemicals & Formulators 2010; BASF - Care Chemicals Devision 2015b). Cross-linking of the monomers occurs via their functional imine groups which react to form primary, secondary or tertiary amines (Wang et al. 2006; Robbins 2012) (Fig 4.1b).

Apart from PEI-HCl, lead substance of investigated polyvinyl amine (PVAm)-HCl solution represents a copolymer of N-vinyl formamide and vinylamine with primary and secondary amine groups attached to the carbon polymer backbone. Therein, amine groups are separated by three carbon atoms, while each repeating unit consists of a pentane backbone with respective amine side chains (Fig 4.1c). It has a nearly completely hydrolyzed linear structure and an average molecular weight of 10,000 g/mol (Wu et al. 2008; BASF - Care Chemicals Devision 2015a).

In contrast to these polymers, tested dimethyl piperazine (DMP) constitutes a rather small piperazine molecule having a molecular weight of only 114 g/mol. Its chemical structure features two tertiary amine groups (Fig 4.1d).

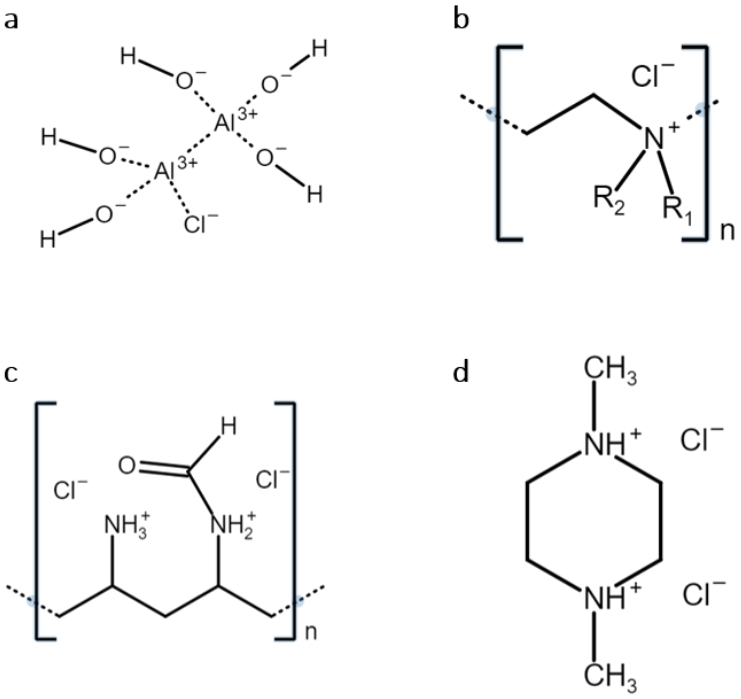

Fig 4.1: Molecular structure of chloride-containing test substances.
Depicted are the molecular structures of test substances as present in aqueous, with hydrochloric acid acidified solutions. Positive charges of the polycation of aluminum chlorohydrate (ACH) are carried by the aluminum ions. ACH forms large polycationic complexes in aqueous solutions with chloride ions acting as counterions (**a**). Primary, secondary, and tertiary aminic nitrogen atoms get protonated under acidic conditions carrying the positive charge in branched polyethyleneimine (PEI). -R_1 and -R_2 represent -H, or other aminic alkyl chains. Average molecular mass equals 1,300 g/mol (**b**). Positive charges of the PVAm molecule are located at protonated primary or secondary amine groups. Average molecular mass is stated as 10,000 g/mol (**c**). Nitrogen atoms of tertiary amine groups in dimethyl piperazine get protonated in acidic solutions. Its molecular mass is small with only 114 g/mol (**d**). Structures were created with Marvin JS software.

Although none of these test substances has a quaternary structure per se, they share the same characteristic of the amine groups getting protonated at acidic pH resulting in (poly)cationic molecules. Thus, all tested compounds attain a quaternary ammonium chloride structure in investigated HCl-supplemented aqueous solutions. At least for the polymeric molecules PEI and PVAm, this is paired with an enormous buffer capacity over a broad pH range (Kichler et al. 2001; Akinc et al. 2005; Wu et al. 2008; Robbins 2012). For PEI, a ratio of 1:1 of protonated to unprotonated amines at pH 4 was determined (Robbins 2012). Therefore, protons got readily accepted by present amine groups inherent to the test substances in acidic solution with HCl, whereas residual Cl^- served as the counterions outbalancing the positive charges and got carried along accordingly. Due to their different structure, each, PEI, PVAm, and DMP, required a distinct amount of HCl to attain a pH of 3.5 of the respective stock solutions. Based on this known amount of added HCl the Cl^- content of each prepared dilution could be calculated. Similarly, the Cl^- content of ACH dilutions was determined by the amount of ACH present.

Highly interesting, all tested ammonium chloride solutions were shown to exert similar ion prints as ACH in 2D eccrine sweat gland co-culture cells (refer to Fig 3.2 and Tab 3.1). Their effects were characterized by concentration-dependent reduction of $[Na^+]_i$ and simultaneous increase of $[Cl^-]_i$. Astonishingly, the same ion pattern was observed for PEI-HCl solutions adjusted to different pH values with HCl. In this case, intensity of $[Na^+]_i$ diminution and $[Cl^-]_i$ elevation was correlated to adjusted pH with more neutral pH values resulting in fainter descend of $[Na^+]_i$ and weaker increase of $[Cl^-]_i$ (refer to Fig 3.3).

In contrast to these herein obtained results, previous research using X-ray microanalysis to determine intracellular ion concentrations in isolated ape sweat glands revealed elevated Na^+ and decreased Cl^- levels after sweating stimulation with methacholine (Saga and Sato 1989; Takemura et al. 1991). Strikingly, these changes associated with onset of sweating are directly opposite those reported in this work after application of possible sweating inhibitors to human eccrine sweat gland cells. Therefore, postulation of ACH to possess an additional cellular AP mode of action is strongly reinforced by these findings and, more specific, ACH is presumed to interfere with cellular ion equilibria (Gordon and Maibach 1968; McWilliams et al. 1987).

Similar testing results of herein scrutinized ammonium chloride solutions strongly suggest those substances to also exert sweat-reducing properties *in vivo*. Based on these findings a mechanism of biochemically inhibited sweating is proposed. It is assumed to be steered via influencing of cellular ion levels as no physical plug formation or even flocculation was observed with neither PEI-HCl, nor PVAm-HCl, nor DMP-HCl. More precise, elicited intracellular responses are attributed to the amount of Cl^- present in the applied test solutions, which is considered the key component of the inhibitory molecular mechanisms. Based on this assumption the innovative parameter of chloride equivalent was introduced enabling cross-substance comparison of cellular effects. Although being a multilevel testing procedure, alteration of $[Na^+]_i$ was given priority as the most informative cell-based readout parameter as this variable showed highest consistency across all performed tests. In comparison, $[Cl^-]_i$ is most likely biased by application of huge amounts of Cl^- to the extracellular medium and not solely influenced by cellular processes. The main focus on changes in $[Na^+]_i$ and associated simplification of described results and correlations is justified by the closely linked transport process of Na^+ and Cl^- across the sweat gland cell membranes (Reddy et al. 1999). Thus,

$[Na^+]_i$ represents an externally rather undisturbed measurement parameter merely reflecting substance-triggered cellular effects.
On a cellular mechanistical level the high amount of extracellular Cl^- added to the cell-surrounding medium by substance application is supposed to influence cross-membrane ion transport processes in that excessive extracellular Cl^- is transported into the cell cytosol due to the existing chemical gradient. Concomitantly, Na^+ gets attracted to the extracellular space by presence of external Cl^- to outbalance the high free negative charges. Such a dependence of cellular Na^+ and Cl^- transport processes facilitated by ENaC and CFTR/ANO1 in eccrine sweat gland cells has been established before and constitutes a vital factor in salt absorption in the duct (Reddy et al. 1999). Thus, this well explains results of performed *in vitro* tests where $[Na^+]_i$ was diminished but $[Cl^-]_i$ concurrently increased.
Surprisingly, when plotting relative $[Na^+]_i$ against chloride equivalents, data points of ACH, PEI-HCl and PVAm-HCl lay close together while those of DMP-HCl ranged distinctly above (refer to Fig 3.4) signifying a weaker effect of DMP-HCl compared to the other substances. This observation suggests the large polycationic parts of ACH, PEI-HCl and PVAm-HCl to contribute to these *in vitro* results next to Cl^-.
Interestingly, PEI was discovered to form nanoscale pores inside the cell membrane, which is attributed to its polycationic character and made PEI the gold standard for efficient non-viral gene transfection during the last years. Besides, this characteristic facilitates non-specific, free flux of ions across membranes (Akinc et al. 2005; Dréan et al. 2017). The same ability of effective gene delivery was proven for other polycationic polymers including polyvinyl amines and its derivatives to which herein tested PVAm-HCl belongs (Dréan et al. 2017). Thus, it is postulated for the PVAm polycation to exert similar effects by forming nanoscale membrane pores in eccrine sweat gland cells, which contributes to the free cross-membrane flux of ions. In general, this characteristic of polycationic counterions to induce some degree of membrane porosity is considered an accelerator of ionic transport processes occurring in eccrine sweat gland cells.
As another aspect, these polycationic substances possess an enormous buffer capacity over a wide pH range due to their outstandingly high ration of protonatable amine groups to carbon atoms (Kichler et al. 2001). In line with the proton sponge theory postulated for PEI (Akinc et al. 2005) this high proton uptake capacity is coupled here with a high load of Cl^- counterions. Similar effects are supposed to occur in case of PVAm-HCl (Dréan et al. 2017).
However, for the rather small cationic DMP-HCl molecule neither pore formation properties nor high buffering capacity are expected. This then well explains why it reacts differently from PEI-HCl and PVAm-HCl regarding its effect on intracellular ion changes as observed here.
Strikingly, ACH was determined to react similarly to PEI-HCl and PVAm-HCl. Therefore, it is speculated for this standard AP active to also exert a cellular effect accelerating the free ion flux across membranes. Interestingly, already in 1967 Papa and Kligman proposed aluminum salts to enhance duct cell permeability comparable to above described polycationic-induced formation of membrane pores (Papa and Kligman 1967). In accordance with this, majority of ACH was described to adopt a polycationic structure described as $Al_{13}O_4(OH)_{24}(H_2O)_{12}^{7+}$ with strong attraction of Cl^- (Teagarden et al. 1981). In this form ACH is comparable to PEI-HCl and PVAm-HCl cations, structurally, chemically and regarding its effect on intracellular ion equilibria as demonstrated here.

Adding to this hypothesis, reports on the detailed scrutiny of plug building steps of ACH revealed aluminum polycations to interact and agglutinate with proteins in the sweat duct responsible for its occlusion. Likewise, interconnection of ACH polycations with membrane proteins of luminal duct cell walls were also mentioned (Bretagne et al. 2017). Pointing in the same direction, intercellular dilatation after treatment with aluminum salts was reported to occur in cells of native eccrine glands (McWilliams et al. 1987). Such an interaction of ACH with the cellular membrane might well explain herein observed cellular effects and their similarity to changes evoked by membrane-interacting PEI-HCl and PVAm-HCl.

4.1.1.2 pH of the solutions impacts the cellular response

Maintaining of a steady, intracellular pH at a physiological level constitutes a vital factor as many cellular processes underlie a pH-sensitive regulation. Controlling of intracellular pH is achieved by ion transport across membranes involving passive flux of ions as well as their active conveyance through carrier proteins. Most important for actively mediated transport processes are ion exchangers and cotransporters like Na^+/H^+-exchanger, Cl^-/HCO_3^--exchanger, and Na^+-HCO_3^- cotransporter (Yatani et al. 1984; Boron 1986; Busche et al. 1993; Bischof et al. 1996).

During sweating the pH in the gland lumen varies between 4.5 and 7.8, which poses an additional challenge for retention of steady intracellular pH (Herrmann and Mandol 1955; Bijman and Quinton 1987; Reddy et al. 2008). However, investigations on the influence of changing luminal pH on salt absorbing transport processes in isolated eccrine sweat gland ducts revealed key regulatory proteins CFTR and ENaC to be unaffected by prevailing conditions in the lumen. Transport activity of these carriers was only decreased when cytosolic, intracellular pH became acidic (Reddy et al. 1998; Reddy et al. 2008). Above mentioned ion exchange and transport processes are presumed to take place in eccrine sweat gland coil and duct cells keeping the intracellular pH constant as indicated by presence of Na^+/H^+-exchanger 1 (NHE1) (Li et al. 2014; Granger et al. 2003). pH regulation might not solely be achieved by Na^+/H^+-exchanger but might include other cotransporters and exchangers such as Cl^-/HCO_3^-exchanger, whose existence in eccrine sweat gland cells has been proposed before (Sato and Sato 1987b; Louie et al. 2016).

Due to these known influences of ambient pH on cellular processes impact of pH of the test solutions on $[Na^+]_i$ was also considered in this study (refer to Fig 3.5). Similar to plotting of $[Na^+]_i$ against chloride equivalent exchanging the latter for measured pH of applied solutions revealed the same grouping of ACH, PEI-HCl and PVAm-HCl while data points of DMP-HCl ranged above. To control for chloride-independent, purely extracellular pH-driven alterations of $[Na^+]_i$, DMEM-based solutions acidified with glycolic acid were tested. Interestingly, these additional measurements displayed glycolic acid to clustered with DMP-HCl. This suggests changes in $[Na^+]_i$ triggered by DMP-HCl and glycolic acid in eccrine sweat gland co-culture cells to be attributable to decrease of the extracellular pH without any substantial effect of the substance itself. Acidification of the extracellular environment inevitably increases the amount of H^+ present and most likely also leads to an acidification of the intracellular cytosol as was determined for monolayer epithelial cells of intestinal origin (Osypiw et al. 1994; Perdikis et al. 1998). In case of Na^+/H^+-exchanger being the transporter in eccrine sweat gland cells

responsible for counteracting elevation of intracellular pH, extrusion of H^+ in exchange for Na^+ would involve temporary increase in $[Na^+]_i$. However, acidic cytosolic conditions were determined to inhibit transport activity of ENaC prohibiting Na^+ influx into sweat gland cells as (Reddy et al. 2008). Since in this study an overall decrease of $[Na^+]_i$ after treatment with slightly acidic substance solutions (pH ranging between 5 and 7.4) was determined, this observed effect is presumed to occur from one or several overlapping processes such as deactivated, ENaC-mediated Na^+ intrusion, Na^+-involving regulation of intracellular pH and above-described extracellular attraction of Na^+ by excessive Cl^-. In any case, disclosure of the exact processes involved requires further detailed studies including selective but not limited to inhibition of distinct ion transporters and exchangers.
Clustering of data points of ACH, PEI-HCl, and PVAm-HCl implies these substances to share a common mechanism of action. As they evoked stronger reduction of $[Na^+]_i$ at more neutral pH values compared to DMP-HCl and glycolic acid, determined effects on the intracellular Na^+ equilibrium are proposed to be elicited by the acidic pH as well as by the impact of the substances themselves. This assumption is supported by observed proportional relation between pH of the test solutions and respective chloride equivalents (refer to Fig 3.6) which was comparable for all test substances. Thus, acidic conditions of ACH, PEI-HCl, and PVAm-HCl could not be the sole factor determining lower levels of $[Na^+]_i$ after treatment. Rather, polycationic counterions of these three substances are postulated to aid to the overall effect by increasing the permeability of the cell membrane (Chen et al. 2009), thereby facilitating and accelerating the efflux of Na^+, which is triggered by excessive presence of Cl^- in the extracellular medium. Additionally, proton scavenging properties reported for PEI and presumed for PVAm polycations might also contribute (Akinc et al. 2005) as explained in the chapter above (refer to 4.1.1.1). In any case, the exact mechanisms involved in pH regulation remain to be elucidated.

Overall, these *in vitro* generated data observed in cultivated 2D eccrine sweat gland co-culture cells strongly imply the standard AP active ACH to exert cellular effects additional to the purely physical, plug-forming properties. Both, physical blockage and physiological interaction with cellular ion equilibria, are proposed to determine the sweat-reducing efficacy of ACH. Similar *in vitro* ionic changes seen with PEI-HCl and PVAm-HCl suggest those test substances to also feature sweat-reducing properties without any observation of precipitation of the substances. Besides, these cell-based results indicate the interplay between Cl^- content and the nature of the polycationic counterpart to be decisive for overall observed effects.

4.1.1.3 Chloride content influences *in vivo* sweat reduction

After uncovering of identical *in vitro* effects of ACH, PEI-HCl and PVAm-HCl those results remained to be related with actual *in vivo* sweat-reducing efficacy of the test substances. For that, data from externally conducted *in vivo* studies quantifying the amount of sweat output on the back of volunteers were kindly provided for comprehensive assessment.
Based on *in vitro* test results, $[Na^+]_i$ is hypothesized to represent as an appropriate parameter for estimation of *in vivo* sweat-reducing efficacy, therewith connecting *in vitro* results to *in vivo* sweat reduction. Taking this idea further, *in vitro* data suggest stronger AP action of ACH, PEI-

HCl and PVAm-HCl due to those substances exerting stronger effects on $[Na^+]_i$ compared to DMP-HCl when applied at similar chloride equivalents.

Astonishingly, 2 and 3% AS (w/w) aqueous solutions of PEI-HCl with pH 3.5 evoked sweat reduction effects in the range of or even slightly above those of the benchmark ACH when determined 24 h after the last application (refer to Fig 3.7a). *in vivo* efficacy of PEI-HCl was dependent on concentration and pH of the applied solution: While an increasing sweat-reducing effect was recorded for rising concentrations of PEI-HCl at constant pH, AP efficacy was also elevated with more acidic pH at constant amounts of PEI. In contrast, 5% TQ (w/w) and 2.5% TQ (w/w) solutions of PVAm-HCl and DMP-HCl, respectively, evoked nearly no sweat reduction *in vivo* (refer to Fig 3.7b).

As with *in vitro* results, comparison of *in vivo* gathered AP effects of the different test substances was done via the respective chloride equivalents (refer to Fig 3.8 and Tab 3.2). In case of *in vivo* studies, the chloride equivalent denotes the amount of Cl^- put on the back of volunteers at each application time point. Strikingly, a good linear relation between chloride equivalent of the solution and resulting sweat-reducing potential was disclosed for PEI-HCl. To determine the contribution of Cl^- to these outstanding AP properties, a PEI solution adjusted to pH 3.5 with citric acid served as the chloride-free control. Due to this Cl^- -devoid solution eliciting no sweat reduction, the assumption of the chloride content to convey the major sweat-reducing effect, both *in vivo* and *in vitro*, was corroborated (Welzel et al. 2021).

In contrast to PEI-HCl, PVAm-HCl and DMP-HCl evoked overall weaker sweat reduction and evoked less sweat reduction when referred to their chloride equivalent. However, for those two test substances no such extensive *in vivo* studies as for PEI-HCl were performed yet.

ACH elicited slightly stronger AP effects than PEI-HCl when related to its Cl^- content.

Strikingly, all these *in vivo* observed sweat-reducing potentials correspond well with *in vitro* determined efficacies of Cl^--related $[Na^+]_i$ reduction (refer to Fig 3.4). This correlation strongly implies a cellular physiological effect of those substances, including ACH, in reducing sweating.

During the natural sweating process, negative net charge is built in the duct lumen due to active resorption of Na^+ into eccrine sweat gland duct cells facilitated by ENaC (Bovell 2015). Consequently, this charge difference between intracellular cytosol and extracellular lumen is assumed to become excessive when more Cl^- is added leading to perturbed ion equilibria as is the case when Cl^--containing substances diffuse down the sweat gland orifice. Positive charges of simultaneously added polycations are supposed to be hidden by the bulky structure, thus creating an overall more negative charge density in the lumen. Intracellular Na^+ then gets attracted to the extracellular space while Cl^- enters the cytosol down the concentration gradient. These ion displacements lead to altered ion equilibria in the duct lumen as well as the cellular cytosol which in turn are proposed to influence sweat generation resulting in reduced sweat secretion (Welzel et al. 2021). This hypothesis is supported by the fact that salt solutions like KCl and NaCl having small cations did not exert any effect, neither *in vitro* nor *in vivo*. Therefore, sweat-reducing potential of Cl^--containing solutions is postulated to originate from the enormous amount of present Cl^- together with the specific polycationic structure of the substances.

Overall, the mechanistic hypothesis presented here well explains *in vitro* gathered results as well as *in vivo* elicited sweat-reducing effects while, and because, it contradicts cellular ionic

changes observed during perspiration. As mentioned above, detailed studies demonstrated an increase in $[Na^+]_i$ and simultaneous reduction of $[Cl^-]_i$ in cells of sweat-stimulated eccrine glands (Saga and Sato 1989; Takemura et al. 1991). With this study showing the exact opposite impact of Cl^--containing substances in cultured eccrine sweat gland cells and together with established *in vivo* AP properties, a biophysiological, cellular mode of sweating inhibition is strongly implied.

Apart from the Cl^--content of the solutions other factors already mentioned to contribute to *in vitro* effects might also affect *in vivo* sweat reduction. Those are the nature of the cationic counter ion as well as the pH of the solution (refer to 4.1.1.1 and 4.1.1.2). Concerning the polycationic structure, the ability of PEI to form small pores in cell membranes *in vivo* is also assumed based on demonstrate efficient gene delivery in living organisms (Boussif et al. 1995; Lecocq et al. 2000; Kichler et al. 2001). As sweat reduction elicited by PEI-HCl increases with PEI-HCl concentration and, thus, the amount of polycations, formation of micropores is assumed to contribute to this effect. As a result, higher membrane porosity would enhance free flux of Na^+ out of and Cl^- into the cell cytosol from the gland lumen.

Influence of pH on sweat reduction might be explained by associated different charge densities of the polycations: At low, acidic pH more amine groups are protonated and polycations carry more positive charges. As transfection efficiency is dependent on charge density of PEI polycations, pore forming properties are supposed to increase with cationic charge density governed by interaction with negative charges on the membrane surface (Boussif et al. 1995; Lecocq et al. 2000).

In any case, amount of Cl^- rises with both, higher amount of PEI-HCl and more acidic pH of the solutions and is therefore tightly and inseparably interwoven with these factors. Interference of Cl^- with the ion equilibrium in the gland is seen as the key component of the sweat-reducing effect as a 3% AS (w/w) PEI citrate solution at pH 3.5 failed to elicit any substantial sweat reduction. Simultaneously Cl^- content, resp chloride equivalent, is believed to link PEI-HCl concentration with corresponding pH (Welzel et al. 2021).

Diverging sweat-reducing potentials of the Cl^--containing test substances are also assumed to relate to properties of their cations. As mentioned before, DMP cations constitute the only tested counterion assumed to lack pore forming properties which in turn limits cross-membrane ion flux to protein-assisted transport activities (refer to 4.1.1.1). This coincides well with DMP-HCl solutions exerting nonsignificant AP effects *in vivo* although owing a substantial chloride equivalent. It was even slightly higher than the one of 3% AS (w/w) PEI-HCl, but PEI-HCl elicited a significant sweat-reduction of 58%.

PVAm cations are believed to increase membrane permeability although, judging from their transfection efficacy, their potency is lower compared to PEI. The reason for this might lie in different basicity and buffer capacity, which is tightly linked to charge density and amount of chloride carried along (Dréan et al. 2017). This might well explain the diminished sweat-reducing efficacy of PVAm-HCl solutions observed in *in vivo* sweat reduction studies.

Regarding ACH, existence of high amounts of Cl^- as well as relatively acidic pH of aluminum salt solutions resulting from liberation of HCl during hydrogel plug formation were named in literature. However, so far no explanations were brought forward connecting AP efficacy to these parameters (Scholes et al. 1978; Swaile et al. 2012). Results of this work add to clarify

the mode of action of ACH as an effective AP by demonstrating its influence on intracellular ion levels and, thus, indicating a biochemical impact in regulating sweating apart from the widely known duct obstructing properties (Bretagne et al. 2017). This dual mechanism of action might be the reason for herein observed highest sweat-reducing attainment of ACH. Based on chloride equivalent, the benchmark outperformed tested PEI-HCl solutions which is proposed to be attributable to the impact of ACH on cellular ion transport processes coupled with plugging of the eccrine gland orifice; the latter contributing to supply extra AP efficacy. Nonetheless, a significant sweat-reduction could be achieved without formation of a plug and obstruction of the gland indicating a substantial impact of cellular physiological mechanisms in steering sweating.

In summary, described *in vitro* testing procedure together with *in vivo* verification results indicate the high potential of this combined approach for identification of alternative AP actives and description of underlying mode of action. Lacking effect of carbachol, however, indicates the monolayer eccrine sweat gland co-culture cells to be unresponsive towards muscarinic stimulation, either due to low expression of M3 or due to disruption of the signaling cascade in the isolated, cultured cells. Considering this, impact of standard AP ingredient ACH on intracellular ion levels in eccrine sweat gland co-culture cells suggested its effect to be triggered by affecting other present ion transport processes and proved the biochemical steering of intracellular ion equilibria. Derived from that, the long-assumed cellular effect of aluminum salts was demonstrated and is postulated to contribute to well-known AP effect of ACH (Scholes et al. 1978; Ellis and Scurr 1979; McWilliams et al. 1987; Welzel et al. 2021).
Strikingly, estimating sweat-reducing efficacy of test substances based on *in vitro* determined changes of $[Na^+]_i$ and related chloride equivalents was mostly confirmed by *in vivo* studies. However, chemical properties of cationic counterions also seemed to contribute to the overall performance. To elucidate their impact in detail additional experiments using Cl^--containing and -free substance solutions with varying sizes and charge densities of the (poly)cations are necessary and recommended. These might include aluminum chloride ($AlCl_3$) and aluminum chloride hexahydrate ($AlCl_3 \cdot 6H_2O$) as examples for Cl^--containing aluminum salts or aluminum sulfate ($Al_2(SO_4)_3$) and aluminum acetate ($Al(OOCCH_3)_3$) as Cl^--free equivalents. Although several *in vivo* studies using some of these exemplary substances haven been performed (Papa and Kligman 1967; Quatrale et al. 1981; Swaile et al. 2012; Swary et al. 2015), no structured approach focusing on the chloride equivalent has been pursued.
Concerning herein tested ammonium chloride substances, a specific toxicological concern exists due to possible presence of nitrosamines which are common contaminants of alkyl amine-containing products. In cosmetics, nitrosamines are restricted in products due to their proven genotoxicity and carcinogenicity (European Parliament and Council 2009; Scientific Committee on Consumer Safety 2012). This aspect should be kept in mind for further experiments to elucidate the impact of other polycations such as PVA, poly-L-lysine, as well as poly(amidoamine) derivatives. Besides, small primary and secondary amine molecules should also be tested such as dimethylamine, N-dimethylamine, and derivatives thereof to corroborate herein postulated hypothesis although they are restricted form use in cosmetics by the Cosmetics Regulation.

4.1.2 Insights from polyol substances

4.1.2.1 Polyols as another chemical class triggering cellular effects

Ammonium chloride solutions scrutinized in *in vitro* screening procedures using primary eccrine sweat gland co-culture cells shared some chemical similarities with common AP ingredients belonging to the group of aluminum salts, especially ACH. Additionally, substances from other chemical classes were also investigated within this work regarding their *in vitro* impact on cellular ion equilibria and *in vivo* observed sweat-reducing potential.
Polyols of various kinds and chain lengths are commonly found in cosmetic products serving as humectants, solvents, denaturants, emulsifiers, fragrance ingredients, skin conditioning agents and moisturizers (Biel et al. 2008; Fiume et al. 2012; Fowles et al. 2013; Guertin 2018; Becker et al. 2019). A sweat-reducing effect of diols was disclosed some years ago by Beiersdorf AG declaring the AP effect of vicinal short-chained diols such as 1,2-PD, but without trying to explain the effect on a mechanistic level (Biel et al. 2008). They first focused on small molecules with two to four carbon atoms and later extended to aromatic and aliphatic diols (Biel et al. 2009). To achieve good sweat reduction results *in vivo* application of high concentrations of the diols ranging between 10-50% AS (w/w) in cosmetic products was required (Biel et al. 2008; Biel et al. 2009).
Surprisingly, when tested *in vitro* in this work using eccrine sweat gland co-culture cells polyols including diols showed distinct ion prints. They were characterized by concentration-dependent elevation of $[Na^+]_i$ and simultaneous reduction of $[Cl^-]_i$ (refer to Fig 3.9, Fig 3.10 and Tab 3.3). In contrast, intracellular levels of Ca^{2+} and K^+ remained largely unaffected after treatment with polyols. Therefore, detailed and concentration-dependent analyses as well as further screening of substance from this chemical class was focused on influences of $[Na^+]_i$ and $[Cl^-]_i$. Of note, the same ion parameters were decisive for evaluation of effects of Cl^--containing substances adding further relevance of this *in vitro* test system for assessing sweat-reducing potentials of substances based on changes of $[Na^+]_i$ and $[Cl^-]_i$.
Important to point out, the variations evoked by polyols and Cl^--containing substances are opposed: While polyols increase $[Na^+]_i$ and diminish $[Cl^-]_i$, ammonium chloride solutions reduced $[Na^+]_i$ and elevated $[Cl^-]_i$. As another difference, concentrations of polyols which triggered significant effects were about ten times higher compared to those of Cl^--containing substances (refer to Fig 3.2 and Fig 3.10), which is in line with high concentrations of up to 50% AS (w/w) required to result in marked *in vivo* sweat reduction (Biel et al. 2008; Biel et al. 2009). However, these distinctions between Cl^--containing substances and polyols clearly point towards another mechanism of action of polyols in influencing *in vitro* determined changes of ion equilibria in eccrine sweat gland cells. Identical for both substance classes, though, variations in $[Na^+]_i$ and $[Cl^-]_i$ are supposed to result in ion disequilibria between the intra- and extracellular spaces causing raised negative charge densities in the extracellular medium. As a conclusion, also polyols are estimated to evoke a sweat-reducing effect which was corroborated by *in vivo* studies.

Despite the high concentrations of polyols (being in the high mM range) required to evoke measurable alterations of intracellular ions, direct interaction of these substances with

membrane proteins or receptors is assumed as highly improbable (Politi et al. 2009). Instead, high amounts of alcohols in water were shown to interfere with the solvation status of ions in water leading to reduced hydrated ion radii with increasing alcohol concentrations (up to 17 mol%). This phenomenon is explained by water molecules solvating alcohol molecules rather than ions withdrawing outer hydration shell layers from these ions (Hawlicka and Grabowski 1993). A study examining hydrogen bond interactions in aqueous solutions of 1,2-propanediol (PD) reported a reduced overall number of hydrogen bonds compared to pure water. Coincidentally, both hydroxyl groups of 1,2-PD were demonstrated to take part in hydrogen bonding with surrounding water molecules as hydrogen bond acceptors and donors indicating its hydration status in water (Rhys et al. 2016). Due to presence of multiple hydroxy groups, herein studied polyols are assumed to behave similarly as these functional groups are main contributors to hydrogen bond interactions with water molecules (Rhys et al. 2016; Habuka et al. 2020). Number and steric distribution of hydroxyl groups in herein tested polyols 1,2-PD, 1,3-PD, dipropylene glycol (DPG), and diglycerol (DG) are outlined in **Fig 4.2**.

Together with concentration of polyol-water-mixtures the chemical structure of the substances is expected to influence the degree of presumed diminution of hydrated ion radii. The amount of water molecules required for solvation is proposed to be especially dependent on the structure and, in turn, directly impacts the hydration status of present ions (Hawlicka and Grabowski 1993). Thereby, DPG offers three hydrogen bond acceptors and two donors, while DG has five acceptor sites and four donors.

Overall, hydration radii of ions were found to be crucial for their free diffusion in water in that with increased hydration state, meaning more water molecules surrounding the ion, mobility decreased (Impey et al. 1983). Furthermore, permeation of solvated ions through ion channels (and possibly directly through membranes) was also demonstrated to dependent on size of hydrated radii (Sugiharto et al. 2008).

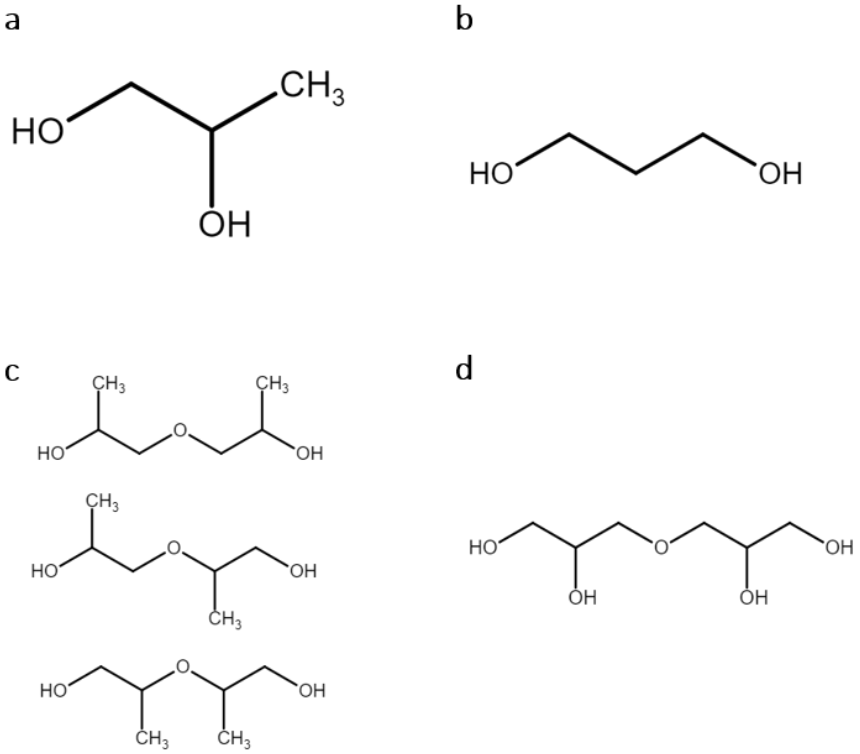

Fig 4.2: Molecular structure of tested polyols.
Depicted are the molecular structures of polyols which were tested *in vitro* for their impact on intracellular ion levels of primary eccrine sweat gland co-culture cells. While 1,2-propanediol (**a**) and 1,3-propanediol (**b**) are represented by one defined chemical structure, dipropylene glycol is an isomeric mixture of three sterically different molecules resulting from varying condensation reactions of two 1,2-propanediol molecules (**c**). Evaluated diglycerol is defined by one specific structure reflecting the condensation product of two glycerol molecules (**d**). Structures were created with Marvin JS software.

Condensed, all these scientific findings clearly delineate the close relation between ions and rather hydrophobic molecules in aqueous solutions which are governed by hydrogen bond interactions and are related to their solubility (Hawlicka and Grabowski 1993; Hribar et al. 2002; Rhys et al. 2016). For the present study of polyols as alternative AP actives this suggests their mode of action to rely on their hydration status as well as the one of present ions. Following hypothesize is postulate for determined effects in primary eccrine sweat gland cells: Upon solvation in aqueous solution polyols are supposed to affect the hydration status of ions, like Na^+ and Cl^-, by reducing the number of hydrating water molecules and, accordingly, the hydrated ion radius (Hawlicka and Grabowski 1993). This smaller hydration radius in turn is perceived to result in increased mobility of the ions as well as elevated cell membrane permeability (Impey et al. 1983). Based on presence of higher extracellular Na^+ concentration compared to the intracellular one (Saga and Sato 1989; Takemura et al. 1991; Baker 2017), this increase in ionic movements is postulated to evoke a cross-membrane influx of Na^+ into eccrine sweat gland cells. For Cl^-, in contrast, intracellular and extracellular levels of this ion are comparable (Saga and Sato 1989; Takemura et al. 1991; Baker 2017) resulting in only slight changes of $[Cl^-]_i$.
This presumed cellular mode of action of polyols satisfactorily explains *in vitro* obtained results characterized by concentration-dependent elevation of $[Na^+]_i$ and only slightly reduced $[Cl^-]_i$ (refer to Fig 3.11).

When comparing the potency of tested polyols, individual solvating properties needed to be considered to explain outstanding performance of DPG compared to 1,2-PD, 1,3-PD and DG. Closely linked to solvation of molecules is their topological polar surface area (TPSA) as well as the *n*-octanol-water partition coefficient (log $P_{O/W}$). The latter together with the hydrogen bond interacting sites of a molecule are important parameters in Lipinski's rule of five (Lipinski et al. 1997). While the TPSA reflects the molecular surface area occupied by polar heteroatoms such as oxygen, nitrogen, and phosphorous as well as thereto attached polar hydrogen atoms, log $P_{O/W}$ is a measure for the actual solubility properties of a molecule. Lately, TPSA was demonstrated to correlate well with hydrogen bonding properties of molecules and to be predictive for water solubility of chemicals (Prasanna and Doerksen 2009; Ali et al. 2012; Vistoli and Pedretti 2016).

Based on these qualities, TPSA of the polyols was taken as the core for introduction of a new figure, the relative TPSA, reflecting the calculated quotient of the molecule's TPSA divided by its molecular weight. This implemented quotient connects traits important for determining solubility of substances with its value displaying the molecule's relative proportion of polar, water-interacting surface (refer to Tab 4.1). Additionally, also the log $P_{O/W}$ was considered reflecting the actual solubility of the three-dimensional substance. Strikingly, both values corresponded well with established potency of polyols to increase $[Na^+]_i$ at a given concentration. E.g., at 2% AS (w/w) DPG elicited by far the strongest reaction while 1,2-PD, 1,3-PD and DG evoked weak or no rise of $[Na^+]_i$. Concomitantly, relative TPSA is markedly lower for DPG but similar for the other three polyols. Small value of relative TPSA signifies a small polar surface area of DPG which could engage in hydrogen bonding. As a result, DPG possess a reduced solubility which requires a higher number of water molecules to completely solvate the more hydrophobic molecule (Ali et al. 2012). This is also reflected in DPG having the highest log $P_{O/W}$ of only -0.46, compared to -0.71 for 1,3-PD, -1.07 for 1,2-PD, and -2.5 for DG (European Chemicals Agency 2020a, 2020b, 2020c, 2020d). Consequently, the structure of hydrogen bonding in water-DPG-mixtures is assumed to be changed leading to less hydration of the ions and thereby reduced ion radii. As explained above, this is speculated to increase the membrane permeability of ions finding expression in elevated $[Na^+]_i$ (Impey et al. 1983; Hawlicka and Grabowski 1993). Of note, the by far lowest log $P_{O/W}$ of DG did not correspond to a comparably low $[Na^+]_i$. Therefore, relative TPSA seemed as a more suited parameter for assessing the *in vitro* performance in this instance.

However, with 1,3-PD and 1,2-PD being constitutional isomers, solely relative TPSA is insufficient to discriminate the *in vitro* effects of these two substances. In this case terminal positioning of the hydroxyl groups in 1,3-PD causes a higher log $P_{O/W}$ compared to their vicinal constitution in 1,2-PD which indicates 1,3-PD to be slightly less hydrophilic and, in turn, to have a slightly reduced water solubility. As a consequence, more disturbance of the hydrogen bonding network in water is assumed, leading to higher changes in the hydrated ion radii (Hawlicka and Grabowski 1993).

With that said, exclusive prediction of *in vitro* performance based on relative TPSA is insufficient, especially when molecules exhibit the same TPSA and molecular weight but possess different chemical structures. In those cases, log $P_{O/W}$ as another parameter indicating water solubility of a chemical, should be considered to support satisfactory discrimination of *in vitro* effects of substances (Prasanna and Doerksen 2009; Ali et al. 2012).

All in all, these cell-based observations corroborate previously outlined relevance of intracellular changes of especially $[Na^+]_i$ and $[Cl^-]_i$ to pose a suitable parameter for indicating magnitude of evoked ion disequilibria between intra- and extracellular space. Simultaneously, parameter of $[Na^+]_i$ is adduced in this thesis for predicting a substance's *in vivo* AP potential from *in vitro* gathered results using primary eccrine sweat gland co-culture cells. Furthermore, outcomes of conducted *in vitro* experiments highlight diverse disturbances of cellular ion equilibria to be indicative for interfering with and reducing sweating *in vivo*: While $[Na^+]_i$ was reduced by application of Cl^--containing substances it increased when cells were treated with polyols. However, both substance classes elicited an *in vivo* sweat-reducing effect.
For investigating whether the proposed mechanism of action of the potency of substances to be governed by relative TPSA together with log $P_{O/W}$ holds true for other polyols, further substances from this chemical class were tested in this study.

4.1.2.2 Molecular size determines the cellular response

Above-described polyols are based on either 1,2-PD, 1,3-PD, or glycerol as monomeric constituents. To evaluate above delineated hypothesis regarding their mode of action in more detail, polymeric substances of these monomeric components were examined for their impact on intracellular ion levels in eccrine sweat gland monolayer cells. With those long-chained substances it was of interest to evaluate their cellular as well as *in vivo* sweat-reducing effects with special emphasis on uncovering the influence of substances with several hydroxyl groups. Chemical structures of the tested polyols are depicted in **Fig 4.3** with the substances being grouped to different families depending on their monomer entity.
For comparison, all those substances were applied to primary eccrine sweat gland cells with an identical molar concentration, reflecting the maximum tolerable concentration of polyglycerol (PG)-10 as determined in cell viability assays. Consistent with reporting of previous results, only effects on changes of intracellular Na^+ and Cl^- levels were determined.
Strikingly, within one family a correlation of increase of $[Na^+]_i$ and chain length of the polyol was observed demonstrating larger molecules to evoke higher elevation of $[Na^+]_i$ (refer to Fig 3.12 and Tab 3.4). However, substances with the same number of carbon atoms evoked comparable alterations across all examined substance families.

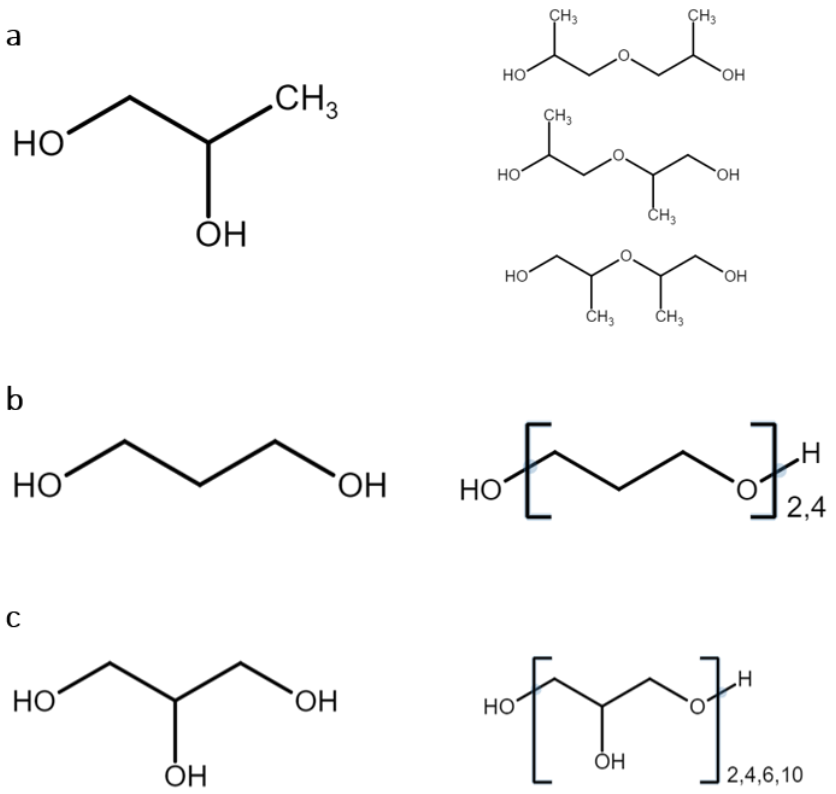

Fig 4.3: Molecular structures of tested polyol families.
Depicted are the molecular structures of polyol families tested *in vitro* for their impact on intracellular ion levels in primary eccrine sweat gland monolayer cells. 1,2-propanediol derivatives only included an isomeric mixture of dipropylene glycol (**a**). 1,3-propanediol family is complemented by polypropanediol-2 and polypropanediol-4 with the figure delineating the average number of combined 1,3-propanediol units (**b**). The largest family based on glycerol constitutes four other members: polyglycerol-2, -4, -6 and -10. Again, the suffix signifies the average number of glycol units per molecule. In case of the polyglycols also branched polymeric molecules are possibly present (**c**). Structures were created with Marvin JS software.

For explanation of these findings, above state hypothesis of relative TPSA playing a crucial role for determining hydration status of the polyols is reviewed. In line with discussed results, quotient of TPSA and molecular weight decreases with increasing chain length of the molecules when compared within one substance family (refer to **Tab 4.1**). Simultaneously, potency of the polyols to elevate $[Na^+]_i$ increased with smaller relative TPSA. These striking correlations confirm above delineated postulation of solvation status of the polyols to influence hydration of ions resulting in improved membrane permeability of ions. This impact finds expression in experimentally determined increase of intracellular Na^+ levels. It is anticipated that larger polyols with lower relative TPSA require more surrounding water molecules for complete solvation resulting in reduced hydration radii of the ions and, thus, enhanced ion mobility (refer to 4.1.2.1) (Impey et al. 1983; Hawlicka and Grabowski 1993; Ali et al. 2012).
In detail, the polyol with the lowest relative TPSA, polypropanediol (PPD)-4, elicited the strongest elevation of $[Na^+]_i$ while glycerol, possessing the highest value, slightly diminished $[Na^+]_i$. Further, molecules with a relative TPSA of higher than 0.5, indicating a predominantly polar property of the substance (more than 50% of the molecule's surface are composed of polar atoms), caused a reduction of $[Na^+]_i$ (Tab 4.1).

Regarding their log $P_{O/W}$, for the families of 1,2-PD and 1,3-PD a similar correlation of this value with determined elevation of $[Na^+]_i$ was observed, showing stronger effects with higher log $P_{O/W}$. However, such a relation could not be shown for molecules of the glycerol family where log $P_{O/W}$ decreased with increasing chain length while determined $[Na^+]_i$ rose. In this case, relative TPSA seems the more predictive parameter. Additionally, number of hydrogen bond acceptors and donors increased within this family with longer chain length. A study scrutinizing the structure of hydrogen bonding interactions of water-glycerol mixtures declared the same number of hydrogen bonds per water molecule in mixtures compared to pure water. Compared to pure glycerol number of hydrogen bonds of glycerol in water was even elevated. These features of water-glycerol mixtures are indicative for easy solvation of glycerol in water (Politi et al. 2009; Towey and Dougan 2012). Furthermore, homogenous mixing of glycerol in water might even promote hydration of ions resulting in increased hydrated ion radii. Although the latter assumption requires experimental verification, it well explains *in vitro* observed slight reduction of $[Na^+]_i$ after application of glycerol.
In contrast, mounting number hydrogen bond interaction sites with increasing chain length of the glycerol derivatives might exert an impact on aqueous structure and, thus, the solvation status of the present ions. Although this well explains results observed with substances from the glycerol family, this postulation requires further investigation.

Tab 4.1: Physicochemical characteristics of different polyols.
Listed are selected physicochemical properties important for solubility of tested polyols including molecular weight in g/mol, topical polar surface area (TPSA) in square angstrom (Å^2), the quotient of these two parameters, the relative TPSA, and *n*-octanol-water partition coefficient (log $P_{O/W}$). The quotient of TPSA divided by molecular weight is an approximation stating the relative proportion of polar, water-interacting surface per molecule for each tested polyol (denoted relative TPSA). When available experimentally determined log $P_{O/W}$ was taken (e), otherwise a calculated value is listed (c). *In vitro* determined intracellular Na^+ are stated again to ease comprehension. 1,2-/1,3-PD: 1,2-/1,3-propanediol, DPG: dipropylene glycol, PPD-2/-4: polypropanediol-2/-4, DG: diglycerol, PG-4/-6/-10: polyglycerol-4/-6/-10. Data of molecular weight, TPSA, and calculated log $P_{O/W}$ were taken from PubChem (National Center for Biotechnology Information).

Test substance	Molecular weight [g/mol]	Topical polar surface area [Å^2]	Relative TPSA: Quotient of TPSA per molecular weight [Å^2 · mol/g]	*n*-octanol-water partition coefficient (log $P_{O/W}$)	Relative intracellular Na^+ concentration [% of untreated]
1,2-PD family					
1,2-PD	76.1	40.5	0.5322	-1.07 (e)	93.75 ± 11.51
DPG	134.2	49.7	0.3704	-0.46 (e)	104.87 ± 12.64
1,3-PD family					
1,3-PD	76.1	40.5	0.5322	-0.71 (e)	96.85 ± 10.16
PPD-2	134.2	49.7	0.3704	-0.6 (c)	116.15 ± 19.84
PPD-4	250.3	68.2	0.2724	-0.2 (c)	257.94 ± 51.86
Glycerol family					
Glycerol	92.1	60.7	0.6591	-1.75 (e)	85.94 ± 9.48
DG	166.2	90.2	0.5428	-2.5 (e)	95.17 ± 11.55
PG-4	314.3	149	0.4740	-4.1 (c)	130.87 ± 17.77
PG-6	462.5	208	0.4497	-5.6 (c)	138.23 ± 33.69
PG-10	758.8	326	0.4296	-8.6 (c)	147.57 ± 27.77

As discussed above 1,3-PD again triggers slightly higher $[Na^+]_i$ compared to its isomer form 1,2-PD. Interestingly, the same tendency is observed for the constitutional isomers DPG and PPD-2. Being formed by two 1,2-PD monomers DPG achieves slightly less elevation of $[Na^+]_i$ than PPD-2 which is the reaction product of two 1,3-PD molecules. However, in this case *in vitro* better performing PPD-2 exhibits minimally lower log $P_{O/W}$ (-0.6 for PPD-2 versus -0.46 for DPG) indicating its higher hydrophilicity meaning minimally reduced water solubility (European Chemicals Agency 2020b; National Center for Biotechnology Information). However, an element of uncertainty remains for the actual log $P_{O/W}$ of PPD-2 as it was only derived by computational modelling. Nonetheless, discrepancies in measured $[Na^+]_i$ of those constitutional isomers might not be satisfactorily explained with available data.

Taken together, *in vitro* results of several polyols built from different monomeric units and having varying chain length clearly demonstrate relative TPSA to correlate well with changes in $[Na^+]_i$ measured in eccrine sweat gland monolayer cells. This indicates postulated hypothesis of solubility and hydration state of polyols in water to be crucial for triggered cellular effects and points out relative TPSA to represent a suited *in silico* parameter for assessment of the substance's cellular effect. Nonetheless, actual solubility of substances reflected by their

log $P_{O/W}$ should also be considered, especially for constitutional isomers and when two molecules exhibit the same relative TPSA. Besides, the number of hydrogen bond interaction sites of the molecules also seems to correlate with *in vitro* determined cellular effects when compared within one substance family. Of note, all those parameters are comprised by Lipinski's rule of five.

Regarding prediction of sweat-reducing effects, *in vitro* findings suggest the long-chained polyols to possess sweat-reducing properties based on comparison with established effects of diols (Biel et al. 2008; Biel et al. 2009). Beyond that, larger polyols such as PPD-4, PG-4, PG-6, and PG-10 might even act as more efficient AP agents compared to smaller diols due to evoking stronger elevation of cellular Na^+ levels *in vitro*. This assumption remains to be verified by testing of long-chained polyols in *in vivo* studies.

Differing ion prints of polyols and Cl^--containing substances highlights the general importance of undisturbed cellular ion equilibria for physiological sweating and concomitantly implies treatment-triggered imbalance of those equilibria to hinder physiological sweat production.

4.1.2.3 Polyols exert a short-time antiperspirant effect *in vivo*

Taking gathered insights from Cl^--containing substances, imbalances in intracellular ion equilibria, especially of Na^+, seems to pose a reliable parameter for predicting AP potential *in vivo* irrespective of the direction of the disturbance. Based on this, *in vitro* results employing primary eccrine sweat gland co-culture cells suggested tested polyol substances to induce sweat-reducing effects *in vivo*.

As for cell-based experiments, also for *in vivo* studies higher concentrations of diols were applied. To obtain significant changes in intracellular ion levels polyol concentrations of at least 1-2% AS (w/w) were required, while effective concentrations of Cl^--containing substances were about ten times lower.

However, testing of high concentrations of 1,2-PD and DPG for their AP effect on the back of volunteers resulted in no significant sweat reduction 24 h after the last application (refer to Fig 3.13) which contradicts published results of AP effects of 1,2-PD (Biel et al. 2008; Biel et al. 2009). Strikingly, short-term AP efficiency determined only 2 h after the last application was impressive and comparable to the effect evoked by the benchmark ACH at that point in time. Tested performance of 1,2-PD, DPG, and DG 6 h after the last substance application revealed intermediate sweat-reducing values with only the one of DPG being significant.

This time-dependence of sweat-reducing efficacy is perceived as another indicator pointing towards an alternative mechanism of AP action of polyols compared to Cl^--containing substances. Due to their rather small molecular size polyols are assumed to diffuse quite quickly and, thus, penetrate deep into the sweat gland, possibly even down into the coil compartment in case of low sweating rates (Wang et al. 2010). There, applied high concentrations of 1,2-PD and DPG are presumed to interfere with the hydration status of ions in the watery sweat just as explained for their *in vitro* mechanism of action (refer to 4.1.2.1). Although their concentration is diluted when mixing with watery sweat, initially high levels of 60% or 40% AS (w/w) of 1,2-PD and DPG, respectively, are proposed to still amount to sufficiently high concentrations inside the gland lumen to elicit changes in hydration radii of sweat ions in line with hypothesized *in vitro* mechanism of action (Hawlicka and Grabowski

1993). Alter hydration radii in the lumen are postulated to trigger imbalances in physiological ion equilibria between luminal sweat and cellular cytosol, finally resulting in reduced sweat production and/or output. Important to note, also *in vivo* higher luminal concentrations of the ions compared to the intracellular situation are stated (Takemura et al. 1991; Baker 2017), which constitutes the basis for enhanced cellular ion influx and caused imbalance.

However, due to high water solubility and mixing of the polyols with sweat they are anticipated to be quickly flushed out of the gland lumen with the sweat flow which is stated to reach up to 17 nl/min per gland (Sato and Sato 1983). In comparison, larger polycations such as ACH and PEI feature lower diffusion coefficients owing to their bulkiness (Beu and Farcaş 2017). Taking this background, it was not surprising to find the highest sweat-reducing efficacy of 1,2-PD and DPG shortly (2 h) after their last application and nearly no effect after 24 h as determined for Cl^--containing substances. Polyols are supposed to be quickly sluiced out with the natural sweat flow which terminates their effect on ion hydration status. Somewhat surprising was the near absence of AP effects already after 6 h which emphasizes rapid washout of polyols from the gland lumen by ubiquitous sweat flow.

Regarding their performance, DPG yielded slightly better sweat reduction than 1,2-PD in all *in vivo* studies although applied at a lower concentration (40% vs 60% AS (w/w)). These outcomes correspond well to results from *in vitro* experiments where DPG provoked the stronger elevation of $[Na^+]_i$ (refer to Fig 3.10 and Fig 3.12). Therefore, postulation of intensity of changes in $[Na^+]_i$ to represent a suitable parameter for estimating qualitative *in vivo* sweat reduction seems verified.

The only so far *in vivo* tested polyol, DG, produced the poorest AP action after 6 h. This agrees with *in vitro* determined effects showing DG to evoke the weakest elevation in $[Na^+]_i$ compared to 1,2-PD and DPG. However, it demonstrates validity of cell-based *in vitro* screening results for assessment of *in vivo* sweat-reducing potential of the substances.

Unfortunately, there was up to now no possibility to assess the sweat-reducing potential of larger polyol molecules in *in vivo* back studies. This would be of high interest, especially in view of their outstanding performance in upregulating $[Na^+]_i$ *in vitro* in primary eccrine sweat gland cells (refer to Fig 3.12).

In vivo results of the benchmark demonstrate highest sweat reduction values of ACH after 6 h, although the effect was already significant after only 2 h. These data open the possibility for further insight into the mode of action of this standard AP ingredient. First, ACH seems to require some time until fully active although formation of the obstructing hydrogel plug is assumed to be completed within few hours (Bretagne et al. 2017). This supports above introduced hypothesis of ACH exerting additional cellular sweat-reducing effects apart from physically plugging the sweat duct. Based on observations from *in vivo* studies, maximal AP efficacy of ACH is achieved when cellular effects due to evoked ion disequilibria and superficial plug obstruction of the orifice are combined. This is most likely the case around 6 h after the last ACH application as evidenced by the highest sweat reduction determined at that time point. Slightly lower AP effect after 2 h are hypothesized to be due to not fully formed ACH hydrogel plugs in combination with fully installed cellular effects. The latter are assumed to act with full force shortly after substance diffusion into the gland as deduced from the rapid transfection ability of other polycations such as PEI (Kichler et al. 2001). 24 h after the last ACH application both impacting mechanisms are supposed to be reduced: Some hydrogel

plugs would already have been ejected and cellular effects would be reduced due to continuous elution with the constant sweat flow (Kichler et al. 2001; Bretagne et al. 2017).
Further detailed investigation on elimination kinetics of all, ACH, Cl^--containing ammonium compounds and polyols out of the eccrine sweat gland are required to validate postulated hypotheses.
In any case, discrepancy of effect duration of Cl^--containing substances versus polyols was not obvious from *in vitro* screenings highlighting one huge limiting factor of this cell-based approach compared to elaborated *in vivo* studies.

Comparison of *in vivo* sweat reduction data used in this work with those of prior studies performed by other research groups is limited as employed *in vivo* methods differ markedly in crucial parameters such as site of substance application (back vs forearm), temperature of sweat stimulation, analytical method (gravimetric determination of sweat amount vs. counting of active glands), concentration of tested solutions, and their incubation method and time. Thus, results of two studies are only comparable regarding the overall AP classification of applied substances but not with respect to numerical values. Taking this into account, sweat-reducing efficacy of aqueous solutions of polyols and ACH published by other groups are therefore only classified as lying in the same efficacy range as data reported in this thesis (Biel et al. 2008; Biel et al. 2009). Tied to this, comparison of *in vivo* performance of 1,2-PD with the one of the constitutional isomer 1,3-PD requires testing of both substances in one *in vivo* study. Results from literature, however, suggest 1,2-PD to be slightly more efficient than 1,2-PD (Biel et al. 2008), which contradicts *in vitro* results of this work showing higher elevation of $[Na^+]_i$ for 1,3-PD.

In summary, available results from *in vivo* sweat reduction studies supported *in vitro*-based estimation of potency of polyols relying on their ability to increase $[Na^+]_i$ in primary eccrine sweat gland cells. Likewise, *in vivo* data confirmed introduced *in silico* parameter of relative TPSA to predict *in vitro* and *in vivo* efficacy.
Additionally, polyols were demonstrated to feature an alternative mechanism of action compared to Cl^--containing substances. While the latter are assumed to interact with cells, hydroxyl group-carrying molecules are supposed to elicit their AP effect via hydrogen bond interaction with water molecules and resulting changes of hydration states of solvated ions. This difference in the substance class's mode of action, in turn, might be the reason for their drastically diverging effect duration, which is proposed to be related to their varying retention in the gland. This needs verification in further experiments by determining the detailed time course of their elimination from the gland.
Although long-chained polyols are not expected to exert effects over a prolonged time owing to their identical mechanism of action, testing of their *in vivo* performance would reveal whether those macromolecules are able to achieve higher sweat reduction values as indicated by their better *in vitro* effectiveness
In any case, results of these comprehensive studies add substantially to understanding of the physiological, cellular processes of sweating and enabled identification of first alternative AP actives.

4.2 Development of eccrine sweat gland models

To get a deeper understanding of physiological processes during sweating, it is relevant to investigate cellular interactions and protein expression patterns of human eccrine sweat gland cells more closely.

For many physiological and toxicological studies as well as in research and development, 3D cell culture models of various tissue types have become a widely used tool as they mimic the *in vivo* situation more closely than conventional monolayer cell cultures could achieve (Kunz-Schughart et al. 2004; Santos et al. 2012; Ravi et al. 2015). Especially attributable to the intensified cell-cell contact several vital physiological processes are more pronounced in 3D cultures (Fennema et al. 2013). One of the first methods to generate such cell aggregates employs the hanging drop technique and was already used in 1907 to cultivate and observe isolated tissue specimen for up to one week (Harrison et al. 1907). Modern platforms and labware formats such as 96- and 384-well plates enable a controlled and more efficient way to generate reproducible, isolated HD spheroids than was possible with initial procedures where drops were hanging from an inverted plate. Furthermore, with these advanced tools defined sizes and compositions of the aggregates are feasible including the combination of different cell types and addition of cells after initial seeding. Also sustenance of 3D models is improved due to easily realizable changes of surrounding culture medium (Fennema et al. 2013). Taking those advantages, generation of 3D eccrine sweat gland models using scaffold-free HD technique was employed in this work to obtain reproducible spheroids combined with the flexibility to easily implemented changes of their composition and size. Most important for the envisaged application is the ability to get single spheroids which can be individually used in further test procedures such as molecular biological and histological analyses as well as in future *in vitro* substance testing. The latter would elevate the testing to include more advanced simulation of physiological processes during sweating.

4.2.1 Improved *in vitro* 3D HD models of the eccrine sweat gland

In vitro 3D HD models of the eccrine sweat gland were initially developed by Klaka et al. and consisted of either co-cultures of coil and duct cells or the respective isolated cell type. Sweat gland co-cultures, however, are mainly made up of coil cells which is why the generated spheroids predominantly showed characteristics of coil cells (Klaka et al. 2017; Klaka 2017). To improve this aspect and to be able to better scrutinize the cell-cell interactions between coil and duct cells, optimized spheroids were described here which consisted of defined numbers of separately cultured coil and duct cells united into one HD. When both cell types were mixed into one suspension prior to addition into the HD plate, HE stainings of prepared spheroids revealed defined regions of coil and duct cells characterized by more intense staining of the duct compartment (Fig 3.15). This defined separation suggests a self-organization potential of the cells and gives first indication for intense cell-cell communication and interaction. Distinction of secretory coil and reabsorbing duct in HE stainings of native human skin due to darker staining of the duct is also established in literature (Gao et al. 2014; Klaka et al. 2017; Ma et al. 2018). This characteristic is based on the different basophilia of the cell cytoplasm which is obviously retained in cultured sweat gland cells.

When consecutively adding the two cell types to one HD this alternative approach only promoted clear separation of the different cell areas but did not alter the 3D HD structure. Initial idea, though, was to generate a tubular like structure of the 3D models by consecutive seeding which should resemble the native eccrine sweat gland tubule more closely. In failing to achieve so, a limitation of the 3D culturing technique becomes evident. Nonetheless, these novel 3D HD models constituted an improvement compared to the initial one described by Klaka et al. in that defined areas of coil and duct cells were distinguishable and, thus, cell type specific and cell-cell interaction-related traits could be scrutinized (Klaka et al. 2017).

Self-organization and -differentiation of coil and duct cells in *in vitro* eccrine sweat gland cell models was also described by other groups. Their models, in contrast, relied on using Matrigel as a scaffold and required implantation into nude mice to fully achieve cellular organization and differentiation (Li et al. 2013; Li et al. 2016a). Even before being implanted, these Matrigel-embedded eccrine sweat gland models developed hollow lumen-like structures in the center of the aggregates during 12 d of culture (Li et al. 2013). In another approach by Lui et al. epidermal progenitor cells were bioprinted into porous hydrogel-based matrices employing a 3D printing technique. Over a time course of 4 weeks sweat gland-like structures formed out of the epidermal progenitor cells, but their differentiation into coil and duct cells was not investigated (Liu et al. 2016a). Such an advanced tubular-like structural organization was not observed with herein described 3D HD models. Rather, the central part of the spheroid was occupied by duct cells. But then, herein described 3D spheroids are scaffold-free models refraining from use of additional material such as Matrigel or hydrogel to obtain single reconstructs which can be directly used in further applications. However, this flexibility of use obviously brings in its wake the downside of less advanced structural orientation with fewer resemblance to the natural morphology of the eccrine gland. Of note though, observed self-organization of the eccrine cell types occurred in these models without further assistance of any scaffold material.

Additionally, cultivation of these 3D HD models was limited to less than 7 d as longer cultivation in HD induced a high amount of cell death (Klaka et al. 2017). This seems as another advantage of scaffold-based models for which cultivation of at least 12 d in Matrigel and up to 4 weeks in bioprinted hydrogels with high viability is reported (Li et al. 2013; Liu et al. 2016a). HE stainings of herein generated coil and duct 3D HD models showed the structural integrity of these spheroids as well as the presence and integrity of the nuclei which indicates vivid cells even in the core of the spheroid. HD models prepared from co-cultures exhibited irregularly shaped loose cells in their center which might either be attributed to apoptotic and/or necrotic cells or formation of a lumen-like structure (Klaka et al. 2017). In any case, the compact core of living cells in the herein described 3D HD models suggests sufficient nutrient and oxygen supply in the center. Insufficient supply is often a problem with voluminous spheroids which have a diameter above 500 µm because a diffusion limit of about 150-200 µm is report. As a result, larger spheroids commonly feature a necrotic center (Lin et al. 2008). The size of herein described eccrine sweat gland models lay below 500 µm ensuring the adequate sustenance of the cells even in the core. Interestingly, the average size of 3D HD models composed of equal numbers of coil and duct cells was markedly smaller than the one reported for the co-culture models (>500 µm), although the overall number of cells was identical with 25,000 cells/HD. Smaller size of the coil and duct HD models is attributed to

more compact cellular structure of especially duct cells in the spheroid core compared to the lose center of co-culture models (Klaka 2017). Interestingly, Matrigel-based models as well as bioprinted hydrogel ones were smaller in size reaching only 100 µm and 400 µm, respectively (Li et al. 2013; Liu et al. 2016a).

Using immunofluorescence staining of selected eccrine sweat gland-specific markers, their distribution and localization in the 3D HD models was determined and compared to the one in native eccrine sweat glands. Included in the analysis were different kinds of proteins ranging from receptors (M3) over ion and water channels (ENaC, AQP5) and cell type-specific proteins (CD44, SSEA-4, CEACAM5) to antimicrobial peptides (dermcidin) (refer to Fig 3.16). With this selection various aspects of sweat gland function and characteristic were covered.
Localization of all those markers in the native gland is well described (Wang et al. 1992; Penneys and Kaiser 1993; Schittek et al. 2001; Inoue et al. 2013; Li et al. 2014; Hubka et al. 2015; Borowczyk-Michalowska et al. 2017; Ma et al. 2018) and stainings of human facial skin sections, carried along in this work as controls, featured the same localization and cell type-specificity as established (Fig 3.16). Further, native skin sections enabled direct comparison of native expression and localization in reconstructed *in vitro* 3D HD models.
Although all selected proteins could be detected in the 3D spheroids, natural distribution of the scrutinized markers was not observed in every case: While dermcidin, ENaC, SSEA-4, and AQP5 showed the same cell type-specific localization in 3D models as in native skin, expression of CD44, M3, and CEACAM5 differed between *in vitro* and *in vivo* tissue.
In detail, expression of glycoprotein CD44 by myoepithelial cells and eccrine secretory coil cells, especially clear cells, is established, while its presence in the native duct compartment is, if any, weak (Wang et al. 1992; Penneys and Kaiser 1993). In the 3D HD models, in contrast, regions of duct cells exhibited more intense coloration than surrounding coil cells indicating a shift in protein expression in this cell type during isolation and culture (Fig 3.16b and c). Li et al. observed emergence of expression of α-SMA in their Matrigel-based eccrine sweat gland models. They postulated presence of this marker to occur due to cellular dedifferentiation of cells into a precursor state (Li et al. 2015). The same explanation is assumed here for duct cells in 3D HD models: During cultivation duct cells dedifferentiate and gain expression of CD44. Pointing in the same direction of altered characteristics, regions of duct cells in 3D spheroids lacked expression of M3 and CEACAM5 while the one of ENaC was markedly reduced compared to presence of these proteins in native duct compartments. Coil cells of the 3D models, in contrast, behaved just as native secretory cells showing marked expression of CD44, M3, dermcidin, AQP5, ENaC, and CEACAM5. This implies cultured *in vitro* coil cells in 3D spheroids to retain their native characteristics *in vitro*.
In native glands, muscarinic acetylcholine receptor M3 is predominantly expressed in secretory coils with only faint presence in the lower part of the duct (Fig 3.16a) (Hubka et al. 2015; Kamiya et al. 2015). In coil and duct 3D HD models, however, M3 was confined to areas of coil cells. Absent expression in duct cell regions might suggest duct cultures to attain characteristics of those cells shaping the upper duct fraction of the native gland where M3 is not expressed. Comparing to initial co-culture 3D HD models, they exhibited staining for this marker only on the outer surface of the spheroid (Klaka et al. 2017). This difference to here

described coil and duct 3D spheroids might be attributed to intensified cell-cell communication of the two cell types in the refined models.
Like native distribution of M3, the antimicrobial peptide dermcidin is produced by dark cells of secretory coils and transported through the duct lumen to the skin surface. Thus, it can be detected in native coil as well as duct compartments (Schittek et al. 2001; Schittek 2012). Matching with this description, only coil cell region exhibited strong expression of this marker in 3D HD models as the active transport into duct cell areas is lacking *in vitro*.
For clear discrimination of coil and duct compartments, the water channel AQP5 constitutes an often employed ideal marker as it is only present in secretory coil cells of the native gland (Inoue et al. 2013; Hubka et al. 2015). Matching with the native distribution, coil cell regions of the improved 3D HD models were also positive for AQP5 while it was absent from duct cell regions. Also mentioned Matrigel-based eccrine sweat gland model demonstrated expression of AQP5 two weeks after subcutaneous injection into nude mice. However, differentiation of coil and duct structures was not performed with APQ5 in this study. Thus, the exact cell type expressing this water channel remains unclear (Li et al. 2015).
Regarding distribution of a general eccrine sweat gland marker, CEACAM5 is present in both, coil and duct compartment, of the native eccrine gland (Fig 3.16m) (Cotton 1986; Li et al. 2009; Gao et al. 2014; Borowczyk-Michalowska et al. 2017; Klaka et al. 2017; Ma et al. 2018). As already mentioned, duct cells in 3D HD constructs lost expression of this protein (Fig 3.16n and o). Comparing to the Matrigel-based model, CEACAM5 expression is weak and confined to the inner parts of the structures in this *in vitro* analogue (Li et al. 2015).
Recently discovered, SSEA-4 is the only identified surface antigen specific for the whole duct compartment of native eccrine sweat glands (Fig 3.16g) (Borowczyk-Michalowska et al. 2017). Interestingly, localization of this duct cell marker was distinctly modified in *in vitro* 3D models as SSEA-4 was weakly detected only in small parts of the duct cell regions which were located next to surrounding coil cells (Fig 3.16h and i). This constitutes the first obvious indication for cell-contact-regulated protein expression in coil and duct HD sweat gland models. It seems likely to assume SSEA-4 expression in 3D eccrine sweat gland HD models to be triggered by crosstalk between eccrine duct and coil cells. Additionally, it indicates the capability of this model as a research tool for mechanistical scrutiny of eccrine sweat gland cell organization under more physiological conditions. Generally, intense cell-cell contact poses a prerequisite for cell organization and polarity in any tissue (Ben-Ze'ev 1984; Wang et al. 1990; Desai et al. 2009). Also for 3D cultures this property is well established as e.g. an *in vitro* 3D HD model of the anterior pituitary showed a high cellular organization potential resulting in a cellular structure which resembled the native rat anterior pituitary (Tsukada et al. 2013).
Taken together, investigation on distribution and localization of all these eccrine sweat gland markers and comparison of the novel 3D eccrine sweat gland models with the native situation in the gland revealed important differences between reconstructed *in vitro* spheroids and the *in vivo* situation. Most obvious, while coil cells largely retained their characteristic protein expression pattern in 3D spheroids as established in the native gland, duct cells underwent some drastic changes. Especially the absence of the sodium channel ENaC, which is crucial for salt reabsorption from primary sweat in the eccrine gland duct *in vivo* (Quinton 1981; Reddy et al. 1999), evidences a profound alteration of the duct cell identity. Loss of CEACAM5 expression further indicates substantially altered duct cell properties as this protein is a

distinctive marker of all eccrine sweat gland cells (Cotton 1986; Li et al. 2009). Absence of ENaC and CEACAM5 strongly suggest the duct cells to shed their sweat gland identity while in return attaining precursor cell features as indicated by gain of CD44 expression (Li et al. 2014; Li et al. 2015).

Shortly discussed at this point should also be intruding possibility of cultured duct cells to be fibroblasts as an explanation for observed divergences between native and cultured duct cells. Substantial fibroblast growth was reported in cultures of eccrine sweat gland explants in presence of high serum concentrations in the medium (Pedersen 1989). Concomitantly, serum constitutes a crucial ingredient in sweat gland cell culture medium for retaining biological traits of sweat gland cells and to prevent their transition into keratinocytes (Sun et al. 2017).
Immunofluorescence staining of transmembrane protein CD276 (also called B7-H3) (Picarda et al. 2016) in 3D HD models comprising coil and duct cells and in 3D HD models made up of fibroblasts revealed solely the duct cells to express this protein, while fibroblast 3D models showed no staining (Supplemental Fig 6.5). Together with presence of eccrine duct-specific marker SSEA-4 this strongly suggests used cells to be eccrine sweat gland duct cells and not fibroblasts. However, CD276 was reported to be constitutively present in skin fibroblasts (Tran et al. 2008) although stainings performed in this study missed to show this.
Furthermore, all cells originating from meticulously isolated duct compartments exhibited the same rather longitudinal-cell shape. If those cells were fibroblasts, it would mean completely missing outgrowth of duct cells from the isolated duct compartment. However, coil cells show a substantial propagation *in vitro*. A suitable explanation for eager *in vitro* growth of coil cells but lacking one of duct cells is elusive seeing as they originate from the same epidermal progenitor cells during ontogenesis (Hashimoto et al. 1965; Li et al. 2009; Lu and Fuchs 2014). Nonetheless, cells derived from whole gland explants predominantly show characteristics of coil cells with only few duct cells interspersed. This might indicate the culture conditions to not be optimal for duct cell growth *in vitro*, while cultured coil cells retained their native traits in 3D models to a great extent as revealed by immunofluorescence analyses. Pointing in the same direction, Pedersen observed drastic morphological changes of growing cells from isolated eccrine duct under different medium conditions. Especially in high serum-containing medium eccrine sweat gland cells differentiated and developed cell type-specific characteristics and morphologies (Pedersen 1989). Therefore, the aspect of influence of culture conditions on cell differentiation requires further exploration.
Nonetheless, these indications strongly suggest cultured cells to be eccrine sweat gland duct cells, but diverging traits compared to their *in vivo* state prompts them to dedifferentiate, at least partially, during isolation and culture.
Loss of protein expression in cells outgrowing from native tissue has been reported multiple times and has become a well-established fact in cell culture research. This dedifferentiation is mainly attributed to the unphysiological growing behavior of cells in tissue culture plates. Accordingly, cells in a 3D alignment regain vital functions including the expression of several proteins and, thus, mimic the *in vivo* situation more closely (Santos et al. 2012; Klaka 2017; Klaka et al. 2017; Li et al. 2017c; Bovell 2018). Based thereon and together with findings of this work it is very likely to assume isolated epithelial cells to attain a more primitive precursor state (e.g., expression of CD44) while cultivation in 3D spheroids triggers partial differentiation

and, thus, expression of cell type specific markers (e.g., SSEA-4, AQP5, M3). Especially cultured duct cells seem to dedifferentiate which corresponds well with reported multipotency of native eccrine duct cells (Lu et al. 2012), but further detailed investigations in this direction are required to fully elucidate these assumptions.

In sum, the novel 3D HD model of the eccrine sweat gland combines coil and duct cells and therefore constitutes a suitable *in vitro* tool for investigating cell type specific differentiation as well as cell-cell contact regulated processes due to the clear spatial separation and morphological discrimination of the two cell types. Furthermore, these 3D models will hopefully prove useful for more elaborate *in vitro* testing of sweat-reducing substances, especially due to detected expression of M3. Based on this, currently missing reaction of the monolayer test system upon stimulation with carbachol will hopefully be overcome. Successful loading of spheroidal cells with ion-sensitive fluorescence dyes was already demonstrated.

4.2.2 Establishment of a sweat gland model in a dermal equivalent

Apart from described *in vitro* 3D HD model of the human eccrine sweat gland several methods were published trying to reconstruct sweat glands *in vitro*. To create a more physiological 3D orientation of cells different scaffold materials like Matrigel (Li et al. 2013; Diao et al. 2019), hyaluronic acid-based hydrogel (Hubka et al. 2015), or 3D bioprinting of gelatin and sodium alginates-mixed hydrogels (Liu et al. 2016a) have been employed. Alternatively, also scaffold-free methods such as the hanging drop technique (Klaka et al. 2017; Klaka 2017) were used. In the last years tissue engineering as well as regenerative medicine have experienced a huge leap forward benefitting from continuous extensive research striving to develop more and more sophisticated *in vitro* models (Santos et al. 2012). Mimicking of the ECM seems to be a crucial factor for achieving close resemblance with native tissue due to enabling cell-ECM interactions apart from mere cell-cell communication. Especially hydrogels including Matrigel have proven beneficial owing to their high resemblance with the natural ECM. They are characterized by high water capacity and formation of pores allowing for unhindered passage of e.g., oxygen and nutrients. Drawbacks include limited possibility to adapt biochemical and -physical parameters and high product variability. Therefore, additional efforts are made to improve tissue reconstruction (Santos et al. 2012).
Although above-mentioned scaffold-based techniques yielded reconstructed sweat glands with good expression of specific and functional markers, separate segments and morphology of the native eccrine gland were not adequately rebuilt (Liu et al. 2016a; Li et al. 2016b; Li et al. 2017a; Li et al. 2017c; Zhang et al. 2018a).
Taking this idea forward and inspired by a recent biomimetic approach which successfully reconstituted a human hair follicle *in vitro* (Abaci et al. 2018), a novel, structurally improved, sweat gland-bearing dermal matrix model was developed in this study. With the help of a 3D-printed plastic mold, collagen type I-based slot-bearing matrices including fibroblasts were produced serving as the dermal equivalent. Separately cultured primary eccrine sweat gland coil and duct cells were then added into the empty slots and cultured for up to 28 d. This constitutes a markedly extended culture time supposedly made possible by to cultivation in artificial ECM as compared to above-described 3D HD models.

Already after 7 d of culture, successful integration of the sweat gland cells into the dermal matrix models was shown derived from on the intense contact between cells and surrounding fibroblasts-supplemented collagen I matrix (Fig 3.17a and b). Additionally, the collagen I-matrix displayed a fibrous, loosely connected network with large pores which should provide unhindered nutrient and oxygen transport (Santos et al. 2012).
While dermal papilla cells and keratinocytes were combined inside the slots of hair follicle models (Abaci et al. 2018), here the different cell types of the eccrine sweat gland were united. In both, hair follicle and sweat gland model, a defined spatial orientation of the cell types was observed clearly recognizable by the different color of the cells in HE stainings. This indicates high self-aggregation and -organization potential of all these cells (Abaci et al. 2018).
Comparing HE with immunofluorescence stainings of cell type specific markers such as AQP5, dermcidin, and M3 revealed duct cells in HE stainings of dermal matrix model to exhibit lighter, more purple coloration whereas coil cells showed a rather reddish hue (Fig 3.17 and Fig 3.19). In dermal matrix models, this observation contradicted staining intensities displayed in the native gland. HE stainings of Matrigel-based constructs, in contrast, revealed all eccrine sweat gland cells to adopt the same coloration although immunofluorescence investigations showed them to differentiate into coil- and duct-like structures based on expression of characteristic proteins (Li et al. 2015; Li et al. 2017c). In both cases, Matrigel models and dermal matrix models of this work, altered HE staining intensities imply the eccrine sweat gland cells to be subject to changes of the basophilia of their cytoplasm.

Dermal matrix models were cultured over a time course of 28 d in this thesis. Therefore, also temporal changes of the structure were scrutinized but revealed no obvious time-related differences as both cell populations were discernible and cells were in close contact and interwoven with the surrounding fibroblast-containing collagen I-matrix at all time points (Fig 3.18). Observed structural discrepancies are rather attributed to naturally occurring variations between individual models and diverging cutting angles when preparing frozen sections. Altogether, this proves collagen I as one of the major collagens in the dermis, to be an adequate basis for reconstruction of the dermal compartment. Integration of skin fibroblasts improves the artificial dermis as fibroblasts are known to produce ECM components and secrete various cytokines, with which they vitally contribute to cell-cell communication (Lai-Cheong and McGrath 2013; Slominski et al. 2015). Similarly, structural junction between collagen I and keratinocytes was also reported for hair follicle models (Abaci et al. 2018).
Seen formation of thin keratinized superficial layers on models after 28 d is in line with reported findings describing eccrine sweat gland cells to be able to rebuild a stratified epidermis *in vitro* (Biedermann 2010).
Although coil cells were seeded into slots 24 h prior to addition of duct cells, the latter arranged at the rim of the slots and exhibited strong connection to the surrounding collagen I-fibroblast matrix while coil cells were found at the bottom and the center of the cavities. Due to stepwise integration of the two cell types a layered structure was anticipated. Observed altered but distinct spatial orientation suggests coil and duct cells to interact with each other and the surrounding artificial matrix, thereby realigning in a way dictated by cell-cell interactions. These cellular and cell-matrix interactions might also be the reason for alignment of duct cells at upper sides of the slots. Possibly this was triggered by intense contact between sweat gland

cells and dermal matrix equivalents favoring close contact of duct cells with the fibroblast-containing collagen I scaffold over those of coil cells. The longitudinal shape of the cavity might also contribute to this, as it posed a completely different environment compared to gravity driven cellular self-aggregation in 3D HD models where duct cells formed the core.
Structural similarities were revealed with published hair follicle model, though: Like coil cells in the sweat gland matrix model, dermal papilla cells formed a spheroid-like structure in the tip of the cavity and were surrounded by differentiated keratinocytes. This also implies intense cell-cell interaction and communication to occur in the hair follicle model (Abaci et al. 2018). Matrigel-embedded sweat gland models, in contrast, exhibited defined cellular orientation characterized by formation of a hollow lumen due to circular alignment of the sweat gland cells (Li et al. 2013). However, emergence of such a lumen was not detected in matrix models of this work.

Investigations concerning the protein expression of cell type-specific and functional markers in sweat gland matrix models was conducted to clarify degree of cellular differentiation.
Observed cell type-specific staining of M3, CD44, dermcidin, AQP5, and CEACAM5 in sweat gland matrix models (Fig 3.19) matched those described for coil and duct 3D HD models (Fig 3.16 and refer to 4.2.1). Solely near absence of SSEA-4 in the dermal constructs poses a marked difference between 3D spheroids and sweat gland matrix models and might indicate missing differentiation of the duct cells in this altered environment.
Additional to mentioned proteins, presence of α-SMA and CFTR as further sweat gland-related markers was also investigated in frozen sections of sweat gland matrix models. Again, simultaneous staining of these proteins in native eccrine sweat glands was consistent with literature reporting myoepithelial marker α-SMA exclusively in these myoepithelial cells surrounding the secretory coil (Kurata et al. 2017; Ma et al. 2018) and CFTR expression predominantly in the duct but only scattered in the coil compartment (Sato and Sato 2000; Sato et al. 2002).
Determined absence of α-SMA in dermal matrix models emphasizes the lack of myoepithelial cells in eccrine sweat gland cell cultures employed here. Comparing to Matrigel-based eccrine sweat gland models, they initially lacked this marker but started to express it after being implanted into nude mice for at least 21 days (Li et al. 2016a; Zhang et al. 2018b). This coincides well with established ontogenetical emergence of α-SMA in fetuses at week 22 (Moll and Moll 1992). Simultaneously it implicates general possibility of rather un- or dedifferentiated eccrine sweat gland cells to differentiate and attain cell type-specific characteristics in a native surrounding (Li et al. 2016a). Keeping complexity of the natural tissue in mind, it seems unlikely to expect eccrine sweat gland cells in dermal matrix models of this study to experience such extensive differentiation with emergence of α-SMA-positive myoepithelial-like cells.
Worth a try, prolonged cultivation of sweat gland matrix models of more than so far tested 28 d might achieve such cellular changes as some markers already exhibited temporal alterations within this time frame implying continuous evolvement of the cells. E.g., the chloride channel CFTR was exclusively detected after 28 d of culture in coil cells. CFTR expression was also demonstrated in Matrigel-based eccrine sweat gland models, but a cell type specificity was not reported there (Li et al. 2015).

Missing CFTR expression in duct cell regions of the matrix models is taken as another indicator for altered characteristics of cultured duct cells as discussed above (refer to 1294.2.1). This assumption is reinforced by determined presence of CD44 and lack of CEACAM5 and SSEA-4 in duct cell parts of the matrix models. Obviously, adopted altered state of cultured duct cells could not be reversed by incorporation into a more elaborate dermal matrix model.
Minor temporal changes of sweat gland matrix models observed in this study included varying expression intensities of M3, dermcidin, CD44 and AQP5 (Supplemental Fig 6.3), which highlights mentioned ongoing differentiation of the cells within the matrix. While presence of CD44 increased with cultivation time, localization of M3, dermcidin, and AQP5 became less and more localized. Strikingly, AQP5 was gradually restricted to a small cell part at the lower border of the cavity which contradicts presence of AQP5 throughout the whole coil compartment in native glands (Brown et al. 2011; Inoue et al. 2013). This might suggest cell-cell and cell-matrix interactions to contribute substantially to shaping of the newly formed *in vitro* structures.
Scattered expression of M3 and dermcidin might be due to insufficient signaling as M3 might require acetylcholine-signaling to be expressed. Although production of dermcidin is reported as constitutive in native (Rieg et al. 2004), this aspect might be different in reconstructed eccrine sweat gland models.
Besides, cultivation over a period of 28 d could be too long under these conditions resulting in observed artificial cell segmentation and marker localization. Yet, it was excluded that these unnatural distributions were due to progressively increasing cell death as HE and immunofluorescence stains proved the cells to be viable.
Increasing and widespread expression of CD44 in matrix models of late cultivation stages corresponds to the one observed in 3D HD models. This suggests the cells in the matrix model to evolve more slowly than in the HD environment.

Overall, cultivation of isolated sweat gland cells in artificial collagen I-based dermal equivalents allowed for an extended cultivation period in the range of the one stated for other established and scaffold-assisted eccrine sweat gland models which were already mentioned (Li et al. 2013; Liu et al. 2016a). Although a certain differentiation of the eccrine cells in the matrix models of this work over time was reported based on protein expression, such a detailed and extensive investigation and description as performed for temporal development of the Matrigel-based, implanted sweat gland model of Li et al. was not conducted (Li et al. 2016a; Li et al. 2016b; Li et al. 2017a; Li et al. 2017c; Zhang et al. 2018a). Therefore, only few parallels could be drawn such as suggested differentiation of the eccrine sweat gland cells.
For the Matrigel-based models, however, examinations of expression of eccrine sweat gland cell-specific markers, keratins, and markers of cell polarity as well as the cellular proliferation behavior over a time course of up to 12 weeks was (Li et al. 2016a; Li et al. 2016b; Li et al. 2017c; Zhang et al. 2018b). Even more, this research group could demonstrate cholinergic and adrenergic innervation as well as vascularization of Matrigel reconstructs 10 weeks after implantation into nude mice based on fluorescence staining of related proteins (Zhang et al. 2018a). Further, using magnetic resonance imaging, fluid secretion of these implanted sweat gland models could be shown 10 weeks post-implantation (Li et al. 2018b).

Taking all these comprehensive studies into account, Matrigel-based and implanted model seems far more advanced than the rather simple models described in this work. Nonetheless, 3D HD models provide easily and fast generated reconstructs while with reliance on collagen I-matrices cell viability and longevity as well as structural organization could be improved. However, to reach the elaborate status of the models reported by Li and group, as well as Liu et al. (2016a) and Diao et al. (2019) most likely implantation into living organisms is required which adds a good amount of complexity. Besides, use of animals is not intended, and allowed, for cosmetic applications for which herein described *in vitro* sweat gland models were primarily designed.
Then again, integration of herein generated eccrine sweat gland constructs into living organisms was never conducted and might reveal striking new aspects and possibilities in the context of medical applications.

Altogether, cultivation of eccrine sweat gland cell in an artificial collagen I-based dermal improved longevity of eccrine sweat gland cells and the structural arrangement. Nonetheless, such an approach seems not ideal to achieve natural differentiation of cells. Although collagen I represents a good scaffold material in terms of pore size, stability, flexibility, fibrous network, nutrient diffusion, and provision of a biologically derived material for the cells to interact with, these mechanical properties are not the only aspects crucial for successful bioengineering of tissue constructs. Moreover, the factor of biochemical signaling constitutes another vital component directing cellular development (Santos et al. 2012; Ravi et al. 2015) as also indicated by other more elaborate sweat gland models which were implanted into living organisms (Li et al. 2016a; Li et al. 2016b; Li et al. 2017a; Li et al. 2017c; Zhang et al. 2018a; Liu et al. 2016a; Diao et al. 2019). In native skin multiple biologically active molecules are contained in the ECM (Slominski et al. 2015). As several of these components are missing in herein presented dermal reconstructs, observed deviations in protein expression are not unexpected but might very well be consequences thereof.
To overcome these limitations and accomplish a differentiated model with native characteristics adjustment of the rebuilt ECM regarding supply with growth factors, morphogens, proteoglycans, glycosaminoglycans, and other soluble biomolecules should be faced (Slominski et al. 2015; Ravi et al. 2015). However, nerval innervation and vascularization is still not achievable with these measures as was demonstrated to be crucial for development of Matrigel models implanted into skin of nude mice (Zhang et al. 2018a). Therefore, this completely *in vitro*-based approach faces limitations which are possible though difficult to overcome with current state of the art (Das et al. 2020).

In conclusion, herein developed dermal matrix model with incorporated eccrine sweat gland cells represents a more sophisticated approach to investigate cell-cell and cell-matrix-related interactions when it comes to differentiation of eccrine sweat gland cell types. Additionally, established continuous temporal succession of cell development poses a chance for more detailed investigation of underlying cellular communication processes using this approach. In the future, this organotypic skin model might also serve as a basis for development of artificial skin equivalents for transplantation purposes.

4.3 Establishment of an immortalized eccrine duct cell line

So far discussed investigations were based on utilization of primary cells. Cell lines, in contrast, represent an advantageous research tool due to the possibility of working with the same cellular material in a multitude of experimental setups. Thereby, interindividual variations are neglectable which are introduced if only limited tissue from one source is available and material from different donors needs to be taken (Buchanan et al. 1990). Creation of a stably immortalized cell line required genetic changes in e.g., cell cycle-related processes. This is most often achieved with the help of lentiviral vectors as vehicles for gene delivery (Maqsood et al. 2013). Thereby, different cell types exhibit varying degrees of transduction efficiency as this process is highly dependent on tropism of vector particles and their compatibility with membrane receptors expressed on target cells (Cronin et al. 2005).
To assess the efficiency of transduction of herein used eccrine sweat gland duct cells, they were firstly transduced with a GFP-containing lentiviral control vector. Flow cytometric measurements demonstrated the ability of the lentiviral vector to integrate into the duct cell genome and showed a MOI of 10 to be insufficient for maximal transduction efficiency (Tab 3.2). Therefore, sweat gland duct cells were finally transfected with SV40T-containing lentiviral vector at a MOI of 50 to yield a high transduction rate while simultaneously not straining the cells too much leading to cell death. Using this approach, a pool of SV40T-transduced eccrine sweat gland duct cells (SGDC-SV40T) was generated and selected by presence of 1 µg/ml of puromycin in the culture medium.
After induction of genomic alterations and while working with a cell line its continuous authentication is crucial to ensure its suitability for the research at hand. Derived cell lines should maintain characteristic traits of parental cells with features as similar as possible to the original tissue to represent a suitable research tool. Methods for authentication include simple techniques such as morphological observations, more advanced ones like karyotyping, immunological determination or isoenzyme analysis, or modern approaches like DNA profiling and CO1-barcoding to establish inter- and intraspecies cell specificity (Nims and Reid 2017).
Adapting this concept to establishment of an immortalized eccrine sweat gland duct cell line, growth and shape of transduced cells was monitored, gene as well as protein expression of sweat gland-associated and functional markers determined, and reactivity of selected clones upon treatment with established AP actives recorded. Whenever possible results were compared with parental cells, cell of a standard donor, and the native eccrine sweat gland.

4.3.1 Characteristics of transduced eccrine sweat gland duct cell pool

First and foremost, comparison of morphology is an easily observable trait giving valuable information about conservation of characteristic traits and cellular identity (Nims and Reid 2017). In case of SV40T-transduced eccrine sweat gland duct cell pool (SGDC-SV40T), they maintained their typical rather longitudinal cell shape and characteristic scattered widespread growth pattern (Fig 3.21). Apart from maintenance of their morphology continuing proliferation of transduced cell when parental cells entered a senescent stage constituted first indications for successful transduction with SV40T leading to an at least prolonged lifespan (Fig 3.20 and Fig 3.21). Further, they exhibited population doubling times (PDT) in the range of young parental cells.

Although SV40T is essential for stable viral infection, regulation of transcriptional process, and cellular transformation this protein might not be sufficient to induce immortality. As its core function, the oncogene SV40T binds cell cycle regulating proteins p53 and Rb leading to their reduced activity and, therewith, resulting in absence of G_1 cell cycle arrest and increased proliferation. Those effects of SV40T reflect essential components for successful transformation of primary cells (Sáenz-Robles et al. 2001; Kirchhoff et al. 2004; Pipas 2009). However, in some reported cases cells transduced with this oncogene retained low p53 activity expressed as abolished cell cycle arrest but still functional apoptosis (Kohli and Jorgensen 1999). Several other studies stated SV40T transduction to be sufficient for establishment of an immortal cell line (Kirchhoff et al. 2004; Shin et al. 2018), although a low frequency of stable immortalization was reported with most cells entering a crisis after an extended lifespan (Seigneurin-Venin et al. 2000; Kim et al. 2001; Macera-Bloch et al. 2002). Cellular crisis often occurs before transduced cells finally become immortal (Maqsood et al. 2013).

In line with these reports, SV40T-transduced eccrine sweat gland duct cells established in this work also exhibited slowed growth when propagated beyond passage 16 (P16) (Fig 3.20 and Fig 3.22). Around P19, at the peak of the crisis, SGDC-SV40T exhibited PDT of up to 150 h. Strikingly, at this age SV40-transduced duct cells had a prolonged lifespan of about 20-30 population doublings compared to parental duct cells which encompasses exactly the time span gained by overcoming of the senescence stage due to absorption of p53 and Rb by SV40T activity (Kim et al. 2001). This indicates SV40T-transduction to be insufficient for stable immortalization.

Gradually decreasing and stable PDT of about 30-40 h post-P20 and concomitant slight morphological changes towards a more cuboidal rather than longitudinal cell shape (Fig 3.23) are proposed to be attributed to gained further mutations. These assumed additional genetic changes are held responsible for overcoming of the apoptotic state and should induce an immortal state of the transduced duct cells.

Generally, inherent genetic instability of cells occurs even in immortalized clones and randomly affects any part of the genome. As a result, not even those cellular copies derived from one ancestor cell exhibit a stable genome over several rounds of passage but rather are subject to a continuous genetic drift (Sato et al. 2016; Ben-David et al. 2018; Gutbier et al. 2018). Based on other studies trying to establish immortalized human cell lines, additional genomic changes in SGDC-SV40T might affect genes related to telomerase activity such as transcription factor c-myc. Transcription factor c-myc is important for initiation of hTERT transcription and related telomerase activity (Kim et al. 2001). Upregulated telomerase activity then circumvents shortening of telomeric ends, which normally constitutes a vital process in limiting cellular lifespan by triggering DNA damage responses and associated cell senescence (Maqsood et al. 2013). Importance of c-myc was demonstrated by successful immortalization of human fibroblasts using in a one-step process of simultaneous transduction with SV40T and c-myc (Kim et al. 2001).

In association with those reports, overcoming of the crisis seen with SGDC-SV40T possibly resulted from overexpression of SV40T together with an acquired mutation influencing activity of telomerase and/or c-myc. Thereby, both bottlenecks crucial for infinite cellular replication would have been overcome – cell cycle regulation as well as telomer shortening.

To prove these assertions whole genome analysis of one selected clone should be performed. This would identify postulated mutations in telomerase-related genes and would reveal insertion side of the SV40T DNA as its integration occurs randomly in a chromosome (Pipas 2009). Alternatively, quantitative protein analysis of hTERT and related genes such as c-myc would be suited to specifically determine the contribution of these proteins on immortalization of SGDC-SV40T.

4.3.2 Characterization of individual eccrine sweat gland duct cell clones

Single cell cloning of immortalized cells is supposed to increase genetic homogeneity of derived clonal cultures (Sato et al. 2016). This assumption holds true for young clones, but with ongoing passaging and putatively slightly differing culture conditions, natural genetic drift and random mutations inevitably result in genetically heterogenous clonal populations (Ben-David et al. 2018).
Also in this study several clones were isolated from SV40T-transducted duct cell pool to obtain a defined cell line derived from one cell with initially limited genetic heterogeneity. The first 15 clonal cultures to reach confluency after limiting dilution were examined regarding their individual molecular biological traits with comparison to parental primary cells when possible. Noticeably, colony forming of singly seeded cells was only achieved when cells were cultured in conditioned medium which was previously removed from SGDC-SV40T cultures. Generally, cells continuously release chemical factors and signaling molecules which substantially affect the growth, replication and survival of neighboring cells (Reid 1979). As those additional cells were lacking when performing single cell cloning assays, required nutrients and signals were supplied via the conditioned medium. Although eccrine sweat gland duct cells featured a singular, scattered growth with limited cell-cell contact when seeded in a low density, their need for surrounding cells including their secreted chemical factors became obvious during single cell cloning.
Those 15 clones growing confluent in 96-well plates were transferred into incrementally larger culture plates as individual clonal cultures. For all of them the average PDT from single cell seeding to reaching confluency was comparable indicating similar growth behavior. Therefore, no clone was excluded from further characterization at this stage.

4.3.2.1 Analysis of molecular biological characteristics

Gene expression profile of a biological material gives valuable information for deduction of phenotypic features from the genotype. Besides, it constitutes a standard procedure to gather indications for divergence of cellular characteristics between native tissue and thereof derived cultured cells (Sun et al. 2017; Klaka 2017; Klaka et al. 2017).
Regarding the SV40T-transduced duct cell clone cultures, gene expression analysis via RT-qPCR was used as a tool to reduce the selection of clonal cultures in search for the best one as the basis for the immortalized eccrine sweat gland duct cell line. Gene expression of selected sweat gland-related markers encompassed CEACAM5, ENaC, and CFTR which are all expressed in native eccrine duct cells. Thereby, ion transporters ENaC and CFTR are important for sweat reabsorption (Cui and Schlessinger 2015; Ma et al. 2018).

Results showed especially marked differences in expression of the sweat gland marker CEACAM5 among the clonal cultures (Fig 3.25). Varying results were also obtained for CFTR, while those of ENaC diverged less among the tested clones. Strikingly, for both, CEACAM5 and CFTR, quantitative gene expressions of the clonal cultured relative to the one of native eccrine sweat glands were exceptionally low (see Supplementary **Fig 6.4**). Hence, observed huge variances of those markers are led back to these low expression values as minor differences become potentiated when amplified on a higher scale. This which was the case for CFTR and CEACAM5 expression values (Fig 3.25) when relative expressions were related to the one of clonal culture 1B10 randomly set to 1.0.
However, this does not change the fact of markedly reduced mRNA presence of CFTR and CEACAM5. For CEACAM5 a lowered gene expression was already reported to occur in cultured eccrine sweat gland cells, although the decline was not that pronounced when cells were analyzed in passage 3. Unfortunately, no functional markers like CFTR or ENaC were investigated in referred study (Sun et al. 2017).
Comparison of gene expression results with above mentioned immunofluorescence stainings of 3D HD and dermal matrix models of the eccrine sweat gland, indicated SV40T-transduced duct cell clones as well as cultured eccrine sweat gland duct cells of this work in general to be subject to changes in expression and translation of CFTR and CEACAM5. This points towards the culture conditions to exert a substantial influence on de- and differentiation of the propagated cells as already described in literature (Brayden et al. 1988; Pedersen 1989), although an individual tissue dependency might not be ruled out. Interestingly, expression of the sodium channel ENaC seemed less affected by culture conditions, although relative presence of this marker was also noticeably reduced in all selected clones.
Overall, neither clonal culture showed outstanding expression values for all markers. Therefore, those eight clones with highest expression values for either ENaC, CFTR or CEACAM5 were chosen as a sub-selection and characterized for their protein expression using 3D HD models.

Presence of eccrine sweat-gland-related genes was investigated in *in vitro* coil on duct 3D HD models consisting of either parental duct cells or thereof derived SV40T-transduced clones surrounded by parental, primary coil cells (all from donor 19-01). Additionally, 3D models were generated with primary coil and duct cells from donor 15-24, which was employed to in generating above-described *in vitro* models of the eccrine sweat gland (refer to 3.2 and 4.2). To note, close proximity and intensified cell-cell-contact of eccrine sweat gland coil and duct cells in 3D spheroids was presumed to trigger more physiological gene expression (Fennema et al. 2013; Ravi et al. 2015), which is the reason why this approach was chosen.
A broader selection of genes was analyzed to gather more detailed information about genetic traits of transduced duct cell clones using RT-qPCR. These analyses encompassed sweat-relevant functional markers such as AQP5, M3, ANO1, CFTR, ENaC, and NKCC1 as well as structural genes COL1 and COL3 (Fig 3.26) with relative expression values of 3D models prepared with cells of donor 15-24 arbitrary set to 1.0.
Comparing relative gene expression of the selected markers in 3D HD models comprising primary cells from donor 19-01 or 15-24 revealed similar expression values for both cell cultures suggesting similar features and changes to occur for all cells independent of the tissue

of origin. Comparable findings were reported by a study scrutinizing the interindividual and tissue-related genetic variances in cultured murine cells. They reveal similar genetic changes to occur in the same tissue culture independent of the individual. In contrast, different tissues from the same mouse underwent varying alternations of the gene expression (Cowley et al. 2009). This confirms herein discovered results of cultured eccrine sweat gland cells having nearly identical gene expression profiles when propagated under the same conditions but originating from distinct donors.

Interestingly, though, expression of the chloride channel CFTR was reduced in 3D models prepared with parental as well as SV40T-transduced cells derived from donor 19-01. CFTR ion channel plays a central role in case of cystic fibrosis, a genetic disease caused by mutations in the CFTR gene which is substantially involved in secretory processes of epithelial tissue. Widely prevailing diagnosis of CF is based on elevated Cl^- concentrations in sweat, often also termed as exceptionally salty sweat, which results from defective Cl^- absorption in the gland duct due to malfunctioning CFTR (Mickle et al. 1998; Saint-Criq and Gray 2017). A further study demonstrated a direct correlation between the abundance of CFTR protein in the duct membrane and Cl^- concentrations secreted sweat. This was also the case for non-CF individuals who albeit had an elevated sweat salt content (Brown et al. 2011). Given this background, low CFTR mRNA transcript levels in cells of donor 19-01 might be caused by genetic mutations affecting gene expression. Simultaneously, these results prove existence of donor-specific, interindividual variances which are manifested in all derived cells.

Only small differences existed regarding expression of ion channels ANO1, ENaC, and NKCC1 between SV40T-transduced duct cell clone cultures and primary cells which are assumed to reflect normal biological variations.

Divergence concerning mRNA levels of coil cell-specific markers AQP5 and M3 among the transduced duct cell cultures were more pronounced. As immunofluorescence stainings confirmed their absence in duct cells (refer to Fig 3.16, Fig 3.19, and Fig 3.28) measured difference are ascribed, either, to varying amounts of coil cells adhering to the duct cell core, or individual duct cell clonal cultures to trigger different degrees of AQP5 and M3 expression in surrounding coil cells via cellular interactions.

Most prominent, expression of COL1 and COL3 was detected in both primary cell cultures but was not detected in any transduced duct cell clone culture, with immunofluorescence stainings confirming these results on a protein level (refer to 4.3.2.2). As chromosomal integration of SV40T transcripts occurs randomly in the cell genome (Pipas 2009), lacking transcription of these collagens might indicate integration of SV40T DNA at the site coding for COL1 or COL3 which would prohibit their correct transcription and translation specifically in the transduced clonal cultures. For verification of this proposal genomic analysis and determination of the SV40T integration site should be undertaken.

Anyway, missing mRNA transcription of these structural genes might well explain observed easier detachment of SV40T-transduced clonal cells from culture plates during trypsinization as compared to parental cells. Together with other structural components they serve as anchoring elements of cells to the culture plate which are cleaved by trypsin (Keech 1954).

Besides, one might argue the expression of collagens to indicate presence of fibroblasts. At this point, reference is given to the discussion above stating outgrowing cells from isolated ducts to be duct cells based on stainings for proteins CD276 and SSEA-4 (4.2.1).

4.3.2.2 Comparison of structure and protein expression

Apart from transcription of genes their translation into proteins represents another vital step of overall cellular functioning. Although those two processes are closely linked, they possess individual regulatory mechanisms steering their respective production. As a result, genome, transcriptome, and proteome reflect individual sub-sets of the large protein expression machinery. From a molecular analytical perspective this implies the quantity of mRNA in a cell not to be a direct indicator for abundance of its protein (Liu et al. 2016b).

Therefore, mRNA expression data were extended by analyses of protein localization via immunofluorescence staining in frozen sections of 3D HD models comprising primary or SV40T-transduced duct cell clones and surrounding primary coil cells.

First, HE stainings of those models showing their overall structure were identical to the ones described before (refer to 4.2.1) and also revealed no differences between primary and SV40T-transduced duct cells. Likewise, cell-specific markers α-SMA, CD44, dermcidin, SSEA-4, and CEACAM5 and sweating-related functional proteins M3, AQP5, CFTR, and ENaC exhibited the same distribution pattern and cell-specificity in *in vitro* spheroids containing primary and SV40T-transduced duct cell clones (Fig 3.28 and Fig 3.29) as observed and discussed previously for 3D HD models of the eccrine sweat gland (refer to 3.2.1 and 4.2.1). Therefore, the same explanations for protein expression apply as stated above (Fig 3.28refer to 4.2.1 and 4.2.2).

Most importantly, gain of CD44 and simultaneous loss of CEACAM5 expression in all, primary duct cells and transduced duct cell clones, indicates the same dedifferentiation to occur with duct cells from donor 19-01 as was seen and proposed before for cells from donor 15-24 (Fig 3.28e, f, k, and l) (Li et al. 2015). Further, absence of myoepithelial cells from SV40T-transduced eccrine sweat gland duct cell cultures was verified by missing presence of the specific marker α-SMA (Fig 3.28b and c) (Kurata et al. 2017; Ma et al. 2018). Astonishingly, duct-specific marker SSEA-4 was clearly expressed in regions of primary and transduced duct cells in 3D HD models suggesting also those cells from donor 19-01 to retain some duct-specific characteristics as was already demonstrated for duct cells from donor 15-24 (Fig 3.28h and i) (Borowczyk-Michalowska et al. 2017).

To characterize especially these SV40T-transduced duct cell clone cultures further, localization and distribution of additional proteins was examined including ion channels ANO1 and NKCC1 as well as surface proteins CD9 and CD276 and structural markers, COL1 and 3, and CK15 which all showed a distinct staining pattern (Fig 3.29). Once again, expression of these proteins in frozen sections of human facial skin was identical to established localization described in literature (Bovell 2018).

Interestingly, Ca^{2+}-dependent chloride channel ANO1 was exclusively detected in coil cells on the inner border towards duct cell areas but was mostly absent in other parts of the 3D constructs (Fig 3.29b and c). This suggests cell-cell-interactions to be a factor for expression of this chloride channel and for this cellular communication to occur with both, primary and transduced duct cells. Likewise, inner localization of the coil cells seemed to play a role as in native eccrine glands also only luminal parts of secretory coils were stained (Fig 3.29a) (Bovell 2018). Furthermore, in conventional co-culture 3D HD models ANO1 was also detected in the core of the spheroids, reflecting the luminal part of the construct (Klaka et al. 2017).

For sodium-potassium-chloride cotransporter NKCC1 weak staining was detected in the primary as well as transduced duct cell parts of the 3D spheroids while it was stronger expressed in areas of coil cells (Fig 3.29b and c). This coincides well with its crucial function in sweat secretion (Cui and Schlessinger 2015). Further, *in vitro* observed distribution reflected the one in native eccrine sweat glands as shown (Fig 3.29a) and described in literature (Cui and Schlessinger 2015), which indicates primary and SV40T-transduced eccrine duct cell clones to retain at least some of their specific characteristics and expression of those genes not to be affected by the transduction process.

The cell surface protein CD9 represents another marker protein apart from CD44 indicating an undifferentiated cell state (Petschnik et al. 2010). Stainings revealed CD9 expression primarily in the coil compartment of native eccrine sweat glands while in the duct only the basal side was positive (Fig 3.29d). Up to now, description of detailed distribution and localization of this marker in native eccrine glands was elusive but results of this work suggest CD9 as another marker to distinguish eccrine sweat gland coil from duct compartments. Adding to this, similar distribution of CD9 was detected in *in vitro* spheroids with strong expression in areas of coil cells whereas duct cell regions showed light and scattered staining (Fig 3.29e and f). This indicates the isolated sweat gland coil and duct cells to retain some of their characteristics seen *in vivo.* In comparison, presence of the related marker protein CD44 is limited to the coil of native eccrine sweat glands but missing in the duct compartment (Li et al. 2015; Xie et al. 2016; Ma et al. 2018) which implies these to proteins to be slightly differently expressed.

Another cluster of differentiation, CD276, was previously mentioned in this work as the marker for distinguishing of sweat gland duct cells from fibroblasts (refer to 4.2.1 and Fig 6.5). CD276 showed noticeable staining in transduced duct cell clones (Fig 3.29i) but was not detected in sections of native human skin and in primary duct cells (Fig 3.29g and h). This suggests especially isolated, transduced duct cells to attain distinct characteristics that differ from duct cells *in vivo*. Due to CD276 expression predominantly reported for tumor cells (Picarda et al. 2016) it implies SV40T-transduced cell clones to gather tumor-like features. Additionally, this observation suggests for the transduction procedure to affect intrinsic traits of the duct cells.

Based on the results obtained for mRNA quantification, protein expression and localization of the structural proteins COL1 and 3 was also investigated (Fig 3.29d, e, f, g, h, and i). In alignment with previously reported studies, both collagens were expressed in native dermal tissue especially around and slightly interwoven with the eccrine gland structure (Vitellaro-Zuccarello et al. 1992). Based on this, it is supposed here that those fibers give structural support by encasing the tangled tubule of the eccrine gland. In 3D HD models, in contrast, both collagens were expressed by primary duct cells, but only COL3 was detected in SV40T-transduced duct cell clones. While absence of COL1 in transduced cell clones coincides with above-stated results of mRNA quantification, presence of COL3 contradicts them. As gene transcription into mRNA and translation into proteins are individually regulated cellular processes it is not unusual to find contradicting measures for both endpoints (Liu et al. 2016b). In any case, these finding further indicate the SV40T-transgene to be inserted in the cell's genome at the site of COL1 coding. Noteworthy, duct cells were transduced while growing on COL1 coated culture plates, which might influence its cellular expression.

Representing another structural component, intermediate filament CK15 was only detected in coil cell areas of 3D HD models (Fig 3.29k and l), which coincides with is native *in vivo* expression specifically in luminal coil cells (Fig 3.29j) (Gao et al. 2014; Li et al. 2016a; Ma et al. 2018). This corroborates postulated hypothesis of coil cells retaining their cellular identity when cultured *in vitro* and incorporated into a natural-like environment such as hanging drops. Similarly, in Matrigel-based eccrine sweat gland reconstructs some parts were CK15-positive and those were classified as coil-like regions as well (Li et al. 2016a).

To sum up, comparable to improved 3D HD models with coil on duct seeding immunohistological investigations demonstrated the constructs with incorporated SV40-transduced duct cell clones to show similar protein distribution. Those results indicate all selected duct cell clones to retain their characteristic protein expression with exception of absence of COL1. Nonetheless, due to the close resemblance of parental and transduced cells authentication of the latter was successfully established. Besides, all SV40T-transduced clones appear suitable as source of the eccrine sweat gland duct cell line regarding characteristic protein expression.

4.3.2.3 Establishment of functional behavior

Apart from investigation cell-cell interactions in a physiological environment, another intention of establishing an immortalized eccrine sweat gland duct cell line was its application in *in vitro* assays for testing of alternative AP actives (refer to 3.1 and 4.1). To ascertain suitability of SV40T-transduced eccrine sweat gland duct cell clones for this purpose their functional behavior was established by treating them with previously well-described substances from the two identified classes of sweat-reducing chemicals, PEI-HCl and DPG. For comparison, primary duct cells from the standard donor 15-24 and primary, parental duct cells from donor 19-01 were treated simultaneously.

In accordance with results from initial substance screenings (refer to 3.1.1.1 and 4.1.1.1), PEI-HCl evoked a reduction of $[Na^+]_i$ with concomitant elevation of $[Cl^-]_i$ in all cells, primary and SV40T-transduced ones (refer to Fig 3.30). Although the intensity of triggered alterations varied among the different cell cultures, those originating from donor 19-01 exhibited the strongest reactions verifying their applicability for further testing procedures.

Likewise, intracellular changes evoked by application of the diol DPG in duct cells were identical to the ones determined previously in eccrine sweat gland co-culture cells and were characterized by increase of $[Na^+]_i$ and diminution of $[Cl^-]_i$ (refer to Fig 3.30b as well as 3.1.2.1 and 4.1.2.1). Thus, also regarding polyol substances suitability of SV40T-transduced duct cells for application in *in vitro* screening assays was assured. However, measured exceptionally low $[Cl^-]_i$ of clone 1C6 might not be satisfactorily explained at the moment.

In further experiments generated transduced duct cell cultures should also be examined regarding their reactivity towards adrenergic, purinergic and cholinergic stimulation as was performed for the coil cell lines NCL-SG3 (Lee and Dessi 1989; Bovell et al. 2008) and EC23 (Robles-Munoz 2014). Additionally, cAMP-dependent activation of CFTR and amiloride-triggered response of ENaC could also be examined similar to experiments performed with SV40T-transduced duct cell line RD2(NL) (Bell and Quinton 1995).

Taken together, due to functional behavior of the SV40-transduced duct cells being in line with those of primary duct cells and initially established results from eccrine sweat gland co-culture cells, all clones are considered suited for employment in future *in vitro* substance testing. Variations observed in reaction intensities are attributed to ubiquitous biological fluctuations. Besides, those results imply the previously postulated modes of action of Cl^--containing and polycationic substances derived from tests with primary eccrine sweat gland co-culture cells to hold true also in purely duct cell cultures. Beyond that, it suggests a universal mode of action of these substances, irrespective of the eccrine sweat gland cell type used.

4.3.2.4 Characteristics of clone 1D10 as basis for the immortalized cell line

The assumption of clonal cells, which originate from one single ancestor cell, to possess identical genomes is obsolete given scientific reports stating genetic drift and genomic instability including mutation to alter the clonal cell line over time (Ben-David 2018, Gutbier 2018). With this background, even more importance should be put on sufficient authentication of the cell line to verify preservation of its identity and associated characteristic traits. This control should be done while establishing the cell line as well as from time to time during culturing to verify maintenance of its cellular identity (Nims and Reid 2017).
Concerning the scrutiny of SV40T-transduced eccrine sweat gland cells clone 1D10 was selected as the basis for generation of an immortalized cell line due to exhibiting overall the most suitable traits of all investigated clonal cultures. In the further course, its growth behavior and protein expression were characterized over several rounds of passaging.
Importantly, the clonal cells' morphology remained unchanged over observed culturing from P22 to P31 (Fig 3.32). This indicates the 1D10 clonal cell line to exhibit stable traits and excludes cross-contamination of the culture with other cells (Nims and Reid 2017).
Furthermore, growth rate of 1D10 clones was monitored to gather information about the immortality status of the culture. Although there was an initial slowed growth with exceptionally high PDT detected, PDT stabilized within few passages adopting doubling times identical to parental cells (Fig 3.31). This initially observed slowed growth is attributed to cellular damages and cell death induced by the freezing-thawing-procedure (McGann et al. 1988; Sandell and Sakai 2011). However, stable growth behavior in later passages after continuous culturing showed propagation rates of the SV40-transduced clonal cells comparable to the ones of primary, parental duct cells. This constitutes an important factor indicating the post-crisis selected clone 1D10 to have entered a stage of immortality and having overcome senescence and upregulated cell death. Thus, the clonal 1D10 culture is perceived as an SV40T-immortalized eccrine sweat gland duct cell line (termed SGDC-1D10).

Apart from growth behavior, genetic stability is another important factor in characterizing cell lines. In general, chromosomal instability induces genetic alterations which might also affect gene expression. This in turn might also influence the functional behavior of the cell line (Ben-David et al. 2018).
Evaluating this aspect in SGDC-1D10 changes in expression of genes coding for sweating-related proteins was monitored over several passages (Fig 3.33). Strikingly, in later passages (from P25 onwards) there was a tendency towards reduced gene expression of those proteins involved in sweat reabsorption, especially the chloride channels ANO1 and CFTR as well as

the sodium channel ENaC. These might be first indications of the cell line to be subject to genetic drift under prevailing culture conditions as environmental influences pose a sensitive factor for sub-clonal selection (Ben-David et al. 2018). However, relative to parental duct cells no outstanding differences were recorded.

To determined genetic stability of the cell line in the future, SGDC-1D10 should be more closely scrutinized including determination of expression of further proteins as well as the cell's functional behavior. Similar investigations as were performed for the selection of SV40T-transduced clones are suggested to achieve this (refer to 3.3.3.2 and 3.3.3.3 as well as 4.3.2.2 and 4.3.2.3). Occurring genetic drift should be revealed by continued passaging of the cells. If such a drift was detected, impact of the culture conditions on sub-clonal selection should be tested and, if necessary, improvements of the culture medium considered to prevent massive genetic drift of the population. Simultaneously, this continuous culturing will verify the immortality status of the 1D10 cells.
Whole genome sequencing of some cell line cultures of varying age is also recommended to determine the integration side of the SV40T transgene in the cellular genome and to reveal possible further acquired mutations. This might help to identify those genetic changes responsible for overcoming of the crisis and onset of immortality.

In conclusion, although indications for the culture to undergo genetic changes need to be kept in view, presented results of characterization of the SV40T-transduced eccrine sweat gland duct cell clone 1D10 suggest this culture to be successfully immortalized and to be free of cross-contamination (cell line SGDC-1D10). Therewith, a defined cell material is available which enables standardized sweat gland-related research in the future and prevents introduction of interindividual variations.

5 Summary

Sweating constitutes a vital mechanism for maintaining human body temperature in a physiologically healthy range. Visible signs of sweating are commonly reduced with the help of topically applied antiperspirants based on aluminum salts. However, their exact mechanism of action of not fully disclosed, especially regarding possible cellular effects.

Given this background, aim of this thesis was to develop an *in vitro* organotypic model of the human eccrine sweat gland to elaborate sweating on a cellular basis and to identify substances which are able to regulate sweating. To achieve this, three main aspects were targeted: a) Establishment of a cell-based *in vitro* test procedure and its application for investigating physiological effects of different substances on sweating; b) Discovering cellular interactions of human eccrine sweat gland cells with the help of a novel organotypic three-dimensional cell model; and c) Generation of a standardized cellular material for future sweat gland research by introducing a novel immortalized eccrine sweat gland duct cell line.

Successful establishment of a reliable *in vitro* test system facilitated the detailed investigation of the sweating process on a cellular level. It included broad testing of multiple substances, which revealed two distinct classes of chemicals as having sweat-regulating properties: Cl^--containing ammonium compounds as well as polyols. Even more, first indications for their cellular mode of action could be given indicating the chloride content of the ammonium solutions and the topological polar surface area of the polyols to markedly contribute to observed antiperspirant effects. Most strikingly, Cl^--containing solutions evoked a long-term antiperspirant effect lasting up to 24 h, which is comparable to the performance of commonly used aluminum chlorohydrate. In contrast, tested polyols evoked only a short-term sweat reduction reaching its maximum after about 2 h. This difference of the substance effects is attributed to their diverging mechanism of action. Overall, these results contribute markedly to deeper understanding of the physiological mechanism of sweating.

To investigate cellular interdependency in eccrine sweat glands, novel *in vitro* 3D models were generated in which sweat gland coil and duct cells were combined. This unpreceded approach unveiled cell type-specific differentiation and cell-cell contact-regulated processes including distinct distribution of specific proteins. In a more advanced step, integration of coil and duct cells into artificial dermal matrix models revealed cell-matrix-related interactions to contribute to defined orientation of eccrine sweat gland cells within the organotypic constructs.

For standardization of future sweat gland-related research an SV40T-transduced, immortalized eccrine sweat gland duct cell line was successfully generated. Especially its close resemblance to parental cells together with its extended lifespan renders these immortalized cells an ideal research tool for getting a more profound understanding of the physiology of sweating.

In conclusion, herein described cell-based *in vitro* evaluation process, the organotypic *in vitro* 3D models of the human eccrine sweat gland, and the generated immortalized duct cell line constitute a sophisticated research package which is ideal for standardized evaluation of physiological sweating as well as investigating cell-cell independencies. Altogether, this adds substantially to understanding of the sweating process and its physiological regulation.

6 Outlook

Herein presented *in vitro* testing approach revealed Cl^--containing amines as well as well-known AP active ACH to exert a long term sweat-reducing effect. To confirm proposed theory for their mechanism of action, further Cl^--supplemented polycationic and small monoamine substance solutions should be tested.
Additionally, polyol substances were discovered to exert a short-term antiperspirant effect. As *in vitro*, cell-based results showed stronger impacts of polyols with increasing chain length those macromolecules, especially PPG-4, -6, and -10, should also be tested *in vivo*. Those results will then show if *in vitro*-based, postulated hypothesis of long-chained polyols to exert better sweat reductions will hold true. Besides, *in vitro* screening of more polyols is also recommended to underpin delineated postulation of their mechanism of action.

Regarding cellular interactions between eccrine sweat gland coil and duct cells, further markers should be analyzed. Established dermal matrix models bearing eccrine sweat gland analogues pose a suitable tool for more detailed investigation of continuous, temporal succession of cell development and underlying cellular communication processes. Special focus should be put on exploring possible dedifferentiation of duct cells during culture in more detail. Darting in the same direction, further analysis of generated immortalized duct cell clone 1D10 should be performed including determination of the chromosomal integration site of the SV40T transgene. Besides, extended cultivation of the clonal culture would ascertain assumed immortalization status of the 1D10 duct cell line and would enable monitoring of possible genetic drift occurring during continuous cellular expansion.
To determine functional characteristics of the immortalized duct cell line, it should be scrutinized regarding its reaction towards adrenergic and cholinergic stimulation which would give information about the reactivity and physiological behavior of the cell line.

II. Bibliography

Abaci, H.E.; Coffman, A.; Doucet, Y.; Chen, J.; Jacków, J.; Wang, E. et al. (2018): Tissue engineering of human hair follicles using a biomimetic developmental approach. *Nat Commun* 9(1): 5301. DOI: 10.1038/s41467-018-07579-y.

Abd, E.; Yousef, S.A.; Pastore, M.N.; Telaprolu, K.; Mohammed, Y.H.; Namjoshi, S. et al. (2016): Skin models for the testing of transdermal drugs. *Clinical Pharmacology: Advances and Applications* 8: 163–176. DOI: 10.2147/CPAA.S64788.

Adolph, E.F. (1923): The nature of the activities of the human sweat glands. *Am J Physiol* 66(3): 445–452.

Akinc, A.; Thomas, M.; Klibanov, A.M.; Langer, R. (2005): Exploring polyethylenimine-mediated DNA transfection and the proton sponge hypothesis. *J Gene Med* 7(5): 657–663. DOI: 10.1002/jgm.696.

Ali, J.; Camilleri, P.; Brown, M.B.; Hutt, A.J.; Kirton, S.B. (2012): Revisiting the general solubility equation: in silico prediction of aqueous solubility incorporating the effect of topographical polar surface area. *J Chem Inf Model*: 420–428. DOI: 10.1021/ci200387c.

Anderson, J.L.; Martin, R.G. (1976): SV40 transformation of mouse brain cells: critical role of gene A in maintenance of the transformed phenotype. *J Cell Physiol* 88(1): 65–76. DOI: 10.1002/jcp.1040880109.

Arosio, D.; Ratto, G.M. (2014): Twenty years of fluorescence imaging of intracellular chloride. *Front Cell Neurosci* 8: 258. DOI: 10.3389/fncel.2014.00258.

Baker, L.B. (2017): Sweating Rate and Sweat Sodium Concentration in Athletes: A Review of Methodology and Intra/Interindividual Variability. *Sports Medicine* 47(Suppl 1): 111–128. DOI: 10.1007/s40279-017-0691-5.

Baker, L.B. (2019): Physiology of sweat gland function: The roles of sweating and sweat composition in human health. *Temperature* 6(3): 211–259. DOI: 10.1080/23328940.2019.1632145.

Barltrop, J.A.; Owen, T.C.; Cory, A.H.; Cory, J.G. (1991): 5-(3-carboxymethoxyphenyl)-2-(4,5-dimethylthiazolyl)-3-(4-sulfophenyl)tetrazolium, inner salt (MTS) and related analogs of 3-(4,5-dimethylthiazolyl)-2,5-diphenyltetrazolium bromide (MTT) reducing to purple water-soluble formazans as cell-viability indicators. *Bioorganic & Medicinal Chemistry Letters* 1(11): 611–614. DOI: 10.1016/S0960-894X(01)81162-8.

BASF - Care Chemicals & Formulators (2010): Techinical Information. Lupasol(R) types. Edited by BASF - Care Chemicals Devision. Available online at https://chemical.carytrad.com.tw/uploads/1/2/3/8/123848866/tds_lupasol_types_en.pdf, checked on 1/9/2021.

BASF - Care Chemicals Devision (2015a): Technical Information. Lupamin(R) 1595. Edited by BASF - Care Chemicals Devision.

BASF - Care Chemicals Devision (2015b): Technical Information. Lupasol(R) G 20 Waterfree. Edited by BASF - Care Chemicals Devision.

Becker, L.C.; Bergfeld, W.F.; Belsito, D.V.; Hill, R.A.; Klaassen, C.D.; Liebler, D.C. et al. (2019): Safety Assessment of Glycerin as Used in Cosmetics. *Int J Toxicol* 38(3_suppl): 6S-22S. DOI: 10.1177/1091581819883820.

Bell, C.L.; Quinton, P.M. (1995): An immortal cell line to study the role of endogenous CFTR in electrolyte absorption. *In Vitro Cell Dev Biol Anim* 31(1): 30–36. DOI: 10.1007/BF02631335.

Ben-David, U.; Siranosian, B.; Ha, G.; Tang, H.; Oren, Y.; Hinohara, K. et al. (2018): Genetic and transcriptional evolution alters cancer cell line drug response. *Nature* 560(7718): 325–330. DOI: 10.1038/s41586-018-0409-3.

Ben-Ze'ev, A. (1984): Differential control of cytokeratins and vimentin synthesis by cell-cell contact and cell spreading in cultured epithelial cells. *J Cell Biol* 99(4 Pt 1): 1424–1433. DOI: 10.1083/jcb.99.4.1424.

Best, A.; Kamilar, J.M. (2018): The evolution of eccrine sweat glands in human and nonhuman primates. *J Hum Evol* 117: 33–43. DOI: 10.1016/j.jhevol.2017.12.003.

Best, A.; Lieberman, D.E.; Kamilar, J.M. (2019): Diversity and evolution of human eccrine sweat gland density. *J Therm Biol* 84: 331–338. DOI: 10.1016/j.jtherbio.2019.07.024.

Beu, T.A.; Farcaş, A. (2017): Structure and dynamics of solvated polyethylenimine chains. In. TIM17 PHYSICS CONFERENCE. Timisoara, Romania, 25–27 May 2017: Author(s) (AIP Conference Proceedings): 20001.

Biedermann, T.; Pontiggia, L.; Böttcher-Haberzeth, S.; Tharakan, S.; Braziulis, E.; Schiestl, C. et al. (2010): Human Eccrine Sweat Gland Cells Can Reconstitute a Stratified Epidermis. *Journal of Investigative Dermatology* 130(8): 1996–2009. DOI: 10.1038/jid.2010.83.

Biel, S.; Gläser, K.; Thielecke, I.; Terstegen, L.; Keyhani, R. (2008): Verwendung von kurzkettigen vicinalen Diolen als antitranspirantwirksame Mittel. Applied for by Beiersdorf AG on 7/8/2008. App. no. PCT/EP2008/005549. Patent no. WO 2009/007089. Priority no. DE 102007032642.

Biel, S.; Mätzold, K.; Miertsch, H.; Meyer, M.; Weinert, K. (2009): Diole als antitranspirantwirksames Mittel. Applied for by Beiersdorf AG on 12/18/2009. App. no. PCT/EP2009/009105. Patent no. WO 2010/078932 A2. Priority no. 10 2009 004 269.5.

Bijman, J.; Quinton, P.M. (1987): Lactate and bicarbonate uptake in the sweat duct of cystic fibrosis and normal subjects. *Pediatr Res* 21(1): 79–82. DOI: 10.1203/00006450-198701000-00017.

Billet, A.; Hanrahan, J.W. (2013): The secret life of CFTR as a calcium-activated chloride channel. *Journal of Physiology* 591(21): 5273–5278. DOI: 10.1113/jphysiol.2013.261909.

Bird, G.S.; DeHaven, W.I.; Smyth, J.T.; Putney, J.W. (2008): Methods for studying store-operated calcium entry. *Methods* 46(3): 204–212. DOI: 10.1016/j.ymeth.2008.09.009.

Bischof, G.; Cosentini, E.; Hamilton, G.; Riegler, M.; Zacherl, J.; Teleky, B. et al. (1996): Effects of extracellular pH on intracellular pH-regulation and growth in a human colon carcinoma cell-line. *Biochimica et Biophysica Acta (BBA) - Biomembranes* 1282(1): 131–139. DOI: 10.1016/0005-2736(96)00050-8.

Blackwenn, S.; Kruse, I.; Springmann, G.; Bielfeldt, S.; Wilhelm, K.-P. (2018): Perspiration and Odor Testing Methods and New Opportunities for Claim Development. *SOFW Journal* 144(04/18): 22–28.

Boron, W.F. (1986): Intracellular pH regulation in epithelial cells. *Annu Rev Physiol* 48: 377–388. DOI: 10.1146/annurev.ph.48.030186.002113.

Borowczyk-Michalowska, J.; Zimolag, E.; Waligorska, A.; Dobrucki, J.; Madeja, Z.; Drukala, J. (2017): Stage-specific embryonic antigen-4 as a novel marker of ductal cells of human eccrine sweat glands. *Br J Dermatol* 176(6): 1541–1548. DOI: 10.1111/bjd.15154.

Boussif, O.; Lezoualc'h, F.; Zanta, M.A.; Mergny, M.D.; Scherman, D.; Demeneix, B.; Behr, J.P. (1995): A versatile vector for gene and oligonucleotide transfer into cells in culture and in vivo: polyethylenimine. *Proc Natl Acad Sci U S A* 92(16): 7297–7301. DOI: 10.1073/pnas.92.16.7297.

Bouwstra, J.; Honeywell-Nguyen, P. (2002): Skin structure and mode of action of vesicles. *Advanced Drug Delivery Reviews* 54: 41-55. DOI: 10.1016/S0169-409X(02)00114-X.

Bovell, D. (2015): The human eccrine sweat gland. Structure, function and disorders. *Journal of Local and Global Health Science* 2015(1): 5. DOI: 10.5339/jlghs.2015.5.

Bovell, D.L. (2018): The evolution of eccrine sweat gland research towards developing a model for human sweat gland function. *Exp Dermatol* 27(5): 544–550. DOI: 10.1111/exd.13556.

Bovell, D.L.; Holub, B.S.; Odusanwo, O.; Brodowicz, B.; Rauch, I.; Kofler, B.; Lang, R. (2013): Galanin is a modulator of eccrine sweat gland secretion. *Exp Dermatol* 22(2): 141–143. DOI: 10.1111/exd.12067.

Bovell, D.L.; MacDonald, A.; Meyer, B.A.; Corbett, A.D.; MacLaren, W.M.; Holmes, S.L.; Harker, M. (2011): The secretory clear cell of the eccrine sweat gland as the probable source of excess sweat production in hyperhidrosis. *Exp Dermatol* 20(12): 1017–1020. DOI: 10.1111/j.1600-0625.2011.01361.x.

Bovell, D.L.; Santic, R.; Kofler, B.; Hermann, A.; Wilson, D.; Corbett, A.; Lang, R. (2008): Activation of chloride secretion via proteinase-activated receptor 2 in a human eccrine sweat gland cell line--NCL-SG3. *Exp Dermatol* 17(6): 505–511. DOI: 10.1111/j.1600-0625.2007.00659.x.

Brandt, M.; Bielfeldt, S.; Springmann, G.; Wilhelm, K.-P. (2008): Influence of climatic conditions on antiperspirant efficacy determined at different test areas. *Skin Res Technol* 14(2): 213–219. DOI: 10.1111/j.1600-0846.2007.00282.x.

Brayden, D.J.; Cuthbert, A.W.; Lee, C.M. (1988): Human eccrine sweat gland epithelial cultures express ductal characteristics. *Journal of Physiology* 405(1): 657–675. DOI: 10.1113/jphysiol.1988.sp017354.

Bretagne, A.; Cotot, F.; Arnaud-Roux, M.; Sztucki, M.; Cabane, B.; Galey, J.-B. (2017): The mechanism of eccrine sweat pore plugging by aluminium salts using microfluidics combined with small angle X-ray scattering. *Soft Matter* 13(20): 3812–3821. DOI: 10.1039/c6sm02510b.

Brodell, L.A.; Rosenthal, K.S. (2008): Skin Structure and Function. *Infectious Diseases in Clinical Practice* 16(2): 113–117. DOI: 10.1097/IPC.0b013e3181660bf4.

Brown, M.B.; Haack, K.K.V.; Pollack, B.P.; Millard-Stafford, M.; McCarty, N.A. (2011): Low abundance of sweat duct Cl− channel CFTR in both healthy and cystic fibrosis athletes with exceptionally salty sweat during exercise. *American Journal of Physiology - Regulatory, Integrative and Comparative Physiology* 300(3): 605-615. DOI: 10.1152/ajpregu.00660.2010.

Buchanan, J.A.; Yeger, H.; Tabcharani, J.A.; Jensen, T.J.; Auerbach, W.; Hanrahan, J.W. et al. (1990): Transformed sweat gland and nasal epithelial cell lines from control and cystic fibrosis individuals. *J Cell Sci* 95 (Pt 1): 109–123.

Bundesinstitut für Risikobewertung (2019a): Fragen und Antworten zu Aluminium in Lebensmitteln und verbrauchernahen Produkten. Aktualisierte FAQ des BfR vom 18. November 2019. Bundesinstitut für Risikobewertung. Berlin. Available online at https://mobil.bfr.bund.de/cm/343/fragen-und-antworten-zu-aluminium-in-lebensmitteln-und-verbrauchernahen-produkten.pdf, updated on 11/18/2019, checked on 11/25/2019.

Bundesinstitut für Risikobewertung (2019b): Reduzierung der Aluminiumaufnahme kann mögliche Gesundheitsrisiken minimieren. Stellungnahme Nr. 045/2019 des BfR vom 18. November 2019. Bundesinstitut für Risikobewertung. Available online at https://www.bfr.bund.de/cm/343/reduzierung-der-aluminiumaufnahme-kann-moegliche-gesundheitsrisiken-mindern.pdf, updated on 11/18/2019, checked on 11/25/2019.

Bundesministerium der Justiz und für Verbraucherschutz sowie Bundesamt für Justiz (9/4/2007): Gesetz über die Spende, Entnahme und Übertragung von Organen und Geweben, revised 11/20/2019. Source: §8 ff. In : Transplantationsgesetz. Available online at https://www.gesetze-im-internet.de/tpg/TPG.pdf, checked on 1/2/2020.

Bunting, H.; Wislocki, G.B.; Dempsey, E.W. (1948): The chemical histology of human eccrine and apocrine sweat glands. *Anat. Rec.* 100(1): 61–77. DOI: 10.1002/ar.1091000106.

Busche, R.; Jeromin, A.; Engelhardt, W. von; Rechkemmer, G. (1993): Basolateral mechanisms of intracellular pH regulation in the colonic epithelial cell line HT29 clone 19A. *Pflugers Arch - Eur J Physiol* 425(3-4): 219–224. DOI: 10.1007/BF00374170.

Cao, L.; Chen, L.; Li, H.; Wei, Z.; Xie, S.; Zhang, M. et al. (2019): Differential antigen expression between human eccrine sweat glands and hair follicles/pilosebaceous units. *J Mol Histol* 50(4): 335–342. DOI: 10.1007/s10735-019-09830-2.

Capasso, J.M.; Cossío, B.R.; Berl, T.; Rivard, C.J.; Jiménez, C. (2003): A colorimetric assay for determination of cell viability in algal cultures. *Biomol Eng* 20(4-6): 133–138. DOI: 10.1016/S1389-0344(03)00037-6.

Chamcheu, J.C.; Siddiqui, I.A.; Syed, D.N.; Adhami, V.M.; Liovic, M.; Mukhtar, H. (2011): Keratin gene mutations in disorders of human skin and its appendages. *Arch Biochem Biophys* 508(2): 123–137. DOI: 10.1016/j.abb.2010.12.019.

Chao, A.C.; Dix, J.A.; Sellers, M.C.; Verkman, A.S. (1989): Fluorescence measurement of chloride transport in monolayer cultured cells. Mechanisms of chloride transport in fibroblasts. *Biophysical Journal* 56(6): 1071–1081. DOI: 10.1016/S0006-3495(89)82755-9.

Chao, A.C.; Widdicombe, J.H.; Verkman, A.S. (1990): Chloride conductive and cotransport mechanisms in cultures of canine tracheal epithelial cells measured by an entrapped fluorescent indicator. *J Membr Biol* 113(3): 193–202. DOI: 10.1007/BF01870071.

Chen, J.; Hessler, J.A.; Putchakayala, K.; Panama, B.K.; Khan, D.P.; Hong, S. et al. (2009): Cationic nanoparticles induce nanoscale disruption in living cell plasma membranes. *J Phys Chem B* 113(32): 11179–11185. DOI: 10.1021/jp9033936.

Chen, X.; Gasecka, P.; Formanek, F.; Galey, J.-B.; Rigneault, H. (2016): In vivo single human sweat gland activity monitoring using coherent anti-Stokes Raman scattering and two-photon excited autofluorescence microscopy. *British Journal of Dermatology* 174(4): 803–812. DOI: 10.1111/bjd.14292.

Cheshire, W.P.; Fealey, R.D. (2008): Drug-Induced Hyperhidrosis and Hypohidrosis. incidence, prevention and management. *Drug Safety* 31(2): 109–126. DOI: 10.2165/00002018-200831020-00002.

Concepcion, A.R.; Vaeth, M.; Wagner, L.E.; Eckstein, M.; Hecht, L.; Yang, J. et al. (2016): Store-operated Ca2+ entry regulates Ca2+-activated chloride channels and eccrine sweat gland function. *The Journal of Clinical Investigation* 126(11): 4303–4318. DOI: 10.1172/JCI89056.

Conn, P.J.; Jones, C.K.; Lindsley, C.W. (2009): Subtype-selective allosteric modulators of muscarinic receptors for the treatment of CNS disorders. *Trends in Pharmacological Sciences* 30(3): 148–155. DOI: 10.1016/j.tips.2008.12.002.

Cotton, D.W. (1986): Immunohistochemical staining of normal sweat glands. *Br J Dermatol* 114(4): 441–449. DOI: 10.1111/j.1365-2133.1986.tb02848.x.

Cowley, M.J.; Cotsapas, C.J.; Williams, R.B.H.; Chan, E.K.F.; Pulvers, J.N.; Liu, M.Y. et al. (2009): Intra- and inter-individual genetic differences in gene expression. *Mamm Genome* 20(5): 281–295. DOI: 10.1007/s00335-009-9181-x.

Cronin, J.; Zhang, X.-Y.; Reiser, J. (2005): Altering the tropism of lentiviral vectors through pseudotyping. *Curr Gene Ther* 5(4): 387–398. DOI: 10.2174/1566523054546224.

Cui, C.-Y.; Kunisada, M.; Esibizione, D.; Douglass, E.G.; Schlessinger, D. (2009): Analysis of the temporal requirement for eda in hair and sweat gland development. *J Invest Dermatol* 129(4): 984–993. DOI: 10.1038/jid.2008.318.

Cui, C.-Y.; Piao, Y.; Campbell, D.P.; Ishii, R.; Michel, M.; Sharov, A.; Schlessinger, D. (2017): miRNAs Are Required for Postinduction Stage Sweat Gland Development. *J Invest Dermatol* 137(7): 1571–1574. DOI: 10.1016/j.jid.2017.03.003.

Cui, C.-Y.; Schlessinger, D. (2006): EDA signaling and skin appendage development. *Cell Cycle* 5(21): 2477–2483. DOI: 10.4161/cc.5.21.3403.

Cui, C.-Y.; Schlessinger, D. (2015): Eccrine sweat gland development and sweat secretion. *Exp Dermatol* 24(9): 644–650. DOI: 10.1111/exd.12773.

Cui, C.-Y.; Yin, M.; Sima, J.; Childress, V.; Michel, M.; Piao, Y.; Schlessinger, D. (2014): Involvement of Wnt, Eda and Shh at defined stages of sweat gland development. *Development* 141(19): 3752–3760. DOI: 10.1242/dev.109231.

Darbre, P.D. (2001): Underarm cosmetics are a cause of breast cancer. *European Journal of Cancer Prevention* 10(5): 389–394. DOI: 10.1097/00008469-200110000-00002.

Das, S.; Gordián-Vélez, W.J.; Ledebur, H.C.; Mourkioti, F.; Rompolas, P.; Chen, H.I. et al. (2020): Innervation: the missing link for biofabricated tissues and organs. *NPJ Regenerative medicine* 5: 11. DOI: 10.1038/s41536-020-0096-1.

Dencker, D.; Thomsen, M.; Wörtwein, G.; Weikop, P.; Cui, Y.; Jeon, J. et al. (2012): Muscarinic Acetylcholine Receptor Subtypes as Potential Drug Targets for the Treatment of Schizophrenia, Drug Abuse, and Parkinson's Disease. *ACS Chem Neurosci* 3(2): 80–89. DOI: 10.1021/cn200110q.

Desai, R.A.; Gao, L.; Raghavan, S.; Liu, W.F.; Chen, C.S. (2009): Cell polarity triggered by cell-cell adhesion via E-cadherin. *J Cell Sci* 122(Pt 7): 905–911. DOI: 10.1242/jcs.028183.

Despa, S.; Vecer, J.; Steels, P.; Ameloot, M. (2000): Fluorescence Lifetime Microscopy of the Na+ Indicator Sodium Green in HeLa Cells. *Anal Biochem* 281(2): 159–175. DOI: 10.1006/abio.2000.4560.

Diao, J.; Liu, J.; Wang, S.; Chang, M.; Wang, X.; Guo, B. et al. (2019): Sweat gland organoids contribute to cutaneous wound healing and sweat gland regeneration. *Cell Death Dis* 10(3): 238. DOI: 10.1038/s41419-019-1485-5.

Dréan, M.; Debuigne, A.; Goncalves, C.; Jérôme, C.; Midoux, P.; Rieger, J.; Guégan, P. (2017): Use of Primary and Secondary Polyvinylamines for Efficient Gene Transfection. *Biomacromolecules*: 440–451. DOI: 10.1021/acs.biomac.6b01526.

Du, L.; Zhang, X.; Chen, L.; Zhang, L.; Li, H. (2020): K31 as a novel marker for clear secretory cells in human eccrine sweat glands. *J Mol Histol*. DOI: 10.1007/s10735-020-09855-y.

Dufait, I.; Liechtenstein, T.; Lanna, A.; Bricogne, C.; Laranga, R.; Padella, A. et al. (2012): Retroviral and lentiviral vectors for the induction of immunological tolerance. *Scientifica (Cairo)* 2012. DOI: 10.6064/2012/694137.

Dull, T.; Zufferey, R.; Kelly, M.; Mandel, R.J.; Nguyen, M.; Trono, D.; Naldini, L. (1998): A third-generation lentivirus vector with a conditional packaging system. *J Virol* 72(11): 8463–8471. DOI: 10.1128/JVI.72.11.8463-8471.1998.

Dutta, R.C.; Dutta, A.K. (2009): Cell-interactive 3D-scaffold; advances and applications. *Biotechnol Adv* 27(4): 334–339. DOI: 10.1016/j.biotechadv.2009.02.002.

Eisenbrand, G.; Pool-Zobel, B.; Baker, V.; Balls, M.; Blaauboer, B.; Boobis, A. et al. (2002): Methods of in vitro toxicology. *Food and Chemical Toxicology* 40(2-3): 193–236. DOI: 10.1016/S0278-6915(01)00118-1.

Ellis, H.; Scurr, J.H. (1979): Axillary hyperhidrosis - topical treatment with aluminium chloride hexahydrate. *Postgrad Med J* 55(650): 868–869. DOI: 10.1136/pgmj.55.650.868.

Ellsworth, D.L.; Ellsworth, R.E.; Love, B.; Deyarmin, B.; Lubert, S.M.; Mittal, V. et al. (2004): Outer breast quadrants demonstrate increased levels of genomic instability. *Ann Surg Oncol* 11(9): 861–868. DOI: 10.1245/ASO.2004.03.024.

Ertongur-Fauth, T.; Hochheimer, A.; Buescher, J.M.; Rapprich, S.; Krohn, M. (2014): A novel TMEM16A splice variant lacking the dimerization domain contributes to calcium-activated chloride secretion in human sweat gland epithelial cells. *Exp Dermatol* 23(11): 825–831. DOI: 10.1111/exd.12543.

Ertongur-Fauth Torsten; Hochheimer Andreas; Krohn Michael (2016): A Novel Calcium-activated Chloride Channel Involved In Human Sweat Formation. Applied for by Brain Biotechnology Res And Information Network Ag on 2016. App. no. EP 2013067044 W. Patent no. WO 2014/027050 A1.

European Chemicals Agency (Ed.) (2020a): Oxybispropanediol. Registration dossier. Available online at https://echa.europa.eu/registration-dossier/-/registered-dossier/13661, checked on 1/9/2021.

European Chemicals Agency (Ed.) (2020b): Oxydipropanol. Registration Dossier. Available online at https://echa.europa.eu/registration-dossier/-/registered-dossier/16016/4/8, checked on 1/9/2021.

European Chemicals Agency (Ed.) (2020c): Propane-1,2-diol. Registration dossier. Available online at https://echa.europa.eu/registration-dossier/-/registered-dossier/16001/4/8, checked on 1/9/2021.

European Chemicals Agency (Ed.) (2020d): Propane-1,3-diol. Registration dossier. Available online at https://echa.europa.eu/registration-dossier/-/registered-dossier/2099/4/8, checked on 1/9/2021.

European Parliament and Council (2009): Regulation (EC) No 1223/2009 on cosmetic products. 2009/1223/EC. *Official Journal of the European Union*(L342): 59–209. Available online at http://eur-lex.europa.eu/legal-content/EN/TXT/PDF/?uri=CELEX:02009R1223-20160812&from=EN.

Exley, C. (2004): Aluminum in antiperspirants: more than just skin deep. *Am J Med* 117(12): 969–970. DOI: 10.1016/j.amjmed.2004.11.003.

Farkaš, R. (2015): Apocrine secretion: New insights into an old phenomenon. *Biochim Biophys Acta* 1850(9): 1740–1750. DOI: 10.1016/j.bbagen.2015.05.003.

Fennema, E.; Rivron, N.; Rouwkema, J.; van Blitterswijk, C.; Boer, J. de (2013): Spheroid culture as a tool for creating 3D complex tissues. *Trends Biotechnol* 31(2): 108–115. DOI: 10.1016/j.tibtech.2012.12.003.

Filingeri, D.; Fournet, D.; Hodder, S.; Havenith, G. (2014): Why wet feels wet? A neurophysiological model of human cutaneous wetness sensitivity. *J Neurophysiol* 112(6): 1457–1469. DOI: 10.1152/jn.00120.2014.

Filingeri, D.; Havenith, G. (2015): Human skin wetness perception. psychophysical and neurophysiological bases. *Temperature* 2(1): 86–104. DOI: 10.1080/23328940.2015.1008878.

Fischer, A.H.; Jacobson, K.A.; Rose, J.; Zeller, R. (2008): Hematoxylin and eosin staining of tissue and cell sections. *CSH Protoc* 2008: pdb.prot4986. DOI: 10.1101/pdb.prot4986.

Fischer, L. (2014): Wie gefährlich ist Aluminium? 5 Fakten. In : Spektrum - Die Woche. 29. KW. Available online at http://www.spektrum.de/wissen/wie-gefaehrlich-ist-aluminium-5-fakten/1300812.

Fiume, M.M.; Bergfeld, W.F.; Belsito, D.V.; Hill, R.A.; Klaassen, C.D.; Liebler, D. et al. (2012): Safety assessment of propylene glycol, tripropylene glycol, and PPGs as used in cosmetics. *Int J Toxicol* 31(5 Suppl): 245S-60S. DOI: 10.1177/1091581812461381.

Fowles, J.R.; Banton, M.I.; Pottenger, L.H. (2013): A toxicological review of the propylene glycols. *Crit Rev Toxicol* 43(4): 363–390. DOI: 10.3109/10408444.2013.792328.

Gao, Y.; Li, M.; Zhang, X.; Bai, T.; Chi, G.; Liu, J.Y.; Li, Y. (2014): Isolation, culture and phenotypic characterization of human sweat gland epithelial cells. *Int J Mol Med* 34(4): 997–1003. DOI: 10.3892/ijmm.2014.1851.

Gerard, G.F.; Fox, D.K.; Nathan, M.; D'Alessio, J.M. (1997): Reverse transcriptase. The use of cloned Moloney murine leukemia virus reverse transcriptase to synthesize DNA from RNA. *Mol Biotechnol* 8(1): 61–77. DOI: 10.1007/BF02762340.

Gordon, B.I.; Maibach, H.I. (1968): Studies on the mechanism of aluminum anhidrosis. *Journal of Investigative Dermatology* 50(5): 411–413. DOI: 10.1038/jid.1968.66.

Granger, D.; Marsolais, M.; Burry, J.; Laprade, R. (2003): Na^+/H^+ exchangers in the human eccrine sweat duct. *American Journal of Physiology - Cell Physiology* 285(5): C1047-C1058. DOI: 10.1152/ajpcell.00581.2002.

Guertin, P. (2018): How safe are glycerin and polyglycerin-10 as key ingredients in personal care products. *Journal of Clinical Pharmacology and Toxicology Research* 1(2): 1–2.

Guinaugh, O. (2020): Bodycare and Deodorant: Inc Impact of COVID-19 - US - June 2020. Edited by Mintel Group Ltd. Available online at https://reports.mintel.com/display/1025217/?fromSearch=%3Ffreetext%3Daluminum-free, checked on 8/11/2020.

Gutbier, S.; May, P.; Berthelot, S.; Krishna, A.; Trefzer, T.; Behbehani, M. et al. (2018): Major changes of cell function and toxicant sensitivity in cultured cells undergoing mild, quasi-natural genetic drift. *Arch Toxicol* 92(12): 3487–3503. DOI: 10.1007/s00204-018-2326-5.

Habecker, B.A.; Malec, N.M.; Landis, S.C. (1996): Differential regulation of adrenergic receptor development by sympathetic innervation. *J Neurosci* 16(1): 229–237. DOI: 10.1523/JNEUROSCI.16-01-00229.1996.

Habuka, A.; Yamada, T.; Nakashima, S. (2020): Interactions of Glycerol, Diglycerol, and Water Studied Using Attenuated Total Reflection Infrared Spectroscopy. *Appl Spectrosc*: 767–779. DOI: 10.1177/0003702820919530.

Hamad, M.I.K.; Krause, M.; Wahle, P. (2015): Improving AM ester calcium dye loading efficiency. *J Neurosci Methods* 240: 48–60. DOI: 10.1016/j.jneumeth.2014.11.010.

Harrison, R.G.; Greenman, M.J.; Mall, F.P.; Jackson, C.M. (1907): Observations of the living developing nerve fiber. *Anat. Rec.* 1(5): 116–128. DOI: 10.1002/ar.1090010503.

Hashimoto, K.; Gross, B.G.; Lever, W.F. (1965): The ultrastructure of the skin of human embryos. I. The intraepidermal eccrine sweat duct. *Journal of Investigative Dermatology* 45(3): 139–151. DOI: 10.1038/jid.1965.110.

Hashimoto, M.; Nozoe, T.; Nakaoka, H.; Okura, R.; Akiyoshi, S.; Kaneko, K. et al. (2016): Noise-driven growth rate gain in clonal cellular populations. *Proc Natl Acad Sci U S A* 113(12): 3251–3256. DOI: 10.1073/pnas.1519412113.

Hawlicka, E.; Grabowski, R. (1993): Solvation of Ions in Aqueous Solutions of Hydrophobic Solutes. *Zeitschrift für Naturforschung A* 48(8-9). DOI: 10.1515/zna-1993-8-912.

Hayflick, L.; Moorhead, P.S. (1961): The serial cultivation of human diploid cell strains. *Exp Cell Res* 25(3): 585–621. DOI: 10.1016/0014-4827(61)90192-6.

Herrmann, F.; Mandol, L. (1955): Studies of pH of Sweat Produced by Different Forms of Stimulation. *Journal of Investigative Dermatology* 24(3): 225–246. DOI: 10.1038/jid.1955.36.

Hibbs, R.G. (1958): The fine structure of human eccrine sweat glands. *Am J Anat* 103(2): 201–217. DOI: 10.1002/aja.1001030204.

Hohmann-Jeddi, C. (2014): Aluminiumhaltige Deos. Risiken unklar. In : Pharmazeutische Zeitung. Augabe 10/2014. Available online at http://www.pharmazeutische-zeitung.de/index.php?id=51218.

Holyoke, J.B.; Lobitz, W.C. (1952): Histologic Variations in the Structure of Human Eccrine Sweat Glands. *Journal of Investigative Dermatology* 18(2): 147–167. DOI: 10.1038/jid.1952.18.

Hribar, B.; Southall, N.T.; Vlachy, V.; Dill, K.A. (2002): How ions affect the structure of water. *J Am Chem Soc* 124(41): 12302–12311. DOI: 10.1021/ja026014h.

Hu, Y.; Converse, C.; Lyons, M.C.; Hsu, W.H. (2017): Neural control of sweat secretion: a review. *British Journal of Dermatology*. DOI: 10.1111/bjd.15808.

Hu, Y.; Converse, C.; Lyons, M.C.; Hsu, W.H. (2018): Neural control of sweat secretion. A review. *Br J Dermatol* 178(6): 1246–1256. DOI: 10.1111/bjd.15808.

Hubka, K.M.; Wu, D.; Harrington, D.A.; Langer, J.C.; Pocard, T.; Jammayrac, O. et al. (2015): Dissociative and Nondissociative Models for Culture of Human Eccrine Glands for Toxicology Testing and Tissue Engineering Applications. *Applied In Vitro Toxicology* 1(3): 187–197. DOI: 10.1089/aivt.2015.0013.

Im, K.; Mareninov, S.; Diaz, M.F.P.; Yong, W.H. (2019): An Introduction to Performing Immunofluorescence Staining. *Methods Mol Biol* 1897: 299–311. DOI: 10.1007/978-1-4939-8935-5_26.

Impey, R.W.; Madden, P.A.; McDonald, I.R. (1983): Hydration and mobility of ions in solution. *J. Phys. Chem.* 87(25): 5071–5083. DOI: 10.1021/j150643a008.

Inoue, R.; Sohara, E.; Rai, T.; Satoh, T.; Yokozeki, H.; Sasaki, S.; Uchida, S. (2013): Immunolocalization and translocation of aquaporin-5 water channel in sweat glands. *J Dermatol Sci* 70(1): 26–33. DOI: 10.1016/j.jdermsci.2013.01.013.

Iwakuma, T.; Cui, Y.; Chang, L.J. (1999): Self-inactivating lentiviral vectors with U3 and U5 modifications. *Virology* 261(1): 120–132. DOI: 10.1006/viro.1999.9850.

Jindal, S. (2020): Reinvest in personal care essentials. Edited by Mintel Group Ltd. Available online at https://clients.mintel.com/insight/reinvest-in-personal-care-essentials?fromSearch=%3Ffreetext%3Daluminum-free, checked on 8/11/2020.

Kalogria, E.; Varvaresou, A.; Papageorgiou, S.; Protopapa, E.; Tsaknis, I.; Matikas, A.; Panderi, I. (2014): Pre-Column Derivatization HPLC Procedure for the Quantitation of Aluminium Chlorohydrate in Antiperspirant Creams Using Quercetin as Chromogenic Reagent. *Chromatographia* 77(19-20): 1275–1281. DOI: 10.1007/s10337-014-2722-9.

Kamiya, K.; Sakabe, J.-I.; Yamaguchi, H.; Suzuki, T.; Yatagai, T.; Aoshima, M. et al. (2015): Gross cystic disease fluid protein 15 in stratum corneum is a potential marker of decreased eccrine sweating for atopic dermatitis. *PLoS One* 10(4): e0125082. DOI: 10.1371/journal.pone.0125082.

Keech, M.K. (1954): The effect of collagenase and trypsin on collagen. An electron microscopic study. *Anat. Rec.* 119(2): 139–159. DOI: 10.1002/ar.1091190202.

Kenney, W.L.; Fowler, S.R. (1988): Methylcholine-activated eccrine sweat gland density and output as a function of age. *J Appl Physiol (1985)* 65(3): 1082–1086.

Kennon, L. (1965): Some Aspects of Toiletries Technology. *Journal of Pharmaceutical Sciences* 54(6): 813–831. DOI: 10.1002/jps.2600540602.

Kichler, A.; Leborgne, C.; Coeytaux, E.; Danos, O. (2001): Polyethylenimine-mediated gene delivery: a mechanistic study. *J Gene Med* 3(2): 135–144. DOI: 10.1002/jgm.173.

Kim, H.S.; Shin, J.Y.; Yun, J.Y.; Ahn, D.K.; Le, J.Y. (2001): Immortalization of human embryonic fibroblasts by overexpression of c-myc and simian virus 40 large T antigen. *Exp Mol Med* 33(4): 293–298. DOI: 10.1038/emm.2001.47.

Kim, W.-S.; Park, B.-S.; Sung, J.-H.; Yang, J.-M.; Park, S.-B.; Kwak, S.-J.; Park, J.-S. (2007): Wound healing effect of adipose-derived stem cells: a critical role of secretory factors on human dermal fibroblasts. *J Dermatol Sci* 48(1): 15–24. DOI: 10.1016/j.jdermsci.2007.05.018.

Kirchhoff, C.; Araki, Y.; Huhtaniemi, I.; Matusik, R.J.; Osterhoff, C.; Poutanen, M. et al. (2004): Immortalization by large T-antigen of the adult epididymal duct epithelium. *Mol Cell Endocrinol* 216(1-2): 83–94. DOI: 10.1016/j.mce.2003.10.073.

Klaka, P.; Giesen, M. (2015): Dreidimensionales Zellkulturmodell der humanen Schweißdrüse zur Untersuchung zellphysiologischer Funktionen / Wirkstoffscreening on 2015. App. no. PT033462.

Klaka, P.; Grüdl, S.; Banowski, B.; Giesen, M.; Sättler, A.; Proksch, P. et al. (2017): A novel organotypic 3D sweat gland model with physiological functionality. *PLoS One* 12(8): e0182752. DOI: 10.1371/journal.pone.0182752.

Klaka, Patricia (2017): Entwicklung eines rekonstruierten dreidimensionalen Schweißdrüsenmodells. Düsseldorf. Available online at https://docserv.uni-duesseldorf.de/servlets/DocumentServlet?id=43034, checked on 9/28/2020.

Kleinman, H.K.; Martin, G.R. (2005): Matrigel: basement membrane matrix with biological activity. *Semin Cancer Biol* 15(5): 378–386. DOI: 10.1016/j.semcancer.2005.05.004.

Ko, W.H.; Chan, H.C.; Chew, S.B.; Wong, P.Y. (1996): Ionic mechanisms of Ca^{2+}-dependent electrolyte transport across equine sweat gland epithelium. *Journal of Physiology* 493(3): 885–894. DOI: 10.1113/jphysiol.1996.sp021431.

Kohli, M.; Jorgensen, T.J. (1999): The influence of SV40 immortalization of human fibroblasts on p53-dependent radiation responses. *Biochem Biophys Res Commun* 257(1): 168–176. DOI: 10.1006/bbrc.1999.0389.

Kunisada, M.; Cui, C.-Y.; Piao, Y.; Ko, M.S.H.; Schlessinger, D. (2009): Requirement for Shh and Fox family genes at different stages in sweat gland development. *Hum Mol Genet* 18(10): 1769–1778. DOI: 10.1093/hmg/ddp089.

Kuno, Yas (1956): Human Perspiration. Springfield, Illinois, USA: Charles C. Thomas.

Kunz-Schughart, L.A.; Freyer, J.P.; Hofstaedter, F.; Ebner, R. (2004): The use of 3-D cultures for high-throughput screening: the multicellular spheroid model. *J Biomol Screen* 9(4): 273–285. DOI: 10.1177/1087057104265040.

Kurata, R.; Futaki, S.; Nakano, I.; Fujita, F.; Tanemura, A.; Murota, H. et al. (2017): Three-dimensional cell shapes and arrangements in human sweat glands as revealed by whole-mount immunostaining. *PLoS One* 12(6): e0178709. DOI: 10.1371/journal.pone.0178709.

Laden, K. (1999): Antiperspirants and Deodorants. History of Major HBA Market. In K. Laden (Ed.): Antiperspirants and Deodorants. Second Edition. New York: Marcel Dekker, Inc., pp. 1–7.

Lai-Cheong, J.E.; McGrath, J.A. (2013): Structure and function of skin, hair and nails. *Medicine* 41(6): 317–320. DOI: 10.1016/j.mpmed.2013.04.017.

Lai-Cheong, J.E.; McGrath, J.A. (2017): Structure and function of skin, hair and nails. *Medicine* 45(6): 347–351. DOI: 10.1016/j.mpmed.2017.03.004.

Langmead, C.J.; Watson, J.; Reavill, C. (2008): Muscarinic acetylcholine receptors as CNS drug targets. *Pharmacol Ther* 117(2): 232–243. DOI: 10.1016/j.pharmthera.2007.09.009.

Lecocq, M.; Wattiaux-De Coninck, S.; Laurent, N.; Wattiaux, R.; Jadot, M. (2000): Uptake and intracellular fate of polyethylenimine in vivo. *Biochem Biophys Res Commun* 278(2): 414–418. DOI: 10.1006/bbrc.2000.3809.

Lee, C.M.; Carpenter, F.; Coaker, T.; Kealey, T. (1986): The primary culture of epithelia from the secretory coil and collecting duct of normal human and cystic fibrotic eccrine sweat glands. *J Cell Sci* 83: 103–118.

Lee, C.M.; Dessi, J. (1989): NCL-SG3. A human eccrine sweat gland cell line that retains the capacity for transepithelial ion transport. *J Cell Sci* 92: 241–249.

Lee, K.Y.; Levell, N.J. (2014): Turning the tide. A history and review of hyperhidrosis treatment. *JRSM Open* 5(1): 2042533313505511. DOI: 10.1177/2042533313505511.

Lee, S.; Cobrinik, D. (2020): Improved third-generation lentiviral packaging with pLKO.1C vectors. *BioTechniques* 68(6): 349–352. DOI: 10.2144/btn-2019-0155.

Lee, S.H.; Jeong, S.K.; Ahn, S.K. (2006): An Update of the Defensive Barrier Function of Skin. *Yonsei Med J* 47(3): 293–306. DOI: 10.3349/ymj.2006.47.3.293.

Lefkimmiatis, K.; Zaccolo, M. (2014): cAMP signaling in subcellular compartments. *Pharmacol Ther* 143(3): 295–304. DOI: 10.1016/j.pharmthera.2014.03.008.

Lei, Y.-H.; Li, X.; Zhang, J.-Q.; Zhao, J.-Y. (2013): Important immunohistochemical markers for identifying sweat glands. *Chin Med J* 126(7): 1370–1377. DOI: 10.3760/cma.j.issn.0366-6999.20111924.

Lemoine, C.; Beau, N. (2005a): Use as an antiperspirant agent of a flocculating water-soluble polymer; cosmetic process for treating perspiration. Applied for by L'Oréal on 4/26/2005. App. no. PCT/EP2005/005243. Patent no. WO 2005/120448 A1.

Lemoine, C.; Beau, N. (2005b): Cosmetic composition comprising as antiperspirant agent a flocculating water-soluble polymer; process for treating perspiration. Applied for by L'Oréal on 6/21/2005. App. no. PCT/EP2005/007370. Patent no. WO 2006/018073 A1.

Li, H.; Chen, L.; Zeng, S.; Li, X.; Zhang, X.; Lin, C. et al. (2015): Matrigel basement membrane matrix induces eccrine sweat gland cells to reconstitute sweat gland-like structures in nude mice. *Exp Cell Res* 332(1): 67–77. DOI: 10.1016/j.yexcr.2015.01.014.

Li, H.; Chen, L.; Zhang, M.; Tang, S.; Fu, X. (2013): Three-dimensional culture and identification of human eccrine sweat glands in matrigel basement membrane matrix. *Cell Tissue Res* 354(3): 897–902. DOI: 10.1007/s00441-013-1718-3.

Li, H.; Chen, L.; Zhang, M.; Xie, S.; Cheng, L. (2018a): Expression and localization of Forkhead transcription factor A1 in the three-dimensional reconstructed eccrine sweat glands. *Acta Histochem* 120(6): 520–524. DOI: 10.1016/j.acthis.2018.06.003.

Li, H.; Chen, L.; Zhang, M.; Xie, S.; Zhang, C. (2018b): Detection of fluid secretion of three-dimensional reconstructed eccrine sweat glands by magnetic resonance imaging. *Exp Dermatol*. DOI: 10.1111/exd.13833.

Li, H.; Chen, L.; Zhang, M.; Zhang, B. (2017a): Cells in 3D-reconstitutued eccrine sweat gland cell spheroids differentiate into gross cystic disease fluid protein 15-expressing dark secretory cells and carbonic anhydrase II-expressing clear secretory cells. *Acta Histochem* 119(6): 620–623. DOI: 10.1016/j.acthis.2017.07.001.

Li, H.; Li, X.; Zhang, B.; Zhang, M.; Chen, W.; Tang, S.; Fu, X. (2016a): Changes in keratins and alpha-smooth muscle actin during three-dimensional reconstitution of eccrine sweat glands. *Cell Tissue Res* 365(1): 113–122. DOI: 10.1007/s00441-016-2357-2.

Li, H.; Zhang, M.; Chen, L.; Li, X.; Zhang, B. (2016b): Human eccrine sweat gland cells reconstitute polarized spheroids when subcutaneously implanted with Matrigel in nude mice. *J Mol Histol* 47(5): 485–490. DOI: 10.1007/s10735-016-9690-3.

Li, H.; Zhang, M.; Chen, L.; Zhang, B.; Zhang, C. (2017b): Expression of S100A2 and S100P in human eccrine sweat glands and their application in differentiating secretory coil-like from duct-like structures in the 3D reconstituted eccrine sweat spheroids. *J Mol Histol* 48(3): 219–223. DOI: 10.1007/s10735-017-9721-8.

Li, H.; Zhang, X.; Zeng, S.; Chen, L.; Li, X.; Lin, C. et al. (2014): The cellular localization of Na(+)/H(+) exchanger 1, cystic fibrosis transmembrane conductance regulator, potassium channel, epithelial sodium channel γ and vacuolar-type H+-ATPase in human eccrine sweat glands. *Acta Histochem* 116(8): 1237–1243. DOI: 10.1016/j.acthis.2014.07.005.

Li, H.-H.; Zhou, G.; Fu, X.-B.; Zhang, L. (2009): Antigen expression of human eccrine sweat glands. *J Cutan Pathol* 36(3): 318–324. DOI: 10.1111/j.1600-0560.2008.01020.x.

Li, X.; Li, H.; Zhang, M.; Chen, L.; Zhang, B. (2017c): Cell proliferation and differentiation during the three dimensional reconstitution of eccrine sweat glands. *J Mol Histol* 48(2): 113–120. DOI: 10.1007/s10735-017-9710-y.

Liao, T.; Lehmann, J.; Sternstein, S.; Yay, A.; Zhang, G.; Matthießen, A.E. et al. (2019): Nestin+ progenitor cells isolated from adult human sweat gland stroma promote reepithelialisation and may stimulate angiogenesis in wounded human skin ex vivo. *Arch Dermatol Res*. DOI: 10.1007/s00403-019-01889-x.

Lin, R.-Z.; Lin, R.-Z.; Chang, H.-Y. (2008): Recent advances in three-dimensional multicellular spheroid culture for biomedical research. *Biotechnol J* 3(9-10): 1172–1184. DOI: 10.1002/biot.200700228.

Linhart, C.; Talasz, H.; Morandi, E.M.; Exley, C.; Lindner, H.H.; Taucher, S. et al. (2017): Use of Underarm Cosmetic Products in Relation to Risk of Breast Cancer. A Case-Control Study. *EBioMedicine* 21: 79–85. DOI: 10.1016/j.ebiom.2017.06.005.

Lipinski, C.A.; Lombardo, F.; Dominy, B.W.; Feeney, P.J. (1997): Experimental and computational approaches to estimate solubility and permeability in drug discovery and development settings. *Advanced Drug Delivery Reviews* 23(1-3): 3–25. DOI: 10.1016/S0169-409X(96)00423-1.

Liu, N.; Huang, S.; Yao, B.; Xie, J.; Wu, X.; Fu, X. (2016a): 3D bioprinting matrices with controlled pore structure and release function guide in vitro self-organization of sweat gland. *Sci Rep* 6: 34410. DOI: 10.1038/srep34410.

Liu, Y.; Beyer, A.; Aebersold, R. (2016b): On the Dependency of Cellular Protein Levels on mRNA Abundance. *Cell* 165(3): 535–550. DOI: 10.1016/j.cell.2016.03.014.

Lobitz, W.C.; Osterberg, A.E. (1945): Chemistry of Palmar Sweat. Preliminary Report: Apparatus and Technics. *Journal of Investigative Dermatology* 6(1): 63–74. DOI: 10.1038/jid.1945.7.

Louie, J.C.; Fujii, N.; Meade, R.D.; Kenny, G.P. (2016): The roles of the Na^+/K^+-ATPase, NKCC, and K^+ channels in regulating local sweating and cutaneous blood flow during exercise in humans in vivo. *Physiol Rep* 4(22): e13024. DOI: 10.14814/phy2.13024.

Low, P.A. (2004): Evaluation of sudomotor function. *Clin Neurophysiol* 115(7): 1506–1513. DOI: 10.1016/j.clinph.2004.01.023.

Lu, C.; Fuchs, E. (2014): Sweat Gland Progenitors in Development, Homeostasis, and Wound Repair. *Cold Spring Harb Perspect Med* 4(2): a015222. DOI: 10.1101/cshperspect.a015222.

Lu, C.P.; Polak, L.; Keyes, B.E.; Fuchs, E. (2016): Spatiotemporal antagonism in mesenchymal-epithelial signaling in sweat versus hair fate decision. *Science* 354(6319). DOI: 10.1126/science.aah6102.

Lu, C.P.; Polak, L.; Rocha, A.S.; Pasolli, H.A.; Chen, S.-C.; Sharma, N. et al. (2012): Identification of stem cell populations in sweat glands and ducts reveals roles in homeostasis and wound repair. *Cell* 150(1): 136–150. DOI: 10.1016/j.cell.2012.04.045.

Ma, Y.; Li, M.; Liu, J.; Pang, C.; Zhang, J.; Li, Y.; Fu, X. (2018): Location, Isolation, and Identification of Mesenchymal Stem Cells from Adult Human Sweat Glands. *Stem Cells Int* 2018: 2090276. DOI: 10.1155/2018/2090276.

Macera-Bloch, L.; Houghton, J.; Lenahan, M.; Jha, K.K.; Ozer, H.L. (2002): Termination of lifespan of SV40-transformed human fibroblasts in crisis is due to apoptosis. *J Cell Physiol* 190(3): 332–344. DOI: 10.1002/jcp.10062.

Malgaroli, A.; Milani, D.; Meldolesi, J.; Pozzan, T. (1987): Fura-2 measurement of cytosolic free Ca2+ in monolayers and suspensions of various types of animal cells. *J Cell Biol* 105(5): 2145–2155. DOI: 10.1083/jcb.105.5.2145.

Mandriota, S.J. (2017): A Case-control Study Adds a New Piece to the Aluminium/Breast Cancer Puzzle. *EBioMedicine* 22: 22–23. DOI: 10.1016/j.ebiom.2017.06.025.

Mandriota, S.J.; Tenan, M.; Ferrari, P.; Sappino, A.-P. (2016): Aluminium chloride promotes tumorigenesis and metastasis in normal murine mammary gland epithelial cells. *Int J Cancer* 139(12): 2781–2790. DOI: 10.1002/ijc.30393.

Maqsood, M.I.; Matin, M.M.; Bahrami, A.R.; Ghasroldasht, M.M. (2013): Immortality of cell lines: challenges and advantages of establishment. *Cell Biol Int* 37(10): 1038–1045. DOI: 10.1002/cbin.10137.

McGann, L.E.; Yang, H.; Walterson, M. (1988): Manifestations of cell damage after freezing and thawing. *Cryobiology* 25(3): 178–185. DOI: 10.1016/0011-2240(88)90024-7.

McSwiney, B.A. (1934): The Composition of Human Perspiration (Samuel Hyde Memorial Lecture). *Proc R Soc Med* 27(7): 839–848. DOI: 10.1177/003591573402700710.

McWilliams, S.A.; Montgomery, I.; Jenkinson, D.M.; Elder, H.Y.; Wilson, S.M.; Sutton, A.M. (1987): Effects of topically-applied antiperspirant on sweat gland function. *British Journal of Dermatology* 117(5): 617–626. DOI: 10.1111/j.1365-2133.1987.tb07494.x.

Menon, G.K. (2002): New insights into skin structure. Scratching the surface. *Advanced Drug Delivery Reviews* 54: 3-17. DOI: 10.1016/S0169-409X(02)00121-7.

Méry, B.; Guy, J.-B.; Vallard, A.; Espenel, S.; Ardail, D.; Rodriguez-Lafrasse, C. et al. (2017): In Vitro Cell Death Determination for Drug Discovery. A Landscape Review of Real Issues. *Journal of Cell Death* 10: 1–8. DOI: 10.1177/1179670717691251.

Meuwis, K.; Boens, N.; Schryver, F.C. de; Gallay, J.; Vincent, M. (1995): Photophysics of the fluorescent K+ indicator PBFI. *Biophysical Journal* 68(6): 2469–2473. DOI: 10.1016/S0006-3495(95)80428-5.

Mickle, J.E.; Macek, M.; Fulmer-Smentek, S.B.; Egan, M.M.; Schwiebert, E.; Guggino, W. et al. (1998): A mutation in the cystic fibrosis transmembrane conductance regulator gene associated with elevated sweat chloride concentrations in the absence of cystic fibrosis. *Hum Mol Genet* 7(4): 729–735. DOI: 10.1093/hmg/7.4.729.

Moll, I.; Moll, R. (1992): Changes of expression of intermediate filament proteins during ontogenesis of eccrine sweat glands. *Journal of Investigative Dermatology* 98(5): 777–785. DOI: 10.1111/1523-1747.ep12499950.

Montagna, W.; Chase, H.B.; Lobitz, W.C. (1953): Histology and Cytochemistry of Human Skin. IV. The Eccrine Sweat Glands. *Journal of Investigative Dermatology* 20(6): 415–423. DOI: 10.1038/jid.1953.52.

Montenier, J.B. (1941): Astringent preparation on 1941. App. no. 309,830. Patent no. US2230084A.

Montgomery, I.; Jenkinson, D.M.; Elder, H.Y.; Czarnecki, D.; MacKie, R.M. (1984): The effects of thermal stimulation on the ultrastructure of the human atrichial sweat gland. I. The fundus. *British Journal of Dermatology* 110(4): 385–397. DOI: 10.1111/j.1365-2133.1984.tb04652.x.

Moore, W.C. (1935): Perspiration-inhibiting composition. Applied for by US IND ALCOHOL CO on 11/25/1935. App. no. US5148035A. Patent no. US2087162A.

Mörk, A.C.; Euler, A. von; Roomans, G.M.; Ring, A. (1996): cAMP-induced chloride transport in NCL-SG3 sweat gland cells. *Acta Physiol Scand* 157(1): 21–32. DOI: 10.1046/j.1365-201x.1996.450223000.x.

Murakami, M.; Ohtake, T.; Dorschner, R.A.; Schittek, B.; Garbe, C.; Gallo, R.L. (2002): Cathelicidin anti-microbial peptide expression in sweat, an innate defense system for the skin. *Journal of Investigative Dermatology* 119(5): 1090–1095. DOI: 10.1046/j.1523-1747.2002.19507.x.

Murota, H.; Matsui, S.; Ono, E.; Kijima, A.; Kikuta, J.; Ishii, M.; Katayama, I. (2015): Sweat, the driving force behind normal skin. An emerging perspective on functional biology and regulatory mechanisms. *J Dermatol Sci* 77(1): 3–10. DOI: 10.1016/j.jdermsci.2014.08.011.

Nagel, S.; Rohr, F.; Weber, C.; Kier, J.; Siemers, F.; Kruse, C. et al. (2013): Multipotent nestin-positive stem cells reside in the stroma of human eccrine and apocrine sweat glands and can be propagated robustly in vitro. *PLoS One* 8(10): e78365. DOI: 10.1371/journal.pone.0078365.

Nail, S.L.; White, J.L.; Hem, S.L. (1976): Structure of Aluminum Hydroxide Gel I. Initial Precipitate. *Journal of Pharmaceutical Sciences* 65(8): 1188–1191. DOI: 10.1002/jps.2600650814.

Nakatani, M.; Maksimovic, S.; Baba, Y.; Lumpkin, E.A. (2015): Mechanotransduction in epidermal Merkel cells. *Pflugers Arch* 467(1): 101–108. DOI: 10.1007/s00424-014-1569-0.

Nathanson, N.M. (2008): Synthesis, Trafficking, and Localization of Muscarinic Acetylcholine Receptors. *Pharmacol Ther* 119(1): 33–43. DOI: 10.1016/j.pharmthera.2008.04.006.

National Center for Biotechnology Information (Ed.): PubChem. U.S. National Library of Medicine. Available online at https://pubchem.ncbi.nlm.nih.gov/, checked on 4/24/2021.

Natsch, A. (2015): What Makes Us Smell: The Biochemistry of Body Odour and the Design of New Deodorant Ingredients. *Chimia (Aarau)* 69(7-8): 414–420. DOI: 10.2533/chimia.2015.414.

Natsume, K.; Ogawa, T.; Sugenoya, J.; Ohnishi, N.; Imai, K. (1992): Preferred ambient temperature for old and young men in summer and winter. *Int J Biometeorol* 36(1): 1–4. DOI: 10.1007/BF0120872.

Nejsum, L.N.; Kwon, T.-H.; Jensen, U.B.; Fumagalli, O.; Frøkiaer, J.; Krane, C.M. et al. (2002): Functional requirement of aquaporin-5 in plasma membranes of sweat glands. *Proc Natl Acad Sci U S A* 99(1): 511–516. DOI: 10.1073/pnas.012588099.

Nims, R.W.; Reid, Y. (2017): Best practices for authenticating cell lines. *In Vitro Cell Dev Biol Anim* 53(10): 880–887. DOI: 10.1007/s11626-017-0212-8.

Notley, S.R.; Park, J.; Tagami, K.; Ohnishi, N.; Taylor, N.A.S. (2017): Variations in body morphology explain sex differences in thermoeffector function during compensable heat stress. *Exp Physiol* 102(5): 545–562. DOI: 10.1113/EP086112.

Ogawa, T.; Sugenoya, J. (1993): Pulsatile Sweating and Sympathetic Sudomotor Activity. *The Japanese Journal of Physiology* 43(3): 275–289. DOI: 10.2170/jjphysiol.43.275.

Ohtsuyama, M.; Sato, F.; Toyomoto, T.; Sato, K. (1994): Stimulation of Cl conductance by minoxidil sulfate and K conductance by minoxidil in eccrine clear cells. *J Pharmacol Exp Ther* 269(2): 823–831.

Okada, N.; Kitano, Y.; Morimoto, T. (1983): Isolation of a Viable Eccrine Sweat Gland by Dispase. *Arch Dermatol Res* 275(2): 130–133. DOI: 10.1007/BF00412889.

Osserman, G. (2020): Deodorants - Germany - 2020. Edited by Mintel Group Ltd. Available online at https://clients.mintel.com/report/deodorants-germany-2020?fromSearch=%3Ffreetext%3Ddeodorants%2520-%2520Germany, checked on 1/9/2021.

Osypiw, J.C.; Gleeson, D.; Lobley, R.W.; Pemberton, P.W.; McMahon, R.F. (1994): Acid-base transport systems in a polarized human intestinal cell monolayer: Caco-2. *Exp Physiol* 79(5): 723–739. DOI: 10.1113/expphysiol.1994.sp003803.

Ouyang, Z.; Li, H.-H.; Zhang, M.-J.; Xie, S.-T.; Cheng, L.-H.-H. (2018): Differential Innervation of Secretory Coils and Ducts in Human Eccrine Sweat Glands. *Chin Med J* 131(16): 1964–1968. DOI: 10.4103/0366-6999.238142.

Papa, C.M.; Kligman, A.M. (1967): Mechanisms of Eccrine Anidrosis. II. The Antiperspirant Effect of Aluminium Salts. *Journal of Investigative Dermatology* 49(2): 139–145. DOI: 10.1038/jid.1967.115.

Pedersen, P.S. (1989): Human sweat duct cells in primary culture. Basic bioelectric properties of cultures derived from normals and patients with cystic fibrosis. *In vitro cellular & developmental biology : journal of the Tissue Culture Association* 25(4): 342–352. DOI: 10.1007/BF02624597.

Penneys, N.S.; Kaiser, M. (1993): Cylindroma expresses immunohistochemical markers linking it to eccrine coil. *J Cutan Pathol* 20(1): 40–43. DOI: 10.1111/j.1600-0560.1993.tb01247.x.

Perdikis, D.A.; Davies, R.; Zhuravkov, A.; Brenner, B.; Etter, L.; Basson, M.D. (1998): Differential effects of mucosal pH on human (Caco-2) intestinal epithelial cell motility, proliferation, and differentiation. *Dig Dis Sci* 43(7): 1537–1546. DOI: 10.1023/A:1018871016691.

Petschnik, A.E.; Klatte, J.E.; Evers, L.H.; Kruse, C.; Paus, R.; Danner, S. (2010): Phenotypic indications that human sweat glands are a rich source of nestin-positive stem cell populations. *British Journal of Dermatology* 162(2): 380–383. DOI: 10.1111/j.1365-2133.2009.09512.x.

Picarda, E.; Ohaegbulam, K.C.; Zang, X. (2016): Molecular Pathways: Targeting B7-H3 (CD276) for Human Cancer Immunotherapy. *Clinical cancer research : an official journal of the American Association for Cancer Research* 22(14): 3425–3431. DOI: 10.1158/1078-0432.CCR-15-2428.

Pipas, J.M. (2009): SV40: Cell transformation and tumorigenesis. *Virology* 384(2): 294–303. DOI: 10.1016/j.virol.2008.11.024.

Poblet, E.; Jimenez, F.; Escario-Travesedo, E.; Hardman, J.A.; Hernández-Hernández, I.; Agudo-Mena, J.L. et al. (2018): Eccrine sweat glands associate with the human hair follicle within a defined compartment of dermal white adipose tissue. *British Journal of Dermatology* 178(5): 1163–1172. DOI: 10.1111/bjd.16436.

Politi, R.; Sapir, L.; Harries, D. (2009): The impact of polyols on water structure in solution: a computational study. *J Phys Chem A* 113(26): 7548–7555. DOI: 10.1021/jp9010026.

Prasanna, S.; Doerksen, R.J. (2009): Topological polar surface area: a useful descriptor in 2D-QSAR. *Curr Med Chem* 16(1): 21–41. DOI: 10.2174/092986709787002817.

Prescott, S.L.; Larcombe, D.-L.; Logan, A.C.; West, C.; Burks, W.; Caraballo, L. et al. (2017): The skin microbiome. Impact of modern environments on skin ecology, barrier integrity, and systemic immune programming. *World Allergy Organ J* 10(1): 29-44. DOI: 10.1186/s40413-017-0160-5.

Prompt, C.A.; Quinton, P.M. (1978): Functions of calcium in sweat secretion. *Nature* 272(5649): 171–172. DOI: 10.1038/272171a0.

Quatrale, R.P.; Waldman, A.H.; Rogers, J.G.; Felger, C.B. (1981): The mechanism of antiperspirant action by aluminum salts. I. The effect of cellophane tape stripping on aluminum salt-inhibited eccrine sweat glands. *Journal of the Society of Cosmetic Chemists*(32): 67–73.

Quinton, P.M. (1981): Effects of Some Ion Transport Inhibitors on Secretion and Reabsorption in Intact and Perfused Single Human Sweat Glands. *Pflügers Archiv* 391(4): 309–313. DOI: 10.1007/BF00581513.

Quinton, P.M. (2007): Cystic Fibrosis. Lessons from the Sweat Gland. *Physiology* 22(3): 212–225. DOI: 10.1152/physiol.00041.2006.

Quinton, P.M.; Tormey, J.M. (1976): Localization of Na/K-ATPase Sites in the Secretory and Reabsorptive Epithelia of Perfused Eccrine Sweat Glands. A Question to the role of the enzyme in secretion. *J Membr Biol* 29(4): 383–399. DOI: 10.1007/BF0186897.

Ram, S.J.; Kirk, K.L. (1989): Cl^- permeability of human sweat duct cells monitored with fluorescence-digital imaging microscopy. Evidence for reduced plasma membrane Cl^- permeability in cystic fibrosis. *Proc Natl Acad Sci U S A* 86(24): 10166–10170. DOI: 10.1073/pnas.86.24.10166.

Randall, W.C. (1946): Quantitation and regional distribution of sweat glands in man. *Journal of Clinical Investigation* 25(5): 761–767. DOI: 10.1172/JCI101760.

Ravi, M.; Paramesh, V.; Kaviya, S.R.; Anuradha, E.; Solomon, F.D.P. (2015): 3D cell culture systems: advantages and applications. *J Cell Physiol* 230(1): 16–26. DOI: 10.1002/jcp.24683.

Reddy, M.; Quinton, P. (2003): Functional interaction of CFTR and ENaC in sweat glands. *Pflügers Archiv* 445(4): 499–503. DOI: 10.1007/s00424-002-0959-x.

Reddy, M.M.; Kopito, R.R.; Quinton, P.M. (1998): Cytosolic pH regulates G_{Cl} through control of phosphorylation states of CFTR. *American Journal of Physiology - Cell Physiology* 275(4): 1040-1047.

Reddy, M.M.; Light, M.J.; Quinton, P.M. (1999): Activation of the epithelial Na^+ channel (ENaC) requires CFTR Cl^- channel function. *Nature* 402(6759): 301–304. DOI: 10.1038/46297.

Reddy, M.M.; Quinton, P.M. (1987): Cl- permeability of sweat duct cell membranes: intracellular microelectrode analysis. *Prog Clin Biol Res* 254: 45–57.

Reddy, M.M.; Quinton, P.M. (1994): Rapid regulation of electrolyte absorption in sweat duct. *J Membr Biol* 140(1): 57–67. DOI: 10.1007/BF00234486.

Reddy, M.M.; Quinton, P.M. (2009): PKA Mediates Constitutive Activation of CFTR in Human Sweat Duct. *J Membr Biol* 231(2-3): 65–78. DOI: 10.1007/s00232-009-9205-1.

Reddy, M.M.; Wang, X.F.; Quinton, P.M. (2008): Effect of Cytosolic pH on Epithelial Na^+ Channel in Normal and Cystic Fibrosis Sweat Ducts. *J Membr Biol* 225(1): 1–11. DOI: 10.1007/s00232-008-9126-4.

Reid, L.C. (1979): [12] Cloning. In : Cell Culture, vol. 58: Elsevier (Methods in Enzymology), pp. 152–164.

Reyes-Reali, J.; Mendoza-Ramos, M.I.; Garrido-Guerrero, E.; Méndez-Catalá, C.F.; Méndez-Cruz, A.R.; Pozo-Molina, G. (2018): Hypohidrotic ectodermal dysplasia: clinical and molecular review. *Int J Dermatol* 57(8): 965–972. DOI: 10.1111/ijd.14048#.

Rhys, N.H.; Gillams, R.J.; Collins, L.E.; Callear, S.K.; Lawrence, M.J.; McLain, S.E. (2016): On the structure of an aqueous propylene glycol solution. *J Chem Phys* 145(22): 224504. DOI: 10.1063/1.4971208.

Rieg, S.; Garbe, C.; Sauer, B.; Kalbacher, H.; Schittek, B. (2004): Dermcidin is constitutively produced by eccrine sweat glands and is not induced in epidermal cells under inflammatory skin conditions. *British Journal of Dermatology* 151(3): 534–539. DOI: 10.1111/j.1365-2133.2004.06081.x.

Ring, A.; Mörk, A.C.; Roomans, G.M. (1995): Calcium-activated chloride fluxes in cultured NCL-SG3 sweat gland cells. *Cell Biol Int* 19(4): 265–278. DOI: 10.1006/cbir.1995.1069.

Robbins, Clarence R. (2012): Chemical and Physical Behavior of Human Hair. 5th ed. 2012. Berlin, Heidelberg: Springer Berlin Heidelberg. Available online at http://site.ebrary.com/lib/alltitles/docDetail.action?docID=10537673.

Robles-Munoz, V.D. (2014): The Development of an in vitro 3D Histotypic Model of The Human Eccrine Sweat Gland. Edited by Queen Mary University of London. Centre for Cutaneous Research. London. Available online at https://qmro.qmul.ac.uk/xmlui/handle/123456789/12910?show=full, checked on 9/2/2020.

Rodrigues-Peres, R.M.; Cadore, S.; Febraio, S.; Heinrich, J.K.; Serra, K.P.; Derchain, S.F.M. et al. (2013): Aluminum concentrations in central and peripheral areas of malignant breast lesions do not differ from those in normal breast tissues. *BMC Cancer* 13: 104. DOI: 10.1186/1471-2407-13-104.

Rosenthal, L.; Burchum, J. (2017): Lehne's Pharmacotherapeutics for Advanced Practice Providers. St. Louis: Elsevier Health Sciences. Available online at https://books.google.de/books?id=gfYoDgAAQBAJ.

Rütten, A. (2002): Ekkrine Schweissdrüsenkarzinome der Haut. *Pathologe* 23(1): 79–88. DOI: 10.1007/s00292-001-0516-y.

Sáenz-Robles, M.T.; Sullivan, C.S.; Pipas, J.M. (2001): Transforming functions of Simian Virus 40. *Oncogene* 20(54): 7899–7907. DOI: 10.1038/sj.onc.1204936.

Saga, K. (2001): Histochemical and immunohistochemical markers for human eccrine and apocrine sweat glands: an aid for histopathologic differentiation of sweat gland tumors. *J Investig Dermatol Symp Proc* 6(1): 49–53. DOI: 10.1046/j.0022-202x.2001.00005.x.

Saga, K. (2002): Structure and function of human sweat glands studied with histochemistry and cytochemistry. *Prog Histochem Cytochem* 37(4): 323–386.

Saga, K.; Sato, K. (1989): Electron Probe X-Ray Microanalysis of Cellular Ions in the Eccrine Secretory Coil Cells during Methacholine Stimulation. *J Membr Biol* 107(1): 13–24. DOI: 10.1007/BF01871079.

Saint-Criq, V.; Gray, M.A. (2017): Role of CFTR in epithelial physiology. *Cellular and Molecular Life Sciences* 74(1): 93–115. DOI: 10.1007/s00018-016-2391-y.

Sandell, L.; Sakai, D. (2011): Mammalian Cell Culture. *Current Protocols Essential Laboratory Techniques* 5(1). DOI: 10.1002/9780470089941.et0403s5.

Santos, E.; Hernández, R.M.; Pedraz, J.L.; Orive, G. (2012): Novel advances in the design of three-dimensional bio-scaffolds to control cell fate: translation from 2D to 3D. *Trends Biotechnol* 30(6): 331–341. DOI: 10.1016/j.tibtech.2012.03.005.

Sato, F.; Sato, K. (1987a): Effect of periglandular ionic composition and transport inhibitors on rhesus monkey eccrine sweat gland function in vitro. *Journal of Physiology* 393(1): 195–212. DOI: 10.1113/jphysiol.1987.sp016819.

Sato, F.; Sato, K. (2000): cAMP-dependent Cl^- channel protein (CFTR) and its mRNA are expressed in the secretory portion of human eccrine sweat gland. *J Histochem Cytochem* 48(3): 345–354. DOI: 10.1177/002215540004800304.

Sato, F.; Soos, G.; Link, C.; Sato, K. (2002): Cystic fibrosis transport regulator and its mRNA are expressed in human epidermis. *Journal of Investigative Dermatology* 119(6): 1224–1230. DOI: 10.1046/j.1523-1747.2002.19601.x.

Sato, K. (1973): Sweat induction from an isolated eccrine sweat gland. *Am J Physiol* 225(5): 1147–1152.

Sato, K. (1977a): Pharmacology and function of the myoepithelial cell in the eccrine sweat gland. *Experientia* 33(5): 631–633. DOI: 10.1007/BF01946542.

Sato, K. (1977b): The Physiology, Pharmacology, and Biochemistry of the Eccrine Sweat Gland. In R. H. Adrian, E. Helmreich, H. Holzer, R. Jung, K. Kramer, O. Krayer et al. (Eds.): Reviews of Physiology, Biochemistry and Pharmacology, Volume 79. Berlin, Heidelberg: Springer (Reviews of Physiology, Biochemistry and Pharmacology, 79), pp. 51–131.

Sato, K.; Dobson, R.L. (1971): Glucose Metabolism of the Isolated Eccrine Sweat Gland. I. The Effects of Mecholyl, Epinephrine and Ouabain. *Journal of Investigative Dermatology* 56(4): 272–280. DOI: 10.1111/1523-1747.ep12261004.

Sato, K.; Kang, W.H.; Saga, K.; Sato, K.T. (1989a): Biology of sweat glands and their disorders. I. Normal sweat gland function. *J Am Acad Dermatol* 20(4): 537–563. DOI: 10.1016/S0190-9622(89)70063-3.

Sato, K.; Kang, W.H.; Saga, K.; Sato, K.T. (1989b): Biology of sweat glands and their disorders. II. Disorders of sweat gland function. *J Am Acad Dermatol* 20(5): 713–726. DOI: 10.1016/S0190-9622(89)70081-5.

Sato, K.; Leidal, R.; Sato, F. (1987): Morphology and development of an apoeccrine sweat gland in human axillae. *Am J Physiol* 252(1): 166-180.

Sato, K.; Sato, F. (1981): Pharmacologic responsiveness of isolated single eccrine sweat glands. *American Journal of Physiology - Regulatory, Integrative and Comparative Physiology* 240(1): R44-R51.

Sato, K.; Sato, F. (1983): Individual variations in structure and function of human eccrine sweat gland. *American Journal of Physiology - Regulatory, Integrative and Comparative Physiology* 245(2): 203-208.

Sato, K.; Sato, F. (1984): Defective beta adrenergic response of cystic fibrosis sweat glands in vivo and in vitro. *Journal of Clinical Investigation* 73(6): 1763–1771. DOI: 10.1172/jci111385.

Sato, K.; Sato, F. (1987b): Sweat secretion by human axillary apoeccrine sweat gland in vitro. *American Journal of Physiology - Regulatory, Integrative and Comparative Physiology* 252(1): 181-187.

Sato, K.; Sato, F. (1988): Relationship between quin2-determined cytosolic [Ca^{2+}] and sweat secretion. *American Journal of Physiology - Cell Physiology* 254(2): 310-317.

Sato, K.; Sato, F. (1990): Na+, K+, H+, Cl-, and Ca2+ concentrations in cystic fibrosis eccrine sweat in vivo and in vitro. *J Lab Clin Med* 115(4): 504–511.

Sato, S.; Rancourt, A.; Sato, Y.; Satoh, M.S. (2016): Single-cell lineage tracking analysis reveals that an established cell line comprises putative cancer stem cells and their heterogeneous progeny. *Sci Rep* 6: 23328. DOI: 10.1038/srep23328.

Savic, I.; Berglund, H.; Gulyas, B.; Roland, P. (2001): Smelling of Odorous Sex Hormone-like Compounds Causes Sex-Differentiated Hypothalamic Activations in Humans. *Neuron* 31(4): 661–668. DOI: 10.1016/s0896-6273(01)00390-7.

SCCS (2016): Note of Guidance for the Testing of Cosmetic Substances and their Safety Evaluation, 9th Revision. SCCS/1564/15. Available online at http://ec.europa.eu/health/scientific_committees/consumer_safety/docs/sccs_o_190.pdf.

Schiefferdecker, P. (1922): Die Hautdrüsen des Menschen und der Säugetiere, ihre biologische und rassenanatomische Bedeutung, sowie die Muscuiaris sexualis. Zoologica - 27_72. Stuttgart: E. Schweizerbart'sche Verlagsbuchhandlung.

Schittek, B. (2012): The multiple facets of dermcidin in cell survival and host defense. *J Innate Immun* 4(4): 349–360. DOI: 10.1159/000336844.

Schittek, B.; Hipfel, R.; Sauer, B.; Bauer, J.; Kalbacher, H.; Stevanovic, S. et al. (2001): Dermcidin: a novel human antibiotic peptide secreted by sweat glands. *Nat Immunol* 2(12): 1133–1137. DOI: 10.1038/ni732.

Schlereth, T.; Dieterich, M.; Birklein, F. (2009): Hyperhidrosis - Causes and Treatment of Enhanced Sweating. *Dtsch Arztebl Int* 106(3): 32–37. DOI: 10.3238/arztebl.2009.0032.

Scholes, K.T.; Crow, K.D.; Ellis, J.P.; Harman, R.R.; Saihan, E.M. (1978): Axillary hyperhidrosis treated with alcoholic solution of aluminium chloride hexahydrate. *Br Med J* 2(6130): 84–85. DOI: 10.1136/bmj.2.6130.84.

Scientific Committee on Consumer Safety (Ed.) (2012): Opinion on Nitrosamines and Secondary Amines in Cosmetic Products. SCCS/1458/11. Available online at https://ec.europa.eu/health/scientific_committees/consumer_safety/docs/sccs_o_090.pdf, checked on 1/9/2021.

Scientific Committee on Consumer Safety (SCCS) (2019): Opinion on the safety of Aluminium in cosmetic products. Preliminary version of 30-31 Ocotober 2019. SCCS/1613/19. Available online at https://ec.europa.eu/health/sites/health/files/scientific_committees/consumer_safety/docs/sccs_o_235.pdf, checked on 2/3/2020.

Seigneurin-Venin, S.; Bernard, V.; Tremblay, J.P. (2000): Telomerase allows the immortalization of T antigen-positive DMD myoblasts: a new source of cells for gene transfer application. *Gene Ther* 7(7): 619–623. DOI: 10.1038/sj.gt.3301132.

Semkova, K.; Gergovska, M.; Kazandjieva, J.; Tsankov, N. (2015): Hyperhidrosis, bromhidrosis, and chromhidrosis: Fold (intertriginous) dermatoses. *Clinics in Dermatology* 33(4): 483–491. DOI: 10.1016/j.clindermatol.2015.04.013.

Seneschal, J.; Clark, R.A.; Gehad, A.; Baecher-Allan, C.M.; Kupper, T.S. (2012): Human Epidermal Langerhans Cells Maintain Immune Homeostasis in Skin by Activating Skin Resident Regulatory T Cells. *Immunity* 36(5): 873–884. DOI: 10.1016/j.immuni.2012.03.018.

Servetnyk, Z.; Roomans, G.M. (2007): Chloride transport in NCL-SG3 sweat gland cells: Channels involved. *Exp Mol Pathol* 83(1): 47–53. DOI: 10.1016/j.yexmp.2007.02.003.

Shelley, W.B.; Horvath, P.N.; Weidman, F.D.; Pillsbury, D.M. (1948): Experimental Miliaria in Man. *Journal of Investigative Dermatology* 11(4): 275–291. DOI: 10.1038/jid.1948.96.

Shibasaki, M.; Crandall, C.G. (2010): Mechanisms and controllers of eccrine sweating in humans. *Front Biosci (Schol Ed)* 2: 685–696.

Shin, H.-Y.; Yang, W.; Lee, E.-J.; Han, G.H.; Cho, H.; Chay, D.B.; Kim, J.-H. (2018): Establishment of five immortalized human ovarian surface epithelial cell lines via SV40 T antigen or HPV E6/E7 expression. *PLoS One* 13(10): e0205297. DOI: 10.1371/journal.pone.0205297.

Sidiropoulos, M.; Sade, S.; Al-Habeeb, A.; Ghazarian, D. (2011): Syringoid eccrine carcinoma: a clinicopathological and immunohistochemical study of four cases. *J Clin Pathol* 64(9): 788–792. DOI: 10.1136/jclinpath-2011-200069.

Simmers, P.; Li, S.K.; Kasting, G.; Heikenfeld, J. (2018): Prolonged and localized sweat stimulation by iontophoretic delivery of the slowly-metabolized cholinergic agent carbachol. *J Dermatol Sci* 89(1): 40–51. DOI: 10.1016/j.jdermsci.2017.10.013.

Slominski, A.; Wortsman, J. (2000): Neuroendocrinology of the skin. *Endocr Rev* 21(5): 457–487. DOI: 10.1210/edrv.21.5.0410.

Slominski, A.T.; Manna, P.R.; Tuckey, R.C. (2015): On the role of skin in the regulation of local and systemic steroidogenic activities. *Steroids* 103: 72–88. DOI: 10.1016/j.steroids.2015.04.006.

Slominski, A.T.; Zmijewski, M.A.; Skobowiat, C.; Zbytek, B.; Slominski, R.M.; Steketee, J.D. (2012): Sensing the environment. Regulation of local and global homeostasis by the skin neuroendocrine system. *Adv Anat Embryol Cell Biol* 212: 1-115. DOI: 10.1007/978-3-642-19683-6_1.

Slominski, A.T.; Zmijewski, M.A.; Zbytek, B.; Tobin, D.J.; Theoharides, T.C.; Rivier, J. (2013): Key Role of CRF in the Skin Stress Response System. *Endocr Rev* 34(6): 827–884. DOI: 10.1210/er.2012-1092.

Smith, C.J.; Alexander, L.M.; Kenney, W.L. (2013): Nonuniform, age-related decrements in regional sweating and skin blood flow. *American Journal of Physiology - Regulatory, Integrative and Comparative Physiology* 305(8): 877-885. DOI: 10.1152/ajpregu.00290.2013.

Smith, J.L.; Lee, L.C.; Read, A.; Li, Q.; Yu, B.; Lee, C.-S.; Luo, J. (2016): One-step immortalization of primary human airway epithelial cells capable of oncogenic transformation. *Cell Biosci* 6: 57. DOI: 10.1186/s13578-016-0122-6.

Song, Y.; Sonawane, N.; Verkman, A.S. (2002): Localization of aquaporin-5 in sweat glands and functional analysis using knockout mice. *Journal of Physiology* 541(2): 561–568. DOI: 10.1113/jphysiol.2001.020180.

Sonner, Z.; Wilder, E.; Heikenfeld, J.; Kasting, G.; Beyette, F.; Swaile, D. et al. (2015): The microfluidics of the eccrine sweat gland, including biomarker partitioning, transport, and biosensing implications. *Biomicrofluidics* 9(3): 31301. DOI: 10.1063/1.4921039.

Steinberg, T.H.; Newman, A.S.; Swanson, J.A.; Silverstein, S.C. (1987): Macrophages possess probenecid-inhibitable organic anion transporters that remove fluorescent dyes from the cytoplasmic matrix. *J Cell Biol* 105(6 Pt 1): 2695–2702. DOI: 10.1083/jcb.105.6.2695.

Strober, W. (2015): Trypan Blue Exclusion Test of Cell Viability. *Curr Protoc Immunol* 111: A3.B.1-3. DOI: 10.1002/0471142735.ima03bs111.

Sugiharto, S.; Lewis, T.M.; Moorhouse, A.J.; Schofield, P.R.; Barry, P.H. (2008): Anion-cation permeability correlates with hydrated counterion size in glycine receptor channels. *Biophysical Journal*: 4698–4715. DOI: 10.1529/biophysj.107.125690.

Sun, Q.; Deng, X.-M.; Wang, Y.-L.; Zhen, Y.-F.; Li, F.; Chen, R.-H. et al. (2017): Serum is an indispensable factor in the maintenance of the biological characteristics of sweat gland cells. *Molecular Medicine Reports* 16(3): 2691–2699. DOI: 10.3892/mmr.2017.6909.

Swaile, D.F.; Elstun, L.T.; Benzing, K.W. (2012): Clinical studies of sweat rate reduction by an over-the-counter soft-solid antiperspirant and comparison with a prescription antiperspirant product in male panelists. *British Journal of Dermatology* 166 Suppl 1: 22–26. DOI: 10.1111/j.1365-2133.2011.10786.x.

Swary, J.H.; West, D.P.; Kakar, R.; Ortiz, S.; Schaeffer, M.R.; Veledar, E.; Alam, M. (2015): Quantitative comparison of topical aluminum salt solution efficacy for management of sweating: a randomized, controlled trial. *J Cosmet Dermatol* 14(4): E1-6. DOI: 10.1111/jocd.12168.

Takemura, T.; Sato, F.; Saga, K.; Suzuki, Y.; Sato, K. (1991): Intracellular ion concentrations and cell volume during cholinergic stimulation of eccrine secretory coil cells. *J Membr Biol* 119(3): 211–219. DOI: 10.1007/BF01868726.

Teagarden, D.L.; Hem, S.L.; Radavich, J.F.; White, J.L. (1981): Aluminum chlorohydrate II. Physicochemical properties. *Journal of Pharmaceutical Sciences* 70(7): 762–764. DOI: 10.1002/jps.2600700712.

Tegtmeyer, P. (1975): Function of simian virus 40 gene A in transforming infection. *J Virol* 15(3): 613–618.

Titford, M. (2009): Progress in the Development of Microscopical Techniques for Diagnostic Pathology. *Journal of Histotechnology* 32(1): 9–19. DOI: 10.1179/his.2009.32.1.9.

Toedt, J.; Koza, D.; van Cleef-Toedt, K. (2005): Chemical Composition of Everyday Products. Westport: Greenwood Press. Available online at https://books.google.de/books?id=UnjD4aBm9ZcC.

Towey, J.J.; Dougan, L. (2012): Structural examination of the impact of glycerol on water structure. *J Phys Chem B*: 1633–1641. DOI: 10.1021/jp2093862.

Tran, C.N.; Thacker, S.G.; Louie, D.M.; Oliver, J.; White, P.T.; Endres, J.L. et al. (2008): Interactions of T cells with fibroblast-like synoviocytes: role of the B7 family costimulatory ligand B7-H3. *J Immunol* 180(5): 2989–2998. DOI: 10.4049/jimmunol.180.5.2989.

Tsukada, T.; Kouki, T.; Fujiwara, K.; Ramadhani, D.; Horiguchi, K.; Kikuchi, M.; Yashiro, T. (2013): Reassembly of anterior pituitary organization by hanging drop three-dimensional cell culture. *Acta histochemica et cytochemica* 46(4): 121–127. DOI: 10.1267/ahc.13015.

Untied, S. (2004): Antitranspirantien. In Wilfried Umbach (Ed.): Kosmetik und Hygiene. Von Kopf bis Fuß. 3., vollst. überarb. u. erw. Aufl. Weinheim: WILEY-VCH.

Urmacher, C. (1990): Histology of normal skin. *Am J Surg Pathol* 14(7): 671–686.

Vervloessem, T.; Yule, D.I.; Bultynck, G.; Parys, J.B. (2015): The type 2 inositol 1,4,5-trisphosphate receptor, emerging functions for an intriguing Ca^{2+}-release channel. *Biochim Biophys Acta* 1853(9): 1992–2005. DOI: 10.1016/j.bbamcr.2014.12.006.

Vistoli, G.; Pedretti, A. (2016): Molecular Fields to Assess Recognition Forces and Property Spaces☆. In : Reference Module in Chemistry, Molecular Sciences and Chemical Engineering: Elsevier.

Vitellaro-Zuccarello, L.; Garbelli, R.; Rossi, V.D. (1992): Immunocytochemical localization of collagen types I, III, IV, and fibronectin in the human dermis. Modifications with ageing. *Cell Tissue Res* 268(3): 505–511. DOI: 10.1007/BF00319157.

Wang, A.Z.; Ojakian, G.K.; Nelson, W.J. (1990): Steps in the morphogenesis of a polarized epithelium. I. Uncoupling the roles of cell-cell and cell-substratum contact in establishing plasma membrane polarity in multicellular epithelial (MDCK) cysts. *J Cell Sci* 95 (Pt 1): 137–151.

Wang, C.; Tammi, M.; Tammi, R. (1992): Distribution of hyaluronan and its CD44 receptor in the epithelia of human skin appendages. *Histochemistry* 98(2): 105–112. DOI: 10.1007/bf00717001.

Wang, H.; Wang, Y.; Yan, H.; Zhang, J.; Thomas, R.K. (2006): Binding of sodium dodecyl sulfate with linear and branched polyethyleneimines in aqueous solution at different pH values. *Langmuir* 22(4): 1526–1533. DOI: 10.1021/la051988j.

Wang, M.-H.; Soriano, A.N.; Caparanga, A.R.; Li, M.-H. (2010): Binary mutual diffusion coefficient of aqueous solutions of propylene glycol and dipropylene glycol. *Journal of the Taiwan Institute of Chemical Engineers* 41(3): 279–285. DOI: 10.1016/j.jtice.2009.09.001.

Way, S.C.; Memmesheimer, A. (1936): The sudoriparous glands. I. The eccrine glands. *Archives of Dermatology and Syphilology* 34(5): 797–808. DOI: 10.1001/archderm.1936.01470170045003.

Welzel, J. (2017): Development of an in vitro model of the human sweat gland for testing of the efficacy of new antitranspirants and approval of their toxicological safety. Master thesis.

Welzel, J.; Grüdl, S.; Welss, T.; Claas, M.; Sättler, A.; Förster, T.; Banowski, B. (2021): Quantitative ion determination in eccrine sweat gland cells correlates to sweat reduction of antiperspirant actives. *Int J Cosmet Sci* 43(2): 181–190. DOI: 10.1111/ics.12679.

Wilke, K.; Martin, A.; Terstegen, L.; Biel, S.S. (2007): A short history of sweat gland biology. *Int J Cosmet Sci* 29(3): 169–179. DOI: 10.1111/j.1467-2494.2007.00387.x.

Wojcikiewicz, R.J.; Luo, S.G. (1998): Phosphorylation of inositol 1,4,5-trisphosphate receptors by cAMP-dependent protein kinase. Type I, II, and III receptors are differentially susceptible to phosphorylation and are phosphorylated in intact cells. *J Biol Chem* 273(10): 5670–5677. DOI: 10.1074/jbc.273.10.5670.

Wolfe, S.; Cage, G.; Epstein, M.; Tice, L.; Miller, H.; Gordon, R.S. (1970): Metabolic studies of isolated human eccrine sweat glands. *Journal of Clinical Investigation* 49(10): 1880–1884. DOI: 10.1172/JCI106407.

World Health Organization (2005): Handbook for Good Clinical Research Practice (GCP): Guidance for Implementation. France. Available online at https://apps.who.int/iris/bitstream/handle/10665/43392/924159392X_eng.pdf;jsessionid=5D57045A4C9D5D93D08B8C13CF26C10E?sequence=1, checked on 8/20/2020.

World Medical Association (1964): Declaration of Helsinki - Ethical Principles for Medical Research Involving Human Subjects. Available online at https://www.wma.net/policies-post/wma-declaration-of-helsinki-ethical-principles-for-medical-research-involving-human-subjects/, checked on 8/20/2020.

Wu, Y.; Xie, J.; Wang, F.; Chen, Z. (2008): Electrokinetic separation of peptides and proteins using a polyvinylamine-coated capillary with UV and ESI-MS detection. *J Sep Sci* 31(5): 814–823. DOI: 10.1002/jssc.200700518.

Xie, J.; Yao, B.; Han, Y.; Huang, S.; Fu, X. (2016): Skin appendage-derived stem cells: cell biology and potential for wound repair. *Burns Trauma* 4: 38. DOI: 10.1186/s41038-016-0064-6.

Yatani, A.; Brown, A.M.; Akaike, N. (1984): Effect of extracellular pH on sodium current in isolated, single rat ventricular cells. *J Membr Biol* 78(2): 163–168. DOI: 10.1007/bf01869203.

Zancanaro, C.; Merigo, F.; Crescimanno, C.; Orlandini, S.; Osculati, A. (1999): Immunohistochemical evidence suggests intrinsic regulatory activity of human eccrine sweat glands. *Journal of Anatomy* 194(3): 433–444. DOI: 10.1046/j.1469-7580.1999.19430433.x.

Zhang, M.; Li, H.; Chen, L.; Fang, S.; Xie, S.; Lin, C. (2018a): Three-dimensional reconstructed eccrine sweat glands with vascularization and cholinergic and adrenergic innervation. *J Mol Histol*. DOI: 10.1007/s10735-018-9773-4.

Zhang, M.; Li, H.; Xie, S.; Chen, L. (2018b): Time course of differentiation of different cell types in 3D-reconstructed eccrine sweat glands. *J Mol Histol*. DOI: 10.1007/s10735-018-9795-y.

Zirwas, M.J.; Moennich, J. (2008): Antiperspirant and Deodorant Allergy. Diagnosis and Management. *J Clin Aesthet Dermatol* 1(3): 38–43.

Zufferey, R.; Dull, T.; Mandel, R.J.; Bukovsky, A.; Quiroz, D.; Naldini, L.; Trono, D. (1998): Self-inactivating lentivirus vector for safe and efficient in vivo gene delivery. *J Virol* 72(12): 9873–9880. DOI: 10.1128/JVI.72.12.9873-9880.1998.

III. Own Publications

Publications

Contributions to all publications: analysis conception and design, data collection, analysis performance, manuscript writing

Welzel, J.; Grüdl, S.; Welss, T.; Claas, M.; Sättler, A.; Förster, T.; Banowski, B. (2020): Quantitative ion determination in eccrine sweat gland cells correlates to sweat reduction of antiperspirant actives. *Int J Cosmet Sci* 43(2): 181-190. DOI: 10.1111/ics.12679.

Welzel, J.; Gruedl, S.; Banowski, B.; Saettler, A.; Foerster, T.; Welss, T. (2020): New Technologies for Specific Antiperspirant Actions. *sofw journal* 146(03/20): 46-51.

Welzel, J.; Gruedl, S.; Stark, H.; Banowski, B.; Saettler, A.; Welss, T. (in preparation): A novel human eccrine sweat gland duct cell line for investigating sweating physiology.

Patents

Welss, T.; Banowski, B.; Welzel, J.; Gruedl, S. (2018): Three-dimensional cell culture model of the human sweat gland and analysis of stress-associated sweating processes. Patent granted. App. no. DE2018-102018129793, Patent no. DE102018129793.

Banowski, B., Welzel, J., Claas, M. (2019): Lösliche Oligomere von Propandiol als Wirkstoff zur Regulierung der Schweißsekretion / als Antitranspirant-Wirkstoff. Patent filed. App. no. 102019133191.9.

Welzel, J.; Gruedl, S.; Welss, T. (2019): Gewebetechnologisch unterstützte Rekonstruktion einer ekkrine Schweißdrüse. Patent filed. App. no. PCT/EP2020/082003.

Banowski, B., Welzel, J., Claas, M. (2019): Aminozucker, speziell Dimethylglucamin als Wirkstoff zur Regulierung der Schweißsekretion / als Antitranspirant-Wirkstoff. Patent filed. App. no. 102019134443.3.

Banowski, B., Welzel, J., Claas, M. (2019): Lösliche Oligomere von Glycerin als Wirkstoff zur Regulierung der Schweißsekretion / als Antitranspirant-Wirkstoff. Patent filed. App. no. 102020100820.1.

Banowski, B.; Welzel, J.; Gruedl, S.; Welss, T.; Breuer, I.; Claas, M. (2019): Dimethylpiperazin, weitere Piperazine und deren Salze als Wirkstoff zur Verminderung der Schweißsekretion. Patent filed. App. no. 102020101190.3.

Conference presentations

SEPAWA® Congress, Berlin, Germany, 2019 – *Oral presentation: "New Technologies for Specific Antiperspirant Actions".*

IV. Supplementary

1.1 Supplemental figures

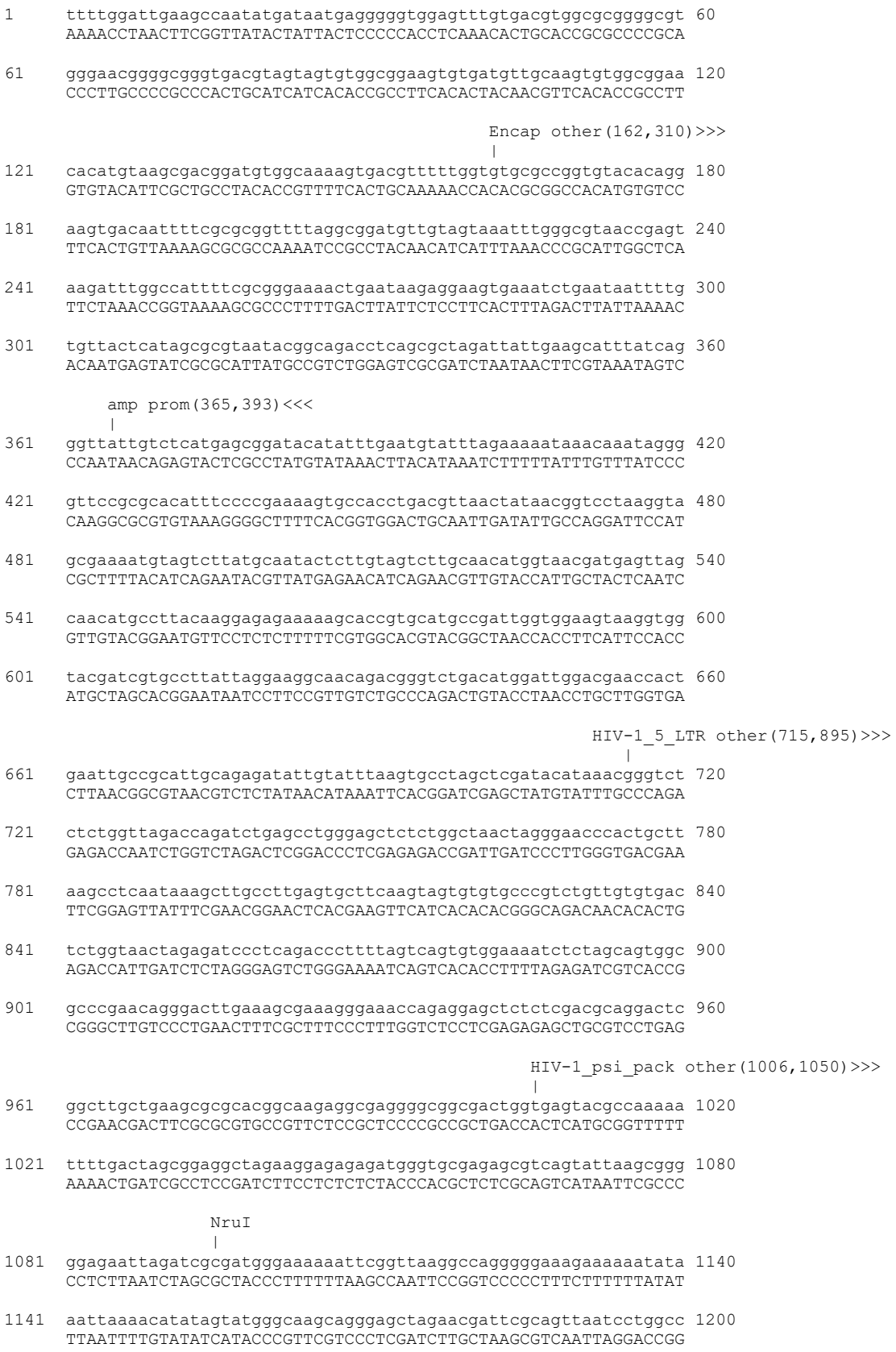

```
1201  tgttagaaacatcagaaggctgtagacaaatactgggacagctacaaccatcccttcaga 1260
      ACAATCTTTGTAGTCTTCCGACATCTGTTTATGACCCTGTCGATGTTGGTAGGGAAGTCT

1261  caggatcagaagaacttagatcattatataataca gtagcaaccctctattgtgtgcatc 1320
      GTCCTAGTCTTCTTGAATCTAGTAATATATTATGTCATCGTTGGGAGATAACACACGTAG

1321  aaaggatagagataaaagacaccaaggaagctttagacaagatagaggaagagcaaaaca 1380
      TTTCCTATCTCTATTTTCTGTGGTTCCTTCGAAATCTGTTCTATCTCCTTCTCGTTTTGT

1381  aaagtaagaccaccgcacagcaagcccgctgatcttcagacctggaggaggagatatgag 1440
      TTTCATTCTGGTGGCGTGTCGTTCGGGCGACTAGAAGTCTGGACCTCCTCCTCTATACTC

1441  ggacattggagaagtgaattatataaatataaagtagtaaaaattgaaccattaggagta 1500
      CCTGTAACCTCTTCACTTAATATATTTATATTTCATCATTTTTAACTTGGTAATCCTCAT

                                                          RRE reg(1557,1790)>>>
                                                          |
1501  gcacccaccaaggcaaagagaagagtggtgcagagagaaaaaagagcagtgggaatagga 1560
      CGTGGGTGGTTCCGTTTCTCTTCTCACCACGTCTCTCTTTTTTCTCGTCACCCTTATCCT

                                          ORF_1 rf(1)(1600,2301)>>>
                                          |
1561  gctttgttccttgggttcttgggagcagcaggaagcactatgggcgcagcgtcaatgacg 1620
      CGAAACAAGGAACCCAAGAACCCTCGTCGTCCTTCGTGATACCCGCGTCGCAGTTACTGC

1621  ctgacggtacaggccagacaattattgtctggtatagtgcagcagcagaacaatttgctg 1680
      GACTGCCATGTCCGGTCTGTTAATAACAGACCATATCACGTCGTCGTCTTGTTAAACGAC

1681  agggctattgaggcgcaacagcatctgttgcaactcacagtctggggcatcaagcagctc 1740
      TCCCGATAACTCCGCGTTGTCGTAGACAACGTTGAGTGTCAGACCCCGTAGTTCGTCGAG

1741  caggcaagaatcctggctgtggaaagatacctaaaggatcaacagctcctggggatttgg 1800
      GTCCGTTCTTAGGACCGACACCTTTCTATGGATTTCCTAGTTGTCGAGGACCCCTAAACC

1801  ggttgctctggaaaactcatttgcaccactgctgtgccttggaatgctagttggagtaat 1860
      CCAACGAGACCTTTTGAGTAAACGTGGTGACGACACGGAACCTTACGATCAACCTCATTA

1861  aaatctctggaacagatttggaatcacacgacctggatggagtgggacagagaaattaac 1920
      TTTAGAGACCTTGTCTAAACCTTAGTGTGCTGGACCTACCTCACCCTGTCTCTTTAATTG

1921  aattacacaagcttaatacactccttaattgaagaatcgcaaaaccagcaagaaaagaat 1980
      TTAATGTGTTCGAATTATGTGAGGAATTAACTTCTTAGCGTTTTGGTCGTTCTTTTCTTA

1981  gaacaagaattattggaattagataaatgggcaagtttgtggaattggtttaacataaca 2040
      CTTGTTCTTAATAACCTTAATCTATTTACCCGTTCAAACACCTTAACCAAATTGTATTGT

2041  aattggctgtggtatataaaattattcataatgatagtaggaggcttggtaggtttaaga 2100
      TTAACCGACACCATATATTTTAATAAGTATTACTATCATCCTCCGAACCATCCAAATTCT

2101  atagtttttgctgtactttctatagtgaatagagttaggcagggatattcaccattatcg 2160
      TATCAAAAACGACATGAAAGATATCACTTATCTCAATCCGTCCCTATAAGTGGTAATAGC

2161  tttcagacccacctcccaaccccgaggggacccgacaggcccgaaggaatagaagaagaa 2220
      AAAGTCTGGGTGGAGGGTTGGGGCTCCCCTGGGCTGTCCGGGCTTCCTTATCTTCTTCTT

2221  ggtggagagagagacagagacagatccattcgattagtgaacggatctcgacggtatcga 2280
      CCACCTCTCTCTCTGTCTCTGTCTAGGTAAGCTAATCACTTGCCTAGAGCTGCCATAGCT

2281  aagcttgggattcgaatttaaaagaaaaggggggattgggggtacagtgcaggggaaag 2340
      TTCGAACCCTAAGCTTAAATTTTCTTTTCCCCCCTAACCCCCCATGTCACGTCCCCTTTC

2341  aatagtagacataatagcaacagacatacaaactaaagaactacaaaaacaaattacaaa 2400
      TTATCATCTGTATTATCGTTGTCTGTATGTTTGATTTCTTGATGTTTTTGTTTAATGTTT

2401  aattcaaaattttcgggtttttcgaacctagggttccgcgttacataacttacggtaaat 2460
      TTAAGTTTTAAAAGCCCAAAAAGCTTGGATCCCAAGGCGCAATGTATTGAATGCCATTTA

2461  ggcccgcctggctgaccgcccaacgacccccgcccattgacgtcaataatgacgtatgtt 2520
      CCGGGCGGACCGACTGGCGGGTTGCTGGGGGCGGGTAACTGCAGTTATTACTGCATACAA

2521  cccatagtaacgccaatagggactttccattgacgtcaatgggtggagtatttacggtaa 2580
      GGGTATCATTGCGGTTATCCCTGAAAGGTAACTGCAGTTACCCACCTCATAAATGCCATT

2581  actgcccacttggcagtacatcaagtgtatcatatgccaagtacgccccctattgacgtc 2640
      TGACGGGTGAACCGTCATGTAGTTCACATAGTATACGGTTCATGCGGGGGATAACTGCAG
```

```
2641  aatgacggtaaatggcccgcctggcattatgcccagtacatgaccttatgggactttcct 2700
      TTACTGCCATTTACCGGGCGGACCGTAATACGGGTCATGTACTGGAATACCCTGAAAGGA

2701  acttggcagtacatctacgtttagtcatcgctattaccatggtgatgcggttttggcagt 2760
      TGAACCGTCATGTAGATGCAAATCAGTAGCGATAATGGTACCACTACGCCAAAACCGTCA

2761  acatcaatgggcgtggatagcggtttgactcacggggatttccaagtctccaccccattg 2820
      TGTAGTTACCCGCACCTATCGCCAAACTGAGTGCCCCTAAAGGTTCAGAGGTGGGGTAAC

2821  acgtcaatgggagtttgttttggcaccaaaatcaacgggactttccaaaatgtcgtaaca 2880
      TGCAGTTACCCTCAAACAAAACCGTGGTTTTAGTTGCCCTGAAAGGTTTTACAGCATTGT

          CMV prom(2885,2966)>>>
          |
2881  actccgccccattgacgcaaatgggcggtaggcgtgtacggtgggaggtctatataagca 2940
      TGAGGCGGGGTAACTGCGTTTACCCGCCATCCGCACATGCCACCCTCCAGATATATTCGT

2941  gagctcgtttagtgaaccgtcagatcgcctggagacgccatccacgctgttttgacctcc 3000
      CTCGAGCAAATCACTTGGCAGTCTAGCGGACCTCTGCGGTAGGTGCGACAAAACTGGAGG

                        tetO reg(3022,3061)>>>
                        |
3001  atagaagaaccgagtttaaactccctatcagtgatagagatctccctatcagtgatagag 3060
      TATCTTCTTGGCTCAAATTTGAGGGATAGTCACTATCTCTAGAGGGATAGTCACTATCTC

            SmaI
            |
          XmaI   ClaI                       KpnI
          | |    |                          |
3061  agctagccccgggatcgatcaattgagtacttacgtaggtaccccagtgtggtggcctgc 3120
      TCGATCGGGGCCCTAGCTAGTTAACTCATGAATGCATCCATGGGGTCACACCACCGGACG

                                                    NotI
                                                    |
       EcoRI               StuI         EcoRV   ApaI
       |                   |            |       |  |
3121  aggtgaattcactagtaccggtaggcctgtcgacgatatcgggcccgcggccgctggatc 3180
      TCCACTTAAGTGATCATGGCCATCCGGACAGCTGCTATAGCCCGGGCGCCGGCGACCTAG

       ORF_3 rf(2)(3182,5308)>>>
       |
3181  catggataaagttttaaacagagaggaatctttgcagctaatggaccttctaggtcttga 3240
      GTACCTATTTCAAAATTTGTCTCTCCTTAGAAACGTCGATTACCTGGAAGATCCAGAACT

3241  aaggagtgcctgggggaatattcctctgatgagaaaggcatatttaaaaaaatgcaagga 3300
      TTCCTCACGGACCCCCTTATAAGGAGACTACTCTTTCCGTATAAATTTTTTTACGTTCCT

3301  gtttcatcctgataaaggaggagatgaagaaaaaatgaagaaaatgaatactctgtacaa 3360
      CAAAGTAGGACTATTTCCTCCTCTACTTCTTTTTTACTTCTTTTACTTATGAGACATGTT

3361  gaaaatggaagatggagtaaaatatgctcatcaacctgactttggaggcttctgggatgc 3420
      CTTTTACCTTCTACCTCATTTTATACGAGTAGTTGGACTGAAACCTCCGAAGACCCTACG

                        SV40_lrgT other(3440,5308)>>>
                        |
3421  aactgagattccaacctatggaactgatgaatgggagcagtggtggaatgcctttaatga 3480
      TTGACTCTAAGGTTGGATACCTTGACTACTTACCCTCGTCACCACCTTACGGAAATTACT

3481  ggaaaacctgttttgctcagaagaaatgccatctagtgatgatgaggctactgctgactc 3540
      CCTTTTGGACAAAACGAGTCTTCTTTACGGTAGATCACTACTACTCCGATGACGACTGAG

3541  tcaacattctactcctccaaaaaagaagagaaaggtagaagaccccaaggactttccttc 3600
      AGTTGTAAGATGAGGAGGTTTTTTCTTCTCTTTCCATCTTCTGGGGTTCCTGAAAGGAAG

3601  agaattgctaagttttttgagtcatgctgtgtttagtaatagaactcttgcttgctttgc 3660
      TCTTAACGATTCAAAAAACTCAGTACGACACAAATCATTATCTTGAGAACGAACGAAACG

3661  tatttacaccacaaaggaaaaagctgcactgctatacaagaaaattatggaaaaatattc 3720
      ATAAATGTGGTGTTTCCTTTTTCGACGTGACGATATGTTCTTTTAATACCTTTTTATAAG

3721  tgtaacctttataagtaggcataacagttataatcataacatactgttttttcttactcc 3780
      ACATTGGAAATATTCATCCGTATTGTCAATATTAGTATTGTATGACAAAAAAGAATGAGG

3781  acacaggcatagagtgtctgctattaataactatgctcaaaaattgtgtacctttagctt 3840
      TGTGTCCGTATCTCACAGACGATAATTATTGATACGAGTTTTTAACACATGGAAATCGAA

3841  tttaatttgtaaaggggttaataaggaatatttgatgtatagtgccttgactagagatcc 3900
```

```
      AAATTAAACATTTCCCCAATTATTCCTTATAAACTACATATCACGGAACTGATCTCTAGG

3901  attttctgttattgaggaaagtttgccaggtgggttaaaggagcatgattttaatccaga 3960
      TAAAAGACAATAACTCCTTTCAAACGGTCCACCCAATTTCCTCGTACTAAAATTAGGTCT

3961  agaagcagaggaaactaaacaagtgtcctggaagcttgtaacagagtatgcaatggaaac 4020
      TCTTCGTCTCCTTTGATTTGTTCACAGGACCTTCGAACATTGTCTCATACGTTACCTTTG

4021  aaaatgtgatgatgtgttgttattgcttgggatgtacttggaatttcagtacagttttga 4080
      TTTTACACTACTACACAACAATAACGAACCCTACATGAACCTTAAAGTCATGTCAAAACT

4081  aatgtgtttaaaatgtattaaaaaagaacagcccagccactataagtaccatgaaaagca 4140
      TTACACAAATTTTACATAATTTTTTCTTGTCGGGTCGGTGATATTCATGGTACTTTTCGT

4141  ttatgcaaatgctgctatatttgctgacagcaaaaaccaaaaaaccatatgccaacaggc 4200
      AATACGTTTACGACGATATAAACGACTGTCGTTTTTGGTTTTTTGGTATACGGTTGTCCG

4201  tgttgatactgttttagctaaaaagcgggttgatagcctacaattaactagagaacaaat 4260
      ACAACTATGACAAAATCGATTTTTCGCCCAACTATCGGATGTTAATTGATCTCTTGTTTA

4261  gttaacaaacagatttaatgatcttttggataggatggatataatgtttggttctacagg 4320
      CAATTGTTTGTCTAAATTACTAGAAAACCTATCCTACCTATATTACAAACCAAGATGTCC

4321  ctctgctgacatagaagaatggatggctggagttgcttggctacactgtttgttgcccaa 4380
      GAGACGACTGTATCTTCTTACCTACCGACCTCAACGAACCGATGTGACAAACAACGGGTT

4381  aatggattcagtggtgtatgacttttttaaaatgcatggtgtacaacattcctaaaaaaag 4440
      TTACCTAAGTCACCACATACTGAAAAATTTTACGTACCACATGTTGTAAGGATTTTTTTC

4441  atactggctgtttaaaggaccaattgatagtggtaaaactacattagcagctgctttgct 4500
      TATGACCGACAAATTTCCTGGTTAACTATCACCATTTTGATGTAATCGTCGACGAAACGA

4501  tgaattatgtgggggggaaagctttaaatgttaatttgcccttggacaggctgaactttga 4560
      ACTTAATACACCCCCCTTTCGAAATTTACAATTAAACGGGAACCTGTCCGACTTGAAACT

4561  gctaggagtagctattgaccagtttttagtagtttttgaggatgtaaagggcactggagg 4620
      CGATCCTCATCGATAACTGGTCAAAAATCATCAAAAACTCCTACATTTCCCGTGACCTCC

4621  ggagtccagagatttgccttcaggtcagggaattaataacctggacaatttaagggatta 4680
      CCTCAGGTCTCTAAACGGAAGTCCAGTCCCTTAATTATTGGACCTGTTAAATTCCCTAAT

4681  tttggatggcagtgttaaggtaaacttagaaaagaaacacctaaataaaagaactcaaat 4740
      AAACCTACCGTCACAATTCCATTTGAATCTTTTCTTTGTGGATTTATTTTCTTGAGTTTA

4741  atttccccctggaatagtcaccatgaatgagtacagtgtgcctaaaacactgcaggccag 4800
      TAAAGGGGGACCTTATCAGTGGTACTTACTCATGTCACACGGATTTTGTGACGTCCGGTC

4801  atttgtaaaacaaatagattttaggcccaaagattatttaaagcattgcctggaacgcag 4860
      TAAACATTTTGTTTATCTAAAATCCGGGTTTCTAATAAATTTCGTAACGGACCTTGCGTC

4861  tgagtttttgttagaaaagagaataattcaaagtggcattgctttgcttcttatgttaat 4920
      ACTCAAAAACAATCTTTTCTCTTATTAAGTTTCACCGTAACGAAACGAAGAATACAATTA

4921  ttggtacagacctgtggctgagtttgctcaaagtattcagagcagaattgtggagtggaa 4980
      AACCATGTCTGGACACCGACTCAAACGAGTTTCATAAGTCTCGTCTTAACACCTCACCTT

4981  agagagattggacaaagagtttagtttgtcagtgtatcaaaaaatgaagtttaatgtggc 5040
      TCTCTCTAACCTGTTTCTCAAATCAAACAGTCACATAGTTTTTTACTTCAAATTACACCG

5041  tatgggaattggagttttagattggctaagaaacagtgatgatgatgatgaagacagcca 5100
      ATACCCTTAACCTCAAAATCTAACCGATTCTTTGTCACTACTACTACTACTTCTGTCGGT

5101  ggaaaatgctgataaaaatgaagatggtggggagaagaacatggaagactcagggcatga 5160
      CCTTTTACGACTATTTTTACTTCTACCACCCCTCTTCTTGTACCTTCTGAGTCCCGTACT

5161  aacaggcattgattcacagtcccaaggctcatttcaggcccctcagtcctcacagtctgt 5220
      TTGTCCGTAACTAAGTGTCAGGGTTCCGAGTAAAGTCCGGGGAGTCAGGAGTGTCAGACA

5221  tcatgatcataatcagccataccacatttgtagaggttttacttgctttaaaaaacctcc 5280
      AGTACTAGTATTAGTCGGTATGGTGTAAACATCTCCAAAATGAACGAAATTTTTTGGAGG

                                      XbaI        XhoI
                                      |           |
5281  cacacctccccctgaacctgaaacataaggatcctctagactgcagctcgagtacccata 5340
      GTGTGGAGGGGGACTTGGACTTTGTATTCCTAGGAGATCTGACGTCGAGCTCATGGGTAT

                                       SV40 prom(5377,5645)>>>
```

```
                                        |
5341  cgacgtcccagactacgcttgagtttaaacacgcgtggtgtggaaagtccccaggctccc 5400
      GCTGCAGGGTCTGATGCGAACTCAAATTTGTGCGCACCACACCTTTCAGGGGTCCGAGGG

5401  cagcaggcagaagtatgcaaagcatgcatctcaattagtcagcaaccaggtgtggaaagt 5460
      GTCGTCCGTCTTCATACGTTTCGTACGTAGAGTTAATCAGTCGTTGGTCCACACCTTTCA

5461  ccccaggctccccagcaggcagaagtatgcaaagcatgcatctcaattagtcagcaacca 5520
      GGGGTCCGAGGGGTCGTCCGTCTTCATACGTTTCGTACGTAGAGTTAATCAGTCGTTGGT

                           SV40 origin(5544,5621)>>>
                           |
5521  tagtcccgcccctaactccgcccatcccgcccctaactccgcccagttccgcccattctc 5580
      ATCAGGGCGGGGATTGAGGCGGGTAGGGCGGGGATTGAGGCGGGTCAAGGCGGGTAAGAG

                                                    SfiI
                                                    |
                                    ORF_2 rf(1)(5611,6279)>>>
                                    |               |
5581  cgccccatggctgactaatttttttttatttatgcagaggccgaggccgcctcggcctctg 5640
      GCGGGGTACCGACTGATTAAAAAAAATAAATACGTCTCCGGCTCCGGCGGAGCCGGAGAC

                                          puro marker(5680,6279)>>>
                                          |
5641  agctattccagaagtagtgaggaggctttttttggaggccatgaccgagtacaagcccacg 5700
      TCGATAAGGTCTTCATCACTCCTCCGAAAAAACCTCCGGTACTGGCTCATGTTCGGGTGC

5701  gtgcgcctcgccacccgcgacgacgtccctcgggccgtacgcaccctcgccgccgcgttc 5760
      CACGCGGAGCGGTGGGCGCTGCTGCAGGGAGCCCGGCATGCGTGGGAGCGGCGGCGCAAG

5761  gccgactaccccgccacgcgccacaccgtggacccggaccgccacatcgagcgggtcacc 5820
      CGGCTGATGGGGCGGTGCGCGGTGTGGCACCTGGGCCTGGCGGTGTAGCTCGCCCAGTGG

5821  gagctgcaagaactcttcctcacgcgcgtcgggctcgacatcggcaaggtgtgggtcgcg 5880
      CTCGACGTTCTTGAGAAGGAGTGCGCGCAGCCCGAGCTGTAGCCGTTCCACACCCAGCGC

5881  gacgacggcgccgcggtggcggtctggaccacgccggagagcgtcgaagcgggggcggtg 5940
      CTGCTGCCGCGGCGCCACCGCCAGACCTGGTGCGGCCTCTCGCAGCTTCGCCCCCGCCAC

5941  ttcgccgagatcggcccgcgcatggccgagttgagcggttcccggctggccgcgcagcaa 6000
      AAGCGGCTCTAGCCGGGCGCGTACCGGCTCAACTCGCCAAGGGCCGACCGGCGCGTCGTT

6001  cagatggaagggctcctggcgccgcaccggcccaaggagcccgcgtggttcctggccacc 6060
      GTCTACCTTCCCGAGGACCGCGGCGTGGCCGGGTTCCTCGGGCGCACCAAGGACCGGTGG

6061  gtcggcgtctcgcccgaccaccagggcaagggtctgggcagcgccgtcgtgctccccgga 6120
      CAGCCGCAGAGCGGGCTGGTGGTCCCGTTCCCAGACCCGTCGCGGCAGCACGAGGGGCCT

6121  gtggaggcggccgagcgcgccggggtgcccgccttcctggagacctccgcgccccgcaac 6180
      CACCTCCGCCGGCTCGCGCGGCCCCACGGGCGGAAGGACCTCTGGAGGCGCGGGGCGTTG

6181  ctccccttctacgagcggctcggcttcaccgtcaccgccgacgtcgaggtgcccgaagga 6240
      GAGGGGAAGATGCTCGCCGAGCCGAAGTGGCAGTGGCGGCTGCAGCTCCACGGGCTTCCT

6241  ccgcgcacctggtgcatgacccgcaagcccggtgcctgaacgcgttccggaaatcaacct 6300
      GGCGCGTGGACCACGTACTGGGCGTTCGGGCCACGGACTTGCGCAAGGCCTTTAGTTGGA

6301  ctggattacaaaatttgtgaaagattgactggtattcttaactatgttgctccttttacg 6360
      GACCTAATGTTTTAAACACTTTCTAACTGACCATAAGAATTGATACAACGAGGAAAATGC

6361  ctatgtggatacgctgctttaatgcctttgtatcatgctattgcttcccgtatggctttc 6420
      GATACACCTATGCGACGAAATTACGGAAACATAGTACGATAACGAAGGGCATACCGAAAG

6421  attttctcctccttgtataaatcctggttgctgtctctttatgaggagttgtggcccgtt 6480
      TAAAAGAGGAGGAACATATTTAGGACCAACGACAGAGAAATACTCCTCAACACCGGGCAA

6481  gtcaggcaacgtggcgtggtgtgcactgtgtttgctgacgcaacccccactggttggggc 6540
      CAGTCCGTTGCACCGCACCACACGTGACACAAACGACTGCGTTGGGGGTGACCAACCCCG

6541  attgccaccacctgtcagctcctttccgggactttcgctttcccctccctattgccacg 6600
      TAACGGTGGTGGACAGTCGAGGAAAGGCCCTGAAAGCGAAAGGGGGAGGGATAACGGTGC

6601  gcggaactcatcgccgcctgccttgcccgctgctggacaggggctcggctgttgggcact 6660
      CGCCTTGAGTAGCGGCGGACGGAACGGGCGACGACCTGTCCCCGAGCCGACAACCCGTGA

6661  gacaattccgtggtgttgtcggggaagctgacgtcctttccatggctgctcgcctgtgtt 6720
      CTGTTAAGGCACCACAACAGCCCCTTCGACTGCAGGAAAGGTACCGACGAGCGGACACAA
```

```
6721  gccacctggattctgcgcgggacgtccttctgctacgtccctttcggccctcaatccagcg 6780
      CGGTGGACCTAAGACGCGCCCTGCAGGAAGACGATGCAGGGAAGCCGGGAGTTAGGTCGC

6781  gaccttccttcccgcggcctgctgccggctctgcggcctcttccgcgtctcgccttcgcc 6840
      CTGGAAGGAAGGGCGCCGGACGACGGCCGAGACGCCGGAGAAGGCGCAGAGCGGAAGCGG

                                                      delta_U3 other(6889,6941)>>>
                                                      |
6841  ctcagacgagtcggatctccctttgggccgcctccccgcctgtccggatggaagggctaa 6900
      GAGTCTGCTCAGCCTAGAGGGAAACCCGGCGGAGGGGCGGACAGGCCTACCTTCCCGATT

                                                HIV-1_5_LTR other(6942,7122)>>>
                                                |
6901  ttcactcccaacgaatacaagatctgctttttgcttgtactgggtctctctggttagacc 6960
      AAGTGAGGGTTGCTTATGTTCTAGACGAAAAACGAACATGACCCAGAGAGACCAATCTGG

6961  agatctgagcctgggagctctctggctaactagggaacccactgcttaagcctcaataaa 7020
      TCTAGACTCGGACCCTCGAGAGACCGATTGATCCCTTGGGTGACGAATTCGGAGTTATTT

7021  gcttgccttgagtgcttcaagtagtgtgtgcccgtctgttgtgtgactctggtaactaga 7080
      CGAACGGAACTCACGAAGTTCATCACACACGGGCAGACAACACACTGAGACCATTGATCT

7081  gatccctcagacccttttagtcagtgtggaaaatctctagcagtagtagttcatgtcatc 7140
      CTAGGGAGTCTGGGAAAATCAGTCACACCTTTTAGAGATCGTCATCATCAAGTACAGTAG

7141  ttattattcagtatttataacttgcaaagaaatgaatatcagagagtgagaggaacttgt 7200
      AATAATAAGTCATAAATATTGAACGTTTCTTTACTTATAGTCTCTCACTCTCCTTGAACA

7201  ttattgcagcttataatggttacaaataaagcaatagcatcacaaatttcacaaataaag 7260
      AATAACGTCGAATATTACCAATGTTTATTTCGTTATCGTAGTGTTTAAAGTGTTTATTTC

7261  catttttttcactgcattctagttgtggtttgtccaaactcatcaatgtatcttatcatg 7320
      GTAAAAAAAGTGACGTAAGATCAACACCAAACAGGTTTGAGTAGTTACATAGAATAGTAC

7321  tctggcatctatgtcgggtgcggagaaagaggtaatgaaatggcattatgggtattatgg 7380
      AGACCGTAGATACAGCCCACGCCTCTTTCTCCATTACTTTACCGTAATACCCATAATACC

7381  gtctgcattaatgaatcggccaacgatcccggtgtgaaataccgcacagatgcgtaagga 7440
      CAGACGTAATTACTTAGCCGGTTGCTAGGGCCACACTTTATGGCGTGTCTACGCATTCCT

7441  gaaaataccgcatcaggcgctcttccgcttcctcgctcactgactcgctgcgctcggtcg 7500
      CTTTTATGGCGTAGTCCGCGAGAAGGCGAAGGAGCGAGTGACTGAGCGACGCGAGCCAGC

7501  ttcggctgcggcgagcggtatcagctcactcaaaggcggtaatacggttatccacagaat 7560
      AAGCCGACGCCGCTCGCCATAGTCGAGTGAGTTTCCGCCATTATGCCAATAGGTGTCTTA

7561  caggggataacgcaggaaagaacatgtgagcaaaaggccagcaaaaggccaggaaccgta 7620
      GTCCCCTATTGCGTCCTTTCTTGTACACTCGTTTTCCGGTCGTTTTCCGGTCCTTGGCAT

             pBR322 origin(7628,8247)<<<
             |
7621  aaaaggccgcgttgctggcgtttttccataggctccgccccccctgacgagcatcacaaaa 7680
      TTTTCCGGCGCAACGACCGCAAAAAGGTATCCGAGGCGGGGGGACTGCTCGTAGTGTTTT

7681  atcgacgctcaagtcagaggtggcgaaacccgacaggactataaagataccaggcgtttc 7740
      TAGCTGCGAGTTCAGTCTCCACCGCTTTGGGCTGTCCTGATATTTCTATGGTCCGCAAAG

7741  cccctggaagctccctcgtgcgctctcctgttccgaccctgccgcttaccggatacctgt 7800
      GGGGACCTTCGAGGGAGCACGCGAGAGGACAAGGCTGGGACGGCGAATGGCCTATGGACA

7801  ccgcctttctcccttcgggaagcgtggcgctttctcatagctcacgctgtaggtatctca 7860
      GGCGGAAAGAGGGAAGCCCTTCGCACCGCGAAAGAGTATCGAGTGCGACATCCATAGAGT

7861  gttcggtgtaggtcgttcgctccaagctgggctgtgtgcacgaaccccccgttcagcccg 7920
      CAAGCCACATCCAGCAAGCGAGGTTCGACCCGACACACGTGCTTGGGGGGCAAGTCGGGC

7921  accgctgcgccttatccggtaactatcgtcttgagtccaacccggtaagacacgacttat 7980
      TGGCGACGCGGAATAGGCCATTGATAGCAGAACTCAGGTTGGGCCATTCTGTGCTGAATA

7981  cgccactggcagcagccactggtaacaggattagcagagcgaggtatgtaggcggtgcta 8040
      GCGGTGACCGTCGTCGGTGACCATTGTCCTAATCGTCTCGCTCCATACATCCGCCACGAT

8041  cagagttcttgaagtggtggcctaactacggctacactagaaggacagtatttggtatct 8100
      GTCTCAAGAACTTCACCACCGGATTGATGCCGATGTGATCTTCCTGTCATAAACCATAGA

8101  gcgctctgctgaagccagttaccttcggaaaaagagttggtagctcttgatccggcaaac 8160
```

```
      CGCGAGACGACTTCGGTCAATGGAAGCCTTTTTCTCAACCATCGAGAACTAGGCCGTTTG

8161  aaaccaccgctggtagcggtggttttttttgtttgcaagcagcagattacgcgcagaaaaa 8220
      TTTGGTGGCGACCATCGCCACCAAAAAAACAAACGTTCGTCGTCTAATGCGCGTCTTTTT

8221  aaggatctcaagaagatcctttgatcttttctacggggtctgacgctcagtggaacgaaa 8280
      TTCCTAGAGTTCTTCTAGGAAACTAGAAAAGATGCCCCAGACTGCGAGTCACCTTGCTTT

8281  actcacgttaagggattttggtcatgagattatcaaaaaggatcttcacctagatccttt 8340
      TGAGTGCAATTCCCTAAAACCAGTACTCTAATAGTTTTTCCTAGAAGTGGATCTAGGAAA

8341  taaattaaaaatgaagttttaaatcaatctaaagtatatatgagtaaacttggtctgaca 8400
      ATTTAATTTTTACTTCAAAATTTAGTTAGATTTCATATATACTCATTTGAACCAGACTGT

8401  gttaccaatgcttaatcagtgaggcacctatctcagcgatctgtctatttcgttcatcca 8460
      CAATGGTTACGAATTAGTCACTCCGTGGATAGAGTCGCTAGACAGATAAAGCAAGTAGGT

8461  tagttgcctgactccccgtcgtgtagataactacgatacgggagggcttaccatctggcc 8520
      ATCAACGGACTGAGGGGCAGCACATCTATTGATGCTATGCCCTCCCGAATGGTAGACCGG

8521  ccagtgctgcaatgataccgcgagacccacgctcaccggctccagatttatcagcaataa 8580
      GGTCACGACGTTACTATGGCGCTCTGGGTGCGAGTGGCCGAGGTCTAAATAGTCGTTATT

8581  accagccagccggaagggccgagcgcagaagtggtcctgcaactttatccgcctccatcc 8640
      TGGTCGGTCGGCCTTCCCGGCTCGCGTCTTCACCAGGACGTTGAAATAGGCGGAGGTAGG

8641  agtctattaattgttgccgggaagctagagtaagtagttcgccagttaatagtttgcgca 8700
      TCAGATAATTAACAACGGCCCTTCGATCTCATTCATCAAGCGGTCAATTATCAAACGCGT

8701  acgttgttgaaaaaggatcttcacctagatccttttcacgtagaaagccagtccgcagaa 8760
      TGCAACAACTTTTTCCTAGAAGTGGATCTAGGAAAAGTGCATCTTTCGGTCAGGCGTCTT

8761  acggtgctgaccccggatgaatgtcagctactgggctatctggacaagggaaaacgcaag 8820
      TGCCACGACTGGGGCCTACTTACAGTCGATGACCCGATAGACCTGTTCCCTTTTGCGTTC

8821  cgcaaagagaaagcaggtagcttgcagtgggcttacatggcgatagctagactgggcggt 8880
      GCGTTTCTCTTTCGTCCATCGAACGTCACCCGAATGTACCGCTATCGATCTGACCCGCCA

                        NEOKAN prom(8900,8949)>>>
                        |
8881  tttatggacagcaagcgaaccggaattgccagctggggcgccctctggtaaggttgggaa 8940
      AAATACCTGTCGTTCGCTTGGCCTTAACGGTCGACCCCGCGGGAGACCATTCCAACCCTT

8941  gccctgcaaagtaaactggatggctttctcgccgccaaggatctgatggcgcaggggatc 9000
      CGGGACGTTTCATTTGACCTACCGAAAGAGCGGCGGTTCCTAGACTACCGCGTCCCCTAG

                                             NTP_II marker(9041,9829)>>>
                                             |
                                          ORF_4 rf(2)(9038,9832)>>>
                                          |  |
9001  aagctctgatcaagagacaggatgaggatcgtttcgcatgattgaacaagatggattgca 9060
      TTCGAGACTAGTTCTCTGTCCTACTCCTAGCAAAGCGTACTAACTTGTTCTACCTAACGT

9061  cgcaggttctccggccgcttgggtggagaggctattcggctatgactgggcacaacagac 9120
      GCGTCCAAGAGGCCGGCGAACCCACCTCTCCGATAAGCCGATACTGACCCGTGTTGTCTG

9121  aatcggctgctctgatgccgccgtgttccggctgtcagcgcaggggcgcccggttctttt 9180
      TTAGCCGACGAGACTACGGCGGCACAAGGCCGACAGTCGCGTCCCCGCGGGCCAAGAAAA

9181  tgtcaagaccgacctgtccggtgccctgaatgaactgcaagacgaggcagcgcggctatc 9240
      ACAGTTCTGGCTGGACAGGCCACGGGACTTACTTGACGTTCTGCTCCGTCGCGCCGATAG

9241  gtggctggccacgacgggcgttccttgcgcagctgtgctcgacgttgtcactgaagcggg 9300
      CACCGACCGGTGCTGCCCGCAAGGAACGCGTCGACACGAGCTGCAACAGTGACTTCGCCC

9301  aagggactggctgctattgggcgaagtgccggggcaggatctcctgtcatctcaccttgc 9360
      TTCCCTGACCGACGATAACCCGCTTCACGGCCCCGTCCTAGAGGACAGTAGAGTGGAACG

9361  tcctgccgagaaagtatccatcatggctgatgcaatgcggcggctgcatacgcttgatcc 9420
      AGGACGGCTCTTTCATAGGTAGTACCGACTACGTTACGCCGCCGACGTATGCGAACTAGG

9421  ggctacctgcccattcgaccaccaagcgaaacatcgcatcgagcgagcacgtactcggat 9480
      CCGATGGACGGGTAAGCTGGTGGTTCGCTTTGTAGCGTAGCTCGCTCGTGCATGAGCCTA

9481  ggaagccggtcttgtcgatcaggatgatctggacgaagagcatcaggggctcgcgccagc 9540
      CCTTCGGCCAGAACAGCTAGTCCTACTAGACCTGCTTCTCGTAGTCCCCGAGCGCGGTCG
```

```
9541  cgaactgttcgccaggctcaaggcgagcatgcccgacggcgaggatctcgtcgtgaccca 9600
      GCTTGACAAGCGGTCCGAGTTCCGCTCGTACGGGCTGCCGCTCCTAGAGCAGCACTGGGT

9601  tggcgatgcctgcttgccgaatatcatggtggaaaatggccgcttttctggattcatcga 9660
      ACCGCTACGGACGAACGGCTTATAGTACCACCTTTTACCGGCGAAAAGACCTAAGTAGCT

9661  ctgtggccggctgggtgtggcggaccgctatcaggacatagcgttggctacccgtgatat 9720
      GACACCGGCCGACCCACACCGCCTGGCGATAGTCCTGTATCGCAACCGATGGGCACTATA

9721  tgctgaagagcttggcggcgaatgggctgaccgcttcctcgtgctttacggtatcgccgc 9780
      ACGACTTCTCGAACCGCCGCTTACCCGACTGGCGAAGGAGCACGAAATGCCATAGCGGCG

9781  tcccgattcgcagcgcatcgccttctatcgccttcttgacgagttcttctgaattttgtt 9840
      AGGGCTAAGCGTCGCGTAGCGGAAGATAGCGGAAGAACTGCTCAAGAAGACTTAAAACAA

9841  aaaatttttgttaaatcagctcatttttttaaccaataggccgaaatcggcaacatccctt 9900
      TTTTAAAAACAATTTAGTCGAGTAAAAAATTGGTTATCCGGCTTTAGCCGTTGTAGGGAA

                                          f1 origin(9937,10242)<<<
                                          |
9901  ataaatcaaaagaatagaccgcgatagggttgagtgttgttccagtttggaacaagagtc 9960
      TATTTAGTTTTCTTATCTGGCGCTATCCCAACTCACAACAAGGTCAAACCTTGTTCTCAG

9961  cactattaaagaacgtggactccaacgtcaaagggcgaaaaaccgtctatcagggcgatg 10020
      GTGATAATTTCTTGCACCTGAGGTTGCAGTTTCCCGCTTTTTGGCAGATAGTCCCGCTAC

10021 gcccactacgtgaaccatcacccaaatcaagttttttgcggtcgaggtgccgtaaagctc 10080
      CGGGTGATGCACTTGGTAGTGGGTTTAGTTCAAAAAACGCCAGCTCCACGGCATTTCGAG

10081 taaatcggaaccctaaagggagcccccgatttagagcttgacggggaaagccggcgaacg 10140
      ATTTAGCCTTGGGATTTCCCTCGGGGGCTAAATCTCGAACTGCCCCTTTCGGCCGCTTGC

10141 tggcgagaaaggaagggaagaaagcgaaaggagcgggcgctagggcgctggcaagtgtag 10200
      ACCGCTCTTTCCTTCCCTTCTTTCGCTTTCCTCGCCCGCGATCCCGCGACCGTTCACATC

10201 cggtcacgctgcgcgtaaccaccacacccgcgcgcttaatgcgccgctacagggcgcgtc 10260
      GCCAGTGCGACGCGCATTGGTGGTGTGGGCGCGCGAATTACGCGGCGATGTCCCGCGCAG

10261 cattcgccattcaggatcgaattaattcttaattaacatcatcaataatatacctt 10316
      GTAAGCGGTAAGTCCTAGCTTAATTAAGAATTAATTGTAGTAGTTATTATATGGAA
```

Fig 6.1: Vector map with nucleotide sequence of herein used SV40T-containing lentiviral vector.

Depicted is the nucleotide sequence of sense and antisense strand of parental SV40T-containing lentiviral vector which was used to transduce primary eccrine sweat gland duct cells in this work. On total, this vector consists of 10,3 kilobases. Digits at the sides represent continuous count of nucleotides. Abbreviations: a/A – adenine, c/C – cytosine, g/G – guanine, t/T – thymine; ORF - open reading frame, origin - replication of origin of denoted gene, other - other gene, prom - start of promotor sequence, puro marker – gene of puromycin selection marker; REBASE – miscellaneous binding site, reg - regulatory sequence.

Taken from: https://www.abmgood.com/vectormap/index/index/?name=pLenti-SV40-T%20(Puro).

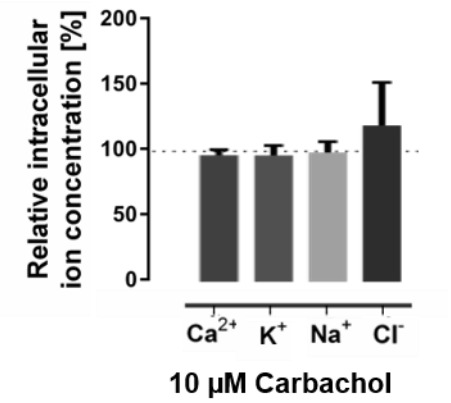

Fig 6.2: *In vitro* ion profile of 10 µM Carbachol.
Depicted are relative intracellular ion concentrations of cations calcium $[Ca^{2+}]_i$, potassium $[K^+]_i$, and sodium $[Na^+]_i$ as well as of the anion chloride $[Cl^-]_i$ evoked by a DMEM-based, aqueous solution with 10 µM Carbachol. Nearly confluent 2D eccrine sweat gland co-culture cells were treated and resulting changes of fluorescence intensities measured with a microplate reader reflecting fluctuation of intracellular ion levels relative to an untreated control which was set as 100%. Data represent mean ± SD of three independent experiments. Modified from Welzel 2017.

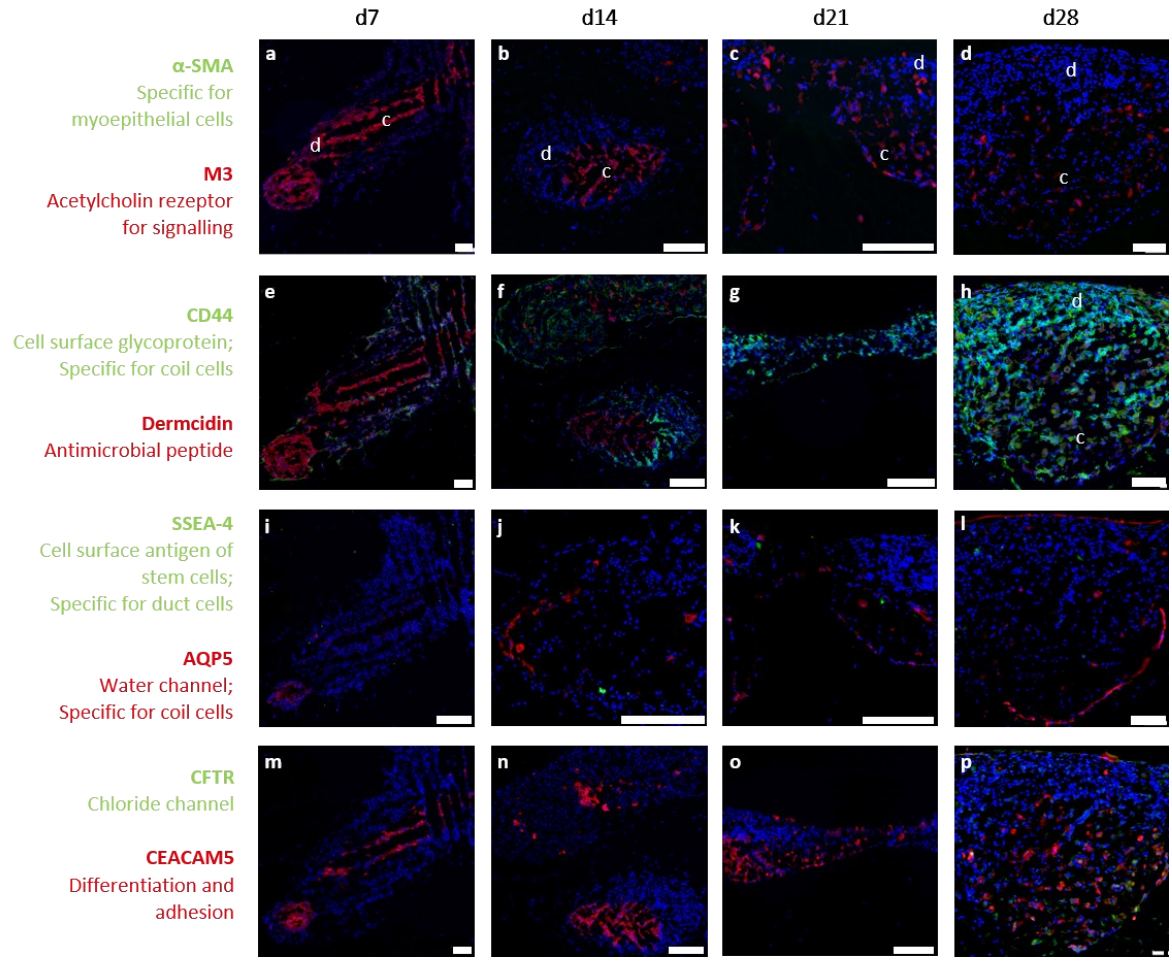

Fig 6.3: Immunofluorescence-based comparison of temporal changes in protein expression of eccrine sweat gland matrix models from d7 to d28.
Localization and distribution of sweat gland-associated proteins was analyzed in frozen sections of sweat gland matrix models after 7 days (d7), 14 days (d14), 21 days (d21), and 28 days (d28) of culturing. Models were built by pre-seeding of coil cells directly into slots in the fibroblast-containing collagen I matrix and addition of duct cells 24 h later. Parts of coil cells are denoted with c, while d signifies duct cells regions as exemplary presented in image a-d. Target proteins are depicted in red (TRITC) and green (FITC) while nuclei are stained in blue (DAPI). Bar represents 200 µm.

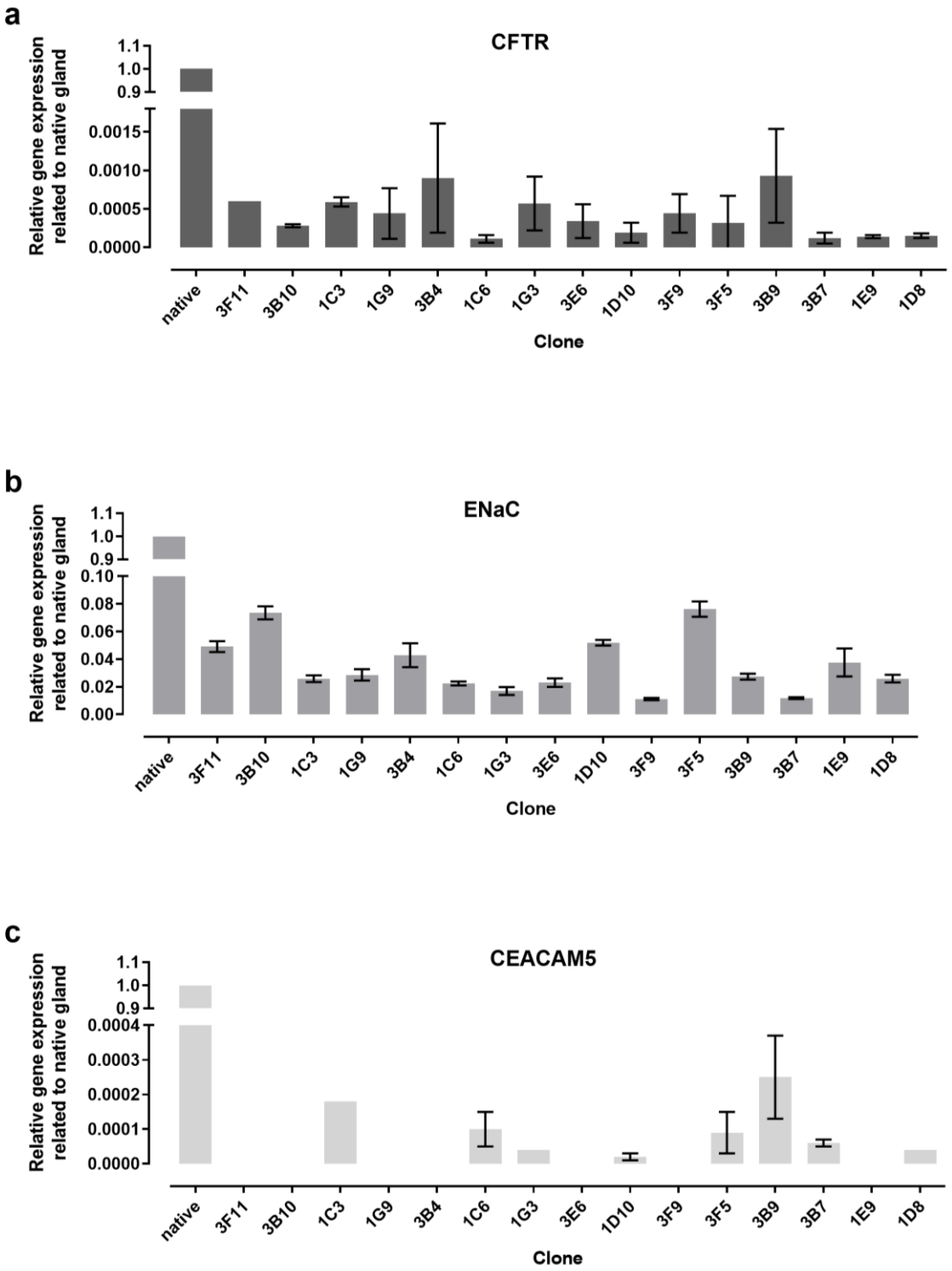

Fig 6.4: Relative gene expressions of isolated SV40T-transduced duct cell clones related to native eccrine glands.

Depicted are relative gene expression levels for cystic fibrosis transmembrane conductance regulator (CFTR) (**a**), epithelial sodium channel (ENaC) (**b**), and carcinoembryonic antigen-related cell adhesion molecule 5 (CEACAM5) (**c**) quantified by RT-qPCR of isolated native eccrine sweat glands and 15 generated SV40T-transduced eccrine sweat gland duct cell clones. Clones were propagated until passage 21 and aliquots sampled for mRNA analysis. Gene expression value of native eccrine glands was set to 1.0. GAPDH served as the housekeeping gene. Data are mean ± SD of one experiment performed in triplicate replicate.

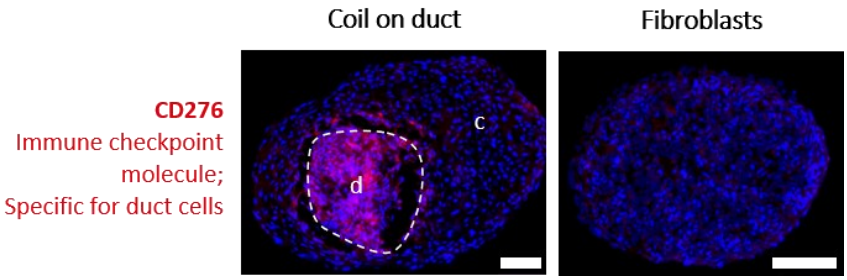

Fig 6.5: Comparable immunofluorescence staining of 3D HD models coil on duct and 3D HD models with fibroblasts.
Localization and distribution of CD276 was compared by immunofluorescence staining in frozen sections of 3D models prepared by pre-seeding of duct cells and addition of the same number of coil cells 24 hours later (coil on duct) or 3D models containing solely fibroblasts. Both 3D hanging drop models were harvested after 3 days of cultivation. Regions of duct cells are denoted by d and surrounding coil cells are marked with c. Target protein CD276 to distinguish duct cells from fibroblasts is depicted in red (TRITC) while nuclei are stained in blue (DAPI). Bar represents 100 µm.

1.2 List of figures

1.3 List of tables

1.4 List of suppliers

Abbreviation	Address
Abcam	Abcam, Cambridge, UK
abm	Applied Biological Materials Inc., Richmond, CAN
Agilent	Agilent Technologies, Inc., Santa Clara, CA, USA
AppliChem	AppliChem GmbH, Darmstadt, GER
BASF	BASF SE, Ludwigshafen, GER
Binder	BINDER GmbH, Tuttlingen, GER
Bio-Rad	Bio-Rad Laboratories, Inc., Hercules, CA, USA
Cell	Cell Signaling Technology, Danvers, MA, USA
ChemAxon	ChemAxon, Budapest, HU
Corning	Corning Incorporated, New York, USA
Dako	Dako Denmark AS, Glostrup, DNK
DuPont	DuPont Tate & Lyle Bio Products Company, LLC, Loudon, TN, USA
Elementis	Elementis plc, London, UK
Eppend	Eppendorf AG, Hamburg, GER
Fisher	Fisher Scientific GmbH, Schwerte, GER
Gibco	Gibco by Life Technologies, Carlsbad, CA, USA
GraphPad	GraphPad Software, La Jolla, CA, USA
Heraeus	Heraeus Holding GmbH, Hanau, GER
HyClone	HyClone by GE Healthcare, Little Chalfont, UK
Inovyn	Inovyn Europe Limited, London, UK
InSphero	InSphero AG, Schlieren, CHE
Invitrogen	Invitrogen Corporation, Carlsbad, California, USA
InvivoGen	InvivoGen Europe, Toulouse, FR
Leica	Leica Mikrosysteme Vertrieb GmbH, Wetzlar, GER
LeicaB	Leica Biosystems, Buffalo Grove, IL, USA
Life	Life Technologies, Carlsbad, CA, USA
Lonza	Lonza Group Ltd, Basel, CHE
Marien	Paul Marienfeld GmbH & Co. KG, Lauda-Königshofen, GER
Merck	Merck KGaA, Darmstadt, GER
Microsoft	Microsoft Corporation, Redmond, USA
Milli	EMD Millipore Corporation, Billerica, MA, USA
Molecular	Molecular Devices, LLC, Sunnyvale, CA, USA
NIH	National Institute of Health, USA
Olympus	Olympus Europe SE & Co. KG, Hamburg, GER
OriGene	OriGene Technologies GmbH, Herford, GER
PEQLAB	PEQLAB Biotechnologie GmbH, Erlangen, GER
Qiagen	Qiagen GmbH, Hilden, GER
Roche	Roche Diagnostics, Mannheim, GER
Roth	Carl Roth GmbH + Co. KG, Karlsruhe, GER
Sakura	Sakura Finetek U.S.A., Inc., Torrance, CA, USA
Schott	Schott Geräte GmbH, Mainz, GER
Sigma	Sigma-Aldrich Chemie GmbH, Hamburg, GER
Solvay	Solvay GmbH, Brussels, BEL
Tecan	Tecan Group AG, Männedorf, CHE
Thermo	Thermo Fisher Scientific, Waltham, MA, USA
WeylChem	WeylChem Internation GmbH, Frankfurt am Main, GER

V. Acknowledgement/Danksagung

Meinen herzlichen Dank möchte ich an Prof. Dr. h.c. Holger Stark richten für seine bereitwillige Übernahme der Erstbetreuung der Arbeit seitens der Universität. Mit seiner hervorragenden chemischen und pharmakologischen Expertise hat er maßgeblich zum erfolgreichen Gelingen dieser Arbeit beigetragen hat. Mein zweiter Dank gilt Prof. Dr. Wilhelm Stahl für die fachliche Betreuung dieser Arbeit als Zweitgutachter.

Ich danke herzlich Dr. Dirk Peterson und Dr. Andrea Sättler von der Firma Henkel AG & Co. KGaA für die Möglichkeit aus, diese spannende und doch alltägliche Thematik bearbeiten zu dürfen sowie für die Überlassung dieses Projektes zur Durchführung meiner Dissertation.

Mein besonderer Dank geht an Dr. Thomas Welss und Bernhard Banowski für die herzliche Aufnahme ins Team, ihre stets vorhandene Bereitschaft zu hilfreichen Diskussionen, der herausragenden fachlichen Betreuung und nicht zuletzt des konstruktiven Korrekturlesens.

Ganz besonders möchte ich mich an dieser Stelle bei Sabine Grüdl bedanken, die in all der ganzen Zeit nicht nur eine wunderbare unterstützende Kollegin, sondern auch eine liebenswürdige Freundin geworden ist. Ich vermisse unsere spontanen Brainstorming-Sessions, die mich immer so viel vorangebracht haben. Vielen Dank auch für die Bemühungen, meine Arbeit Korrektur zu lesen.

Ein weiterer großer Dank geht an mein Team von Advanced Research Biology für Eure hilfreiche Unterstützung: Christoph Backhausen, Gudrun Heinen, Werner Bartmann und Melanie Ludwig.
Außerdem danke ich Marcus Claas, Swenja Kalischke, Marion Merkel, Lars Vierkotten, Claudia Petrick, Nelli Blasius, Patrizia Böttcher, Laura Steinmeier, Kerstin Elias und allen Kollegen für die herzliche Zusammenarbeit. Eure vielen guten Tipps und Eure Hilfe haben maßgeblich zu dieser Arbeit beigetragen. Es war eine wunderbare Zeit mit Euch in Z33.
Auch möchte ich mich auch bei allen bedanken, die mich auf unterschiedlichste Art und Weise unterstützt haben und somit zum Gelingen dieser Arbeit beigetragen haben.

Ein herzliches Dankeschön möchte ich an dieser Stelle auch an Sonja Wrobel und Carolin Neumann richten, die mich als beste Freundinnen in dieser intensiven Zeit ausgehalten und motiviert haben.

Meinen größten Dank möchte ich meiner Familie widmen, die mich in all den Jahren des Studiums immer unterstützt hat. Ohne Eure unermüdliche persönliche Hingabe und motivierenden Worte wäre ich heute nicht an diesem Punkt.

Vielen Dank!

VI. Affidavit/Eidesstattliche Erklärung

I declare under oath that I have produced my thesis independently and without any undue assistance by third parties under consideration of the ‘Principles for the Safeguarding of Good Scientific Practice at Heinrich Heine University Düsseldorf'.

Ich versichere an Eides Statt, dass die Dissertation von mir selbständig und ohne unzulässige fremde Hilfe unter Beachtung der „Grundsätze zur Sicherung guter wissenschaftlicher Praxis an der Heinrich-Heine-Universität Düsseldorf“ erstellt worden ist.

Date/Datum	Signature/Unterschrift